Reliability and Efficiency of Vehicular Network Applications

A thesis submitted in fulfilment of the requirements for the degree of Doctor of Philosophy in the School of Information Technologies at

University of Sydney

Saeed Bastani

2014

Declaration

I declare that this thesis is my work. If information is used from other sources, I confirm that it is properly referenced in the thesis.

To my son who kept me motivated and to my wife for all her sacrifices and belief in me.

Acknowledgements

I would like to express my deepest appreciation to my main supervisor Prof. Bjorn Landfeldt for the continuous support of my PhD study and research. His patience, enthusiasm, and specially his profound knowledge kept me motivated all the time. Even after his moving to Lund University, I was never deprived of his continuous support. Among many things, he provided me with a great opportunity to visit the highly prestigious Lund University where I was introduced to the people with vast knowledge and experience in my field. I could not have imagined finishing the most challenging part of my research without being enlightened by the people at Lund University.

I sincerely thank my honorary supervisor Prof. Albert Y. Zomaya, my co-supervisor at the University of Sydney, Dr. Taso Viglas, my co-supervisor at National ICT Australia (NICTA), Prof. Aruna Seneviratne, for their full support and valuable advices.

I would like to especially thank Dr. Joachim Gudmundsson at the University of Sydney for his precious scientific supports, Dr. Lavy Libman at the University of New South Wales for helping me technically and in preparing parts of my publications, Prof. Michal Pioro at Lund University for his enthusiastic discussions on my research and for the great course I was honoured to attend, Dr. Fredrik Tufvesson and Taimoor Abbas at Lund University for enlightening me in several ways including the application of a radio propagation model.

The last but not the least, I am indebted to my wife for her sacrifices in many ways, and to my little son whose birth during my PhD brought inspiration and warmth to my life.

Abstract

The DSRC/WAVE initiative is forecast to enable a plethora of applications, categorised in two broad classes of safety and non-safety applications. With the improvement of driver awareness being the primary objective of the safety applications, the performance and hence the users' satisfaction are driven foremost by the reliability of applications in providing the users with fresh kinematic and warning information about hazardous events. However, due to limited tasks performed in the application layer, the reliability of these applications reduces substantially to the reliability of the underlying communication system. In non-safety applications, on the other hand, many different tasks are performed and decisions are made in the application layer. To gain a holistic view of the impacts of such diverse tasks and decisions on the efficiency of information dissemination as the primary task of these applications, it is required that a comprehensive application framework be designed in the first place.

In this dissertation, we adopt a systematic approach to analytically investigate the reliability of the communication system in a symbiotic relationship with the host system comprising a vehicular traffic system and radio propagation environment. To this aim, the *interference* factor is identified as the central element of the symbiotic relationship. Our approach to the investigation of interference and its impacts on the communication reliability departs from previous studies by the degree of realism incorporated in the host system model. In one dimension, realistic traffic models are developed to describe the vehicular traffic behaviour in urban traffic systems as the major overlooked scenario in the previous studies. In a second dimension, a state-of-the-art radio propagation model targeted to vehicular network (VANET)

environments is employed to capture the unique signal propagation aspects of the host system. Our key findings are summarised as follows: (i) in urban traffic scenarios, the use of lower data rates in the nominal range stipulated by DSRC/WAVE initiative to fulfil the load demand of applications is questionable, unless the transmission range is controlled effectively, (ii) the worst-case reliability takes place in positions behind the traffic light queue where vehicles are decelerating from high velocity. Such positions are arguably the most important for timely alerting of dangerous traffic conditions, (iii) the hidden terminal interference causes a significant decline in the reachable distance of broadcast safety messages, which in several cases drop to distances shorter than the minimum required coverage of medium range safety applications, and (iv) the hidden terminal interference happens to be the most severe within a short distance from the intersection, implying the likeliness of severe reliability degradation in safety applications targeted to intersection scenarios.

This dissertation addresses the case of non-safety applications by proposing a generic framework as a capstone architecture for the development of new applications and the evaluation of existing ones. This framework, while being independent from the underlying networking technology, enables accurate characterization of the various information dissemination tasks that a node performs individually and in cooperation with others. As the central element of the framework, we propose a game theoretic model to describe the interaction of meeting nodes aiming to exchange information of mutual or social interests. An adaptive mechanism is designed to enable a mobile node to measure the social significance of various information topics, which is then used by the node to prioritize the forwarding of information objects. Our study reveals that the physical structure of the network is not the sole factor driving the behaviour of the dissemination task. Instead, the logical structure characterized by the contact and interest patterns of the participating nodes is the key influential factor.

Highlighted Findings

- ✓ In our study of radio overlapping and channel load in the urban traffic scenario, we found a strong evidence that the use of data rates in the lower part of the nominal range specified for VANETs operation in the DSRC/WAVE standard is highly questionable in urban areas when the wireless transmission range grows to the required coverage of long range applications. (Chapter 3)
- ✓ In our study of the reliability performance in the urban scenario, we observe that the worst case results take place in positions behind the traffic light queue where vehicles are decelerating from high velocity. It is notable that, from a traffic safety point of view, these positions are arguably the most important for timely alerting of dangerous traffic conditions, and their lower reliability may correspondingly lead to an increased risk of serious incidents. (Chapter 4)
- ✓ In our study of the hidden terminal problem in safety-critical traffic scenarios, we observe that the hidden terminal interference causes a significant decline in the reachable distance of broadcast safety messages, which in several cases drop to distances shorter than the minimum required coverage of medium range safety applications. (Chapter 5)
- ✓ Our study of the hidden terminal problem in traffic scenarios with the presence of intersections reveals that the aggregate interference power induced by hidden terminals may amount to values several times larger than the induced interference power in an equivalent road scenario, but in the absence of intersections. Our results also show that the most severe interference occurs within a short distance ($\sim$ 200 meters) from the intersection center. These observations indicate the likeliness of severe reliability degradation in safety applications targeted to intersection scenarios. (Chapter 5)
- ✓ In our study of information dissemination in non-safety applications, we observe that the physical structure of the network is not the sole factor driving the outcome behaviour of the dissemination task. Instead, the logical structure formed by the contact and interest patterns of the participating nodes is the key influential factor. (Chapter 7)

Publications

Some of the material in this thesis are published in peer-reviewed conferences or submitted for review as a journal article.

S. Bastani, B. Landfeldt, and L. Libman, “A Traffic Density Model for Radio Overlapping in Urban Vehicular Ad hoc Networks”, The 36$^{\text{th}}$ IEEE Conference on Local Computer Networks (LCN), Bonn, Germany, October 2011. [23]

S. Bastani, B. Landfeldt, and L. Libman, “On the Reliability of Safety Message Broadcast in Urban Vehicular Ad hoc Networks”, The 14$^{\text{th}}$ ACM/IEEE International Conference on Modeling, Analysis and Simulation of Wireless and Mobile Systems (MSWIM), Miami, USA, October 2011. [24]

S. Bastani, B. Landfeldt, and Ch. Rohner, P. Gunningberg, “A Social Node Model for Realizing Information Dissemination Strategies in Delay Tolerant Networks”, The 15$^{\text{th}}$ ACM/IEEE International Conference on Modeling, Analysis and Simulation of Wireless and Mobile Systems (MSWIM), Cyprus, October 2012. [25]

S. Bastani, B. Landfeldt, T. Abbas, and F. Tufvesson, “Hidden Terminal Interference in Vehicular Ad Hoc Networks with Forced-Flow Traffic Conditions”, submitted for journal publication.

Contents

List of Figures

List of Tables

Chapter 1

Introduction

With the introduction of DSRC/WAVE [2; 121] as candidate technology for enabling Vehicular Ad hoc NETworks (VANETs), a broad range of applications spanning from safety to traffic monitoring and control, urban sensing, mobile trading and more, are envisioned for deployment in the near future [3; 5; 87]. A primary class of applications, with Forward Collision Warning (FCW) [5] as an example, is targeted for the enhancement of traffic safety, while others are of convenience nature with the objective of facilitating information and content access or discovery of local services while on the move. Such a rich range of applications from safety to convenience or commercially-oriented is highly interesting from the standpoint of car manufacturers, communication network providers, and service providers. Other parties such as transportation authorities and policy makers are more interested in enhancing the safety of drivers and pedestrians.

For various players from business or industry, achieving sustainable gain from an application is significantly driven by the user satisfaction of the application once deployed. To this end, the achievable service quality is the key to satisfy the user expectations. However, the user expectation of service quality differs in safety and non-safety (i.e., convenience) applications. In a safety application with the objective of improving drivers' awareness of potential hazards, the reliability of the application is highly influential in the user experience of the service quality and the level of his/her trust in the application. Furthermore, in these applications, the decisions made in the application layer of a node are very limited. Hence, the reliability of applications is mainly dependent on the reliability of the underlying communication system.

In non-safety applications with information or content-centric nature, many different tasks are carried out by a typical mobile node participating in the dissemination of information. Also, the node faces various decisions to be made on which information objects to exchange at the time of meeting with others. Above all, the degree of the node's participation in the dissemination process is determined by the node's state and constraints in terms of the available resources, contact duration, the relevance of information offered by other nodes, etc. This, in turn, influences the ultimate efficiency of the application in terms of dissemination performance and the utility accrued by the individual participating nodes. Previous studies have addressed some aspects of information dissemination as the enabling mechanism for information-centric applications. However, they stop short of addressing other key functionalities and the interplay of those functionalities in a holistic view.

While safety and non-safety applications have some causes of performance degradation in common, they exhibit some intrinsic differences mainly attributed to the application layer architecture. This, in turn, triggers differentiation in the approaches to be employed for the exploration of the degradation causes and the countermeasures to be designed and deployed for the improvements. Because of these differences, we opt to approach the two types of applications separately, while we acknowledge the fact that these applications are potentially deployed in the same environment (i.e., vehicular traffic network) and realized by the same communication technology (i.e., DSRC/WAVE).

In the following, we introduce our work on safety applications in Section 1.1 followed by our work on information-centric non-safety applications in Section 1.2.

1.1 Reliability Performance of Safety Applications

In safety applications, such as Blind Spot Warning (BSW) [5], the driver's expectation of the application reliability is highly strict, meaning that few failures are likely to result in driver's distrust in the application. Efforts for the improvement of the application reliability and thus the acceptance by users should in the first place concentrate on the underlying communication system to identify its potential bottlenecks. In view of this, a critical step is to understand the behaviour of the communication system with respect to the characteristics of the host system as the platform for the realization of the application. By host system, we mean the vehicular traffic system and the environment encompassing the traffic system. The traffic system, in turn, consists of the traffic network topology and the regulations governing vehicles' motion. The traffic environment encompasses all physical objects including vehicles and the buildings surrounding the traffic system which influence the performance of the communication system.

1.1.1 Symbiotic Modelling of Host and Communication Systems

Accurate study of the behaviour of a VANET's application requires that the underlying host and communication systems are modelled in symbiosis. The symbiotic relationship is interpreted as the impact(s) of one system on the other:

- *Impacts of the Host System on the Communication System:* the host system affects the communication system in two major ways. First, the traffic system determines the density of vehicles potentially using an application via message communication. Also, the relative spatial arrangement of vehicles at any time instant is determined by the mobility of vehicles and other influential factors such as road structure, traffic regulation, etc. From the standpoint of a sender and receiver of application data, both vehicle density and the spatial arrangement affect the quality of data received in the receiver side. The vehicle density affects the reception quality by giving rise to the radio overlapping of vehicles competing for access to the communication channel, which potentially results in increased packet collisions. The relative arrangement of vehicles, on the other hand, determines the distance of the sender and the intended receiver(s), which in turn determines the strength of the received signal carrying application's data. The physical objects in the environment account for another kind of impact of the host system on the communication system in terms of radio propagation behaviour. The moving (e.g., vehicles) and static (e.g., buildings) objects give rise to signal attenuation and the variation in the received signal power. Such adverse environmental effects are attributed to signal diffraction, signal reflection, multi path fading, and Doppler effects [120], which collectively determine the quality of received signals, and thus the ultimate performance of the application.

- *Impacts of the Communication System on the Host System:* the communication system facilitates the exchange of instant kinematic and global traffic information among vehicles. On the reception of such information, some responses (or feedbacks) are triggered in the recipients. The responses can take many forms including instant braking, slowing down, lane changing, and planning new routes. They affect the microscopic traffic parameters such as vehicle spacing and the macroscopic parameters including density, flow, and the average velocity of the traffic.

To study the symbiotic relationships of the two systems in terms of mutual impacts, it is required to represent the systems by appropriate models. As such, the degree of accuracy in characterizing the mutual impacts relates to the extent of realism captured by the representative models. Although the two symbiotic relationships described above are equally important for the purpose of studying an application's behaviour, in this thesis we focus on the first type of relationship, that is, the impacts of host system on the communication system. To this end, the host system is represented by appropriate traffic and radio propagation models. These models are expected to facilitate the investigation of the communication and application level factors on realistic grounds.

1.1.2 Communication and Application Level Factors

The communication level factor addressed in this thesis is interference and the application level metric of interest is reliability. While other factors including data rate, transmission power, and MAC layer parameters merit further study, our focus on interference and reliability is justified by the following reasons:

- The reliability of a safety application is the key factor influencing the acceptance of the application by drivers.

- The application reliability relates to the intensity of interference in the communication level, which in turn is driven by the intensity of radio overlapping of the vehicles using the application.

- The amount and variation of interference, collectively describing the interference behaviour, are highly impacted by the characteristics of the host system. This is explained by the strong relationship between interference and traffic density and also the radio propagation environment. Bearing in mind the fact that the building blocks of the host system, that is, the traffic system and the environment encompassing the traffic system, are uncontrolled and dynamic entities, to the same extent one can consider the interference as an uncontrolled and challenging factor.

- Hidden terminal interference as a typical realization of the broad concept of interference is a primary cause of performance degradation of applications relying on the broadcast communication paradigm [78; 106; 108; 164; 165]. The applications relying on other forms of broadcast communication (e.g., geocast) are also highly vulnerable to the hidden terminal effect. The high impact of the hidden terminal problem in broadcast mode is due to the fact that virtual carrier sensing is not used in this mode and the applications rely only on physical carrier sense [78; 108; 164]. This leads to a wide range of hidden terminal activity in broadcast communication [108].

1.1.3 Motivations

While in the context of vehicular networks the interference and reliability factors have been the focus of extensive research, in previous studies the traffic and radio propagation models used for the representation of the host system do not accurately capture the real world features of the host system. Our approach in this thesis departs from previous studies by addressing the aforementioned factors on more realistic grounds. More specifically, we identify three major directions where realistic approaches are absent in previous research or otherwise biased to particular scenarios.

1.1.3.1 Realistic and Comprehensive Modelling of Vehicular Traffic

A major shortcoming in previous research on VANETs is found in the assumptions and models applied to the vehicular traffic. To clarify this, we introduce some fundamental concepts from traffic science.

Three macroscopic traffic parameters including traffic density, velocity, and flow describe the traffic state by the following well-known expression termed fundamental traffic equation [140]:

$$Q = V \times K \tag{1.1}$$

where Q, V, and K are the traffic flow, average velocity, and traffic density, respectively. Depending on the density and velocity, several traffic states emerge. The detailed features of these traffic states can be found in [140; 182]. In the following, we present a brief introduction to the major traffic states as shown in Figure 1.1.

In a road segment with sparse traffic conditions, the arriving and departing flows are identical and queues do not emerge on the road segment. In this situation, the traffic flow is stable [182]. While the flow is in stable state, if the density of traffic is low enough that drivers can drive as fast as they wish, the traffic is presumed to be in free-flow situation [182]. The stable-flow state persists up to a point where the density reaches a threshold termed optimal (or critical) density (K_o) [140]. At this point, the traffic flow reaches its maximum, which is known as the capacity of the road (Q_{max}) [142]. By increasing the density beyond the critical density K_o, vehicles are forced to interact with their surrounding vehicles in order to keep a safe distance. The traffic state corresponding to this situation is termed forced-flow [182]. In forced-flow state, when the density reaches its maximum (K_j), the traffic is known to be in jam state and vehicles are forced to stop [182].

Each traffic state shown in Figure 1.1 imposes unique challenges on the vehicular communication system. This, in particular, translates to heterogeneous

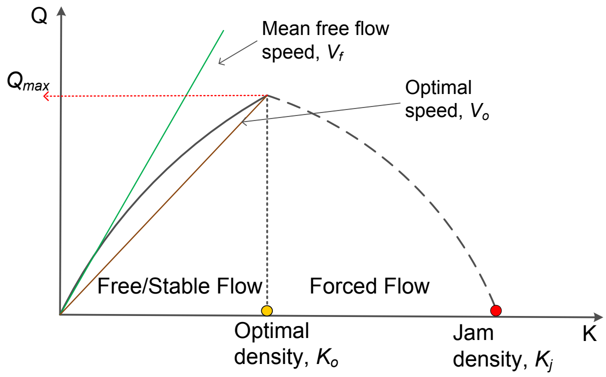

Figure 1.1: Fundamental diagram of traffic flow [140]

performance of the communication system in reaction to various traffic states potentially coexisting on a road segment. Hence, the challenges attributed to a traffic state are required to be addressed both exclusively and also in relation to other traffic states simultaneously present on the road segment. Previous studies on VANETs are rather selective in addressing the challenges of the traffic states on the communication system. Apart from few simulation studies which suffer from the lack of generalization, the analytical studies adopt some questionable assumptions when they address traffic scenarios. The first widely-adopted assumption is that the traffic is in steady-state. Following this assumption, a number of distribution functions including uniform, Poisson, exponential, and Poisson point process are employed for the modelling of traffic distribution on a road. Second, they assume traffic is homogeneous, that is, at a given time instant only a single traffic state exists on a road. Thus, the coexistence of various traffic states is ignored. While these assumptions may be valid in highway scenarios with free-flow traffic as the dominant traffic state, the extent to which they are applicable to other traffic states (e.g., forced-flow) and to the scenarios with several simultaneous traffic states is arguable. More specifically, in urban traffic systems, the emergence of heterogeneous traffic states is inevitable due to the presence of signalised (and give-way) intersections. Besides, in urban scenarios, the presence of forced-flow traffic state is undoubted due to the relatively dense traffic and also the impact of intersections. Furthermore, the steady-state assumption is not generally valid due to diverse drivers' behaviour and the complex transitions of traffic states. Therefore, previous models which are highly biased towards steady state, free-flow, and homogeneous traffic are not applicable to urban traffic scenarios.

To be able to design control mechanisms and countermeasures for the improvement of applications' reliability, in the first place, it is required that the bottlenecks of the communication system are identified using realistic traffic models and based on valid assumptions. It is therefore necessary to develop new model(s) able to capture the core traffic properties and in the meantime comply to the real-world traffic features. We acknowledge that currently there are many synthetic traffic models suitable for simulation purposes; however, these models are not tractable for generalised analytical studies of VANET issues. This motivates us to develop parsimonious and tractable traffic models based on macroscopic traffic aspects. Along the line of the arguments, we believe *traffic density* is a suitable macroscopic parameter facilitating the study of interference and reliability issues in vehicular communication networks.

1.1.3.2 Significance of Safety-Critical Scenarios

While addressing various traffic scenarios is a valuable effort for accurate understanding of the behaviour of communication system, identifying the safety-critical traffic scenarios and studying the performance of communication system in such scenarios is highly prominent. In safety-critical scenarios, the velocity of vehicles is relatively high and the vehicles' spacing or so-called *headway distance* is shorter compared to drivers' reaction time. These scenarios account for accident-prone situations where the safety applications, in order to be useful, are required to be extremely reliable. The mapping from a traffic scenario to the safety dimension facilitates better understanding of the bottlenecks of DSRC/WAVE technology in fulfilling stringent reliability requirements of the applications. In particular, by addressing safety-critical scenarios, one can predict the reliability of the communication system in worst case conditions, resembling the performance test of industrial systems or software applications under stress. Surprisingly, safety-critical scenarios and their implications for the communication system are not addressed in previous studies in the context of VANETs. Those studies addressing various vehicle densities do not characterise the criticality of such densities from traffic safety perspective.

In view of the demand for addressing safety-critical scenarios, we believe that the traffic scenarios corresponding to intersections and also the scenarios associated with the capacity of roads are examples of safety-critical and accident-prone scenarios requiring dedicated research.

1.1.3.3 Application of Radio Propagation Models Targeted to Vehicular Network Environment

The accuracy of conclusions derived from a study on the communication aspects of VANETs also depends on the assumptions on the radio propagation and the extent of realism captured by the propagation model used in the study. For the purpose of clarification, we present an example of hidden terminal interference which highlights the dependency of the outcome communication behaviour on the radio propagation model employed. In this example, we borrowed the concepts of coordinated and uncoordinated transmissions from [164], but to serve a different purpose. As shown in Figure 1.2, three vehicles are situated on a traffic network. Vehicle A is the target transmitter, vehicle B is the intended recipient of a message from A, and C is a potential hidden terminal with respect to A. We assume vehicle B is obstructing the Line of Sight (LOS) between A and C. Figure 1.2a demonstrates the case of using a propagation model without the capability of detecting or distinguishing LOS obstruction. In this case, the extra attenuation due to LOS obstruction is not taken into account in the signal received in C from A ($\mathrm{P_{CA}}$). Hence, it is likely that the signal is received with a power greater than a Carrier Sense threshold ($\mathrm{CS_{th}}$). This results in a coordinated transmission by vehicle C, because C detects the channel busy and defers its transmission. This ultimately leads to a successful reception in vehicle B, if the impacts of other factors are ignored. Consequently, C is not considered as a hidden terminal. If, on the other hand, a realistic radio propagation model is used (Figure 1.2b), the extra attenuation due to signal obstruction is captured by the model. Therefore, the signal from A is likely to be received in C with a power ($\mathrm{P_{CA}}$) less than $\mathrm{CS_{th}}$. In this case, vehicle C plays the role of hidden terminal whose uncoordinated transmission potentially results in packet collision in B. The difference of the outcome communication behaviour with respect to the employed radio propagation model can be witnessed in numerous other cases, including Non Line of Sight (NLOS) situations frequently occurring at intersection corners.

The above examples and many others drive us to conclude that the use of realistic radio propagation models developed for the VANET environment will highly add to the accuracy of the study.

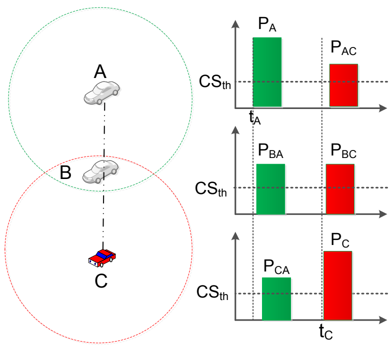

(a) Unrealistic radio propagation model

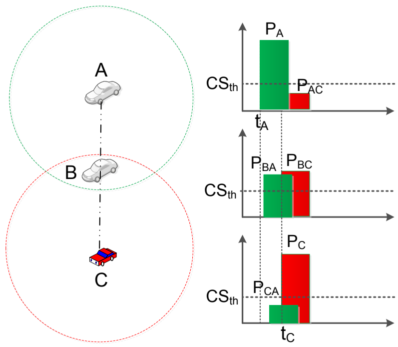

(b) Realistic radio propagation model

Figure 1.2: The dependency of hidden terminal interference on the radio propagation model

1.1.4 Contributions

The contributions of this thesis to the interference and reliability issues in vehicular communication networks are as follows:

1. We develop a novel traffic density model for urban traffic scenarios. To model the traffic density, we consider the impacts of urban intersections on the traffic dynamic. We employ the traffic density model to characterise the spatial-temporal behaviour of radio overlapping as a predictor of communication interference. Accordingly, a radio overlapping model is developed and used for the study of channel load associated with periodic beaconing as a fundamental mechanism for safety message communication in VANETs. This contribution is presented in Chapter 3 and appears as a conference publication [23].

2. An analytical model is developed to predict the reliability indicators of safety applications in urban traffic scenarios. Focusing on a road segment

linked to a signalized intersection as the building blocks of urban traffic systems, we apply the traffic density model mentioned in the first contribution to investigate the spatial-temporal behaviour of the reliability metrics. Also, we characterize the region(s) on the road segment according to the achieved safety level. The proposed analytical model covers both periodic and event-driven messaging mechanisms and integrates them in a single universal model. This contribution is presented in Chapter 4 and appears as a conference publication [24].

3. We develop an analytical framework to investigate the severity of hidden terminal interference under realistic grounds and with focus on safety-critical traffic scenarios. A state-of-the-art measurement-based shadow-fading path loss model is used as the radio propagation model. Also, focusing on urban traffic scenarios with forced-flow traffic, we identify two major safety-critical traffic scenarios and find the upper-bound interference power induced by hidden nodes and the lower-bound reachable distance of the safety messages. The proposed analytical framework has the capability of being used as a benchmark for the assessment of the reliability risks of safety applications under safety-critical traffic scenarios. To the best our knowledge, the approach of studying reliability issues under safety-critical conditions, and also the degree of realism captured in the host system representation within an analytical framework is unique to our work. This contribution is presented in Chapter 5. Also, it is submitted as a journal article.

Our approach to addressing the real-world aspects of the host system is progressive; contributions 1 and 2 emphasize the real-world aspects of vehicular traffic (modelled as part of the first contribution) and the implications for radio overlapping, interference, and reliability issues. In contribution 3, the real-world aspects of both radio propagation environment and the traffic system are taken into account. The radio propagation environment is represented by a state-of-the-art radio propagation model targeted to vehicular network environments, and the traffic scenarios are derived from traffic theory and are represented by well-established Cellular-Automaton (CA) modelling approach [47; 161].

1.2 Efficiency of Information-Centric Non-Safety Applications

Convenience and commercial VANET applications are information or content-centric in nature. The performance of these applications relates to the satisfaction of the users with the information of interest they fetch opportunistically in a course of meetings with the peers or the infrastructure. More specifically, from the standpoint of an individual user, the performance of the application is interpreted as the degree of matching between the topic(s) of information delivered to the user and the information interest(s) of user expressed in a measurable fashion. From a network-wide or social perspective, the performance is determined by the proportionality of the dissemination rate of information objects to the significance of the objects. The significance of an information object is interpreted as the popularity level of the topic(s) covered by the object.

There are a number of key features driving the performance of an information-centric application as follows:

- *Appropriate representation of user interests:* the quality of information delivered by the application depends on the degree of matching between the user interests and the topics of information delivered to the user. In line with this, the application should provide the users with mechanisms to facilitate the representation and the advertisement of users' interests. In particular, such mechanisms must be flexible in the representation of multiple information interests attributed to a single user.

- *Fine granularity of information representation:* an information object (e.g., file, message, video clip, etc.) may cover multiple topics or so-called *attributes*, simultaneously. The application must be flexible in representing information objects with as many attributes as they cover.

- *Matching of compound information objects and user interests:* with the compound information objects (i.e., with multiple attributes) and user interests as described above, the appropriate functionality must be available to measure the similarity of the two compound entities.

- *Adaptation to the shift of user interests:* the interest(s) of a user may change with time. The application should provide mechanisms to react to the shift in user interests, discover new interests, and apply the most recent interests in the upcoming dissemination sessions.

- *Timely access to the information of interest:* users lose their patience when facing prolonged access to their information of interest. Besides, some information are only valid within a certain time frame. The application should provide mechanisms for fast dissemination of information of high priority, high popularity, or time-limited.

- *Location awareness:* if an information object is bounded to a geographical region, the application should provide the functionality for representing such property in the meta-data section of the information object and also activate location-aware dissemination for this type of information.

- *Individual and social satisfaction:* in an individual-oriented dissemination mechanism, the goal is to address the information interests of nodes individually, whereas in social-oriented mechanism the objective is to enhance the overall satisfaction of nodes. The dissemination outcomes in the two modes are not necessarily identical. Depending on the information type and the current satisfaction level of the meeting nodes, an appropriate mechanism should be activated to achieve maximum performance. The application should provide sophisticated functionalities to choose or alternate between these two modes, if necessary.

In a broader dimension, the efficiency of an application is interpreted as the superposition of the performance (with the features mentioned above) and several other properties not directly related to performance. Two properties of this kind are related to the network and node resources with the following descriptions:

- *Resource awareness:* the contact time of meeting nodes and the communication bandwidth are precious network level resources. To use resources optimally, nodes are required to maintain a sufficient level of awareness about the resources prior to and during the sessions of information exchange.

- *Indiscriminate resource utilization:* with the limitation of resources of a typical user device in mind, efficiency is related to the pattern of resource usage of the application. Recalling that information muling is the major enabling mechanism for information dissemination, the application should not put the burden on a certain number of nodes, leading to resource depletion in those nodes while leaving others intact.

1.2.1 Motivations

Realizing an application framework that exhibits the aforementioned properties is an important task. However, addressing all properties and the associated challenges demands a vast amount of research and it is beyond the scope of this thesis to address all those challenges. For this reason, we are motivated to address the most fundamental aspects of the problem listed as follows:

- A fundamental study of various aspects of the information dissemination process, including efficiency aspects, demands the design of a generic framework. The main objective of such a framework is to describe the various tasks that a participating node performs individually and by cooperation with others. To the best of our knowledge, such a framework has not been addressed in previous studies.

- We are also motivated to address the case of network-wide efficiency of information dissemination. While the efficiency of conventional publish/subscribe methods [51] in satisfying the individual interests of nodes is acknowledged, we opt to develop a social-oriented information dissemination mechanism. To this aim, we believe a distributed and adaptive mechanism for the measurement of information popularity plays the key role.

1.2.2 Contributions

This thesis advances the state of the art in information dissemination frameworks targeted to DTNs, in general, and VANETs, in particular, by means of the following main contribution:

- A generic framework is designed to describe the characteristics of information dissemination among participating nodes in a network. The proposed framework describes the various tasks a node performs individually and in cooperation with others to facilitate the dissemination of information objects with various degrees of significance. Our proposed framework involves the following components and functionalities:

  (a) A distributed and adaptive information popularity measurement is developed. On a meeting incidence, the nodes employ the popularity of information to determine the ordering of information objects to be exchanged.

  (b) A user model is proposed with the capability of representing users with compound interests.

  (c) An information model is proposed with the capability of representing information objects with compound attributes.

  (d) A game theoretic interaction model is designed which takes into account the network and node resources together with the current states and constraints of the meeting nodes intending for information exchange. Using a utility function as part of the game problem, the meeting nodes are able to calculate the payoff they achieve by participating in the information exchange. Also, the degree to which a node participates in the exchange process is determined by the utility function.

  (e) A novel matching technique is proposed for the ranking of the information objects with respect to the individual and/or social interests of the meeting nodes.

The proposed framework with the aforementioned components and functionalities is presented in Chapter 7 and appears as a conference publication [25].

1.3 How to Read this Thesis

The remainder of this dissertation is organised as follows. In Chapter 2, we build our background on interference and reliability issues in vehicular communication networks. Additionally, in this chapter, we present evidence from previous studies to show that the application of realistic traffic and radio propagation models for the purpose of simulation or analytical studies is crucial for deriving accurate results. Chapter 3 presents our first contribution to reliability issues mentioned in Section 1.1.4. The second and third contributions mentioned in Section 1.1.4 are presented in Chapters 4 and 5, respectively. Chapter 6 presents the background and related work on information dissemination issues. Chapter 7 presents our contributions to information dissemination mentioned in Section 1.2.2. Chapter 8 summarises this dissertation and proposes new directions for future work. Appendix A introduces DSRC/WAVE technology and the various applications envisioned for future deployment. In Appendix B, we present concepts, theories, and modelling mechanisms applied to the context of vehicular traffic. Finally, Appendix C contains the detailed experimental results used in our analysis in Chapter 5.

Chapter 2

Reliability of Safety Applications: Background and Related Work

This chapter begins by introducing the concept of reliability in a broad term (Section 2.1), followed by an overview of the major factors affecting the reliability of safety applications (Section 2.2). In that regard, interference is highlighted as the most challenging factor influenced by uncontrolled characteristics of the radio propagation environment and the vehicular traffic system. In addition, the reliability indicators addressed frequently in the literature are discussed and the use cases of each indicator are highlighted (Section 2.3). A significant body of the chapter is dedicated to the related analytical and simulation studies on reliability issues (Section 2.4). In Section 2.5, we report some crucial evidence from the literature indicating that the way the host system is modelled will highly impact the credibility of the conclusions drawn from studies in the context of VANETs. Such evidence covers a broad range of issues including reliability.

2.1 Definition and Interpretations

In a safety application relying on safety message broadcast, the *reliability* is defined as the possibility that all *intended recipients* of a message will receive it successfully and in a timely manner [108]. In the context of vehicular communications, the intended recipients are generally referred to as the vehicles in the transmission range of a vehicle currently broadcasting a safety message. From the perspective of traffic safety, those vehicles situated in a critical traffic situation with respect to the location of the transmitter or the location of a hazardous incident reported by the transmitter are considered as intended recipients. The *timely delivery* of a safety message is also meaningful when it is related to the reaction time of drivers as well as the relative position of the intended recipients with respect to the position of the transmitter or the present hazardous event. Characterizing the exact relationship between the intended recipients and the traffic characteristics is a complex task and demands inter-disciplinary research. Due to the lack of mature research, most of previous studies in the context of VANETs have adopted the conventional definition of intended recipients as those vehicles in the communication range of a vehicle broadcasting safety messages.

2.2 Key Influential Factors

There are several factors influencing the reliability of safety applications. These factors are generally classified in two categories: controlled and uncontrolled factors [21]. Controlled factors include the internal functionalities of the safety application, the MAC layer functionalities, transmission power, data rate, modulation scheme, and many others [21; 106; 108; 183]. In the uncontrolled category, the communication interference is the primary factor. The significance of interference arises from the fact that it is highly dependent on the characteristics of the host system, that is, the radio propagation environment and the vehicular traffic system. Interference as a broad term is viewed in two main categories; internal and external interference [78]. Internal interference is caused by concurrent transmissions of two nodes having radio overlap. This results in packet collision, affecting the packet delivery rate of the transmitting node and the packet reception rate in some intended recipients. On the other hand, external interference relates to the overlapping radios of hidden node(s) and the intended recipient(s) of a given target transmitting node. In this case, an overlapped transmission (in time dimension) of the hidden node(s) and the target transmitter *potentially* affect the probability of successful reception in some intended recipients. It should be noted that the radio overlap is not a sufficient condition for a reception to fail. Indeed, reception failure also relates to the relative strength of the received signals propagated by the target transmitter and the hidden node(s) [164; 165].

2.2.1 Interference Issues

Radio Overlapping and Interference

In the literature, the communication interference is generally characterized by overlapping radios. In line with this, the intensity of radio overlap is considered as a predictor for the intensity of the communication interference. Depending on the radio overlap as perceived from a sender or a receiver perspective, the interference is investigated within two broad directions: sender-centric and receiver-centric.

The pioneering studies of interference with a sender-centric view are [119] and [36]. [119] addressed the interference in relation with the traffic and congestion level of the network. In [36], the authors proposed an explicit sender-centric definition for interference. According to this study, given a communication range R of nodes, the interference is described by the number of nodes within the overlapped region of the disks with radius R centred at various nodes. By applying this sender-centric definition, the authors argued that, opposed to the widely adopted assumption in the context of wireless communications, in sparse networks the intensity of interference is not necessarily low.

A pioneering study on interference with a receiver-centric view can be found in [174]. According to the authors, the interference from the perspective of a node w relates to the number of distinct radios overlapping the node w. Using this receiver-centric notion of interference, [122] addressed the minimization of interference in a given network while preserving some desired topological features, e.g., network connectivity. To this aim, the authors introduced the notion of average interference defined as the ratio of the total number of interference incidents to the number of passive nodes [122]. Given a network topology, the nodes are divided into passive and active nodes, where the active nodes are intended to maintain some topological features while their radios may cover some other nodes (i.e., passive nodes) [122].

In [70], Jain *et al.* adopted a hybrid sender and receiver-centric notion of interference to define pairwise successful transmission or reception. According to [70], a transmission from a node u with another node v as the intended receiver is successful if: $d_{uv} \leq R_u$, and any node w provided that its distance from v satisfies $d_{wv} \leq R_w$ or its distance from u satisfies $d_{wu} \leq R_w$ does not commit any transmission. d is the Euclidean distance between two nodes. R_u and R_w are the transmission ranges of u and w, respectively.

In [53], the definition by Jain *et al.* was employed to investigate the interference issues in the context of vehicular communications. Given a predetermined traffic density λ and free-flow mobility of vehicles in a highway scenario, the authors characterized the interference behaviour. Also, the impacts of driving habits defined by three types of drivers and the impacts of various traffic densities on the interference behaviour were taken into account; however, in all cases, the authors assumed that the traffic density is homogeneous and the traffic mobility is in steady state. Therefore, the impacts of heterogeneous traffic states occurring frequently in urban traffic systems were not addressed.

In our study presented in Chapter 3, we adopt a receiver-centric definition of interference based on radio overlapping, defined as the number of nodes covering a target node by their radios. Our work departs from the mentioned studies, including [53], by addressing radio overlap dynamics in urban traffic scenarios with heterogeneous traffic states.

Hidden Terminal Interference

Hidden terminals are a pair of nodes situated outside the interference range of each another, but they share some nodes in the overlapping part of their transmission ranges [32]. Hidden terminal interference is a major factor influencing the performance of wireless ad hoc networks [106; 108; 109; 164; 165]. To alleviate the adverse effects of hidden terminals, the IEEE 802.11 standard proposed two different mechanisms including virtual carrier sensing realized by RTS/CTS handshaking and physical carrier sensing. In unicast communications, which rely on both mechanisms, the size of the potential hidden terminal area is determined with respect to the distance between transmitter Tx and receiver Rx. However, in a broadcast communication paradigm, virtual carrier sensing is suppressed and the transmitting nodes rely only on physical sensing of the channel. The potential hidden terminal region in broadcast mode expands to the interference range of all intended recipients, Rx, situated in the transmission range of the Tx [108]. Consequently, the potential hidden terminal region in broadcast communication mode can be significantly larger than in the unicast counterpart [108]. This implies that safety applications, relying mainly on broadcast communication, are highly vulnerable to interference caused by hidden terminals.

The uncoordinated transmissions in random access MAC protocols, as in IEEE 802.11p for vehicular networks, is known to give rise to interference caused by hidden terminals [32]. However, this phenomenon is not solely attributed to the MAC functionality, but also to signal propagation properties. A node A commits an uncoordinated transmission with respect to a currently transmitting node B if the signal propagated by A arrives in B with a power too weak to detect that the channel is busy. In such a case, a transmission from B is considered as uncoordinated [164; 165]. The extent to which the uncoordinated transmissions affect successful reception from A in an intended receiver C depends on the relative strength of the received power in C from A and B. This, in turn, is dependent on several controlled and uncontrolled factors. The controlled factors include, but are not limited to, the data rate and transmission powers, whereas the uncontrolled factors consist of the relative distance of the intended receiver C from A and B, the propagation environment, and the nodes' mobility [20]. Therefore, a study of the hidden terminal problem owes much of its credibility to the radio propagation model used and the traffic model adopted in the study. This motivates us to investigate the hidden terminal problem within a realistic framework consisting of realistic radio propagation and traffic models (Chapter 5).

2.3 Reliability Indicators

The reliability indicators applied to one-hop and multi-hop safety message broadcasts are different in nature. Since the focus of this dissertation is the one-hop broadcast, we opt to introduce the associated reliability indicators with a great detail.

2.3.1 Packet Delivery Ratio (PDR)

PDR describes the reliability from the standpoint of a target transmitter. It is quantified as the ratio of the number of packets received successfully in all intended recipients of a target transmitter to the total number of transmitted packets [108]. PDR can be further characterized based on distance d of the potential receivers from the transmitter. Thus, PDR factor describes the percentage of error-free packets received by the intended recipients within the distance d from a target transmitter [108]. PDR is strongly related to the degree of drivers' awareness about a hazardous event reported by a target node realizing the event. An ideal PDR corresponds to the case that all packets of a safety message transmitted by a target sender are received by all concerned vehicles. If the delivery latency of a safety message is negligible compared to the driver reaction time, an ideal PDR implies guaranteed and timely reaction of the concerned vehicles. This indicator was employed in a number of works including [17; 102; 177] to address the reliability of safety applications targeted to vehicular networks.

2.3.2 Packet Reception Ratio (PRR)

In contrast to PDR, the PRR indicator describes the receivers' perception of reliability. It is quantified as the percentage of nodes receiving a packet from a target transmitter without error [108]. PRR in conjunction with PDR indicator can be employed to assess the potential contribution of a safety application in improving the awareness level of drivers. As with PDR indicator, PRR can be characterized for a distance d from the target transmitter [101]. In contrast with the average PRR which is measured over the entire communication range of a transmitter, the distance-based PRR facilitates more accurate understanding of the reliability as the distance from the transmitter grows. In a number of studies including [101; 165; 179], the PRR indicator was employed to investigate the reliability performance of vehicular communication networks.

2.3.3 Probability of Successful Reception ($\mathbf{p_{sr}}$)

p_{sr} is the probability that a node situated in the communication range of a target transmitter receives a packet from the transmitter successfully [108]. In contrast with packet delivery and reception ratios, which measure the reliability on average basis, p_{sr} relates to the reception quality of safety messages in a certain vehicle(s). The rationale for p_{sr} is that in some vehicular network applications, safety messages are important only to a certain vehicle(s) [108]. Given a network setting, the average indicators may imply that the reliability is in a satisfactory level, whereas the p_{sr} indicator measured in the same network may exhibit weak reliability in some nodes [108].

2.3.4 Delivery Latency (DL)

The delivery latency of a packet is the time interval from the time point when a packet is generated in the application layer to the time point when the packet is received in an intended recipient [106]. The internal contention in the application or MAC layers of the sender contributes to a time interval it takes for a packet to become the head of the internal transmission queue. Once a packet of a message is at the top of the transmission queue, another time interval is spent to access the channel. The third element of DL is the packet propagation time. Correspondingly, the delivery latency of a message is the aggregate latency of all packets comprising the message. The DL indicator has been addressed in a number of studies including [77; 101; 106; 177; 183]. Most of these studies addressed the packet level latency. The issue of message level latency is considered to be a research gap, and hence it merits a dedicated investigation.

2.3.5 Inter-Reception Time (IRT)

In safety applications relying on event-driven messages, the reliability is mainly determined by the successful packet reception probability (p_{sr}) and the geographical coverage of the broadcast message. On the other hand, in case of periodic messages, inter reception time (IRT) of messages is deemed to better describe the reliability of the application [55]. According to Elbatt *et al.* [55], who first introduced the indicator, IRT integrates the variability of packet reception time and packet reception probability into a single parameter. Intuitively, from the perspective of an intended recipient vehicle, a high probability of message reception from neighbouring vehicles implies better overall awareness of the recipient about their neighbourhood. Furthermore, the high frequency of message reception enhances the freshness of the information that a vehicle receives from its neighbouring vehicles or from the infrastructure. This, in turn, improves the reaction time of drivers to unpredicted hazardous events. Also, from the sender's point of view, the higher the chance that the neighbouring vehicles receive a message successfully and timely, the better the achieved safety level will be. In a recent study by Sepulcre *et al.* [151], the IRT indicator was used for the evaluation of the reliability of cooperative safety applications relying on periodic message dissemination. In our work in Chapter 4, we also apply the IRT indicator for the performance evaluation of periodic safety message dissemination.

2.3.6 Effective Range (ER)

According to Yousefi *et al.* [184], ER is the distance from a transmitter where a minimum service quality can be gained. The authors proposed the ER as a reliability indicator and defined it as the distance from the transmitter where: (i) the minimum delivery ratio is larger than a given threshold, and (ii) the maximum latency is smaller than a given threshold. Yousefi *et al.* highlighted the ER indicator as the most meaningful indicator for the reliability analysis of safety applications, arguing that the contribution of a safety application to the improvement of the safety level is equally important to all vehicles within a certain range of a transmitter and must be guaranteed to a certain degree. According to Yousefi *et al.*, the service quality thresholds are dependent on the type of safety application. In safety applications with the objective of assisting the drivers, p_{sr} should be in the range $[0.95, 0.99]$, whereas in more stringent safety applications it must be larger than 0.99. A similar notion of ER indicator can be found in [108], where the authors employed it for the study of reliability in one-hop broadcast.

2.3.7 Reachable Distance

Reachable Distance (RD) is introduced as a reliability metric for the first time in this dissertation (Chapter 5). RD is generally defined as the average distance to which a safety message can reach in a one-hop broadcast, taking into account the impacts of degradation caused by various factors including interference, channel load, MAC issues, and the adverse effects of the radio propagation environment. As a particular, yet significant case, the worst case reachable distance corresponds to the distance to which a message can reach while the adverse factors are most severe. In Chapter 5, we investigate the worst case (or lower bound) reachable distance in one-hop broadcast with respect to severe interference caused by hidden terminals.

2.4 Related Work

2.4.1 Analytical Studies

A pioneering study on one-hop broadcast can be found in [46], where the authors proposed an analytical model for broadcast communication mode and investigated the throughput in the presence of hidden terminals. They used unit disk graph as the radio model. Their traffic model was comprised of random placement of nodes within the communication range of a transmitter. Li *et al.* [95] also used the unit disk graph as the radio model to analytically predict the optimal range for maximizing broadcast coverage in one-hop mode. As in [46], they addressed the case of traffic with nodes randomly placed around a transmitter. Yadumurthy *et al.* [177] proposed a new MAC protocol to overcome the hidden terminal problem in omni-directional and directional broadcasts. They used real traffic traces for verification; however, the applicability of the proposed protocols in real world situations is limited due to the assumption of perfect channel adopted in their work. Balon and Guo [22] studied MAC-layer recovery of broadcast frames using a congestion detection mechanism. Assuming that the channel is in perfect condition, they addressed the freeway scenario to evaluate the packet delivery ratio. Lee *et al.* [85] developed a position-based broadcast suppression protocol for vehicular communications and compared the PDRs achieved by their protocol with those of the neighbour-based broadcast suppression mechanisms. As with the aforementioned studies, Lee *et al.* adopted a perfect channel model in their study. Regarding the traffic model, they addressed a group-based node mobility where the velocity of nodes is chosen randomly from a predetermined range. Such a mobility model is not realistic since the random velocity does not reflect the actual interaction of moving vehicles. In [83], a new broadcast protocol termed R-OB-VAN was proposed to overcome the shadowing problem caused by large vehicles. PDR and DL indicators were the subject of improvement in their study. A two-lane road segment with nodes distributed uniformly formed their traffic model. For the channel model, they used a proprietary shadowing model implemented in a simulator. An analytical model was proposed in [179] to address the reliability of one-hop broadcast. The Rayleigh propagation model was used and a one-dimensional network with random placement of nodes was addressed to evaluate the packet reception ratio as the reliability indicator. A drawback of their study is that they considered solely the channel issues as the cause of packet reception failures. In particular, they stopped short of addressing the impacts of other adverse factors such as interference caused by hidden terminals. Furthermore, the generic propagation model used in their study does not represent the vehicular environment well.

In [78], Khabazian *et al.* adopted a cautionary view in addressing the effects of hidden terminals on the reliability of vehicular communications. Opposed to the traditional assumption on hidden terminals, they argued that hidden terminals are not isolated. With this assumption and using a one dimensional network with predetermined traffic densities, they addressed some reliability aspects such as the probability of reception failures due to interference caused by hidden terminals. Khabazian *et al.* used a similar network and traffic settings in [77] to investigate the average delay of event-driven messages in the presence of low priority regular safety messages. The radio propagation issues were not taken into account in this study. Also, given a traffic density, the authors assumed that the nodes are randomly placed in the network, which is not a realistic assumption. Furthermore, the one dimensional network topology does not represent the real topology of vehicular networks.

In a series of works, Vinel *et al.* studied the reliability of periodic beaconing. In [171], the authors used a D/M/1 queueing system to model the MAC functionalities and obtained the average delay incurred by beacon transmission. Vinel *et al.* also investigated the p_{sr} indicator corresponding to periodic beacons in [170] and [169]. In the former study, the beaconing rate was assumed saturated, while in the latter work it was assumed unsaturated. There are three arguable assumptions adopted in the work of Vinel *et al.*: (i) beacon messages arrive randomly, and hence, the periodic nature of beacon messages and its impact on the IRT indicator is not considered, (ii) traffic density was assumed homogeneous, which is not applicable to urban scenarios, and (iii) the reception failures due to channel issues were not taken into account in deriving the reliability indicators corresponding to periodic messages.

In a series of works, Ma *et al.* studied different aspects of the broadcast paradigm in MANETs and VANETs. In [102; 103], the authors addressed the back-off process of IEEE 802.11 MAC. To this aim, they developed analytical models using Markov chains and investigated the PDR indicator in a wireless local area network under the assumptions of perfect channel and saturated packet generation. With similar network settings, Ma *et al.* investigated the case of unsaturated packet generation described by a random process [104]. In [44], Chen *et al.* extended their previous models to address the case of safety message broadcast in vehicular communication networks. In [180], Yin *et al.* developed a model based on Markov process to characterize the continuous time behaviour of channel contention and the MAC layer back-off process in broadcast communication mode. In all the aforementioned studies conducted by Ma and co-workers, PDR was the main reliability indicator for the evaluation of the proposed models. In [105], they addressed the PRR indicator corresponding to a one dimensional mobile ad hoc network operating in multi hop communication mode. The case of two dimensional network topology was addressed in [107; 108]. In [101; 106], analytical models were developed to investigate the reliability performance of vehicular broadcast communications in highway scenarios with steady state vehicular traffic and assuming the IEEE 802.11a as the MAC layer protocol. In this work, the event-driven and periodic beacon messages were addressed with different priorities. In [109], Ma *et al.* employed most of their findings in previous studies and proposed new broadcast schemes, aiming at better reliability of the broadcast mechanism in vehicular communication networks. Unfortunately, their studies are limited to highway scenarios and the random distribution of nodes. These drawbacks can be observed in the analytical models as well as the simulations conducted for verification purposes. Another drawback of their studies is attributed to the unrealistic assumptions on the radio propagation model. They either assumed the channel is perfect or it can be described by Bit Error Rate (BER) (or Packet Error Rate) derived from generic radio propagation models. We argue that BER as an indicator for channel description must be derived from a realistic channel model or from measurements, otherwise it will be too optimistic for estimating the channel quality.

On the assumption that wireless communications are inherently unreliable, Lidstrom *et al.* [97; 98] pursued a notably different approach to address the enhancement of driver safety. In [97], the authors proposed a model realized by direct and relay-based observations of the traffic environment. The observation data are fed to an inference system to predict those potentially hazardous situations not easily detectable by relying only on the node's self-knowledge. In particular, their proposed solution is able to predict communication disruptions corresponding to the obstructed nodes and the potential disruptions due to traffic congestion. In [98], Lidstrom *et al.* proposed models to predict dangerous traffic situations. The models describe two major factors including vehicle and environment, and infer the driver intention quantified as the probability distribution of path choices. The authors claim that such a capability, if enabled in the vehicles in the form of a warning or driver recommendation system, will improve the safety level of drivers; notwithstanding, they stop short of characterizing an example application of that kind.

Torrent-Moreno [162] proposed a position-based forwarding mechanism termed contention-based dissemination (CBD) together with a distributed power adaptation algorithm to improve the reception of safety messages while maintaining the channel load below a given threshold. In this study, Nakagami model was employed as the channel model characterizing signal propagation in a highway traffic scenario. Sepulcre *et al.* [149] adopted a novel top-down approach to studying the reliability issues in vehicular networks. They stressed the necessity of mapping from application-level requirements to the network-level performance metrics. To this aim, the authors identified a minimum warning distance (D_w) for two example applications. Then, using a parametric warning time frame (TWindow), the reliability of applications (p_{app}) were expressed as a function of successful packet reception (p). Through experiments and given a target application reliability threshold, the authors further explored the optimal parameter settings for transmission power, message frequency, and TWindow. The study in [54] addressed the prioritization of message dissemination based on message benefit. To calculate the utility of a given message, individual nodes should independently identify some context-based metrics extractable from the message itself, vehicle, and exogenous information context (e.g. time of day). To maximize network utilization, the authors suggest that the protocol architecture in the MAC and data link layers should be designed in a way that it reflects the benefit-based dissemination paradigm. Practically, a proprietary architecture designed from the scratch or derived by modifying the existing IEEE 802.11e EDCA mechanism are two candidate ways to implement the proposed approach. Li *et al.* [93] argued that the conventional methods applied in the multi-hop forwarding of emergency messages do not provide sufficient reliability, and do not scale properly when the traffic is dense or the size of network grows. To improve scalability, the authors proposed a controlling mechanism for the selection of forwarders. To guarantee a minimum reliability characterized by a given threshold, they proposed additional forwarding of messages performed by intermediate nodes located between any pair of subsequent main forwarders.

2.4.2 Simulation Studies

Elbatt *et al.* [55] investigated the reliability of Cooperative Collision Warning (CCW) as a representative safety application relying on periodic beaconing. Several reliability indicators including PDR, IRT, and DL were evaluated in their study. They addressed two types of traffic densities in an eight-lane highway scenario: high traffic density and sparse traffic density. In both density scenarios, the velocities were chosen either randomly or deterministically from a set of given velocities. Furthermore, they adopted a channel model characterized by measurement-based BER and SNR parameters [55]. Yousefi *et al.* [183] studied the delivery ratio and delay of beacon messages with varying packet transmission intervals and packet sizes. They addressed one-hop broadcast in a large highway scenario with stationary vehicles and a fixed communication range of the vehicles. According to their simulation results, packet delay was in the order of a few milliseconds, which generally does not cause a bottleneck for safety applications. They also showed that the packet reception rate decreases significantly by increasing the distance of the receiver from the transmitter, a phenomenon previously observed in [55]. In their study, a deterministic channel model was employed and the hidden node problem was identified as the primary cause of performance degradations, particularly in long distances from the transmitter. Similar traffic settings and channel model were used in [184] to investigate the effective range of safety critical applications relying on one-hop broadcast.

Torrent-Moreno *et al.* [163; 164; 165] were the first to introduce the probabilistic propagation models in the study of the one-hop broadcast scheme. They introduced the notion of Packet Level In-coordination (PLI) to characterise the hidden terminal interference. The failed receptions were separated into 4 categories with the hidden terminal problem being identified as the primary reason for low reception rate, particularly at distances beyond 66% of the intended communication range [164; 165]. Using the findings from previous studies, they implemented a distributed fair power adjustment mechanism to improve the reception rate [163]. In their studies, they used Rayleigh and Nakagami radio propagation models. For the simulation, they used a number of topologies ranging from a wireless local area network (as in [164; 165]) to a multi-lane highway scenario in a recent study [163].

The exploration of the key factors influencing the performance of safety message communications was performed in [114], where Martinez *et al.* identified the transmission range, radio propagation model, and traffic density as the major factors determining the ultimate performance of warning message dissemination. The performance metrics investigated in this work included notification time of messages, percentage of blind vehicles (i.e. vehicles without reception), and the number of packets received per vehicle. The authors suggested that a compound metric obtained by combining the three identified metrics is sufficient for the assessment of message dissemination performance in VANETs.

2.4.3 Other Related Work

We also build our background on generic models of the IEEE 802.11 Distributed Coordination Function (DCF) and its internal back-off process. Many analytical models have been developed in the literature for the study of the performance of IEEE 802.11 coordination function. For the most part, the proposed approaches are variations of the Markov-based performance evaluation method presented by Bianchi [28] and Cali *et al.* [37]; for instance, the implications of an error prone channel were modelled in [127], while transmission retries and seizing phenomenon were taken into account in [42] and [172], respectively. This framework was extended to IEEE 802.11e QoS differentiation by Engelstad *et al.* [56], who also investigated the channel and application layer performance indicators with respect to non-saturation traffic. In [100], Lyakhov *et al.* studied the performance of IEEE 802.11 networks operating in broadcast mode. They assumed Poisson packet arrival and applied Markov chains to analytically express the mean notification time of broadcast packets. Ma *et al.* [103] studied the impact of backoff counter freezing on IEEE 802.11 performance in a scenario termed Continuous Freeze Process (CFP). In another study, Ma *et al.* [106] modelled the performance of IEEE 802.11a as the initial MAC layer protocol proposed for vehicular networks. Using two Markov chains, they analysed the broadcast performance of event-driven and periodic safety messages. Arguably, they used a Poisson distribution to model the arrival process of both types of safety messages.

2.4.4 Drawbacks of Previous Studies

A number of drawbacks can be identified in the above mentioned studies with respect to the real world aspects of vehicular traffic and the propagation environment. First and foremost, the traffic scenarios are limited to random and uniform node distribution, which in the best case are only applicable to highway traffic. In spite of performance evaluation under various traffic densities, the impacts of non-uniform and heterogeneous traffic densities attributed to urban traffic systems were not addressed. Moreover, it is not clear how the traffic scenarios addressed in those studies relate to safety-critical conditions. Forced-flow traffic states that frequently dominate urban traffic systems and intersections are examples of safety-critical scenarios that were not addressed in previous studies. Furthermore, the assumption of one-dimensional network topology adopted in a major body of the studies does not apply to vehicular networks. The final drawback of the previous studies relates to the radio propagation models employed either for analytical development or simulation purposes. Obviously, the assumptions of perfect channel and unit disk graph applied in many studies are not realistic. Also, the generic propagation models used in some studies do not fully capture the uncontrolled environment factors in vehicular traffic systems, and thus do not provide good accuracy for the study of vehicular communication networks [81].

2.5 Implications of Host System Model for Communication Aspects

The credibility of conclusions drawn in studies conducted on vehicular networks is significantly driven by the way the host system is modelled and the assumptions adopted in the studies. In that regard, the major components representing the host system including the vehicular traffic model and the radio propagation model have been shown to be highly influential. In the following sections, evidence is reported from the literature which highlights the impacts of the choice of traffic and radio propagation models on the results derived from studies on vehicular communication networks. The evidence covers a broad range of vehicular network aspects and is not limited only to reliability issues.

In the following sections, we frequently refer to traffic and radio propagation models. For the interested reader, Appendix B presents the theories and modelling paradigms associated with vehicular traffic systems. The fundamental concepts and the various radio propagation models employed frequently in the context of wireless communications can be found in [116; 120; 137]. [120] is particularly focused on the radio propagation aspects of vehicular environments. Hereafter, for the sake of distinction, we refer to those radio propagation models not specifically developed for vehicular environments as "generic" or "simplistic" models.

2.5.1 Implications of Traffic Model

The impacts of the traffic model on the communication aspects of vehicular communications were addressed in a number of studies. In [41], the authors emphasized that, in routing protocols proposed for vehicular networks, the performance indicators such as the PDR are significantly influenced by the degree of realism incorporated in the traffic model. The authors suggested that if simplistic traffic models are used for the evaluation of VANETs, the results significantly deviate from those obtained in the case of realistic models. Bai *et al.* [18; 19] studied the effects of mobility on the topological aspects of ad-hoc networks and verified the high dependence of connectivity behaviour on the mobility model. Mahajan *et al.* [110] showed that the packet delivery ratio and latency are significantly impacted in the presence of intersections causing vehicular clusters. Their study involved the development of several mobility models to capture the motion pattern of vehicles in urban traffic systems. Choffnes *et al.* [45] developed STreet RAndom Waypoint (STRAW), an integrated mobility model based on car following. They compared the routing performance of the vehicular networks using the STRAW model and a classic random waypoint model. They showed that the performance of wireless network protocols in urban environments is significantly different under the two mobility models. The results of this study suggest that both the mobility model and the topological aspects of a traffic network must be realistic in order to reflect the actual performance of the communication network. Fiore *et al.* [60] evaluated the impacts of various mobility models on link duration, node degree, and node cluster sizes. They showed that the choice of mobility model significantly impacts the topological properties of a vehicular network. In particular, they suggested that various models exhibit different clustering and link-level features. This motivates the use of realistic traffic models instead of inaccurate, generic models. In [157], the authors employed various vehicular mobility models ranging from realistic to random models to investigate the impacts of the traffic model on the topological features of the network. The results of this study confirm those conclusions drawn in the Fiore *et al.* study [60].

2.5.2 Implications of Radio Propagation Model

The generic radio propagation models do not fully capture the environmental factors in vehicular traffic systems, and thus do not provide good accuracy for VANET scenarios [81]. These models are mainly developed for cellular networks and may well adapt to the properties of such networks. However, as highlighted in [116; 120], VANET environments have several unique characteristics, hindering the direct application of the generic propagation models. There are several intrinsic differences between propagation environments of the vehicular and cellular networks. These include the relative elevation of the transmitter and the receiver, the motion patterns, and the frequency band used in the two technologies [120].

A recent campaign investigating the radio propagation aspects in VANET environments was notably triggered by the limited capacity of the existing generic radio models. In the following, we review a number of these studies.

Gozalvez *et al.* [64] revealed that the results obtained in a study of safety and data applications in VANETs change dramatically with respect to the choice of the radio propagation model. They showed that ignoring any component of a realistic radio propagation model including path loss, multi-path fading, shadowing, and shadowing correlation significantly changes the results of the study. In their study, two applications representing safety and data services in VANETs were addressed: a traffic safety application operating in an urban intersection scenario without visibility, and data routing protocols in a Manhattan-like urban scenario. The results obtained for the intersection scenario and using a simplistic path loss model shows that, with a given transmission power, there is a high probability that safety messages are received successfully. On the other hand, if a realistic propagation model is used, the communication channel is not as reliable as in the case of the simple path loss model. Their results for the data routing scenario indicate a noticeable performance degradation under realistic models compared to the simple path loss model. In a similar work, Martinez *et al.* [113] compared the performance of warning message dissemination in various scenarios distinguished by the degree of realism incorporated in the radio propagation model. They investigated three performance metrics, namely, message notification time, percentage of blind vehicles, and the number of message receptions per vehicle, and revealed that such metrics significantly deteriorate when the attenuation due to obstruction by surrounding buildings is taken into consideration in the propagation model. [21] is another study on the propagation properties in vehicular traffic environments. This study was conducted by means of field measurements using off-the-shelf DSRC radios. In this study, a very rich set of traffic scenarios including urban, suburban, and rural traffic were addressed, and the impacts of uncontrollable (e.g., node mobility) and controllable (e.g., transmission power) factors on the packet delivery ratio and also the link level reliability were investigated. According to their results, the perfect reception zone does not exist in vehicular networks. Instead, intermediate reception regions prevail throughout the entire communication range of a target transmitter. The authors in [148] and [27] identified street intersections and tunnels as the highly important environmental elements requiring dedicated characterization in the radio propagation model. They suggest that the traditional classification of vehicular environment into urban/suburban/rural should be extended to cover these new elements. Studies in [33; 117] revealed that Line Of Sight (LOS) obstruction caused by moving vehicles is frequently observed in urban traffic settings, and the obstructing vehicles impose significant attenuation and packet loss. Signal attenuation in urban intersections is studied in [111]. Also in [111], field experiments using DRSC radios were conducted and a path loss model for Non Line Of Sight (NLOS) situations was developed. In another work, Mangel *et al.* [112] highlighted the NLOS at intersections as a key factor affecting the performance of DSRC applications targeted to intersection scenarios. They argue that, despite the similarity of some intersections, not all of them have similar signal propagation characteristics. Furthermore, due to the non-negligible cost involved in field measurements, it is of vital demand to enforce abstraction and clustering of intersections and conduct field tests only on few representative intersections within each cluster. To this aim, Mangel *et al.* proposed a clustering mechanism based on the key intersection parameters including the distance of intersection center from the building, intersection type (e.g. 3 and 4 legs), and the spanning length of buildings at the corners of the intersection. In [150], the authors stressed that unrealistic assumptions about the fading issues leads to wrong conclusions on the reliability of safety applications at intersections. In [29], the necessity of distinguishing between the LOS and NLOS shadowing cases in traffic simulators is emphasized.

Sommer *et al.* [156] identified physical obstacles (e.g. buildings) as the major cause of signal attenuation, and developed a computationally efficient channel fading model to deterministically calculate the amount of attenuation. The proposed model distinguishes between various obstacles in terms of the material used and also the fraction of the line of sight of two communicating nodes being obstructed by a given obstacle. Another channel simulation model termed UM-CRT was proposed in [84] for vehicular communications. UM-CRT is a semi-deterministic channel model and is claimed to achieve the accuracy of ray-tracing and the computational efficiency of stochastic models [34].

In a recent class of developments, scientific channel sounding equipment was used to characterize signal propagation in vehicular network environments. The main objective of such studies was the development of new radio propagation models adapted to vehicular environments. One such study is found in [8], where Abbas *et al.* developed a shadow fading model using measurements conducted in urban and highway scenarios. The details of this radio propagation model including the path loss functions developed for LOS, NLOS and Obstructed LOS (OLOS) situations appear in Chapter 5.

2.5.3 Implications for Our Work

An important aspect of the studies on VANETs is the demand for a traffic model reflecting the real behaviour of vehicular traffic. On one hand, the accuracy of studies on DSRC/WAVE protocols and safety applications are highly related to the accuracy of the traffic model used in the studies. On the other hand, the inherent difficulties in conducting large-scale and comprehensive field experiments of traffic mobility, leaves simulation the sole choice for validation purposes. Consequently, the accuracy of a study highly depends on the extent of realism captured in the traffic model used in the simulation. In analytical studies, on the other hand, a common practice is to simplify the traffic model as much as possible to make it tractable for the underlying analytical development. Consequently, the achievable accuracy and generalization of such simplified models depend foremost on the extent of adherence to the key traffic features. The evidence reported above stresses that the choice of traffic model, including the traffic network topology, significantly impacts the results to be derived. This evidence indicates that realistic traffic models need to be applied for the validation of the studies throughout this thesis. Furthermore, care should be taken to base the analytical models on valid assumptions about traffic features. Thus, in the present study, wherever necessary, the traffic models are developed in compliance with Car Following (CF) [142] and Cellular Automaton (CA) [161] modelling paradigms, which have been proven to efficiently describe traffic behaviour in various scenarios.

Similar implications arise regarding the choice of the radio propagation model. As highlighted above, the recent studies on the aspects of radio propagation in vehicular environments reveal that the application of generic radio models for VANET studies is not a wise choice. Instead, it is highly recommended that models exclusively developed for vehicular environments should be used. An example of such radio propagation models is proposed by Abbas *et al.* [8]. To our best knowledge, this model is the most comprehensive in terms of the various shadowing conditions taken into account, including LOS, obstruction by vehicles (OLOS), and obstruction by static objects such as buildings (NLOS), all integrated in a number of simple path loss functions. Due to the comprehensiveness and the relative simplicity of this model compared to other models, we use this model in our analytical study of hidden terminal interference in Chapter 5.

2.6 Summary

There are many controlled and uncontrolled factors affecting the reliability of safety applications. Among those factors, the interference is highly influenced by the characteristics of the host system, that is, the radio propagation environment and the traffic system. Although many important aspects of reliability are addressed in the literature, previous studies stopped short of realistically addressing the interference issues in relation to the host system. More specifically, the unrealistic assumptions on radio propagation and also the extreme simplification of the underlying traffic models compromise the accuracy of the results derived from previous studies.

Chapter 3

A Traffic Density Model for Radio Overlapping Analysis in Urban Vehicular Ad hoc Networks

3.1 Introduction

Viewing vehicles as *moving radios* with potential overlapping in time and space dimensions is key to understand the dynamic of communication interference, which by itself is known as a primary cause of performance degradation of wireless communications. From the perspective of vehicular communications, *traffic density* is a major factor influencing the behaviour of radio overlapping. As such, it determines the channel load dynamics and hence the performance of data and safety message communications. Consequently, an accurate characterization of the performance of applications demands a thorough understanding of the traffic density dynamics. In this chapter, we propose a novel traffic density model for urban traffic systems and employ this model for the purpose of spatial-temporal analysis of radio overlapping. To model traffic density, we consider a signalized intersection and the road segments connected to the intersection as the basic building blocks of urban traffic systems. The density model is used as a framework to describe the trends and the critical regions of radio overlapping corresponding to the road segments of the intersection. We apply the radio overlapping model derived from the traffic density to study the channel load associated with periodic beaconing, a fundamental mechanism for safety message communication in VANETs. Considering the fact that radio overlapping is a predictor for interference behaviour, this study also provides a generic analytical framework to investigate other performance aspects of data and safety message communication influenced by interference issues.

The remainder of this chapter is organized as follows. In Section 3.2, the assumptions adopted throughout this study are presented. In Section 3.3, we introduce the approach used in the development of the traffic density model. Section 3.4 describes the proposed traffic density model. Using this model, an analytical framework is presented in Section 3.5 to characterize radio overlap in spatial and temporal dimensions. In Section 3.6, we characterize the channel load imposed by periodic beaconing. Numerical evaluation is presented in Section 3.7. Finally, Section 3.8 summarises the chapter.

3.2 Assumptions

A traffic density model is designed to capture the basic characteristics of an urban traffic system. More specifically, a signalized intersection and road segments linked to that intersection are considered as the basic components comprising an urban traffic system (Figure 3.1). Such a traffic density model is expected to express traffic density as a function of position x (along the road segment L_E) and time t during a traffic light cycle at the intersection. For simplicity, we assume traffic is unidirectional with flow q *vehicles/hour/lane* approaching the intersection from a l-lane road segment L_E. The maximum velocity of the road segment is limited to V *meters/second*, in line with regulations imposed on urban transportation systems. The intersection is signalized and operates with fixed timing consisting of red and green phases denoted by t_{red} and t_{gr}, respectively. We assume the amber phase is equally shared between the red and green phases of the traffic light. Accordingly, the duration of a traffic light cycle denoted by t_{cycle} is equal to $t_{cycle} = t_{red} + t_{gr}$. We assume the intersection operates in near-saturation or so-called *perfect mode*, i.e. the queue forming during a red phase entirely discharges during the green phase of the same traffic light cycle and no overflow queue emerges in a cycle. With this setting, traffic densities corresponding to under-saturation and over-saturation scenarios can be numerically compared to the near-saturation scenario.

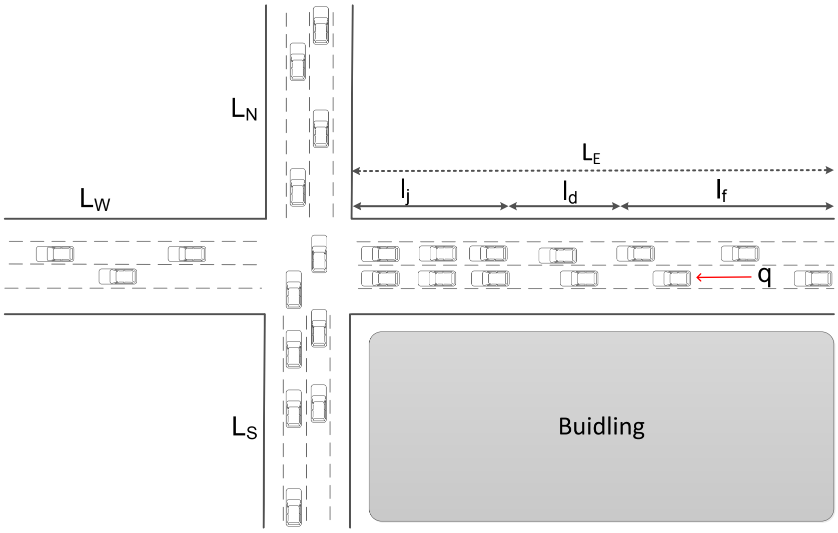

Figure 3.1: Signalized intersection scenario

3.3 Modelling Approach

There are numerous studies in the literature investigating different aspects of traffic in the presence of signalized intersections. Queuing behaviour at signalized intersections has been widely studied and many models have been proposed [12; 160; 173]. However, few works address global traffic behaviour throughout an urban road segment. By global traffic model, we mean a model capable of describing traffic characteristics, e.g. traffic density, throughout a road segment or a large traffic system formed by a network of connected road segments. Local traffic models, on the other hand, are only capable of estimating traffic behaviour in an immediate vicinity of a vehicle or a position along a road segment. An example of models predicting local traffic density is a model proposed by Pipes [135] and used by Artimy *et al.* [14] for dynamic assignment of the transmission range in VANETs. In this model, instant velocity of a vehicle and a sensitivity factor were used to estimate local density around vehicles. We argue that the existing queue models or local traffic density models cannot adequately capture the general behaviour of traffic throughout an entire road segment. Instead, a global traffic density model is needed to describe the traffic behaviour at any given position throughout the road segment under investigation.

3.4 Traffic Density Model

Our proposed traffic density model is inspired by observations from 100 simulation runs conducted with single- and multi-lane scenarios implemented in *Paramics* [1], a traffic simulator compliant with car-following traffic model [142]. Our findings of traffic characteristics on a road segment ($\mathrm{L_E}$ in Figure 3.2), are summarized in the following main points:

(a) During a red phase, three regions with different traffic densities coexist along the road segment: (i) a jam traffic density caused by vehicles building up a queue, (ii) a growing traffic density caused by vehicles decelerating as they approach a queue ahead, and (iii) an almost constant light traffic density caused by vehicles driving in free or stable flow traffic state. The regions with the three different densities are denoted by l_j, l_d, and l_f, respectively (Figures 3.1 and 3.2).

(b) During a green phase, a fourth region associated with a different traffic density emerges as vehicles in front of the previously formed queue gradually discharge the queue. This region is denoted by l_a in Figure 3.2.

(c) The shape and dynamics of the three density regions formed during a red phase and partly during a green phase are analogous to the shape and dynamic of a logistic curve [79].

Due to significant differences between the traffic dynamics associated with red and green phases of a traffic light cycle, we address traffic density corresponding to each phase separately. According to observation (c) above, traffic density can be expressed by a simplified logistic curve defined as follows:

$$K(x,t) = A + \frac{K_j - A}{1 + \exp\left(B(x - M)\right)} \tag{3.1}$$

where:
A is the lower bound traffic density associated with stable/free flow traffic state;
K_j is the upper bound traffic density associated with jam traffic density (if $A = 0$ then K_j is called the carrying capacity);
B is the growth rate of traffic density from lower bound (A) to upper bound (K_j);
M is the inflection point of the logistic curve;
$K(x,t)$ is the traffic density at position x at time instant t during a traffic light cycle.

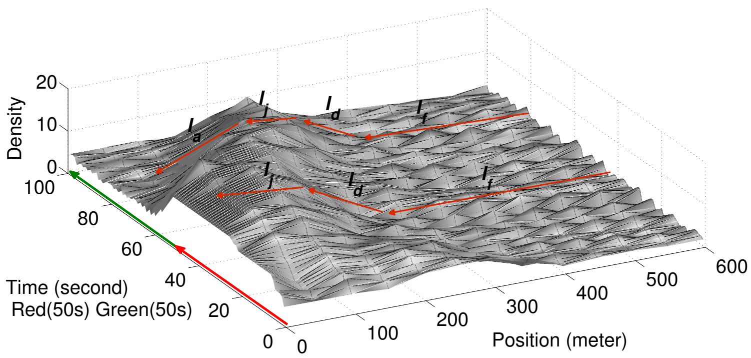

Figure 3.2: Traffic density defined as the number of vehicles in 40 m intervals on a 3-lane road segment linked to a signalized intersection (cycle length=100 s)

To model traffic density using Equation 3.1, the above mentioned parameters must be determined. We start with A, defined as the lower bound of traffic density, which is equivalent to traffic density in stable and/or free flow traffic state (region l_f in Figure 3.2). Assuming a deterministic traffic arrival q *vehicles/hour/lane* and road speed limit V, the inter-arrival time of vehicles is $\frac{3600}{q}$ measured in seconds and the headway distance is $\frac{3600\,V}{q}$ measured in meters. In a stable flow traffic state, a following vehicle must keep a safe headway distance from a leading vehicle to avoid rear end collision. According to car-following properties [142], the safe headway distance, also known as the braking distance, is proportional to the distance that the following vehicle with velocity V and average deceleration R_d should maintain in order to be able to make a full stop when the leading vehicle brakes suddenly. Consequently, the braking distance can be expressed as $d_b = \frac{V^2}{2R_d}$. Taking the braking distance and vehicles' inter-arrival time into consideration, the headway distance in free and stable flow traffic states can be expressed as $HD = \max\left(\frac{V^2}{2R_d}, \frac{3600\,V}{q}\right)$ and traffic density can be expressed as follows:

$$A = \frac{l}{HD} \tag{3.2}$$

In Equation 3.2, A is measured in $vehicles/meter$ and l is the number of lanes. For traffic arrivals with other distribution functions such as Poisson, q in the definition of HD and hence in Equation 3.2 is replaced with the expected traffic arrival $E(q)$.

To obtain K_j in Equation 3.1, we use the fact that K_j is the traffic density associated with vehicles queued up at the intersection (region l_j in Figure 3.2) and is inversely related to jam headway distance l_{hj}, i.e.,

$$K_j = \frac{l}{l_{hj}} \tag{3.3}$$

where l_{hj} is the average jam headway distance and is a known parameter.

To calculate parameters B, we use the properties of deceleration region l_d in Figure 3.2. By definition, the length of this region is equal to the braking distance, which was obtained as $d_b = \frac{V^2}{2R_d}$. Also, the logistic function $K(x,t)$ can be rewritten with respect to x as $x = \frac{1}{B}\ln\left(\frac{K_j - K}{K - A}\right) + M$ (we substitute $K(x,t)$ by K for brevity). Define x_1 and x_2 as the start and end positions of the braking region and K_1 and K_2 as the traffic densities corresponding to x_1 and x_2, respectively. The difference between x_1 and x_2 must be equal to d_b (braking distance), and, hence, $d_b = x_1 - x_2 = \frac{1}{B}\left(\ln\left(\frac{K_j - K_1}{K_1 - A}\right) - \ln\left(\frac{K_j - K_2}{K_2 - A}\right)\right)$. Solving for B, we obtain

$$B = \frac{2R_d}{V^2}\left(\ln\left(\frac{K_j - K_1}{K_1 - A}\right) - \ln\left(\frac{K_j - K_2}{K_2 - A}\right)\right) \tag{3.4}$$

The last parameter to be determined is M, which is the inflection point of the logistic curve. Assuming that the logistic curve is symmetric in the deceleration region, M is equal to the queue length at the current time instant t plus half the braking distance d_b. Thus, we obtain M as follows:

$$M = q\,t\,l_{hj} + \frac{d_b}{2} \tag{3.5}$$

where term $q\,t\,l_{hj}$ represents the queue length (in meters), which is a function of the average traffic arrival rate (q), current time instance (t), and the headway distance corresponding to jam traffic.

Finally, the calculated parameters are consolidated into the logistic function described by Equation 3.1 to obtain the following expression:

$$K(x,t) = \begin{cases} A + \frac{K_j - A}{1+\exp\left(B(x-M)\right)} & where: \\ A = \frac{l}{HD},\quad K_j = \frac{l}{l_{hj}},\quad M = q.t.l_{hj} + \frac{d_b}{2} \\ B = \frac{2R_d}{V^2}\left(\ln\left(\frac{K_j-K_1}{K_1-A}\right) - \ln\left(\frac{K_j-K_2}{K_2-A}\right)\right) \end{cases} \tag{3.6}$$

where x is measured relative to the intersection position. M and B in Equation 3.6 are scenario dependent and can be used to fine tune the mobility behaviour. However, they do not greatly impact the general model.

During a red phase, $K(x,t)$ defined by Equation 3.6 measures traffic density at any given time instant for any position x within the road segment. However, during a green phase, due to the presence of a queue discharge region (denoted by l_a in Figure 3.2), the density function will be different from the red phase. The approach to model density during a green phase is to decrement from Equation 3.6 the rate of density reduction (D_{rate}) due to the queue discharge, that is:

$$K(x,t) = A + \frac{K_j - A}{1+\exp\left(B\left(x-M\right)\right)} - D_{rate} \tag{3.7}$$

where D_{rate} is a function of vehicles' average acceleration a and drivers' average reaction time t_r.

To obtain D_{rate}, we utilize a snapshot of vehicles' trajectory shown in Figure 3.3. Assume v_1, v_2, v_3, $\cdots$, v_n are currently queued up at a junction. At the beginning of a green phase, these vehicles are located at positions $x = 0$, l_{hj}, $2l_{hj}$, $\cdots$, $(n-1)l_{hj}$, respectively (Figure 3.3a), where l_{hj} is the jam headway distance. We define $t' = t - t_{red}$, the time elapsed since the start of the green phase. v_1 starts moving after $t' = t_r$ (Figure 3.3b), v_2 starts moving after $t' = 2t_r$ (Figure 3.3c), v_3 starts moving after $t' = 3t_r$, etc. At a time t' such that $t_r < t' \leq 2t_r$, vehicle v_1 has travelled the distance $\frac{1}{2}a\,(t' - t_r)^2$ and the positions of v_2, v_3, $\cdots$, v_n are unchanged. At time t' where $2t_r < t' \leq 3t_r$, vehicles v_1 and v_2 have travelled distance $\frac{1}{2}a\,(t' - t_r)^2$ and $\frac{1}{2}a\,(t' - 2t_r)^2$, respectively and the positions of v_3, $\cdots$, v_n are unchanged. This process can be similarly continued for subsequent time instants and for the remaining vehicles in the queue. Generally, at time t' such that $(i+1)\,t_r < t' \leq (i+2)\,t_r$ the locations of vehicles i and $i+1$ are $i\,l_{hj} - \frac{1}{2}a\,(t' - it_r)^2$ and $(i+1)\,l_{hj} - \frac{1}{2}a\,(t' - (i+1)\,t_r)^2$, and the distance between the two vehicles is $l_{hj} + \frac{1}{2}a\,t_r\,(2t' - (2i+1)\,t_r)$. Consequently, the initial distance l_{hj} of the two vehicles i and $i+1$, queued up during a red phase, increases at time instant t' during a green phase where $t' > i\,t_r$, and the increase rate is obtained as $a\,(t' - i\,t_r)\,t_r$. It is straightforward to generalize the rate increase by describing the vehicle number (i.e. i) as a function of its position (i.e. x), namely $i = \lceil \frac{x}{l_{hj}} \rceil$. Bearing this in mind, and noting that the initial density of queued vehicles is $\frac{l}{l_{hj}}$, the density at position x at time t' in a l lane scenario becomes $\frac{l}{l_{hj} + a\,(t' - \lceil \frac{x}{l_{hj}} \rceil\, t_r)\, t_r}$ and the rate of density reduction (D_{rate}) can be expressed as follows:

$$D_{rate} = \begin{cases} \frac{l\,a\left(t' - \lceil \frac{x}{l_{hj}} \rceil\, t_r\right)\, t_r}{l_{hj}\left(l_{hj} + a\left(t' - \lceil \frac{x}{l_{hj}} \rceil\, t_r\right)\, t_r\right)} & x < \frac{l_{hj}\, t'}{t_r} \\ 0 & o.w \end{cases} \tag{3.8}$$

Having D_{rate} obtained by Equation 3.8, and considering that the lower bound traffic density is A, Equation 3.7 can be rewritten as follows:

$$K(x,t) = \begin{cases} \max\left(A, A + \frac{K_j - A}{1 + \exp(B(x-M))} - D_{rate}\right) & x < \frac{l_{hj}\,(t - t_{red})}{t_r} \\ A + \frac{K_j - A}{1 + \exp(B(x-M))} & o.w \end{cases} \tag{3.9}$$

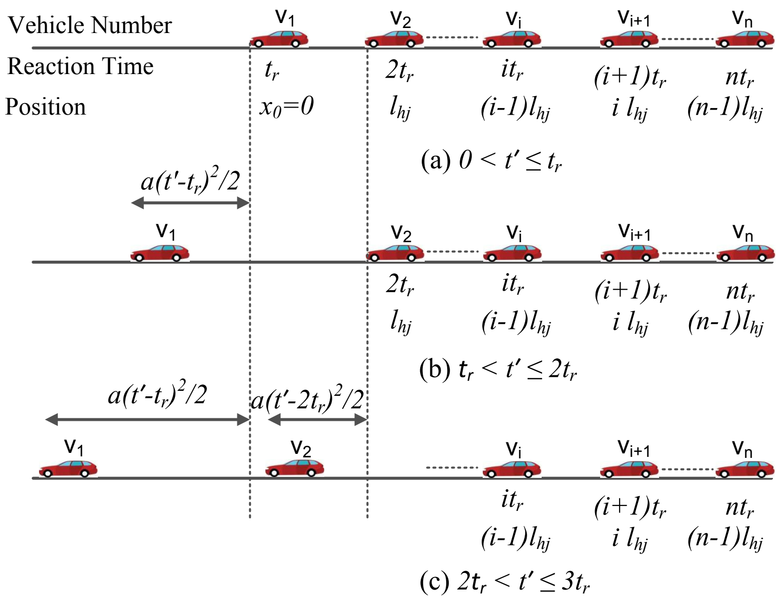

Figure 3.3: Evolution of traffic discharge from a queue

3.5 Radio Overlapping

To address radio overlapping, we define the Radio Overlapping Number (RON) at position x_v along the road segment L_E as the number of unit disks covering a vehicle positioned at x_v, where each unit disk corresponds to a vehicle on the road segment. In our analysis, we assume that the radius of all unit disks is equivalent to the nominal transmission range R of vehicles. Accordingly, RON is simply translated into the number of nodes situated in the transmission range of a vehicle located at position x_v, and is determined by calculating the integral over the density function $K(x,t)$ described by Equations 3.6 and 3.9, corresponding to red and green phases of the traffic light cycle. Incorporating the temporal dimension into the definition of RON, it can be expressed as follows:

$$RON_{x_v}^{t} = \int_{x_s}^{x_e} K(x,t)\,\mathrm{d}x \tag{3.10}$$

where $x_s = max(x_{min}, x_v - R)$, $x_e = min(x_{max}, x_v + R)$, and x_{min} and x_{max} are the coordinates of the start and end positions of the road segment under consideration. In an unbounded road segment, the bounds of the above integral will simply become $[x_v - R, x_v + R]$. Depending on whether or not the radios of vehicles situated on the two perpendicular road segments (denoted by L_E and L_S in Figure 3.1) overlap, two extreme cases can be identified: full overlapping and non-overlapping segments. Full overlapping is attributed to the situation where the area surrounding the two road segments (shadowed area in Figure 3.1) is an open space and no obstacles are present within this area. Hence, radios belonging to vehicles on one road segment can potentially overlap with those on the other road segment. The non-overlapping segments scenario, on the other hand, is attributed to a situation where the entire surrounding area is covered by obstacles (e.g., buildings). Therefore, vehicles on segment L_S do not contribute to RON of vehicles located on segment L_E. Other scenarios of segment overlapping, e.g. partial overlapping, fall within these two extreme scenarios. Hereafter, we focus on road segment L_E as the main road segment and derive RON corresponding to the positions on this road segment. In deriving RON, we address the two aforementioned overlapping scenarios separately.

Non-overlapping segments: Due to different descriptions of density functions corresponding to red and green phases, we derive RON in each phase separately. At any given time instant t during a red phase ($0 \leq t \leq t_{red}$) and for any position x_v on road segment L_E, substituting $K(x,t)$ in Equation 3.10 with the density function expressed by Equation 3.6 determines RON as follows:

$$RON^t_{x_v,L_E} = \left[\left(Kx + \frac{\ln(1 + \frac{1}{e^{B(M-x)}})(A-K)}{B} \right) - I_{D_{rate}} \right] \Bigg|_{x_e}^{x_s} \tag{3.11}$$

Likewise the description of RON for a red phase, substituting $K(x,t)$ in Equation 3.10 with the density function described by Equation 3.9, determines RON at position x_v at a given time instant t during a green phase (i.e. $t_{red} < t \leq t_{cycle}$) where x is bounded as in Equation 3.8. We define x_b as the upper bound of x in Equation 3.8, i.e. $x_b = \frac{l_{hj}\,(t-t_{red})}{t_r}$. Depending on the relative values of x_v and x_b, different expressions for RON are derived as follows.

Case 1: $x_v + R < x_b$

$$RON^t_{x_v,L_E} = \left[\left(Kx + \frac{\ln\left(1 + \frac{1}{e^{B(M-x)}}\right)(A-K)}{B} \right) - I_{D_{rate}} \right] \Bigg|_{x_s}^{x_e} \tag{3.12}$$

where $I_{D_{rate}}$ is the integral of D_{rate} defined by Equation 3.8, i.e. $I_{D_{rate}} = \frac{l\,x}{l_{hj}} + \frac{l\,l_{hj}\ln(a\,t_r^2\,x - a\,(t-t_{red})\,t_r\,l_{hj} - l_{hj}^2)}{a\,t_r^2}$.

Case 2: $x_v - R \leq x_b \leq x_v + R$

$$\begin{aligned} RON^t_{x_v,L_E} &= \left[\left(Kx + \frac{\ln\left(1+\frac{1}{e^{B(M-x)}}\right)(A-K)}{B}\right) - I_{D_{rate}}\right]\Bigg|_{x_s}^{x_b} \\ &+ \left(\frac{\ln\left(1+\frac{1}{e^{B(M-x)}}\right)(A-K)+K\,x\,B}{B}\right)\Bigg|_{x_b}^{x_e} \end{aligned} \tag{3.13}$$

Case 3: $x_b \leq x_v - R$

$$RON^t_{x_v,L_E} = \left[\left(\frac{\ln\left(1+\frac{1}{e^{B(M-x)}}\right)(A-K)+K\,x\,B}{B}\right)\right]\Bigg|_{x_s}^{x_e} \tag{3.14}$$

Full overlapping segments: The radio of a vehicle at position x_v on road segment L_E overlaps with radios of vehicles on road segment L_S if $x_v < R$. If this condition is satisfied, the length of the overlapping sub-segment on L_S will be $\sqrt{R^2 - (x_v)^2}$. With this in mind, the total radio overlapping experienced by a vehicle in position x_v on road segment L_E is equivalent to radio overlapping attributed to the vehicles on this road segment plus the number of vehicles currently existing on the overlapping part of road segment L_S, i.e.,

$$RON^t_{x_v} = RON^t_{x_v,L_E} + I^{t'}_{L_S} \tag{3.15}$$

where $RON^t_{x_v,L_E}$ is determined using Equation 3.11 for $0 \leq t \leq t_{red}$ (red phase) and Equations 3.12-3.14 for $t_{red} < t \leq t_{cycle}$ (green phase). $I^{t'}_{L_S}$ is the number of vehicles driving at time t' (with respect to traffic light timing of road segment L_S) on the $\left[0, \sqrt{R^2-(x_v)^2}\right]$ region of road segment L_S. Calculation of $I^{t'}_{L_S}$ will be straightforward when the symmetry property of traffic light timing for road segments L_E and L_S is taken into consideration. By timing symmetry, we mean that if the traffic light at time instance t is in red phase for road segment L_E, at the same time it is green for road segment L_S, and an equal time duration has elapsed since the beginning of red and green phases as perceived by the two road segments. As a result, Equation 3.15 can be rewritten as follows:

$$RON_{x_v}^{t} = \begin{cases} RON_{x_v,L_E}^{t} + I_{L_S}^{t+t_{red}} & 0 \leq t \leq t_{red} \\ RON_{x_v,L_E}^{t} + I_{L_S}^{t-t_{red}} & t_{red} < t \leq t_{cycle} \end{cases} \tag{3.16}$$

$I_{L_S}^{t+t_{red}}$ is determined by calculating Equation 3.10 with $x_s = 0$, $x_e = \sqrt{R^2 - (x_v)^2}$ and obtaining $K(x,t)$ from Equation 3.9, replacing the traffic parameters of road segment L_E with those of L_S. In a similar manner, $I_{L_S}^{t-t_{red}}$ is determined using $K(x,t)$ by using Equation 3.7 with the parameters corresponding to road segment L_S. It is straightforward to extend the full overlapping scenario to as many road segments linked to the intersection (e.g., L_S in Figure 3.1).

It is insightful to compare the radio overlapping calculated using our proposed density model with that obtained using uniform traffic density, as adopted widely in the literature. Assume traffic is uniformly distributed with density μ vehicles/meter on road segments L_E and L_S. Following the same approach as above, the radio overlapping corresponding to non-overlapping and full overlapping scenarios for a uniform traffic density model can be obtained as follows:

Non-overlapping segments:

$$RON_{x_v} = \begin{cases} 2\mu\, R & x_v \geq R \\ (x_v + R)\, \mu & o.w \end{cases} \tag{3.17}$$

Full overlapping segments:

$$RON_{x_v} = \begin{cases} \mu \left((x_v + R) + \sqrt{R^2 - (x_v)^2} \right) & x_v < R \\ 2\mu\, R & x_v \geq R \end{cases} \tag{3.18}$$

3.6 Channel Load Imposed by Periodic Beaconing

The notion of RON, introduced in Section 3.5, can be readily employed to determine channel load in vehicular ad hoc networks. Obviously, channel load is dependent on the characteristics of the safety or data application. In this section, we focus on channel load associated with beaconing, a basic mechanism for safety message dissemination in VANETs. The channel load of periodic beaconing perceived by a vehicle at position x_v is the total data rate generated by vehicles within radio transmission range (R) of this vehicle. To determine the channel load, two parameters must be known *a priori*: the beacon arrival rate per vehicle (λ beacons/second), and the number of vehicles existing on a stretch of road segment L_E with radius R centered at position x_v (i.e. $RON^t_{x_v,L_E}$). Bearing this in mind, it is easy to show that the channel load of beaconing (denoted by $C^t_{x_v,L_E}$) perceived at position x_v during time instant t can be obtained as follows:

$$C^t_{x_v,L_E} = RON^t_{x_v,L_E}\,\lambda\,B \tag{3.19}$$

where B is size of a beacon message and λ is the beacon arrival rate. Note that in the definition of channel load, it is assumed that the channel is ideal, beacon transmissions are scheduled and thus collision-free, and retransmissions are disabled. In this sense, $C^t_{x_v,L_E}$ can be thought of as a channel load lower bound under real channel conditions.

Given that λ and B are fixed parameters, the maximum possible channel load is obtained when $RON^t_{x_v,L_E}$ has its maximum, which in turn occurs when the entire segment of size $2R$ centred at x_v is in jam traffic condition, e.g. occupied by a long queue. In this case, the maximum channel load can be determined as follows:

$$C^{max} = \frac{2R\,l\,\lambda\,B}{l_{hj}} \tag{3.20}$$

3.7 Numerical Results

To verify the traffic density model derived in Section 3.4, we conduct a set of experiments using the Paramics traffic simulator. The parameters and values corresponding to the traffic scenarios are shown in Table 3.1. The road segment chosen for verification purpose is L_E (Figure 3.1). The verification is performed with three different lane configurations of segment L_E. In all scenarios, the number of lanes in segment L_W are identical to the number of lanes in segment L_E. Traffic flow associated with each lane configuration is set to near saturation flow and determined according to the capacity of the junction. These traffic flow settings correspond to perfect operation of the signalized junction. As a typical setting for major roads in urban environments, we set traffic light timing to $t_{red} = t_{green} = 50$ seconds, speed limit $V = 20$ meters/second, average driver reaction time $t_r = 1$ second. The length of the main road segment (i.e., L_E) is set to 1000 meters with an extra 100 meters dedicated to a traffic zone where vehicles enter the road segment. The lengths of other road segments are shown in Table 3.1.

For each lane configuration scenario, the experiments are conducted with 10 different seeds. With a given seed, the experiment run consists of 2 hours of simulation time. The traces corresponding to the last 20 minutes of each run are extracted for verification purpose. This translates to 12 light cycles per seed. All in all, the verification of a scenario with respect to a lane configuration involves 120 cycles of the traffic light.

The verification metrics used are mean error and mean cross correlation of traffic density, calculated by our model and the traffic density measured in the Paramics. The mean error is obtained using the errors corresponding to the individual traffic light cycles for a given lane configuration scenario. In a traffic light cycle, the errors are calculated in spatial dimension with the granularity of 1 meter. Similarly, the average cross correlation is calculated based on the individual light cycles.

Our results are shown in Table 3.2. According to the table, the mean error of the model is around 14%. Observe that in road segments with higher number of lanes, the mean error increases slightly and the confidence interval widens. This can be attributed to a high probability of takeovers and traffic perturbation in road segments with large number of lanes. However, except for very wide highways with a large number of lanes, the proposed model can be used for most of urban traffic scenarios. As mentioned previously, by fine tuning M and B to the specific scenario, the accuracy can also be slightly improved.

According to the table, the average cross correlation between the model and the traces is around 96% with a 95% confidence interval of around 3.3%. Figure 3.4 depicts the fitting of the model and the traces for a 3-lane scenario. The cross correlation results demonstrate a high capability of the proposed model to reproduce and mimic the traffic behaviour. Therefore, the model can be safely

Table 3.1: Parameters and configuration values

Group	Parameter	Value
Network dimensions	length of main segment (L_E)	1000 meters
	length of segment L_S	1000 meters
	length of segment L_W	300 meters
	length of segment L_N	300 meters
	number of lanes	1, 2, 3
Traffic flow	1-lane	850 vehicles/hour
	2-lane	1800 vehicles/hour
	3-lane	2740 vehicles/hour
Traffic light timing	t_{red}	50 seconds
	t_{green}	50 seconds
	t_c	100 seconds
Others	speed limit (V)	20 meters/second
	driver reaction time (t_r)	1 second
	transmission range (R)	150 meters

Table 3.2: Verification of traffic density model

	1-lane	2-lane	3-lane
Mean error	12%	13.4%	15.5%
95% Confidence Interval (CI)	6.9%	7.4%	8.5%
Average Cross Correlation (CC)	97.5%	95.6%	95.4%
95% Confidence Interval (CI)	2.3%	3.7%	3.7%

employed for the investigation of potentially many cases related to traffic behaviour. This includes the study of radio overlapping behaviour as follows.

3.7.1 Radio Overlapping

We investigate the radio overlapping behaviour using our model for a 3-lane scenario. The road segment under investigation is L_E. The transmission range (R) is set to 150 m. Figures 3.5a and 3.5b show the *RON* corresponding to the non-overlapping and full overlapping scenarios, respectively. In the scenarios, without loss of generality, we only consider the impacts of the external segment

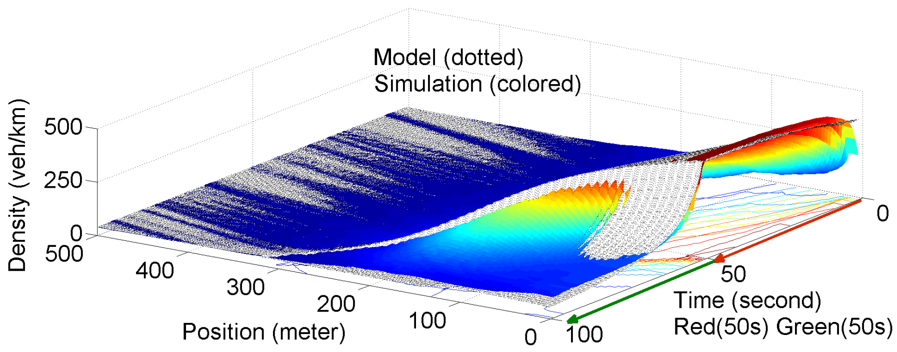

Figure 3.4: Spatial-temporal traffic densities of the main road segment L_E obtained by the model and simulation traces (3-lane scenario)

L_S on the radio overlap induced in the main segment L_E. The number of lanes on the two segments L_E and L_S is assumed identical.

According to Figure 3.5a, RON uniformly increases as new vehicles arrive and join the queue formed at the junction. The maximum RON with magnitude 114 is observed at time t=59 s and in position x=151 m. This can be attributed to the fact that in the beginning of a green phase, up to a time when the queue discharge rate exceeds the traffic arrival rate, the queue length continues to grow in accordance with an extension of the red phase. After 1 second (= reaction time) from the beginning of the green phase, the queue starts to discharge, causing lower RONs in the front region of the queue. As time passes in the green phase, the length of this region increases, leaving more positions with low RONs. Moreover, the region with large RONs are shifted away from the junction towards farther positions on the road segment. This phenomenon is explained by a further queue forming during the green phase as a result of non-zero reaction time and lack of acceleration of all vehicles queued up during the red phase. Specifically, maximum RON with magnitude 114 is shifted from position 151 m to position 219 m at time 75 s and with magnitude 107. Following this shifting process, the maximum RON at the end of the green phase is observed at position 348 m with magnitude 83. It is also important to note that in spite of the queue discharge during the green phase, the number of positions with high RONs is larger compared to the red phase. In the remaining road segment with a flat shape, the average magnitude of RON is 11, and this region is dominated by free/stable flow traffic with no impact from the junction. Compared with the non-overlapping scenario, the full overlapping scenario (Figure 3.5b) shows similar behaviour for the major part of the road segment except for positions with $x < R$, which show high RONs at all times during a cycle. The fluctuations of RONs in this region are attributed to the dynamics of traffic density on the second road segment (i.e. L_S) described by Equations 3.12–3.14. In addition to the global maximum RON produced in region $x < R$ during a green phase, a local maximum RON also emerges as a result of queue shifting in a similar way to the non-overlapping scenario.

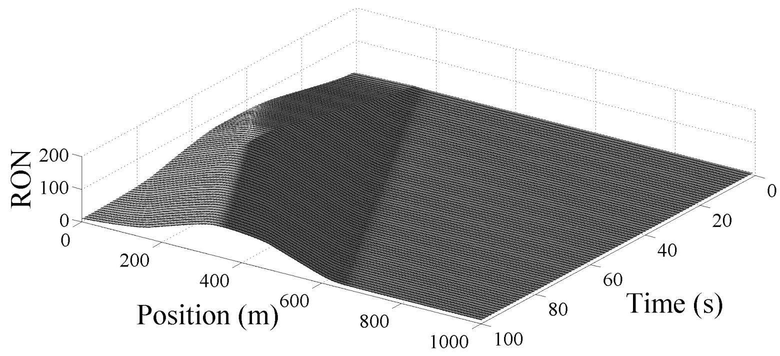

(a) Non-overlapping segments (obstruction by building)

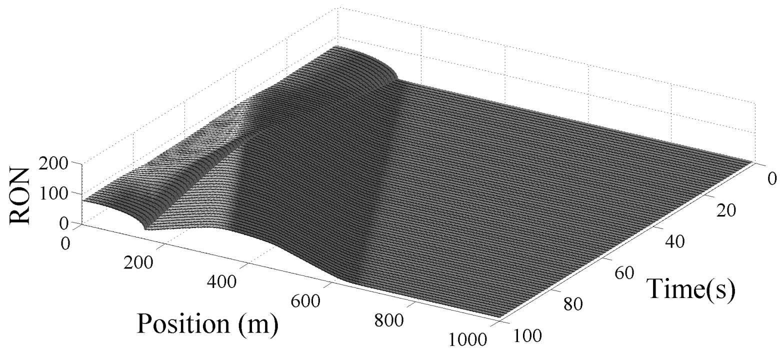

(b) Overlapping segments (existence of Line of Sight)

Figure 3.5: Radio overlapping

3.7.2 Channel Load

To study the channel load of beaconing in VANETs, we conduct a different set of experiments with various transmission ranges and traffic flows. Transmission ranges are selected from those specified in DSRC and cover the required ranges of short, medium, and long range safety applications [17; 43]. Traffic flows are set in a way that they cover a range of flows from 50% below to 50% above saturation flow to reflect different classes of traffic, ranging from sparse to dense conditions. Again, we use a 3-lane scenario, a base saturation flow of 2740 vehicle/hour, and various flows with respect to this base flow. Beaconing parameters B and λ are set to 500 bytes and 10 beacons/second. Figure 3.6a and 3.6b show maximum channel load observed in non-overlapping and full overlapping scenarios, respectively. According to Figure 3.6a, in the non-overlapping scenario, the maximum channel load corresponding to 150 m transmission range grows linearly from 2.25 Mbps associated with traffic flow 1370 to 5.37 Mbps associated with traffic flow 3425. From this point up to higher flows, the channel load approaches its maximum corresponding to a jam traffic condition (described by Equation 3.20). Therefore, the channel load curve becomes flat with only slight change observed. As the transmission range exceeds 150 m, a larger contribution of the overlap comes from vehicles in free flow state. This explains why for transmission ranges larger than 150 m, the growth in channel load is linear within the entire range [1370,4110] of traffic flows. In the full overlapping scenario (Figure 3.6b), due to contribution from vehicles on segment L_S, the maximum possible channel load on segment L_E is reached for longer transmission ranges compared to the non-overlapping scenario (i.e. for 300 m). Observe that for long transmission ranges, e.g. 1000 m, channel load can be as high as 17 Mbps in dense traffic conditions.

3.8 Summary

In this chapter, we proposed a traffic density model for urban traffic systems that takes into account the different phases of vehicle movement between signalized intersections. We have established that the number of overlapping radios behave

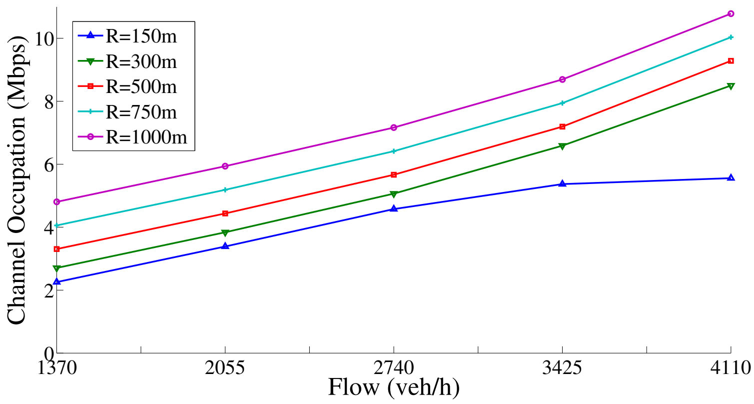

(a) Non-overlapping segments (obstruction by building)

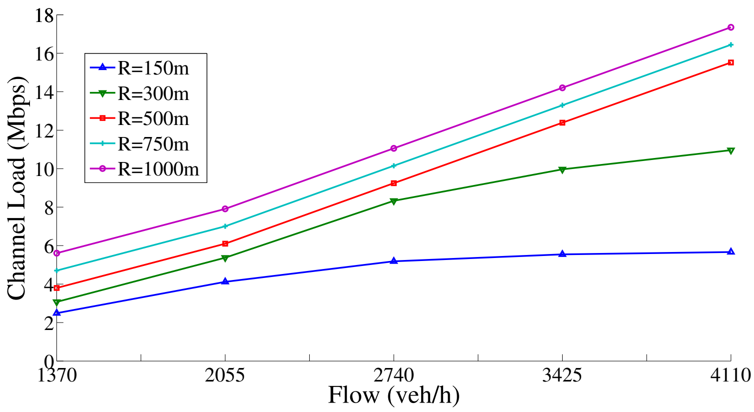

(b) Overlapping segments (existence of Line of Sight)

Figure 3.6: Channel load

in a highly dynamic manner, which cannot be adequately captured by the widely used uniform density model. Based on our density model, we investigated radio overlapping and channel load of safety beacon messages. As a result of traffic heterogeneity, a single data rate and/or transmission power cannot be assigned to all vehicles at all times.

Our evaluation of the *RON* model has been based on a unit disk coverage without retransmissions. This is a rather conservative approach. Using a more realistic propagation model with channel errors would indeed further increase the channel occupancy due to retransmissions. Furthermore, traffic on two-way road segments contributes to higher channel load compared to the one-way scenario investigated in this chapter. Considering the nominal range of data rates specified for VANETs operation in the DSRC standard (3-27 Mbps), it becomes clear that the use of data rates in the lower part of that range is questionable in urban areas when the wireless transmission range is large. The problem is exacerbated when other types of safety messages, in addition to periodic beaconing, are taken into consideration. The scarcity of the radio resource underscores the need for careful design of applications and protocols in urban VANETs in order to mitigate channel load in dense traffic regions, based on vehicles' estimations of their local traffic density or traffic information provided by roadside infrastructure. The design of an adaptive and robust mechanism to adjust transmission power and assign proper data rates based on perceived radio overlapping is a subject of our future work.

Chapter 4

Reliability of Safety Message Broadcast in Urban Vehicular Ad hoc Networks

4.1 Introduction

The reliability of message broadcasts in a safety application is key to its credibility and ultimate acceptance by drivers as the end users. Depending on the type and purpose of a safety message, a subset of parameters describes the reliability of the safety application. For event driven messages, the reliability of the safety application is determined by the successful packet reception probability or, alternatively, the successful packet transmission probability. The former is a receiver-centric reliability indicator, whereas the latter is sender-centric. On the other hand, in case of periodic messages, inter reception time (IRT) of messages is a good candidate metric for describing the application reliability [55]. The IRT metric integrates the variability of message reception time and packet reception probability into a single parameter. Intuitively, from a recipient vehicle perspective, a high probability of message reception from neighbour vehicles leads to high overall awareness by the recipient about its neighbourhood. Furthermore, the reception of messages with high frequency enhances the information freshness a recipient maintains at any time instant, and, in turn, promotes timely reaction to undesired events as they occur. Correspondingly, from a sender point of view, the higher the chance that the neighbour vehicles receive its message successfully and timely, the better the achieved safety level will be.

A key factor impacting the reliability metrics mentioned above is traffic density. In static wireless networks, due to the deterministic distribution of nodes throughout the network area, it is straightforward to characterize the traffic behaviour and thus reliability metrics. On the other hand, in vehicular ad hoc networks (as in mobile ad hoc networks in general), characterizing reliability involves taking into account dynamic topology changes due to vehicles' mobility, which in turn is affected by microscopic and macroscopic traffic parameters [60; 61; 67; 136]. These parameters include, but are not limited to, traffic regulations on intersections and road segments, driver behaviour, traffic flow, road capacity, etc. In vehicular networks, the analysis of the reliability of a safety application is even more complicated than in other mobile ad hoc networks, due to the impact of unexpected drivers' behaviour and variable traffic flow on vehicles' mobility [67]. Moreover, it is also expected that the reliability varies significantly between highway and urban traffic scenarios. This is partly due to the fact that traffic density is homogeneous under free and stable traffic flow regimes, which dominate highways, whereas a mixture of different traffic densities can be observed simultaneously in an urban scenario as simple as a road segment linked to a signalized intersection. Moreover, an urban traffic network must be seen as a 2-dimensional network, compared to a 1-dimensional highway network. This makes the dynamics of traffic density more complicated in urban scenarios, resulting in more complex reliability behaviour, especially near intersection.

The traffic model we proposed in Chapter 3 describes the dynamics of traffic density in a simple urban scenario comprised of an intersection and the road segments connected to that intersection. The noticeably high cross-correlation of $\sim 95\%$ between the model and the synthetic traffic traces, as shown in Chapter 3, indicates a high capability of the model in conducting a behavioural study of reliability in an urban traffic scenario. In this chapter, we take advantage of such property and apply the proposed traffic density model to analytically describe the spatial-temporal reliability behaviour of safety message dissemination in an urban road segment. In the proposed analytical model, the probability of successful message transmission associated with both periodic and warning messages contending for a shared channel are calculated. Additionally, we determine the distribution function corresponding to the IRT of periodic beacon messages. In this study, we are not interested in the per message channel access delay, as it is in the order of a few milliseconds, hence, it is not a key factor impacting the requirements of a safety application [55]. Transmission failures, on the other hand, are of high importance because, in the case of periodic messages, a single transmission failure causes the reception time to exceed a beacon interval as large as 100 ms [55; 183].

Our work differs from the previous studies (described in 2) in several ways: (i) instead of solely adopting a simulation approach, we develop an analytical model to generalize the analysis of safety messages' reliability; (ii) we take into consideration the mutual impact of both types of safety messages, that is, event driven and periodic; (iii) we study the reliability of safety massage dissemination in an urban traffic scenario with heterogeneous and dynamic traffic density.

The remainder of this chapter is organized as follows. In Section 4.2, the assumptions adopted throughout this study are clarified. In Section 4.3, we develop a general Markovian analytical framework to characterize the reliability metrics of safety message broadcast, and apply it with the urban traffic density model proposed in Chapter 3. A numerical evaluation of the model is presented in Section 4.4, and finally, Section 4.5 summarises the chapter.

4.2 Assumptions

We adopt the following assumptions when addressing IEEE 802.11p one hop broadcast communications: (i) the virtual carrier sense mechanism realized by request-to-send and clear-to-send (RTS/CTS) handshaking is disabled, and (ii) ACKs are not transmitted after successful reception. Consequently, no retransmissions are performed and the backoff window size is not adjusted based on the existing load on the channel. Moreover, according to the DSRC/WAVE specifications, it is mandatory that vehicles transmit periodic beacons and event-driven emergency messages on the same channel (channel 178) [2]. Thus, a message can potentially collide with a message of its own type or another type if they are transmitted simultaneously by more than one vehicle.

We assume that the backoff window of event-driven messages, denoted by W_e, is smaller than that of the periodic beacon messages denoted by W_b. This is in agreement with IEEE 802.11p standard and implies that event driven messages are of higher priority than periodic beacons. Additionally, we assume that nodes experience a non-saturated arrival of event-driven messages as a Poisson arrival process with rate λ. Beacon messages, on the other hand, arrive on a periodic basis with inter-arrival time of α time slots. Arrival of a new beacon message cancels out old beacons, since a new beacon is assumed to always contain the most updated vehicle state. As a result, the impact of queuing delay on beacon messages is eliminated.

Our work in this chapter is focused on urban traffic systems. We use the traffic density model proposed in Chapter 3 to characterise the reliability behaviour on a road segment (i.e., $\mathrm{L_E}$ in Figure 4.1) connected to a signalized intersection. The intersection is centred at coordinate $x = 0$, and x increases to the right on segment $\mathrm{L_E}$. For further details of the traffic density model see Chapter 3.

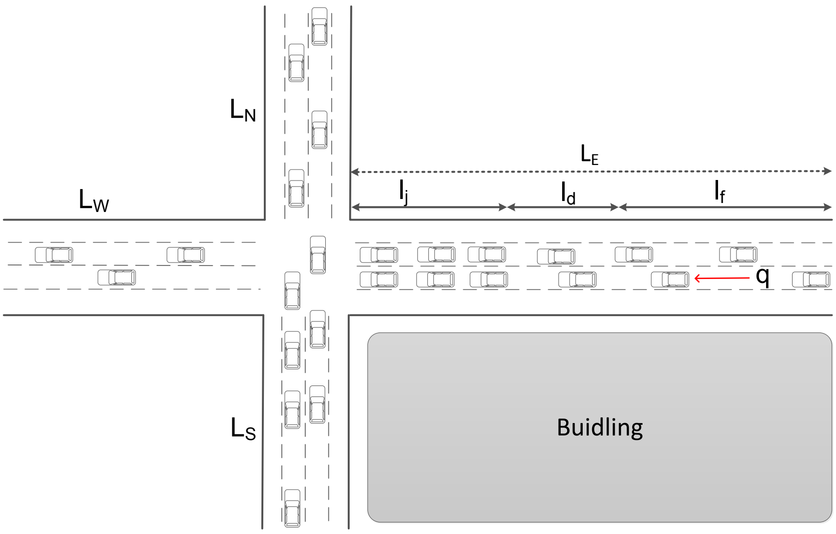

Figure 4.1: Urban traffic scenario

4.3 Analytical Model

To study the aforementioned reliability metrics, in the first step, we need to calculate the probability that a vehicle attempts a transmission in a generic time slot. To this aim, we propose a Markov-chain model for the backoff process corresponding to a combination of periodic beacons and event driven messages.

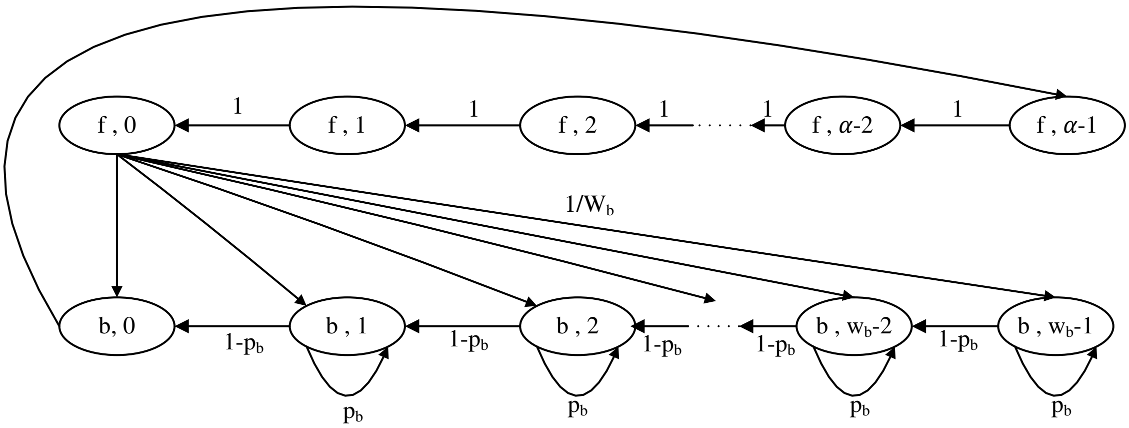

Figure 4.2: Markov chain model of backoff process for periodic beaconing safety messages

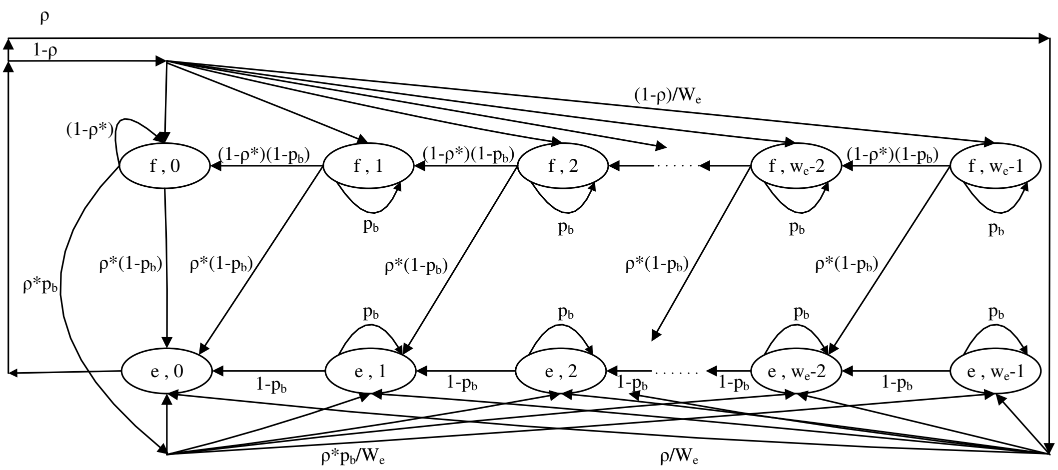

Figure 4.3: Markov chain model of backoff process for event-driven safety messages

We adopt the Markov chain model proposed in [101] as the base model for beaconing process. However, to account for the periodic nature of beacon transmissions, it is required to extend the base model. The extended chain, shown in Figure 4.2, consists of a combination of deterministic post backoff (upper stage) and stochastic backoff processes (lower stage). Whenever a vehicle completes its current channel contention and transmission attempt, it enters the post backoff stage of length equal to beaconing period $\alpha = \lceil \frac{I_b}{\sigma} \rceil$, where I_b and σ are the beacon period and time slot duration, respectively. With probability $\frac{1}{W_b}$, a backoff state (b, k) is selected and channel contention starts. The probability of a transmission attempt is equivalent to the probability that the backoff process enters state $(b, 0)$.

To this end, we solve the Markov chain shown in Figure 4.2 to calculate the probability that a vehicle transmits a beacon in a generic time slot, denoted by τ_b. It is straightforward to verify that the steady-state transition of the chain and the normalization conditions result in:

$$s_{b,k} = \frac{W_b - k}{W_b} s_{b,0} \qquad k \in (0, W_b - 1) \tag{4.1}$$

$$s_{f,k} = s_{b,0} \qquad k \in (0, W_b - 1) \tag{4.2}$$

$$\sum_{k=0}^{W_b-1} s_{b,k} + \sum_{k=0}^{\alpha-1} s_{f,k} = 1 \tag{4.3}$$

and solving for $s_{b,0}$ (equivalent to the probability of transmission attempt τ_b), we obtain:

$$\tau_b = s_{b,0} = \frac{2}{W_b + 1 + 2\alpha} \tag{4.4}$$

The Markov chain corresponding to the backoff process of event-driven messages is shown in Figure 4.3. This chain is obtained by customizing Engelstad *et al.* model [56] to account for broadcast transmission mode. Here, (f, k) are post backoff states during which the queue is empty and the node has to wait for a new message to arrive. (e, k) represent backoff states where there exists a message for transmission. In this case, with probability ρ, the backoff process is immediately invoked by entering one of the backoff states (e, k) chosen randomly. With probability $1-\rho$ the node enters a post backoff stage. While being in a state (f, k), if a new message arrives with probability ρ^* (different from ρ) and the channel is sensed idle, the contention process is immediately triggered by directly entering the state $(e, k-1)$ in the backoff stage. If the channel is sensed busy (with probability p_b), the countdown process is blocked, otherwise a transition to state $(f, k-1)$ takes place.

Applying steady-state conditions recursively through the chain, it is straightforward to show that:

$$s_{f,k} = \frac{1-\rho}{W_e}\frac{1-(1-\rho^*)^{W_e-k}}{1-p_b}\frac{s_{e,0}}{\rho^*} \qquad k \in (1, W_e-1) \tag{4.5}$$

$$s_{f,0} = \frac{1-\rho}{W_e}\frac{1-(1-\rho^*)^{W_e}}{(\rho^*)^2}s_{e,0} \qquad k = 0 \tag{4.6}$$

$$s_{e,k} = \frac{(W_e-k)}{W_e(1-p_b)}s_{e,0} + \frac{(W_e-k)\rho^* p_b}{W_e(1-p_b)}s_{f,k} - s_{f,k} \qquad k \in (0, W_e-1) \tag{4.7}$$

and the normalization condition implies that:

$$\sum_{k=0}^{W_e-1}(s_{e,k}+s_{f,k}) = 1 \tag{4.8}$$

Using Equations 4.5 - 4.8, $b_{e,0}$ and thus the probability of event-driven message transmission (τ_e) in a generic time slot is obtained as follows:

$$\begin{aligned}\frac{1}{\tau_e} &= 1 + \frac{W_e-1}{4(1-p_b)} + \frac{p_b}{(1-p_b)^2}\frac{1-\rho}{W_e^2} \\ &\quad \frac{(\rho^*)^2W_e(W_e-1)+(1-\rho^*)^{W_e}(2\rho^*W_e-2\rho^*+2)+2(\rho^*-1))}{(\rho^*)^2} \\ &\quad + \frac{1-\rho}{W_e}\frac{1-(1-\rho*)^{W_e}}{(\rho^*)^2}\end{aligned} \tag{4.9}$$

4.3.1 Probability of Busy Channel (p_b)

The probability of the event that the channel is sensed busy is equivalent to the probability that at least one vehicle is transmitting a message, either a beacon or an event-driven message. This probability can be expressed as:

$$p_b = 1 - ((1-\tau_b)(1-\tau_e))^{N_r} \tag{4.10}$$

where τ_b and τ_e are the probabilities of transmission attempts corresponding to beacon and event-driven messages, described by Equations 4.4 and 4.9, respectively. N_r is the number of vehicles in the transmission range (R) of the vehicle under investigation. For uniform traffic distribution, e.g. highway scenario, with density β vehicles/meter, $N_r = 2\beta R$. For non-uniform traffic distribution corresponding to urban scenario, we later give an expression for calculating N_r using the density functions proposed in Chapter 3.

4.3.2 Probability of Successful Transmission (p_s)

Without loss of generality, we address the probability of successful transmission separately for beacon and event-driven messages while the mutual impacts are taken into consideration. Denote by p_s^b and p_s^e, the probability of successful transmission of beacon and event-driven messages, respectively. To obtain these probabilities, we account for simultaneous transmissions in the transmission range of a vehicle and transmission(s) from hidden nodes within the hidden area of the sender vehicle. Intuitively, p_s^b and p_s^e are equivalent to the probabilities that exactly one node attempts transmission and no hidden node transmits a message which overlaps in time with the transmission performed by the sender vehicle. This leads us to derive p_s^b and p_s^e as follows:

$$p_s^b = \tau_b\,(1-\tau_b-\tau_e)^{\left(N_r - 1 + \tilde{N}_h \frac{T_h^b}{p_b T_s^b + (1-p_b)\sigma}\right)} \tag{4.11}$$

$$p_s^e = \tau_e\,(1-\tau_b-\tau_e)^{\left(N_r - 1 + \tilde{N}_h \frac{T_h^e}{p_b T_s^e + (1-p_b)\sigma}\right)} \tag{4.12}$$

In Equations 4.11 and 4.12, $\tilde{N}_h$ is the average per-vehicle number of hidden terminals for vehicles within the transmission range of a sender vehicle. For uniform traffic distribution with density β, and adopting unit disk graph as the radio propagation model, we have $\tilde{N}_h = \beta R$. For non-uniform traffic distribution, the hidden terminal nodes fall within the ranges $(x_v - 2R, x_v - R)$ and $(x_v + R, x_v + 2R)$ on the left and right side of a candidate sender vehicle positioned at x_v; we describe the calculation of $\tilde{N}_h$ in greater detail in Section 4.3.5.

T_h in Equations 4.11 and 4.12 is the period during which a transmission from a vehicle may overlap with the transmission from a hidden node; hence, $T_h^r = 2T_s^b$ and $T_h^e = 2T_s^e$, where T_s^b and T_s^e are packet transmission time corresponding to beacon and event-driven messages, respectively. The subscript s in T_s^b and T_s^e is introduced to distinguish between duration of a successful message transmission and the duration of a message collision. The ratios $\frac{T_h^b}{p_b T_s^b + (1-p_b)\sigma}$ and $\frac{T_h^e}{p_b T_s^e + (1-p_b)\sigma}$ in Equations 4.11 and 4.12 are introduced to account for the fact that if a node in the hidden area of the sender vehicle starts transmission, the channel will be sensed busy by the remaining vehicles in the hidden area who thus remain silent.

4.3.3 Calculating ρ^* and ρ

In the proposed Markov model for event-driven messages, ρ^* is the conditional probability for a new event-driven message to arrive in the queue within a generic slot time, given that at the beginning of the slot the queue was empty. Note that a generic slot can have different lengths due to blocking of the backoff process in reaction to busy channel. If the channel is idle (with probability $1 - p_b$), the slot length is σ (nominal slot duration). If a successful beacon or event-driven message transmission occurs on the channel with probability P_s^b and P_s^e, the corresponding generic slot time will be of length T_s^b and T_s^e, respectively. Otherwise, with probability $p_b - P_s^b - P_s^e$, the slot duration is T_c (collision duration). Therefore, for a Poisson arrival process with rate λ, ρ^* can be expressed as:

$$\rho^* \;=\; 1 - \Big((1-p_b)e^{-\lambda\sigma} + P_s^b e^{-\lambda T_s^b} + P_s^e e^{-\lambda T_s^e} + (p_b - P_s^b - P_s^e)e^{-\lambda T_c}\Big) \tag{4.13}$$

Note that P_s^b and P_s^e are different from p_s^b and p_s^e described by Equations 4.11 and 4.12. More specifically, P_s^b (P_s^e) is the probability of the event that a successful beacon (event-driven) message transmission occurs, taking into account all vehicles within the transmission range of a vehicle, but neglecting the impact of hidden vehicles, since the transmitting vehicle does not have any knowledge about its hidden peers. Accordingly, we eliminate the effect of hidden terminals to obtain P_s^b and P_s^e as follows:

$$P_s^b = \frac{N_r p_s^b}{(1-\tau_b-\tau_e)^{\frac{\tilde{N}_h T_h^b}{p_b T_s^b + (1-p_b)\sigma}}} \tag{4.14}$$

$$P_s^e = \frac{N_r p_s^e}{(1-\tau_b-\tau_e)^{\frac{\tilde{N}_h T_h^e}{p_b T_s^e + (1-p_b)\sigma}}} \tag{4.15}$$

To calculate ρ, we need to determine the channel service time, which is the time it takes a head-of-line message to access the channel and complete its transmission, either successfully or with collision. Assume P_e and H_e are the payload and header length (in number of bits) of an event-driven message, and R_d is data rate in bits/second. To obtain ρ, we follow the approach proposed in [56] to derive the Z-transform of the Markov chain in Figure 4.3:

$$\begin{aligned} D(z) &= \frac{z^{\frac{P_e+H_e}{\sigma R_d}}}{W_e} \sum_{k=0}^{k=W_e-1} H_{state}^k(z) \\ &= \frac{z^{\frac{P_e+H_e}{\sigma R_d}}}{W_e} \frac{1-(H_{state}(z))^{W_e}}{1-H_{state}(z)} \end{aligned} \tag{4.16}$$

where $H_{state}(z)$ is the Z-transform of each state, expressed as follows:

$$\begin{aligned} H_{state}(z) &= (1-p_b)z + P_s^b z^{\frac{T_s^b}{\sigma}} + P_s^e z^{\frac{T_s^e}{\sigma}} \\ &\quad + \left(p_b - P_s^b - P_s^e\right) z^{\frac{T_c}{\sigma}} \end{aligned} \tag{4.17}$$

The average service time of an event driven message can be obtained by calculating the derivative of Equation 4.16 in $z=1$ (denoted by $D'(1)$ and measured in number of slots). Correspondingly, ρ is obtained as:

$$\rho = 1 - e^{-\lambda\sigma D'(1)} \tag{4.18}$$

Expressions 4.9, 4.10, 4.11, 4.12, 4.13, and 4.18 are considered as a system of equations to be solved numerically in order to obtain the values of τ_e, p_b, p_s^b, p_s^e, ρ^*, and ρ.

4.3.4 Distribution of IRT

Define $p_I(\gamma)$ as the complementary cumulative probability of the inter-reception time of beacon messages, that is, the probability that the inter-reception time I of messages from a specific sender is greater than γ. Recalling that I_b is the beacon interval, this is equivalent to the probability that at least $\lfloor \frac{\gamma}{I_b} \rfloor$ consecutive messages transmissions end in failure, i.e.,

$$p_I(\gamma) = \sum_{I=\gamma}^{\infty} (1 - p_s^b)^{\lfloor \frac{I}{I_b} \rfloor} = \frac{(1 - p_s^b)^{\frac{\gamma}{I_b}}}{1 - (1 - p_s^b)^{\frac{1}{I_b}}} \tag{4.19}$$

It is also informative to calculate the probability of an event that at least one beacon is received by a vehicle from a sender within a duration γ. Denote by $p_n(\gamma)$ the probability of such an event. We obtain

$$\begin{aligned} p_n(\gamma) &= \sum_{n=1}^{\lfloor \frac{\gamma}{T_b} \rfloor} (1 - p_s^b)^{\lfloor \frac{\gamma}{T_b} \rfloor - n} (p_s^b)^n \\ &= \frac{p_s^b \left((1 - p_s^b)^{\lfloor \frac{\gamma}{T_b} \rfloor} - (p_s^b)^{\lfloor \frac{\gamma}{T_b} \rfloor} \right)}{1 - 2p_s^b} \end{aligned} \tag{4.20}$$

4.3.5 Number of Nodes in Transmission Range (N_r) and Average Number of Hidden Nodes ($\tilde{N}_h$)

Using the traffic density model proposed in Chapter 3, we obtain the number of vehicles within the transmission range of a vehicle at position x_v at time instant t during the light cycle of the intersection. To this aim, we calculate the integral over the density function $K(x,t)$ described by Equations 3.6 and 3.9 in Chapter 3, corresponding to the red and green phases of the traffic light cycle, i.e.,

$$N_r = \int_{max(L_{min},x_v-R)}^{min(L_{max},x_v+R)} K(x,t)dx \tag{4.21}$$

where L_{min} and L_{max} are the coordinates of the start and end positions of the road segment under consideration, and x_v is the position of the vehicle.

To determine $\tilde{N}_h$, we consider the fact that, due to the non-uniform traffic distribution, the average per-vehicle number of hidden nodes affecting packet reception is no longer simply half the total number of hidden nodes in the hidden terminal region, as it is the case in uniform traffic density. To that end, focusing on the transmission range of the sender vehicle, denote by x_m^r the median position such that half of the total number of vehicles to the right of the sender within its transmission range is located to each side of x_m^r; similarly, define x_m^l to be the median point of vehicles to the left of the sender. In other words, if x_v is the position of the sender vehicle, then, x_m is the point on the road segment that minimizes the following objective function:

$$x_m^{(r,l)} = argmin_x \left(\frac{N_x}{N} - \frac{1}{2}\right) \qquad s.t.\ |x - x_v| \leq R \tag{4.22}$$

where $N_x = \int_{x_v}^{min(L_{max},x_v+x)} K(x,t)dx$ and $N = \int_{x_v}^{min(L_{max},x_v+R)} K(x,t)dx$ are in effect when calculating x_m^r, while $N_x = \int_{max(L_{min},x_v-x)}^{x_v} K(x,t)dx$ and $N = \int_{max(L_{min},x_v-R)}^{x_v} K(x,t)dx$ are used for the calculation of x_m^l.

To calculate $x_m^{(r,l)}$ described by Equation 4.22, in the first step, $x_m^{(r,l)}$ is decomposed to right-side and left-side median positions, that is, x_m^r and x_m^l, respectively. The median positions are then calculated using a simple procedure illustrated by Algorithm 4.1. In Algorithm 4.1, ϵ is an arbitrary small value, and the expressions in parentheses correspond to x_m^l.

Correspondingly, the average per-vehicle number of hidden nodes in the right and left directions of the sender are determined as follows:

$$\tilde{N}_h^r = \int_{min(L_{max},x_v+R)}^{min(L_{max},x_v+R+x_m^r)} K(x,t)dx \tag{4.23}$$

Algorithm 4.1 - finding median position to the right (left) of a sender

Require: $K(x,t), x_v, L_{min}, L_{max}, R$
1: $\Delta x \leftarrow \delta(\leq 1)$
2: $x^r_m \leftarrow x_v \quad (x^l_m \leftarrow x_v)$
3: $N_{right} \leftarrow \int_{x_v}^{min(L_{max}, x_v+R)} K(x,t)dx \quad \left(N_{left} \leftarrow \int_{max(L_{min}, x_v-R)}^{x_v} K(x,t)dx\right)$
4: **repeat**
5: $\quad x^r_m \leftarrow x^r_m + \Delta x \quad (x^l_m \leftarrow x^l_m - \Delta x)$
6: $\quad N_{x^r_m} \leftarrow \int_{x_v}^{min(L_{max}, x_v+x^r_m)} K(x,t)dx \quad \left(N_{x^l_m} \leftarrow \int_{max(L_{min}, x_v-x^l_m)}^{x_v} K(x,t)dx\right)$
7: **until** $\left|\frac{N_{x^r_m}}{N_{right}} - \frac{1}{2}\right| \leq \epsilon \quad \left(\left|\frac{N_{x^l_m}}{N_{left}} - \frac{1}{2}\right| \leq \epsilon\right)$
8: **return** $x^r_m \quad (x^l_m)$

$$\tilde{N}^l_h = \int_{max(L_{min}, x_v-R-x^l_m)}^{max(L_{min}, x_v-R)} K(x,t)dx \tag{4.24}$$

where $\tilde{N}^r_h$ and $\tilde{N}^l_h$ are the average number of hidden terminals in the right and left directions of the sender, respectively.
Using $\tilde{N}^r_h$ and $\tilde{N}^l_h$, the average per vehicle hidden nodes can be expressed as follows:

$$\tilde{N}_h = \beta\tilde{N}^r_h + (1-\beta)\tilde{N}^l_h \tag{4.25}$$

where $0 \leq \beta \leq 1$ is a weighting factor and can be determined based on the direction relative to the sender where the reception probability of safety message broadcast is considered. In a forward collision warning application (FCW), message reception is not important for vehicles driving ahead of a sender vehicle, thus $\beta = 0$. On the other hand, in the case of a lane changing or an overtaking vehicle, reception in both directions are deemed to be equally important, and thus $\beta = 0.5$.

4.4 Numerical Results

We numerically study the reliability model derived in Section 4.3 within two directions. First, the numerical results of the model are derived for an 8–lane highway scenario and are validated using the results of Elbatt *et al.* [55] simulation work.

Second, the results of the model are derived for a 3–lane urban intersection scenario illustrated in Figure 4.1. Traffic and network parameters corresponding to these scenarios are specified in Table 4.1. Traffic flow associated with the urban scenario is set to a near-saturation level and determined according to the capacity of the intersection; as explained in Chapter 3, this traffic flow setting corresponds to an ideal signalized intersection, and facilitates predictions for under-saturated and over-saturated traffic conditions near a signalized intersection.

4.4.1 Model Validation

As the scenario simulated in [55] only considers periodic beacons, we set the probability of transmission of event driven messages to zero to align our model with this scenario. In the scenario, the number of vehicles within the transmission range (i.e. N_r) of a candidate sender in high and low density cases are obtained 358 and 38, respectively. The average per-vehicle number of hidden nodes ($\tilde{N}_h$) calculated using Equation 4.25 with $\beta = 0.5$ are 179 and 18 for high and low densities. As the traffic is uniformly distributed, $\tilde{N}_h$ is simply half the number of vehicles in the entire hidden terminal area of a node. The numerical results corresponding to Elbatt *et al.* scenarios are shown in Figure 4.4. According to Figure 4.4a, the probability of successful reception in the dense traffic case decreases with increasing distance from the sender. This can be justified by the fact that for nodes farther from the sender, the number of hidden terminals increases, leading to a higher number of collisions. The mean reception probability achieved by our model and the simulations of Elbatt *et al.* are 0.65 and 0.72, respectively, and the mean difference between the model and simulation results is 7% with standard deviation 4%. The results corresponding to the probability of successful reception in the low density case are depicted in Figure 4.4b. Due to the light traffic density, the impacts of simultaneous transmissions and hidden terminal nodes are negligible. The mean reception probability achieved by the model and simulations are 0.96 and 0.98, respectively, and the mean difference is 2% with standard deviation 0.9%.

We applied the mean probabilities of successful reception measured by Elbatt *et al.* and calculated by the model to measure the distribution of IRT in high and low density scenarios. Figure 4.4c demonstrates the complementary cumulative probability as a function of IRT. The results show that, in the low density case, a message is almost always received in less than 200 ms. On the other hand, in the high density case, this increases to 400 ms for some messages. Furthermore, in the low density case, the probability that the inter-reception time be above 100 ms is significantly small. This means that the vast majority of messages arrive in time. The mean difference between results achieved by the model and simulations in high and low density scenarios are 1% and 0.02%, respectively. It is therefore concluded that the proposed model fits very well with the simulation results of Elbatt *et al.* as the benchmark for scenarios characterized by uniform traffic distribution.

Table 4.1: Simulation parameters and configuration values

Traffic	Elbatt *et al.* Scenario	High density: 1920 vehicles/mile
		Low density: 208 vehicles/mile
	Urban Scenario	Road length =1 km
		Duration of red phase =50 s
		Traffic flow =2740 vehicles/hour
		Speed limit =20 m/s
		Jam headway distance = 6 m
DSRC/WAVE	Transmission range R =150 m	
	Packet length =100 bytes	
	Signal bandwidth = 10 MHz	
	Channel Data Rate = 6 Mbit/s	
	Slot time (σ)=13 μs	
	Propagation delay = 1 μs	
	Preamble length = 40 μs	
	Contention window size W_b = 32	
	Contention window size W_e = 16	
	Arrival rate λ = 1 message/s (event driven msg.)	
	Beacon period (I_b)=100 ms	

4.4.2 Urban Intersection Scenario

Our results for the urban scenario characterised by heterogeneous traffic distribution are shown in Figures 4.5 and 4.6. Figure 4.5a shows traffic density in

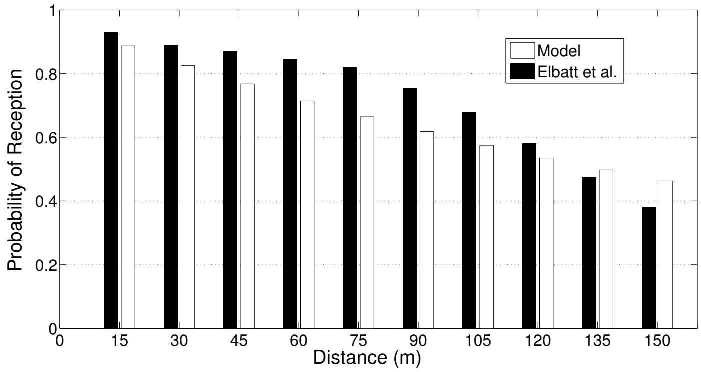

(a) Probability of successful reception in high traffic density

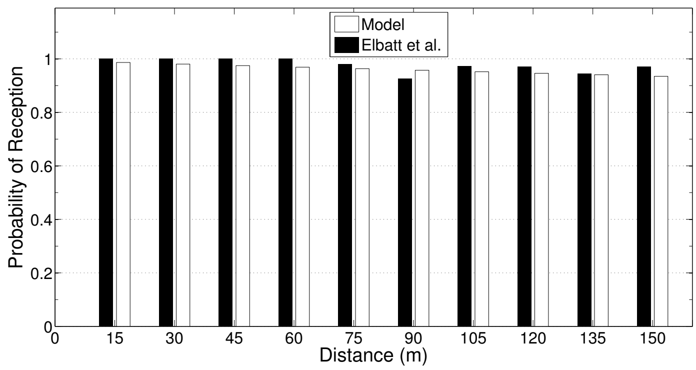

(b) Probability of successful reception in low traffic density

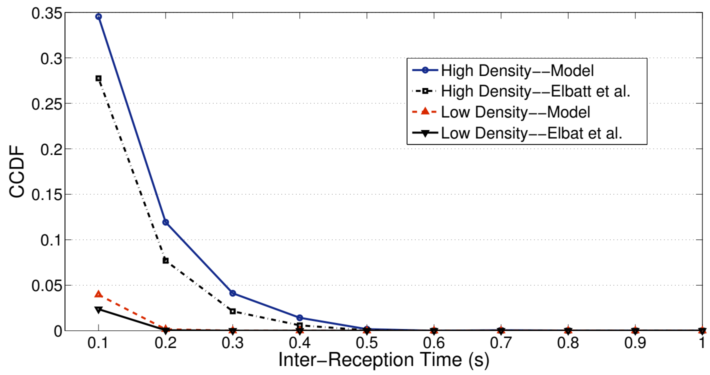

(c) Complementary Cumulative Distribution Function (CCDF) of IRT

Figure 4.4: Comparison of the model and Elbatt *et al.* highway scenario [55]

vehicles/meter along the road segment under investigation during a red phase, and Figure 4.5b depicts the average per-vehicle number of hidden nodes potentially affecting a vehicle on the road segment. Figure 4.5c shows the probability of successful transmission in spatial and temporal dimensions. Observe that, by increasing the queue length at the intersection, the average per vehicle hidden terminals increases at positions behind the queue. A maximum number of hidden nodes is observed at positions 301–334 m with magnitude 37 at time 50 seconds (end of the red phase). In addition to the increase of hidden terminals with time, the area with high number of hidden terminals also widens and expands to distances farther from the intersection. As the queue length grows larger than R (the nominal transmission range), the average per vehicle hidden terminals also increases in positions close to the intersection. This is shown by the rising curve near the intersection from time instant 40 sec to 50 sec.

It follows from Figure 4.5c that the probability of successful transmission of a vehicle is significantly dependent on the average per vehicle number of hidden nodes. Comparing Figures 4.5b and 4.5c reveals that, in areas with large number of hidden nodes, the probability of successful transmission is low. In positions 301–334 m and at time instant 50 sec, for instance, the average successful transmission probability is 0.86, which is the lowest among all positions at the same time instant. In addition, we observe that the density of vehicles within the transmission range of a sender has a very small impact on the probability of successful transmission. At time instance 50 sec, the highest number of vehicles within transmission range of a sender is 104, which is observed at position 150 m. The number of hidden nodes seen at this position is a small number 3. Correspondingly, the probability of successful transmission is 0.95 at this position, which highlights a fact that the hidden terminal effect is the predominant driving factor determining the achievable successful transmission rate.

We continue the numerical study with the distribution of IRT shown in Figure 4.6. For three IRT values 100 ms, 300 ms, and 1 sec, we calculated the probability of inter-reception time using Equation 4.19 and depicted the results in Figure 4.6a, 4.6b, and 4.6c, respectively. Again, the worst-case IRT probabilities occur at positions 301–334 m with average magnitudes 0.13, 0.002, and 10^{-9} corresponding to 100 ms, 300 ms, and 1 sec, respectively.

Our results above were given for the red phase of a traffic light. During the green phase, in the first few seconds of the phase, the probability of unsuccessful

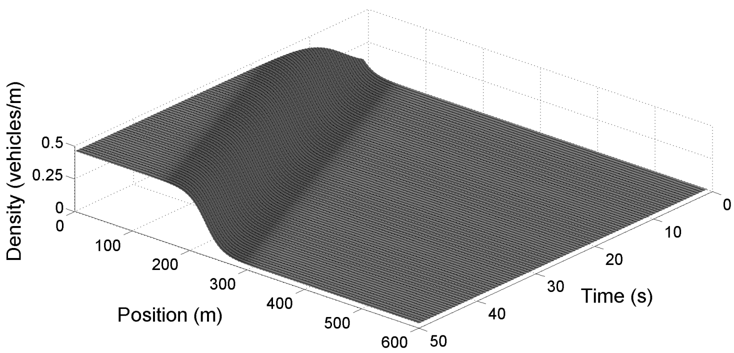

(a) Traffic density

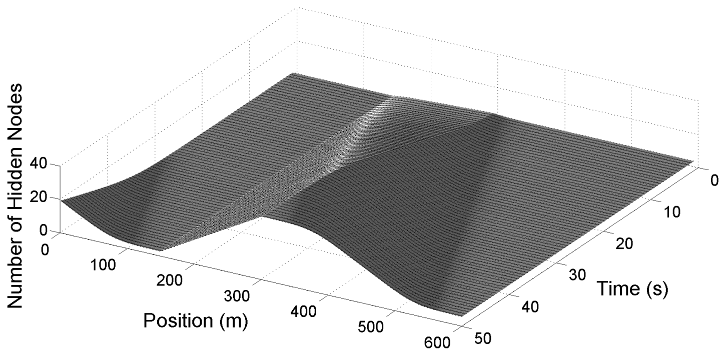

(b) Average per-vehicle hidden terminal nodes

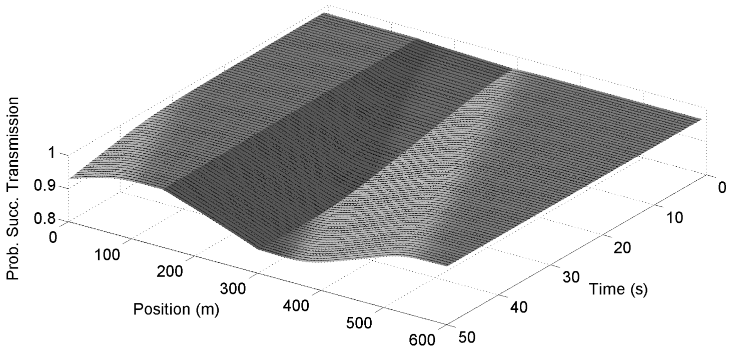

(c) Probability of successful transmission

Figure 4.5: Urban intersection scenario

transmission and probability of high inter-reception time were observed to exacerbate due to a slow initial discharge rate of the queue, indicating that more positions will experience a high average per-vehicle hidden terminals. Afterwards, with increasing velocity, the queue discharges faster and the reliability metrics improve.

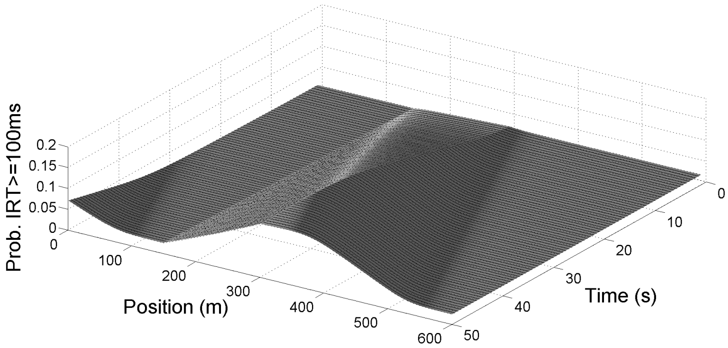

(a) Probability IRT $\geq$ 100 ms

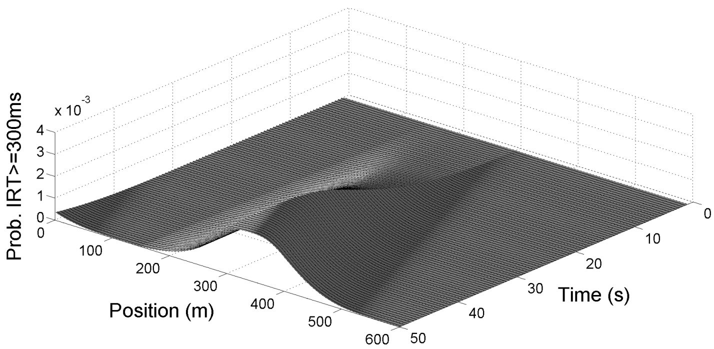

(b) Probability IRT $\geq$ 300 ms

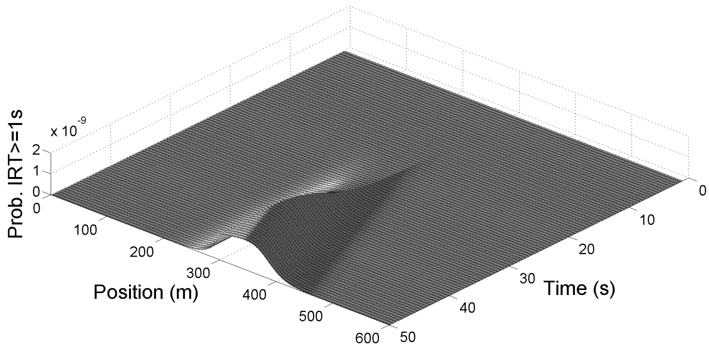

(c) Probability IRT $\geq$ 1 s

Figure 4.6: IRT distribution

4.4.3 Discussion

The impact of the hidden terminal effect on VANETs has previously been studied in several works including [55; 183]. The studies were carried out by simulating free-flow, uniformly distributed vehicular traffic and capturing the packet delivery characteristics. In the validation of our model in Section 4.4.1, we verified and corroborated these results. In our study of the reliability performance in the urban scenario, based on a realistic vehicular mobility model around a signalized intersection, we find strong evidence that these results can be generalized to cover urban settings as well. One would intuitively suspect that the setting of a signalized intersection, characterized by high variations of traffic density, will lead to poor packet delivery performance due to increased overlapping of transmitters. However, our results show that this impact is less significant than the hidden node problem, which is dominant in the urban non-uniform scenario as well. Moreover, we observe that the worst case results take place far from the traffic light queue, where the traffic is either in free-flow or decelerating from high speed. It is notable that, from a traffic safety point of view, these positions are arguably the most important for timely alerting of dangerous traffic conditions, and their lower reliability may correspondingly lead to an increased risk of serious incidents.

Our experiments were carried out at near-saturation traffic conditions, using DSRC communication with moderate (100 bytes) payload length. Increasing the traffic load further, or increasing the packet size, will result in lower performance but generally will not change the negative impact dominance of the hidden nodes. It is possible to mitigate the impact of vehicular density by selecting appropriate radio data rates, but the hidden node problem will still remain a serious issue using the current IEEE 802.11p specifications. In this chapter, we adopted unit disk graph as the radio propagation model. In Chapter 5, we aim to reveal some other aspects of hidden terminal problem using realistic radio propagation models and focusing on safety-critical traffic scenarios, where the reliability requirements are highly stringent. Such analysis is expected to reveal the worst-case reliability from the standpoint of traffic safety.

4.5 Summary

It is paramount to safety applications that the underlying communication network provides stringent reliability characteristics. Previous work in this area has focused on investigating the reliability of communication networks in free-flow traffic scenarios, where vehicles are uniformly distributed or traffic is in steady state. This does not hold true in urban settings, where traffic is regulated by signalized intersections. In this chapter, we addressed the urban case by studying the reliability of safety messages using a realistic vehicular mobility model which captures the heterogeneous node densities at and around signalized intersections. In line with previous work, we constructed Markov models for capturing the delivery probability for event-driven warning messages and the packet inter-reception time for periodic beacons. Combining the Markov models with the urban vehicular density model, for the first time, we are able to accurately capture the resulting performance characteristics in a non-uniform density setting. Through a numerical evaluation, we demonstrated that the major impact of the hidden node problem on the reliability performance of safety messages extends to the urban case as well. Importantly, we found that the impact is most significant in the same road sections where the vehicle velocities are the highest. These findings call for further work on mechanisms to mitigate the effect of hidden nodes in order to ensure the viability of DSRC/WAVE safety applications.

Chapter 5

Hidden Terminal Interference in Vehicular Ad Hoc Networks with Forced-Flow Traffic Conditions

5.1 Introduction

In the DSRC/WAVE standard [2; 121], the recommended paradigm for dissemination of safety messages is one-hop broadcast, even though multi-hop dissemination is also an option for the event-driven warning messages. In broadcast communications, with one-hop as a special case, the virtual carrier sense realized by Request-To-Send (RTS) and Clear-To-Send (CTS) handshaking which is a point to point mechanism does not work and the applications rely solely on physical carrier sense. While the adoption of this approach may benefit the safety applications in the form of latency reduction, the extent to which it affects their performance and reliability is of prominent concern. An immediate consequence of eliminating the virtual carrier sense is to give rise to hidden terminal interference due to the expansion of the hidden terminal region [105]. This concern is indeed recognized in the literature and earlier work addressed the problem in the context of broadcast communications [22; 78; 106; 164; 165; 178]. An extensive background and related work can be found in Chapter 2.

The conventional approach of characterising hidden terminal problem is based mainly on the presence or absence of hidden nodes in a so-called hidden terminal region of a target transmitter. The enumerated hidden nodes account for an interference number, which is then applied to the MAC layer functionalities to calculate the impacts on some performance metrics, e.g., packet delivery ratio. The major drawback of this widely used approach is that all interferers are treated uniformly, no matter where they are located relative to the position of an intended receiver of the target transmitter. In a more advanced approach [164; 165], the interference is characterized by its power, where the power magnitude is determined by a radio propagation model accounting for relative positions of nodes, among other factors [146]. The accuracy of the latter approach is highly dependent on the degree of realism incorporated into the radio propagation and the vehicular traffic models, collectively representing the host system. As an example, suppose there are two choices of radio propagation models for a study on hidden terminal effects. Model A assumes Line of Sight (LOS) always exists, whereas model B is able to detect and capture LOS obstruction. With the model A in use, extra signal attenuation due to signal obstruction is not taken into account in the received signal, whereas with model B it is considered. In effect, with model A, the likelihood of coordinated transmission is larger than with model B. Considering the fact that hidden terminal problem stems from uncoordinated transmissions, the severity of hidden terminal problem is optimistically less in the case of model A compared to the more realistic model B.

The above example and many others also stress that the hidden terminal problem has an uncontrolled nature because its behaviour is foremost driven by uncontrolled elements of the host system such as unpredicted obstructions caused by the static and moving objects. Hence, the accuracy of interference characterization is significantly dependent on the radio propagation model employed to capture the various causes of signal attenuation. It also depends on the degree of realism captured by the traffic model used for describing the relative arrangement of nodes.

In another dimension, the investigation of hidden terminal problem for the case of forced-flow vehicular traffic, in general, and the case of safety-critical scenarios, in particular, is highly demanded. In these scenarios, the safety applications are expected to have the most stringent reliability requirements. By analogy, the study of interference and reliability in safety-critical scenarios resembles the classic test of industrial systems under stress. The difference is that in the former case, the subject of stress is the safety level required by the drivers, whereas in the latter case the stress relates to some form of load assigned to the system.

In line with the aforementioned arguments, in this chapter, we aim to advance the state of the art in the investigation of reliability issues of safety applications by means of the following contributions:

- An analytical framework is developed to investigate the severity of hidden terminal interference under forced-flow traffic scenarios dominating urban traffic systems which is less addressed in the literature, while it is predicted to represent a suitable example of severe interference.

- A state-of-the-art radio propagation model targeted to VANET environment is employed to analytically derive the aggregate interference power induced by hidden nodes.

- Focusing on forced flow traffic, two major safety-critical traffic scenarios are identified. In an urban road stretch operating in capacity state, the upper bound interference power induced by hidden nodes and the lower bound reachable distance of the safety messages are obtained for various velocities and lanes of the road stretch. In a signalized intersection, as another safety-critical scenario, the upper bound interference power is obtained for the intersection with various lanes of the road segments connected to the intersection and also various timings of the traffic light in the intersection.

To the best our knowledge, the case of studying reliability issues in safety-critical conditions, and also the degree of realism captured in the host system representation within an analytical framework is unique to this work.

The remainder of this chapter is organised as follows. In Section 5.2, the radio propagation model employed throughout this work is introduced. Section 5.3 presents the definition of hidden node interference adopted in this study, and presents a theoretical methodology for the calculation of hidden node interference power using the radio propagation model. In Section 5.4, a practical approach is described for the identification of the effective Carrier Sense (CS) distance and hidden terminal range, taking into account the traffic properties and the desired transmission range of various safety applications. Section 5.5 presents an overview of the traffic scenarios addressed in our study. Sections 5.6 and 5.7 present the analytical models developed for the characterization of hidden terminal interference corresponding to the road stretch and intersection scenarios, respectively. The experimental results are presented in Section 5.8, and finally Section 5.9 summarizes and concludes the chapter. In the remainder of this chapter, we use the term "single broadcast" instead of "on-hop broadcast" in order to avoid confusion with the notion of "hop" in the context of vehicular traffic.

For the sake of convenience and readability, the notations used frequently in this chapter are introduced in Table 5.1 .

5.2 Channel Model Overview

We apply a shadow-fading path loss model proposed in [8] to determine the magnitude of the received and interference powers in a node. The channel model was designed by means of extensive field measurements in urban areas and using vehicles as transceivers. The structure and behaviour of urban traffic and also vehicle dimensions are incorporated into the channel model by considering three separate scenarios based on shadowing states. These include Line of Sight (LOS), Obstructed Line of Sight (OLOS), and Non Line of Sight (NLOS). LOS is self-explanatory. OLOS is a shadowing state caused by a vehicle driving in between a transmitter and a receiver node. NLOS is caused by buildings and mainly emerges in intersections where communicating vehicles travel on two cross-road segments of the intersection. The path loss corresponding to the LOS and OLOS is described by a dual slope function expressed as follows:

$$PL(d) = \begin{cases} PL0 + 10n_1 \log_{10}\left(\frac{d}{d_0}\right) + X_\sigma & \text{if } d_0 \leq d \leq d_b \\ PL0 + 10n_1 \log_{10}\left(\frac{d_b}{d_0}\right) + & \text{if } d > d_b \\ 10n_2 \log_{10}\left(\frac{d}{d_b}\right) + X_\sigma & \end{cases} \tag{5.1}$$

Table 5.1: Notations

Symbol	Description
PL	Path Loss
CA	Cellular Automata
Δ	length of a cell in CA (meters)
Γ	width of a cell in CA (meters)
HD	Headway Distance (meters)
HT	Headway Time (seconds)
$\mathrm{H_j}$	Jam spacing (meters)
T_c	cycle duration of a traffic light (seconds)
T_g	green phase duration of a traffic light (seconds)
T_{red}	red phase duration of a traffic light (seconds)
t_r	average reaction time of a driver (seconds)
$\hat{L}_s$	length of a small vehicle (meters)
$\hat{L}_m$	length of a medium vehicle (meters)
$\hat{L}_l$	length of a large vehicle (meters)
p_s	population of small size vehicles in the system
p_m	population of medium size vehicles in the system
p_l	population of large size vehicles in the system
W_l	width of a lane (meters)
SINR	Signal to Interference plus Noise Ratio (dB)
$\mathrm{SINR_{th}}$	SINR threshold (dB)
CSth	Carrier Sense power threshold (dBm)
CSD	Carrier Sense Distance (meters)
NSD	Noise Signal Distance (meters)
LOS	Line Of Sight
OLOS	Obstructed Line Of Sight
NLOS	Non Line Of Sight
P	Transmission Power (dBm)
$\mathrm{P_n}$	Noise power (dBm)
P_{if}	Aggregate Interference Power (dBm)
Tx	A target transmitter node
Rx	An intended recipient node

where d is the distance between Tx and Rx. $PL0$ is the free-space path loss plus the accumulative antenna gain ($PL0 = PLf + Ga$) at a reference distance d_0. n_1 and n_2 are path loss exponents, d_b is the breakpoint distance (or slop point), and X_σ is a zero-mean Gaussian distributed random variable with standard deviation

σ. Except for d_0 and d_b, all parameters have different values for LOS and OLOS cases. $PL0$ is 10 dBm larger in OLOS compared to the LOS case which implies higher attenuation if the signal is obstructed by a vehicle located in between Tx and Rx. To distinguish between LOS and OLOS, appropriate notations are provided wherever necessary throughout this work.

For the NLOS situation, the path loss model is described as follows:

$$PL(d_r; d_t; w_r; x_t; i_s) = 3.75 + i_s\, 2.94$$
$$+ \begin{cases} 10\log_{10}\left(\left(\dfrac{d_t^{0.957}}{(x_t w_r)^{0.81}}\dfrac{4\pi d_r}{\lambda}\right)^{n_{NLOS}}\right) + X_\sigma & \text{if } d \leq d_b \\[2ex] 10\log_{10}\left(\left(\dfrac{d_t^{0.957}}{(x_t w_r)^{0.81}}\dfrac{4\pi d_r^2}{\lambda d_b}\right)^{n_{NLOS}}\right) + X_\sigma & \text{if } d > d_b \end{cases} \tag{5.2}$$

where d_r (d_t) is the distance of Tx (Rx) to intersection center, w_r is the width of the street where Rx is located, x_t is distance of Tx to the wall (e.g., building), and i_s is parameter to distinguish suburban and urban environments; that is, $i_s = 1$ and $i_s = 0$ for suburban and urban cases, respectively. n_{NLOS} is a path loss exponent and X_σ is a zero-mean Gaussian distributed random variable with standard deviation σ and describes the path loss variation.

It is worth mentioning that in the path loss model described by Equation 5.1, only one obstruction instance is taken into account if the signal is obstructed by more than one vehicle. Also, in the path loss model described by Equation 5.2, only the obstruction caused by obstacles other than vehicles are considered.

5.3 Hidden Node Interference

Suppose Tx is a target transmitter and Rx is an intended recipient of Tx. A node f from a set of potential interferers $\mathbb{I}$ contributes as a hidden node of Tx to the interference power in Rx if: (i) Rx can hear the transmission of Tx, (ii) f cannot hear the transmission of Tx , and (iii) a transmission from f can be received (not necessarily decoded) in Rx. This definition, from the perspective of signal power, translates to the following terms: (i) the power of the received signal from Tx in the Rx is larger than or equal to a Carrier Sense threshold (CSth), (ii) the power of Tx signal at the location of f is less than CSth, and (iii) a potential transmission from f will have a signal power greater than or equal to a Noise threshold ($\mathrm{P_n}$) as perceived in the location of Rx, assuming that any signal with power greater than or equal to $\mathrm{P_n}$ can be received in a node. The above definition is based on the assumption that $\mathrm{P_n} < \mathrm{CSth}$.

The probabilistic radio propagation model, described by Equations 5.1 and 5.2, implies that the hidden terminal problem has a probabilistic nature. Denote by HC the event that f as a hidden terminal of Tx contributes to the interference power in Rx. Also, denote by $\mathrm{PGN_f}$ the event that a signal propagated from node f is received in Rx with a power greater than $\mathrm{P_n}$. Furthermore, let $\mathrm{H_{(rx,tx)}}$ and $\mathrm{NH_{(f,tx)}}$ be the events corresponding to the conditions (i) and (ii) mentioned above. The probability of HC can be expressed as follows:

$$Pr(HC) \quad = \quad Pr\left(H_{(rx,tx)} \wedge NH_{(f,tx)} \wedge PGN_f\right) \tag{5.3}$$

The event $\mathrm{PGN_f}$ is determined by the distance between f and Rx ($d_{(f,rx)}$) and their shadowing state, i.e., whether they are in LOS, OLOS, or NLOS situation. This event is independent from events $\mathrm{H_{(rx,tx)}}$ and $\mathrm{NH_{(f,tx)}}$. On the other hand, events $\mathrm{H_{(rx,tx)}}$ and $\mathrm{NH_{(f,tx)}}$ are correlated and potentially dependent. These arguments imply that Equation 5.3 should be rewritten as follows:

$$Pr(HC) \quad = \quad Pr\left(H_{(rx,tx)} \wedge NH_{(f,tx)}\right) Pr\left(PGN_f\right) \tag{5.4}$$

To obtain Pr(HC) using the path loss function, the distances and the shadowing state of each pair of nodes should be given *a priori*. We describe the received power in various situations corresponding to the relative distance of a pair of nodes compared to the breaking point distance d_b, and the shadowing state of the pair of nodes by a set of random variables. Without loss of generality we assume all nodes are located on a road stretch where only LOS and OLOS situations occur. The arguments for the NLOS case are straightforward. Starting by the event $\mathrm{H_{(rx,tx)}}$ and given the distance between the two nodes denoted by $d_{(tx,rx)}$, the random variables corresponding to the received power in Rx from the Tx are shown in Tables 5.2 and 5.3. Table 5.2 describes the random variables for LOS situation and Table 5.3 shows the random variables for the OLOS case.

Table 5.2: Random variables for LOS situation

$d_{(tx,rx)} < d_0$	$X_0 = P_{tx} - IL$
$d_0 \leq d_{(tx,rx)} \leq d_b$	$X_1 \sim N\left(\mu_{LOS}(d_{(tx,rx)}), \sigma_{LOS}\right)$, where $\mu_{LOS}(d_{(tx,rx)}) = P_{tx} - PL0_{LOS} - IL - 10n_{1,LOS}\log_{10}\left(\frac{d_{(tx,rx)}}{d_0}\right)$
$d_{(tx,rx)} > d_b$	$X_2 \sim N\left(\mu_{LOS}(d_{(tx,rx)}), \sigma_{LOS}\right)$, where $\mu_{LOS}(d_{(tx,rx)}) = P_{tx} - PL0_{LOS} - IL - 10n_{1,LOS}\log_{10}\left(\frac{d_b}{d_0}\right) - 10n_{2,LOS}\log_{10}\left(\frac{d_{(tx,rx)}}{d_b}\right)$

Table 5.3: Random variables for OLOS situation

$d_{(tx,rx)} < d_0$	$X_0 = P_{tx} - IL$
$d_0 \leq d_{(tx,rx)} \leq d_b$	$X_3 \sim N\left(\mu_{OLOS}(d_{(tx,rx)}), \sigma_{OLOS}\right)$, where $\mu_{OLOS}(d_{(tx,rx)}) = P_{tx} - PL0_{OLOS} - IL - 10n_{1,OLOS}\log_{10}\left(\frac{d_{(tx,rx)}}{d_0}\right)$
$d_{(tx,rx)} > d_b$	$X_4 \sim N\left(\mu_{OLOS}(d_{(tx,rx)}), \sigma_{OLOS}\right)$, where $\mu_{OLOS}(d_{(tx,rx)}) = P_{tx} - PL0_{OLOS} - IL - 10n_{1,OLOS}\log_{10}\left(\frac{d_b}{d_0}\right) - 10n_{2,OLOS}\log_{10}\left(\frac{d_{(tx,rx)}}{d_b}\right)$

In Tables 5.2 and 5.3, $N(\mu, \sigma)$ is a normal distribution function with mean μ and standard deviation σ, P_{tx} is the transmission power of Tx measured in dBm, and IL is a constant value representing the implementation loss [8]. In the two tables, the original parameters n_1 and n_2 are subscripted by LOS and OLOS terms in order to distinguish the shadowing state of the node pairs. X_0 has a constant value determined by free-space path loss and the implementation loss. X_1, X_2, X_3, and X_4 are random variables representing the received power in Rx if the distance from Tx is greater than or equal to d_0. The Probability Density Functions (PDF) of the random variables are represented by f_{X_1}, f_{X_2}, f_{X_3}, and f_{X_4}, respectively. In a similar way to pair Tx/Rx, we identify the random variables and the PDFs corresponding to the received power in node f from Tx. Let Y_1, Y_2, Y_3, and Y_4 be such random variables and f_{Y_1}, f_{Y_2}, f_{Y_3}, and f_{Y_4} represent the corresponding PDFs. Similar to X_0, Y_0 is a constant value representing the received power when the distance between pair Tx/f (i.e., $d_{(tx,f)}$) is less than d_0.

Once the individual random variables corresponding to events $H_{(rx,tx)}$ and $NH_{(f,tx)}$ are determined as above, a set of bivariate normal density functions $f_{(X_i,Y_j)}$ for i , $j \in \{1,2,3,4\}$ can be identified, where $f_{(X_i,Y_j)}$ is expressed as follows:

$$f_{(X_i,Y_j)} = \frac{1}{2\pi\sigma_{X_i}\sigma_{Y_i}\sqrt{1-\rho_{ij}^2}} \exp\left(-\frac{1}{2(1-\rho_{ij}^2)}\left[\frac{(X_i-\mu_{X_i})^2}{\sigma_{X_i}^2} + \frac{(Y_i-\mu_{Y_j})^2}{\sigma_{Y_j}^2} - \frac{2\rho_{ij}(X_i-\mu_{X_i})(Y_j-\mu_{Y_j})}{\sigma_{X_i}\sigma_{Y_j}}\right]\right) \tag{5.5}$$

where ρ_{ij} is the correlation coefficient of X_i and Y_j. Let $F_{(x_i,y_j)}$ be the Cumulative Density Function (CDF) of joint variables (X_i, Y_j). It follows that:

$$Pr\left(H_{(rx,tx)} \wedge NH_{(f,tx)}\right) = F_{Y_j}(CSth) - F_{(X_i,Y_j)}(CSth, CSth) \tag{5.6}$$

A closed form expression for $F_{(X_i,Y_j)}(CSth, CSth)$ does not exist; however, there are a number of algorithms that estimate it numerically [176].

To that end, it remains to derive the expressions for Pr($\mathrm{PGN_f}$) in order to obtain Pr(HC) in Equation 5.4. Following the same line of arguments applied to events $\mathrm{H_{(rx,tx)}}$ and $\mathrm{NH_{(f,tx)}}$, we identify random variables Z_i, and PDFs f_{Z_i} for $i \in \{1,2,3,4\}$ describing the received (interference) power in Rx from node f. Note that Z_0 is analogous to X_0 and Y_0 and has a constant value $Z_0 = P_f - IL$, where P_f is the transmission power of node f. Given the distance between the pair of nodes f and Rx (denoted by $d_{(f,rx)}$) and recalling the definition of the event $\mathrm{PGN_f}$, it follows that:

$$Pr(GN_f) = \begin{cases} 1 & \text{if } d_{(f,rx)} < d_0 \wedge P_f - IL \geq P_{\mathrm{n}} \\ 0 & \text{if } d_{(f,rx)} < d_0 \wedge P_f - IL < P_{\mathrm{n}} \\ 1 - F_{Z_1}(P_{\mathrm{n}}) & \text{if } d_0 \leq d_{(f,rx)} \leq d_b \wedge LOS \\ 1 - F_{Z_2}(P_{\mathrm{n}}) & \text{if } d_{(f,rx)} > d_b \wedge LOS \\ 1 - F_{Z_3}(P_{\mathrm{n}}) & \text{if } d_0 \leq d_{(f,rx)} \leq d_b \wedge OLOS \\ 1 - F_{Z_4}(P_{\mathrm{n}}) & \text{if } d_{(f,rx)} > d_b \wedge OLOS \end{cases} \tag{5.7}$$

where F_{Z_i} is the CDF of the random variable Z_i.

At this point, the event HC is fully characterized and its probability can be obtained. The next step is to determine the interference power induced by the node f. The event HC, if occurs for node f, implies that the interference power induced by f must be greater than or equal to the noise power. Thus, we define truncated normal random variables $\widehat{Z_i}$ derived from Z_i. The domain of $\widehat{Z_i}$ (measured in dBm) is (P_{n}, ∞) and the corresponding density function is obtained as follows:

$$f_{\widehat{Z_i}} = \frac{f_{Z_i}}{1 - F_{Z_i}(P_{\mathrm{n}})} \tag{5.8}$$

Assuming that a message is being received in Rx from Tx, the expected interference power (due to node f) induced in a time slot of the message can be expressed as follows:

$$PI_{(f,rx)} = Pr\left(HC\right) Pr\left(f_{ovp}\right) \mathbb{E}\left(10^{\left(\frac{\widehat{Z_i}}{10}\right)}\right) \tag{5.9}$$

where $\mathbb{E}\left(.\right)$ is statistical expectation. $PI_{(f,rx)}$ is the expected interference power measured in mW. $Pr\left(f_{ovp}\right)$ is the probability that a transmission from f overlaps with a time slot of the message being received in Rx from Tx. The aggregate interference power in Rx induced by all hidden nodes is the sum of interference contributions of all nodes in the set $\mathbb{I}$:

$$PI_{(rx)} = \sum_{f \in \mathbb{I}} PI_{(f,rx)} \tag{5.10}$$

Accordingly, the expected SINR of a message received in Rx from Tx is as follow:

$$SINR_{(rx)} = \frac{\mathbb{E}\left(10^{\left(\frac{X_i}{10}\right)}\right)}{P_n + PI_{(rx)}} \tag{5.11}$$

Recall that X_i is the i^{th} random variable from the set of random variables representing the power of Tx's signal received in Rx.

It remains to obtain $\Pr(f_{ovp})$, the probability that a potential interferer f transmits a message and overlaps with a time slot of the Tx's message being received in the Rx. The decider module of a device or a simulator usually assesses the interference power within a sequence of time slots of the message time. For simplification, we fix the length of the decision sequence to 1 slot. With this setting, the interference power experienced in a slot time represents the interference power imposed on the entire message. A key MAC layer parameter determining $\Pr(f_{ovp})$ is the probability of message transmission in a time slot. In Chapter 4, the steady state transmission probabilities were derived for periodic and event-driven messages. The transmission probabilities are denoted by τ_b and τ_e, corresponding to periodic and event-driven messages, respectively. Let PE be the event that a periodic message of node f overlaps with a time slot of the message transmitted by Tx. Likewise, denote by EV the event that an event-driven message of the node f overlaps with a time slot of the message transmitted by Tx. It follows that:

$$Pr\left(f_{ovp}\right) = Pr\left(PE\right) + Pr\left(EV\right) - Pr\left(PE \wedge EV\right) \tag{5.12}$$

$\Pr(PE \wedge EV) = 0$, because a node is allowed to transmit one message at a time. The required parameters to determine the $\Pr(PE)$ and $\Pr(EV)$ are the data rate (R), the size of periodic message $\mathrm{M_b}$, the size of event-driven message ($\mathrm{M_e}$), and the slot duration (σ). The message time is obtained as $T_b = M_b/R$ and $T_e = M_e/R$, respectively for periodic and event-driven messages. The total number of slots occupied by periodic and event-driven messages are $N_b = \lceil T_b/\sigma \rceil$ and $N_e = \lceil T_e/\sigma \rceil$ respectively. It follows that $Pr\left(PE\right) = N_b\tau_b$ and $Pr\left(EV\right) = N_e\tau_e$. Albeit, the resultant probabilities are bounded to 1.

5.4 Effective Carrier Sense and Hidden Node Range

In Section 5.3, a theoretical framework was proposed to obtain the expected interference power of a hidden node (Equation 5.9) and the aggregate interference power of all hidden nodes (Equation 5.10). Revisiting Equation 5.9 reveals that potentially all nodes in the network will have some interference contribution in the intended recipients of Tx. This arises from the fact that $\Pr(HC)$ is non-zero for all nodes. Therefore, all nodes in the network are potentially hidden from the transmitter Tx. This hinders the development of an implementable and tractable analytical model characterizing the interference power of hidden nodes. For this reason, we relax the channel model by eliminating the non-deterministic element X_σ. Under this relaxation, the analysis is reduced to average path loss and thus average interference power.

By adopting the relaxed channel model, the probabilistic event HC is eliminated. Instead, it is required to deterministically identify the carrier sense distance (CSD) of Tx where the potential intended recipients are located. Similarly, the range of hidden terminals (HTR) of Tx is identified deterministically. We identify the ranges under question separately for LOS/OLOS and NLOS conditions. Figure 5.1 depicts the carrier sense distance and the hidden terminal range of Tx on the horizontal road RW-RE and vertical road segment RN. For readability, suffixes _H and _V are used to distinguish the ranges on the horizontal and vertical roads.

Finding the carrier sense distance from the path loss model proposed for LOS and OLOS situations (Equation 5.1) is not straightforward; depending on the shadowing state (LOS or OLOS) and whether CSD_H is greater or equal to the breaking point distance d_b, several options emerge. In the following line of argument, we eliminate the unlikely options using the notion of Desired Transmission Range (DTR) in single broadcast. DTR is the distance from the Tx where the received signal has a power greater than a threshold (RCth) and, in the absence of interference, the Signal to Noise Ratio (SNR) is large enough to decode the signal. The DTR for medium range safety applications is around 300 m [17; 43]. Long range safety applications may require single broadcast ranges up to 1 km [43].

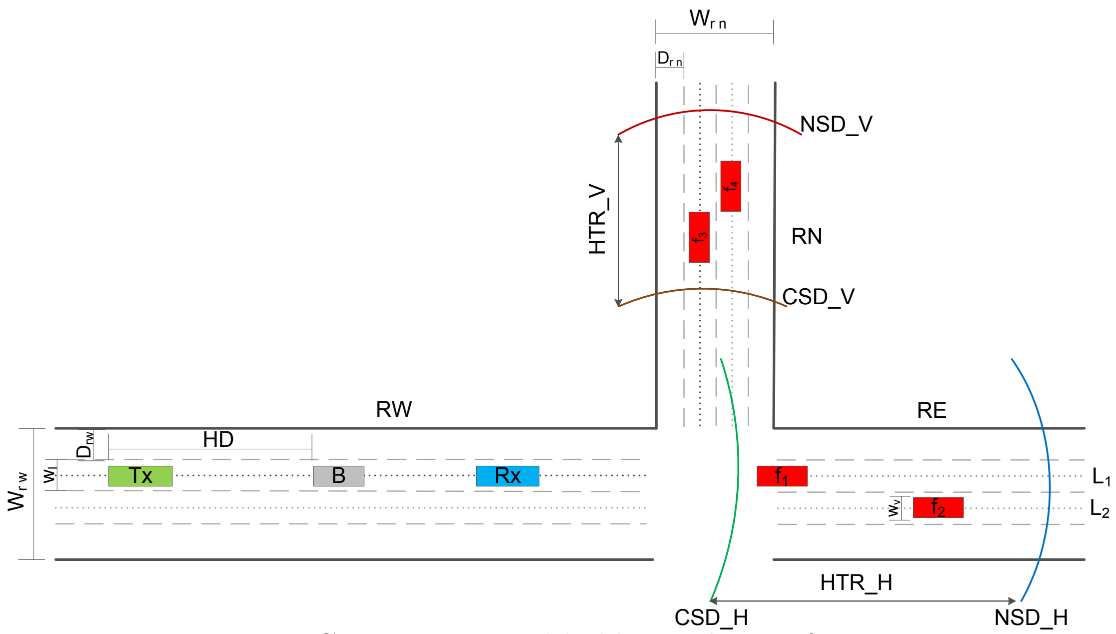

Figure 5.1: Carrier sense and hidden node interference regions

With DTR = 300 m as the presumed minimum DTR, the options corresponding to $CSD\_H < d_0$ and $d_0 \leq CSD\_H \leq d_b$ are eliminated from the set of options because otherwise, given that according to [8] $d_0 = 10$ m and $d_b = 104$ m, the resultant transmission range will be far shorter than the minimum DTR. With such a short transmission range, a number of safety applications are not supported. This leaves two options corresponding to the case $CSD\_H > d_b$ and branching from the two shadowing states LOS and OLOS, that is,

$$PL(CSD\_H) = \begin{cases} PL0_{LOS} + 10n_{1,LOS}\log_{10}\left(\frac{d_b}{d_0}\right) + 10n_{2,LOS}\log_{10}\left(\frac{CSD\_H}{d_b}\right) \\ PL0_{OLOS} + 10n_{1,OLOS}\log_{10}\left(\frac{d_b}{d_0}\right) + 10n_{2,OLOS}\log_{10}\left(\frac{CSD\_H}{d_b}\right) \end{cases} \tag{5.13}$$

Considering the fact that this work is focused on forced-flow traffic, we conjecture that OLOS assumption is a practical assumption in the calculation of the ranges under question. In support of this claim, an empirical study reported in [10] indicates that in the capacity traffic state, the average headway distance on a freeway segment does not exceed 42.5 m. On a multi-lane highway, the distance hardly reaches 38 m. In urban streets, the capacity headway distance is less than

35 m. Assuming that vehicles tend to drive in the middle of the lanes in which they are situated, the above figures imply that the LOS distance on a lane, that is, the distance to which LOS is not obstructed, is far shorter than the DTR of even short range safety applications.

For completeness of the argumentation, we perform a simple numerical study to investigate the LOS distance of a Tx node as a function of mean headway time (HT). We obtain the headway distances (HD) corresponding to a range of prevalent velocities in urban traffic systems using the relationship $HD = HT \times V$, where V stands for velocity. A road segment with 5 lanes in each direction is used for the study. A transmitter Tx and an intended receiver Rx are located on a lane with another vehicle being in the middle (vehicle B in Figure 5.2). The LOS distance from the standpoint of Tx is then calculated assuming that the following vehicle B is located at a distance from Tx equal to the given headway distance, and B is the only source of LOS obstruction. Assuming that vehicles drive in the middle of the lanes in which they are situated, it follows that the LOS distance on the Tx's lane is equal to HD. To determine the LOS distance on a neighbouring lane (i.e., the upper lane in Figure 5.2), it is sufficient to obtain the length of segment s_2. Given the lane width (W_l), vehicle width (W_v), and vehicle length (L_v), it follows that $s_1 = HD - L_v/2$ and $\tan(\alpha) = \frac{2s_1}{W_v} = \frac{2(HD-L_v/2)}{W_v}$. The LOS distance on the neighbouring lane is equal to s_2 and is obtained as: $s_2 = W_l\left(\frac{2(HD-L_v/2)}{W_v}\right)$. It is straightforward to extend this argument to any lane in the network. Assume the lane index of Tx is l_{tx} and the index of the lane under investigation for LOS distance is l_n. It follows that for lane l_n, $s_2 = |l_{tx} - l_n|\, W_l\left(\frac{2(HD-L_v/2)}{W_v}\right)$.

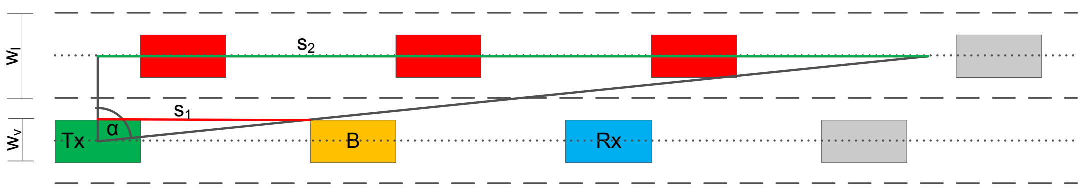

Figure 5.2: The projected LOS distance of Tx on a neighbouring lane

Figure 5.3 depicts the numerical results. The results shown in Figure 5.3a

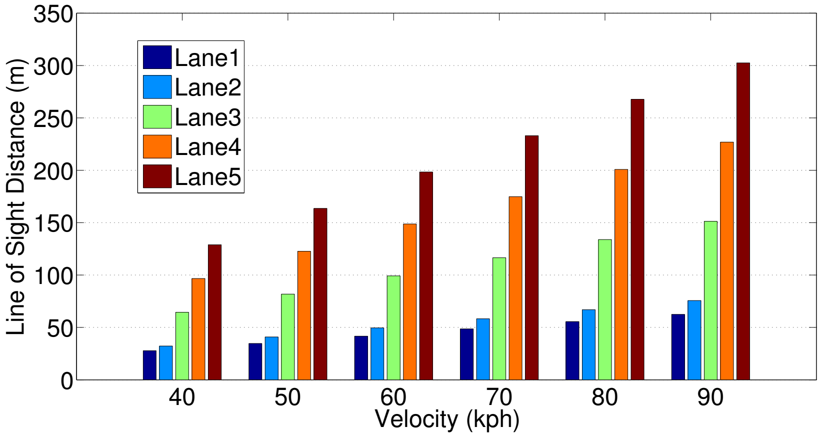

(a) LOS distance in normal traffic density (headway time = 2.5 seconds)

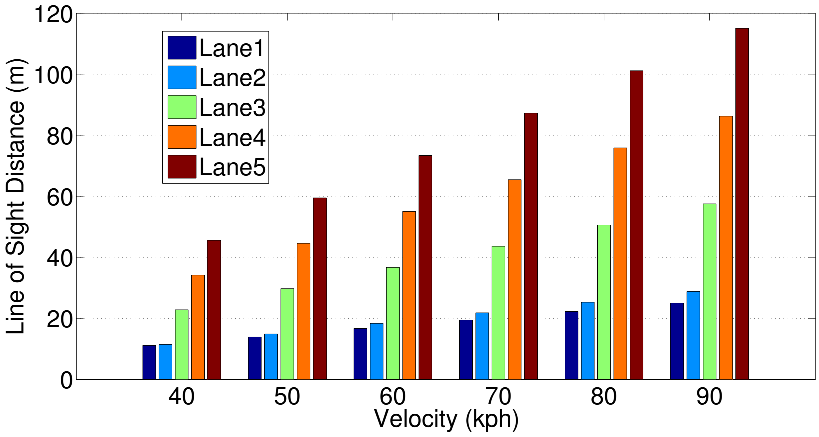

(b) LOS distance in traffic situation near capacity (headway time = 1 second)

Figure 5.3: LOS distance in urban traffic settings

correspond to a forced-flow traffic condition with a relatively large headway time of 2.5 seconds. The results in Figure 5.3b are obtained for HT = 1 second, corresponding to near capacity traffic conditions. In our study, we use passenger vehicles as the dominant vehicle type in urban areas. Accordingly, the width and length of vehicles are set to $W_v = 1.6$ m and $L_v = 4$ m, corresponding to the size of a typical passenger car, according to Paramics traffic simulator [49]. The lane width is set to $W_l = 3.7$ m, representing the width of a typical urban major road. According to Figure 5.3a, the obstruction occurs almost certainly in distances beyond 300 m on all lanes. In near capacity traffic conditions, as our main focus in this work, the largest LOS distance drops to 120 m. Recall that, in the above analysis, only the effect of a following vehicle of Tx is accounted for as the source of obstruction. In practice, due to obstruction by vehicles driving on lanes other than Tx's lane, the LOS distance in farther lanes are predicted to be significantly smaller than the results shown in Figures 5.3a and 5.3b.

The above evidence implies that the LOS distance in forced-flow traffic is shorter than the minimum DTR required for medium range applications. Given that the transmission power is tuned in such a way that the minimum DTR is reached and given that $DTR \leq CSD\_H$, it follows that the OLOS assumption in the calculation of CSD_H is a rational and practical assumption. With OLOS assumption and using the path loss parameters for the OLOS situation, the carrier sense distance for the horizontal road stretch in Figure 5.1 is expressed as follows:

$$CSD\_H = d_b 10^{\left(\frac{P - CSth - PL0_{OLOS} - IL - 10n_{1,OLOS}\log_{10}\left(\frac{d_b}{d_0}\right)}{10n_{2.OLOS}}\right)} \tag{5.14}$$

We discarded the subscript of transmission power (P), assuming that all nodes transmit with the same power.

A further step towards the identification of hidden terminal range is to determine the distance from Rx where an interferer can induce an interference power greater than or equal to the noise threshold ($\mathrm{P_n}$). Denoting such distance on the horizontal road by NSD_H, it is evident that NSD_H > CSD_H. Therefore, the OLOS assumption is also applied in the calculation of NSD_H. Using the path loss parameters for OLOS situation, NSD_H can be expressed as follows:

$$NSD\_H = d_b 10^{\left(\frac{P - P_{\mathrm{n}} - PL0_{OLOS} - IL - 10n_{1,OLOS}\log_{10}\left(\frac{d_b}{d_0}\right)}{10n_{2,OLOS}}\right)} \tag{5.15}$$

Given that CSD_H and NSD_H are determined as above for the horizontal road, we set the hidden terminal range of Tx with respect to Rx to $HTR\_H =$ [CSD_H , NSD_H].

In the NLOS case, the regions under investigation are located on the cross roads linked to the intersection (e.g., segment RN in Figure 5.1). Consider a typical case where Tx and Rx are positioned on segment RW in such a way that

NLOS is certain to occur between them and the nodes on segment RN. The road parameters required for calculating CSD_V and NSD_V are shown in Figure 5.1. W_l is the lane width, and W_{rw} and W_{rn} are the width of horizontal and vertical streets, respectively. D_{rw} (D_{rn}) is the gap between RW (RN) street and the wall to the top (left). Let $d_{j,tx}$ be the distance from the intersection center to Tx. Further assume that the lanes of road RW are indexed in increasing order from top to bottom, and from left to right on road RN. Let l_{tx} be the index of the lane where Tx is located. It follows that the distance of Tx to the wall is $x_{tx} = (l_{tx} - 1)\, W_l + \frac{W_l}{2} + D_{rw}$. It then follows that the CSD_V of Tx, projected to any lane on segment RN, is either

$$CSD\_V = \frac{\lambda(x_{tx}W_{rn})^{0.81}}{4\pi(d_{j,tx})^{0.957}} 10^{\left(\frac{P-CSth-3.75}{10\, n_{NLOS}}\right)} \tag{5.16}$$

or

$$CSD\_V = \left(\frac{\lambda d_b(x_{tx}W_{rn})^{0.81}}{4\pi(d_{j,tx})^{0.957}} 10^{\left(\frac{P-CSth-3.75}{10\, n_{NLOS}}\right)}\right)^{\frac{1}{2}} \tag{5.17}$$

Applying Equation 5.16 to calculate CSD_V must yield $CSD\_V \leq d_b$, whereas by Equation 5.17 $CSD\_V > d_b$. These two cases are not satisfied simultaneously. Thus, the valid CSD_V is unique.

In contrast with CSD_V, the NSD_V on the vertical road RN will have different values for different lanes. The projection of NSD_V on a lane l_n is expressed as follows:

$$NSD\_V(n) = \begin{cases} \left(\frac{\lambda(x_n W_{rw})^{0.81}}{4\pi d_{j,rx}} 10^{\left(\frac{P-P_{\mathrm{n}}-3.75}{10\, n_{NLOS}}\right)}\right)^{\frac{1}{0.957}} & \text{if } d_{j,rx} \leq d_b \\ \left(\frac{\lambda d_b(x_n W_{rw})^{0.81}}{4\pi(d_{j,rx})^2} 10^{\left(\frac{P-P_{\mathrm{n}}-3.75}{10\, n_{NLOS}}\right)}\right)^{\frac{1}{0.957}} & \text{if } d_{j,rx} > d_b \end{cases} \tag{5.18}$$

where x_n is the distance to the left wall of road segment RN from the middle of the lane l_n. This distance is $x_n = (l_n - 1)\, W_l + \frac{W_l}{2} + D_{rn}$, where $d_{j,rx}$ is the distance between Rx and the intersection center.

5.5 Traffic Scenarios

Two major building blocks of urban traffic networks are addressed in this work: an isolated stretch of road and a signalised intersection. The road stretch scenario represents an isolated arterial or transit road or part of a road connected to an intersection, but does not include the region of the intersection where the queueing and traffic discharge take place. In this scenario, a safety-critical traffic state is identified and modelled using cellular automata (CA) [47], proven to capture the traffic behaviour in various scenarios effectively [48; 141; 161]. The traffic model is used in a simple procedure to determine an upper bound interference power at any intended message recipient of a leading vehicle, and a lower bound reachable distance of safety messages transmitted by the vehicle. In the intersection scenario, a probabilistic CA model is proposed to model the traffic scenario, and a procedure is designed to determine an upper bound interference power for the entire intersection. The intersection scenario is generally considered a safety-critical scenario, according to the statistics of road crash investigations [80].

5.6 Road Stretch Scenario

5.6.1 Characterizing a Safety-Critical Traffic State

Traffic safety relates to vehicle velocity and the headway distance preserved by drivers. Given a road segment with speed limit V and assuming that drivers do not violate the speed limit, we characterize a safety-critical state with two conditions met simultaneously: (i) vehicles drive with velocity V, and (ii) vehicles preserve a minimum safe distance. The occurrence of both conditions corresponds to the situation where a road segment operates at its capacity [142]. Capacity is measured in vehicles/hour and is described by the maximum traffic flow that can be accommodated in a single lane of a road segment. The most frequently used expression for capacity is [142]:

$$C = 1000 \frac{V}{S} \tag{5.19}$$

where C is capacity, and S is the average headway distance measured in meters and is expressed by the following equation [142]:

$$S = \alpha + \beta V + \gamma V^2 \tag{5.20}$$

where α is the effective length of a vehicle, β is the driver reaction time also denoted by t_r, and γ is inversely proportional to the deceleration of a following vehicle [142]. Given the average maximum deceleration rates of a leading and a following vehicle denoted by a_l and a_f, an expression for γ is $\gamma = 0.5\left(\frac{1}{a_f} - \frac{1}{a_l}\right)$ [142]. For simplification, we assume vehicles have similar braking performance. This translates to $\gamma = 0$ and the *minimum safe distance* is expressed as follows [189]:

$$S_{min} = \alpha + \beta V \tag{5.21}$$

From the perspective of safety applications envisioned for VANETs, in a traffic network operating at its capacity, vehicles require greater communication reliability and a longer message reachable distance compared to under-capacity traffic states. Failure to fulfil any of these conditions leads to weak driver awareness, and thus affects the reliability of safety applications. Hidden terminal interference is one of the issues which affects the reachable distance of safety messages and thus the reliability of the communication network [163; 164]. In a capacity traffic state, it is deemed that the impact of hidden node interference on the reachable distance of safety messages is non-negligible. This arises from the fact that, in this traffic state, the number of interferers is larger and the distance from interferers to the location of an intended message recipient is smaller compared to under-capacity traffic states. This leads to larger aggregate interference power in a receiver.

The capacity of a road segment is a theoretical upper bound on traffic flow. Despite the efforts of the designers of transportation systems, the capacity is not reached in practice and thus traffic networks operates in under-capacity states. In terms of hidden node interference, we propose that the hidden terminal interference in the theoretic capacity state is an upper bound to the resulting actual capacity. In the following section, the traffic model and the required mechanisms are designed to characterize the hidden node interference for theoretic capacity.

5.6.2 Traffic Model

According to the path loss model introduced in Section 5.2, characterization of interference power in a node requires that the positions of the intended receivers and the potential interferers and also the obstruction information are known. In a real traffic network, vehicle position is a continuous quantity. While using a continuous quantity leads to accurate modelling of traffic, it imposes a side effect on the tractability of the mechanisms used to characterize the interference. To relax the position continuum in favour of model's tractability, the traffic network is discretized by means of cellular automata.

The traffic scenario consists of a bidirectional road stretch operating in capacity state. The number of lanes in each direction is unconstrained. In the CA model, each lane of a road segment is divided into equal size cells (Figure 5.4). In the conventional CA models, a cell is assumed to have a square shape, whereas in this work due to the dependence of shadowing on the length and the width of vehicles, a rectangular cell shape is assumed. The length and width of the cell are denoted by Δ and Γ, and are related to the size of vehicles. With the variety of vehicle sizes, the configuration of Δ and Γ is driven by the objectives pursued in this study. A generic approach is to set the parameter values to the average length and width of vehicles in the network; however, this approach may compromise the accuracy of the study in its entirety. In the current work, the location of antenna installed on top of a vehicle is seen as an important factor influencing the signal strength. The variation of latitudinal dimension of antenna location is limited to the vehicle's width which at most is equal to the lane width, whereas in longitudinal dimension the variation is driven by the length of the longest vehicle, which can be significant. Therefore, for the sake of fine granularity in the longitudinal dimension, Δ is set to the length of the smallest vehicle in the network. Γ is set to the average width of vehicles in the network. Another assumption applied to the CA model is that the longitudinal axis of vehicles coincides with the middle line of the lane they are situated in, corresponding to the situation where vehicles drive in the middle of their current lanes.

The state of a cell (i.e., whether or not it is occupied by a vehicle) is assigned by a set of rules designed to maintain the compliance of the CA model with the traffic parameters and regulations governing the road stretch. The cell state takes a value from a domain $\{-1, 0, 1\}$ and determined by a rule set Λ consisting of the following rule items:

1. *occupation:* if a cell is occupied by a vehicle, the cell state is set to either 1 or -1, otherwise the cell state is set to 0.

2. *antenna location:* this rule is enforced to distinguish between the front cell of a vehicle where the antenna is installed and the trailer cells. If a cell is occupied by the front part of a vehicle, the cell state is set to 1 and for the trailer parts the corresponding cell states are set to -1.

3. *driving direction:* if a vehicle occupies more than a cell, the precedence of cell states 1 and -1 corresponding to the vehicle is determined by the driving direction. The state of the first cell in the driving direction is 1 and the states of the remaining cells are -1.

4. *vehicle length:* according to this rule, if the state of a cell is 1, a number of cells equal to $Lv_c - 1$ must be set to -1 where Lv_c is vehicle length measured in number of cells. The precedence of the trailer cells (i.e., whether they are before or after the current cell) is determined by the driving direction rule.

5. *headway preserving:* in each lane, if the state of a cell is 1, the next cell with state 1 is $HD_c + 1$ cells away from the current cell. $\mathrm{HD_c}$ is the headway distance measured in number of cells.

The implementation of the CA model requires that the real values of the headway distance and vehicle length are transformed to the number of cells. To this aim, we set $HD_c = \lfloor \frac{S_{min}}{\Delta} \rfloor$ and $Lv_c = \lfloor \frac{\hat{L}_v}{\Delta} \rfloor$, where S_{min} and $\hat{L}_v$ are the minimum safe headway distance and the average size of vehicles, respectively. The floor operator ensures that the transformed headway distance does not exceed the actual minimum headway distance. To determine $\hat{L}_v$, without loss of generality, we assume there are three categories of vehicles in the network: small, medium,

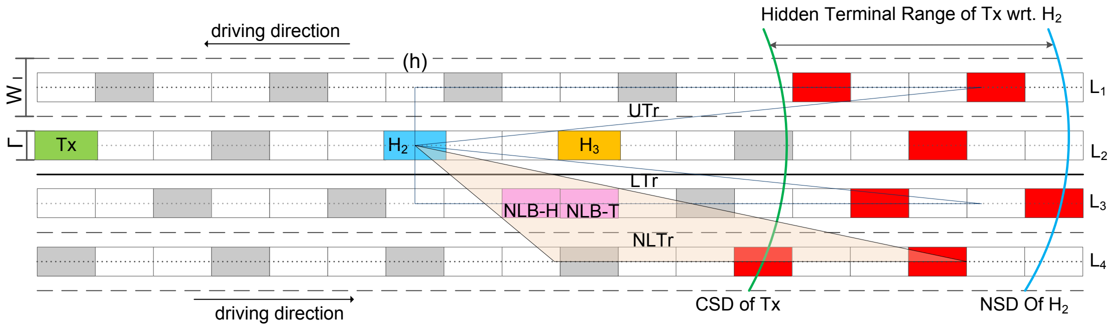

Figure 5.4: Road stretch scenario

and large vehicles. The real lengths of the three categories are denoted by $\hat{L}_s$, $\hat{L}_m$, and $\hat{L}_l$, and the vehicles' populations (%) are represented by p_s, p_m, and p_l, respectively. It follows that

$$\hat{L}_v = p_s\hat{L}_s + p_m\hat{L}_m + p_l\hat{L}_l \tag{5.22}$$

Similarly, the width of the CA cell is obtained as follows:

$$\Gamma = p_s\hat{W}_s + p_m\hat{W}_m + p_l\hat{W}_l \tag{5.23}$$

where $\hat{W}_s$, $\hat{W}_m$ and $\hat{W}_l$ are the real width of the three types of vehicles.

5.6.3 Maximum Aggregate Interference Power

Suppose a transmitter Tx and a number of intended recipients termed "hops" are located on a lane of the road stretch (H_is in Figure 5.4). Lanes are indexed in increasing order from the top lane to the bottom one. Assume the intended recipient under investigation is the hop H_2. Initially, Tx and H_2 are indexed with respect to their relative cell positions on the road stretch. The index of Tx is set to 1 and the index of H_2 is h. The rest of cells on all lanes are indexed in increasing order to the right of Tx. The cells on the same column have identical indices.

In the next step, the parameters CSD and NSD [1] are obtained using Equa-

[1]For readability, the suffix _H corresponding to horizontal road stretch is eliminated.

tions 5.14 and 5.15. Denote by CSD_c and NSD_c the data structures used to maintain, for all lanes, the indices of the boundary cells corresponding to CSD and NSD. On a lane $\mathrm{L_n}$, the index of the cell located on the boundary of CSD is $CSD_{c,n} = \lfloor \frac{\sqrt{CSD^2-(|L_n-L_h|W_l)^2}}{\Delta} \rfloor + 1$, where $\mathrm{L_h}$ is the lane number of the hop. Likewise, the index of the cell located on the boundary of NSD with respect to the cell position of the hop is $NSD_{c,n} = \lceil \frac{\sqrt{NSD^2-(|L_n-L_h|W_l)^2}}{\Delta} \rceil + h$. The flooring and ceiling operators are carefully chosen for larger interference contribution.

The aggregate interference power experienced in the hop situated on cell h is driven by the arrangement of nodes in the region $[h, NSD_c]$ of the road stretch. Given that there are many possible arrangements, we propose a procedure to find the arrangement that yields the maximum aggregate interference power in the hop (Algorithm 5.1).

In Algorithm 5.1, RS is the road stretch represented by the CA model with the initially empty cells. $\mathrm{PAR_{dsrc}}$ and $\mathrm{PAR_{ch}}$ are DSRC and channel model parameters, respectively. Λ is the set of CA rules. UL and HL are the projections of the road segment corresponding to the upper lanes and the hop's lane, respectively. The upper lanes are identified with respect to the hop's lane. The indices of the boundary cells in the hidden terminal region are maintained in HTR_c. Ω is a data structure used to maintain, for all lanes, the indices of occupied cells with state 1 located in the hidden terminal region, and are obstructed from the hop's LOS. D maintains the distance between such cells and the hop. Ψ is the set of all possible arrangements of nodes on the upper lanes, each conforming to the CA rules. j is the index of the first cell among the cells occupied by the vehicle following the hop, and located on the same lane as the hop (e.g., $\mathrm{H_3}$ in Figure 5.4). The parameters Δ and Γ are implicit to the procedure and are retrieved wherever required.

Algorithm 5.1 calculates the maximum aggregate interference power $P_{if,max}$ induced by the hidden nodes situated on the upper lanes UL of the hop and also the nodes located on the hop's lane (L_h). A similar procedure is applied to the lower lanes with the exception that the interference from the hidden nodes on the hop's lane is excluded in order to be accounted for only once. The ultimate interference power is the sum of the powers reported by the two procedures. With an assumption of non-curved road stretch, separating the upper and lower

Algorithm 5.1 Maximum aggregate hidden terminal interference power in a hop

Require: road stretch RS, HD_c, hop lane L_h, hop index h, CSD_c, NSD_c, PAR_{dsrc}, PAR_{ch}
Require: vehicle length LV_c, CA rule set Λ

1: $P_{if,max} \leftarrow 0$
2: $HTR_c \leftarrow [CSD_c, NSD_c]$
3: $UL \leftarrow RS\,(1 : L_h - 1)$
4: $HL \leftarrow singleLaneNodeArrange\,(RS(L_h), h, \Lambda)$
5: $j \leftarrow getFollowingVehIndex(h)$
6: $isObstHTR \leftarrow checkObst(UL, HL, h, j, HTR_c)$
7: **if** $isObstHTR$ **then**
8:     $UL \leftarrow leastDistArrange(UL, HTR_c, \Lambda)$
9:     $\Omega \leftarrow getObstCellIndices\,(UL, HL, h, HTR_c)$
10:     $D \leftarrow getDistanceMap(UL, HL, h, HTR_c)$
11:     $P_{if,max} \leftarrow calcAggPow\,(\Omega, D, PAR_{dsrc}, PAR_{ch})$
12: **else**
13:     $\Psi \leftarrow getAllArrangements(UL, h, \Lambda)$
14:     $n \leftarrow 0$
15:     **while** $n \leq size(\Psi)$ **do**
16:         $UL \leftarrow \Psi(n)$
17:         $\Omega \leftarrow getObstCellIndices\,(UL, HL, h, HTR_c)$
18:         $D \leftarrow getDistanceMap(UL, HL, h, HTR_c)$
19:         $P_{if} \leftarrow calcAggPow\,(\Omega, D, PAR_{dsrc}, PAR_{ch})$
20:         **if** $P_{if} \geq P_{if,max}$ **then**
21:             $P_{if,max} \leftarrow P_{if}$
22:         **end if**
23:         $n \leftarrow n + 1$
24:     **end while**
25: **end if**
26: **return** $P_{if,max}$

lanes does not change the outcome, because the vehicles on the upper lanes do not impact the shadowing status between the hop and the vehicles on the lower lanes, and vice versa. Furthermore, this strategy improves the time complexity of the procedure by eliminating unnecessary computations related to shadowing. In the following paragraph, the core functionalities are briefly described.

The hidden terminal region HTR_c is initialized with the boundary cells in CSD_c and NSD_c (line 2). The projection of RS corresponding to the upper lanes and the hop lane are stored in UL and HL, respectively (line 3 and 4). Also in line 4 an arrangement of nodes is implemented on the hop lane, given the hop index h and the rule set Λ. The index of the first occupied cell of an immediately following vehicle is found (line 5) and checked if this vehicle obstructs the LOS of the hop and the entire HTR region (line 6). If so, the procedure enters a simple phase where the maximum interference is only determined by the distance between the vehicles in HTR and the hop (lines 8–11). This node arrangement is implemented in line 8 and the obstruction and distance map are constructed in lines 9 and 10, respectively. If there is at least one cell in HTR whose LOS with hop is not obstructed, the procedure implements all possible arrangements of nodes on the upper lanes and iterates through each arrangement case to find the arrangement yielding the maximum aggregate interference power (lines 12–25).

a) Generation of node arrangements

In a general CA framework, the number of node arrangements grows exponentially with the number of lanes and the number of cells on each lane. Thus, finding a node arrangement yielding the maximum interference is possibly a NP-hard or NP-complete problem. We reduce the size of the problem by enforcing a number of strategies. The first strategy, as mentioned above, is to divide the problem into sub-problems corresponding to the upper and lower lanes. The second strategy is to restrict the problem only to the cells situated between the hop cell (h) and the boundary cells in $\mathrm{NSD_c}$ for all lanes. This strategy is valid because such cells are the only ones affecting shadowing and the aggregate interference power induced in the hop. With the first and second strategies being implemented, the third strategy is to assess the LOS obstruction caused by the following vehicle of the hop ($\mathrm{H_3}$ in Figure 5.4) on the upper lanes (similarly for lower lanes) prior to the generation of node arrangements. Under certain conditions, as we address later, this strategy leads to the generation of only one arrangement of nodes, and the maximum interference power corresponds to such a node arrangement. This strategy is implemented in lines 4–11 of Algorithm 5.1.

The last and the most promising strategy is to resort to the traffic parameters in order to reduce the size of each sub-problem. Headway distance ($\mathrm{HD_c}$) is a promising parameter as its application can yield a significant reduction in the problem size. The implementation of this strategy on the sub-problem corresponding to upper lanes is as follows. Initially, given the index of the hop cell (i.e.,h), the remainder of nodes are arranged on the hop's lane using the *headway preserving* rule in the rule set Λ. This step is implemented by function *singleLaneNodeArrange* (line 4, Algorithm 5.1). The *headway preserving* rule is used again to arrange the nodes on the other upper lanes (and similarly for lower lanes). This rule implies that exactly one node must be located at the cell range $[h, h + HD_c - 1]$ on any upper lane (similarly on lower lanes). This node will be the first one appearing on an upper lane with respect to the hop cell. Using the *headway preserving* rule, the rest of the nodes are arranged on the upper lane up to the boundary cell in $\mathrm{NSD_c}$ corresponding to this lane. The total number of choices corresponding to the location of the first node on a lane is $HD_c - 1$.

The core task of arrangement generation implemented by function *getAllArrangements* (line 13, Algorithm 5.1) is to generate all possible arrangement of nodes for the upper lanes. Note that the arrangement of nodes on the hop's lane remains fixed in all arrangements. Once the set of all arrangements is known, Algorithm 5.1 iterates through the arrangements (lines 15–24). For each arrangement, functions *getObstCellIndices*, *getDistanceMap*, and *calcAggPow* are invoked to build or update Ω and D, and calculate the aggregate interference power corresponding to the iterated arrangement. Finally, the maximum aggregate interference power is reported at line 26.

The obstruction map Ω plays a key role in the procedure. The obstruction caused by the first following vehicle and also the vehicles on all other lanes are taken into account to build Ω corresponding to a node arrangement. We address the two obstruction cases separately.

b) LOS obstruction by the vehicle following the hop

A projection of the cells from Figure 5.4 located on the hop's lane and also on an upper lane is shown in Figure 5.5. The right triangle $ULTr$ (in Figure 5.4) represents the area on the upper lane with the most of its cells not being obstructed by the vehicle following the hop (i.e., $\mathrm{H_3}$), though some cells located to the rightmost side of the triangle may be obstructed. To find the index of the last non-obstructed cell, we identify three line segments s_1, s_2, and s_3 on the triangle.

s_1 is a segment starting from the middle of the hop's cell and ending at the upper left corner of the cell occupied by H_3. The length of s_1 is $\frac{(2HD_c-1)\Delta}{2}$, where $\mathrm{HD_c}$ is the headway distance. The tangent of the angle α corresponding to the lower vertex of $ULTr$ can be obtained from s_1 as follows:

$$\tan(\alpha) \quad = \quad \frac{2s_1}{\Gamma} = \frac{(2HD_c-1)\Delta}{\Gamma} \tag{5.24}$$

s_2 is a segment starting from the middle of the cell h on the upper lane and ending at the point where the hypotenuse of the triangle intersects the side of a cell on the upper lane. The length of s_2 is $\left(W_l - \frac{\Gamma}{2}\right)\tan(\alpha)$, where W_l is the lane width. A generalized expression for s_2 on any upper or lower lane $\mathrm{L_n}$ is

$$s_2 \quad = \quad \left(|L_n - L_h|\, W_l - \frac{\Gamma}{2}\right)\frac{(2HD_c-1)\Delta}{\Gamma} \tag{5.25}$$

s_3 starts from the center of the cell h on the upper lane. It ends at the intersection point of the hypotenuse and the middle line on the upper lane. It follows that $s_3 = \tan(\alpha)W_l = \frac{(2HD_c-1)\Delta}{\Gamma}W_l$. For any upper/lower lane $\mathrm{L_n}$, s_3 is expressed as follows:

$$s_3 \quad = \quad |L_n - L_h|\,\frac{(2HD_c-1)\Delta}{\Gamma}W_l \tag{5.26}$$

Using line segment s_2, the minimum index of the first obstructed cell on the upper

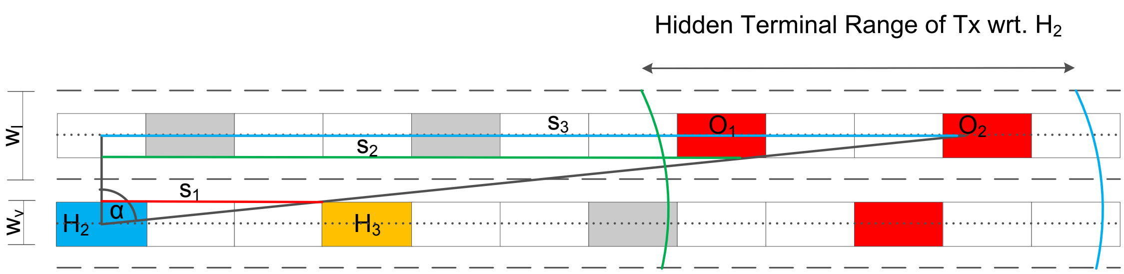

Figure 5.5: Obstruction caused by H_3 as the direct follower of hop H_2

lane is determined (cell o_1 in Figure 5.5). The index of such cell is identified as follows. Define $s' = s_2 - \frac{\Delta}{2}$ and $s'' = s' - \lfloor\frac{s'}{\Delta}\rfloor\Delta$. If $s'' \geq \frac{\Delta}{2}$, the index of o_1 is $\lceil\frac{s'}{\Delta}\rceil + h$ otherwise it is $\lfloor\frac{s'}{\Delta}\rfloor + h$. Using line segment s_3 and following the same arguments, the maximum index of the first obstructed cell (cell o_2 in Figure 5.5) is determined. Applying the above arguments to any lane within the upper-lanes or lower-lanes sub-problems yields a pair of indices o_1 and o_2 corresponding to that lane. For the convenience of the following arguments, notations $\mathrm{o}_{1,\mathrm{n}}$ and $\mathrm{o}_{2,\mathrm{n}}$ correspond to the minimum and maximum indices of obstructed cells on a lane L_n.

Cell indices o_1 and o_2 serve two purposes. Before the implementation of node arrangements, where only the indices of the hop and the following vehicle are known, o_2 will determine whether or not the obstruction from the following vehicle of the hop advances into the hidden node region. For a given lane L_n, such decision is made by comparing $\mathrm{o}_{2,\mathrm{n}}$ and the boundary cell $\mathrm{CSD}_{c,n}$ on the hidden terminal region. In the upper-lanes sub-problem, if for any lane L_n, $\mathrm{o}_{2,\mathrm{n}} < CSD_{c,n}$, then the procedure of implementing all possible node arrangements reduces to a single arrangement whose cells in the hidden terminal region overlapping with the upper lanes are obstructed. For this node arrangement, which is produced by function *leastDistArrange* in Algorithm 5.1, the outcome interference power is only determined by the distances of hidden nodes from the hop. In this situation, the maximum aggregate interference power corresponds to the case where the closest cells to the hop on the hidden terminal region are occupied by vehicles (i.e., cells $\mathrm{CSD}_{c,n} + 1$ for all lanes L_n). Given the location of the first interferer on a lane, the locations of other occupied cells on that lane are determined using the CA rules.

In the case that $\mathrm{o}_{1,\mathrm{n}}$ or $\mathrm{o}_{2,\mathrm{n}}$ indicates an advancement into the hidden node region on a lane L_n, then all possible arrangements of nodes are generated to find the arrangement yielding the maximum aggregate interference power. Given a particular node arrangement, the exact index of the first obstructed cell on lane L_n is found by iterating from cell index $\mathrm{o}_{1,\mathrm{n}}$ to $\mathrm{o}_{2,\mathrm{n}}$ and checking the cells in between. The index of the first cell with state 1 or -1 (occupied by a vehicle) determines the first obstructed cell on the lane L_n. Denote the index of this cell by o_n. The set of the obstructed occupied cells on the lane L_n represented by Ω_n is updated by adding the cell indices in range $[o_n, NSD_{c,n}]$ on condition that the cell state is 1, implying the obstruction of the front part of the vehicle where the antenna is installed. The cells on the lane L_h and beyond the location of H_3 are all considered as obstructed cells. The indices of those cells with state 1 are then added to the h^{th} row of Ω (i.e., Ω_h).

The above arguments are similarly applied to the lanes in the lower-lanes subproblem. It remains to address the case of obstruction caused by occupied cells other than the vehicle following the hop.

c) LOS obstruction by vehicles on other lanes

We investigate the obstruction caused by vehicles situated on lanes different from the hop's lane. Figures 5.6 and 5.7 illustrate projections of Figure 5.4 corresponding to the obstruction caused by a vehicle located on a lane different from the hop's lane. For the sake of generalization, we consider an obstructing vehicle occupying more than a cell, with cell NLB-H representing the header cell and NLB-T the trailer of the vehicle. In the following, we identify the cells on various lanes being obstructed by this vehicle. Assume the indices of NLB-H and NLB-T are j and k, respectively. Further, assume the lane of the obstructing vehicle is L_o. On a lane L_n, we determine the indices of the start and end cells obstructed by this vehicle. The geometry required to find the index of the starting obstructed cell is illustrated in Figure 5.6. For convenience, the cell indices are shown above the cells. All triangles in the figure are right angled triangles. β is the angle of the upper vertex of the largest triangle. The length of the line segment s_1 is obtained as $s_1 = (j-h)\,\Delta - \frac{\Delta}{2}$. Accordingly, the tangent of β is expressed as follows:

$$\tan(\beta) \quad = \quad \frac{s_1}{|L_o - L_h| W_l + \frac{\Gamma}{2}} = \frac{(j-h)\Delta - \frac{\Delta}{2}}{|L_o - L_h| W_l + \frac{\Gamma}{2}} \tag{5.27}$$

s_2, as shown in Figure 5.6, is a line segment starting from the cell with index h on lane L_n and ending at the intersection point of the triangle's hypotenuse with the side of a cell on lane L_n (the upper side of cell (e)). The length of s_2 can be obtained as follows:

$$s_2 \quad = \quad \left(|L_n - L_h|\, W_l + \tfrac{\Gamma}{2}\right) \tan(\beta) = \left(|L_n - L_h|\, W_l + \tfrac{\Gamma}{2}\right) \frac{(j-h)\Delta - \frac{\Delta}{2}}{|L_o - L_h| W_l + \frac{\Gamma}{2}} \tag{5.28}$$

The line segment s_2 determines the index of cell (e), which in turn helps determine the start cell of the sequence of the obstructed cells on lane L_n. Whether the cell (e) itself is the starting obstructed cell depends on how far the intersection

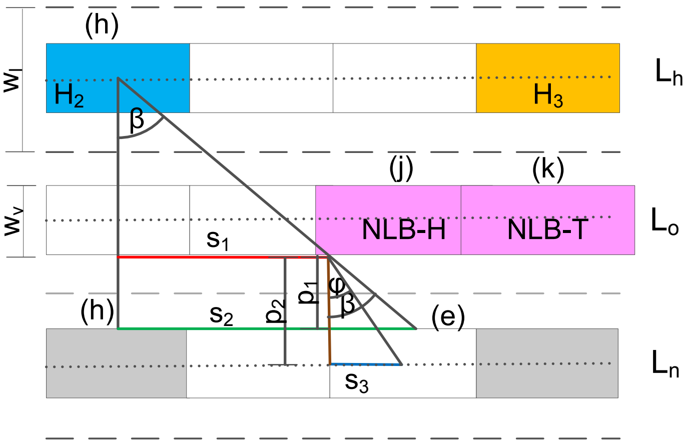

Figure 5.6: The index of the first cell on a lane L_n obstructed by a vehicle on a lane L_o

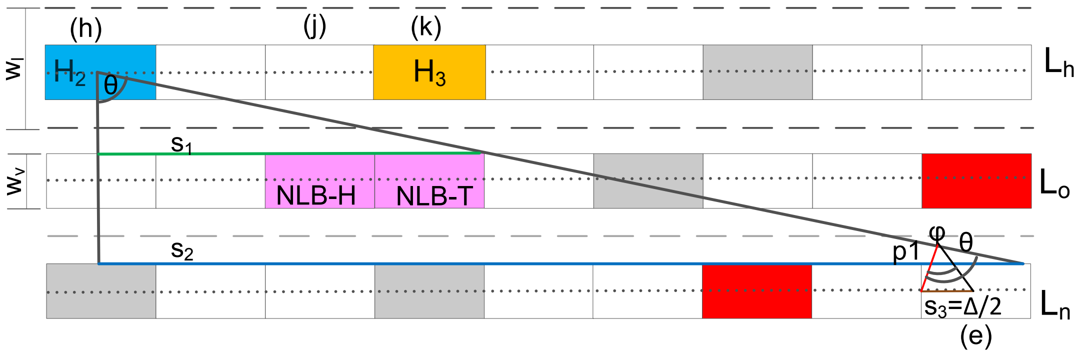

Figure 5.7: The index of the last cell on a lane L_n obstructed by a vehicle on a lane L_o

point of the large triangle's hypotenuse and the cell (e) is from the middle of the cell (e). To determine this, define $s' = s_2 - \frac{\Delta}{2}$. The projection of the hypotenuse on the side of cell (e) is $s'' = s' - \lfloor \frac{s'}{\Delta} \rfloor \Delta$. In the next step, we build another two smaller triangles. A triangle is built with a side (p_1) starting from the upper left corner of cell (e) and intersecting the large triangle's hypotenuse, and the second side is s''. Likewise the largest triangle, the upper angle of this triangle is also equal to β. It follows $p_1 = \frac{s''}{\tan(\beta)}$. The third triangle is build with a side (s_3) equal to $\frac{\Delta}{2}$ and originating from the center of the cell (e). Another side of the triangle denoted by p_2 is the extension of p_1 to the middle of the left side of the cell (e). The upper angle of this triangle is denoted by ϕ. It follows that $p_2 = p_1 + \frac{\Gamma}{2}$ and $\phi = \arctan\left(\frac{\Delta}{2p_2}\right)$. The index of the first obstructed cell on lane L_n denoted by $b_1(L_n)$ is decided based on the angles β and ϕ; if $\beta \geq \phi$ then $b_{1,n} = \lceil \frac{s'}{\Delta} \rceil + h + 1$, otherwise $b_{1,n} = \lceil \frac{s'}{\Delta} \rceil + h$.

We use the geometry depicted in Figure 5.7 to find the index of the last obstructed cell. By a similar approach used to find the starting obstructed cell, the length of segments s_1 and s_2 (shown in Figure 5.7) are obtained. It follows that $s_1 = (k-h)\Delta + \frac{\Delta}{2}$. Accordingly, $\tan(\theta)$ is expressed as follows:

$$\tan(\theta) = \frac{s_1}{|L_o - L_h|W_l - \frac{\Gamma}{2}} = \frac{(k-h)\Delta - \frac{\Delta}{2}}{|L_o - L_h|W_l - \frac{\Gamma}{2}} \tag{5.29}$$

And the length of s_2 is obtained as follows:

$$s_2 = \left(|L_n - L_h|\, W_l - \frac{\Gamma}{2}\right)\tan(\theta) = \left(|L_n - L_h|\, W_l - \frac{\Gamma}{2}\right)\frac{(k-h)\Delta + \frac{\Delta}{2}}{|L_o - L_h|W_l - \frac{\Gamma}{2}} \tag{5.30}$$

Finding the index of the last obstructed cell on a lane L_n is straightforward and is similar to the approach applied to find the start cell. Denote the index of the last obstructed cell by $b_{2,n}$. Once $b_{1,n}$ and $b_{2,n}$ are known, the n^{th} row of the obstruction map (i.e., Ω_n) is updated by adding the indices of those cells in range $[b_{1,n}, b_{2,n}]$ which satisfy the following conditions: (i) they are located on the hidden terminal region, and (ii) the cell state is 1, implying for the occupation of the cell by the front part of the vehicle where the antenna is installed.

d) Construction of distance map

For each generated node arrangement, the data structure D maintains the distance between the hop and the occupied cells (with state 1) which are situated in the hidden terminal region of the Tx. The construction of distance map D is implemented in function *getDistanceMap* and is invoked in lines 10 and 18 of Algorithm 5.1. For ease of computation, cells are separated with respect to the lanes in which they are located. An entry $d_{c,n}$ in D stands for the distance between the hop and a cell with index c situated on a lane with index (L_n). It follows that

$$d_{c,n} \;=\; \sqrt{[(c-h)\,\Delta]^2 + [|L_n - L_h|\,W_l]^2} \tag{5.31}$$

e) Interference power corresponding to a node arrangement instance
The aggregate interference power imposed by hidden nodes and experienced in the hop is implemented in function *calcAggPow* and invoked in lines 11 and 19 of Algorithm 5.1. Given the DSRC and channel model parameters, the obstruction and distance maps Ω and D provide sufficient information for the calculation of the aggregate interference power in the hop. To this aim, Algorithm 5.2 is proposed to calculate the aggregate interference power corresponding to a given node arrangement. This algorithm implements the function *calcAggPow* in Algorithm 5.1. It iterates through the entries in D. For each entry, the cell index and the distance from the hop are fetched. The cell index is then found in the obstruction map Ω to determine the obstruction status of the cell. The distance d of a cell determines which component of the path loss model described by Equation 5.1 should be applied. The obstruction status of the cell determines which of the two parameter settings corresponding to LOS and OLOS should be applied.

5.6.4 Reachable Distance of a Safety Message

The distance to which a safety message can reach in single broadcast is determined by the SINR value of the signal at that distance and a predetermined SINR threshold ($\mathrm{SINR_{th}}$). In an intended Rx, the SINR value is determined by the received signal from the transmitter Tx and the interference power experienced in Rx plus a constant noise power $\mathrm{P_n}$. With some abuse of notations, let h and k represent the h^{th} and k^{th} vehicles among the sequence of vehicles on a lane with transmitter Tx being the leading vehicle. We term such vehicles hops h and k. Let SINR_h and SINR_k be the SINR values at hops h and k, respectively. The reachable distance on a lane is equal to the distance of a hop h from the Tx such that $\mathrm{SINR_h} \leq \mathrm{SINR_{th}}$, and for any other hop k such that $k \leq h$, the condition $\mathrm{SINR}_k \geq \mathrm{SINR}_h$ is satisfied. In the following, we prove that under certain assumptions the reachable distance obtained by the model is a lower bound to the real system. Note that the following proposition and lemmas do not negate the general lower bound property of the model; however, developing proofs

Algorithm 5.2 Implementation of function *calcAggPow* in Algorithm 5.1

Require: D, Ω
Require: $(d_b, IL, n_{1,LOS}, n_{2,LOS}, PL0_{LOS}, n_{1,OLOS}, n_{2,OLOS}, PL0_{OLOS}) \in PAR_{ch}$
Require: transmission power P
Require: overlapping probability $Pr_{ovp} \in PAR_{dsrc}$
$P_{if} \leftarrow 0$
$L \leftarrow$ lane indices in D
$n \leftarrow 1$
while $n \leq size(L)$ **do**
  $C \leftarrow$ all cells in D_n
  for $c \in C$ **do**
    $d \leftarrow D_{c,n}$
    if $c \in \Omega_n$ **then**
      $n_1 \leftarrow n_{1,OLOS}, n_2 \leftarrow n_{2,OLOS}$
      $PL0 \leftarrow PL0_{OLOS}$
    else
      $n_1 \leftarrow n_{1,LOS}, n_2 \leftarrow n_{2,LOS}$
      $PL0 \leftarrow PL0_{LOS}$
    end if
    if $d \leq d_b$ **then**
      $P_{loss} \leftarrow PL0 + IL + 10 n_1 \log_{10}\left(\frac{d}{d_0}\right)$
    else
      $P_{loss} \leftarrow PL0 + IL + 10 n1 \log_{10}\left(\frac{d_b}{d_0}\right) + 10 n_2 \log_{10}\left(\frac{d}{d_b}\right)$
    end if
    $P_{if} \leftarrow P_{if} + Pr_{ovp}\, 10^{\frac{P - P_{loss}}{10}}$
  end for
  $n \leftarrow n + 1$
end while
return P_{if}

for the general cases is extremely difficult. For the general case of lower bound and upper bound properties of the model, we rely on our extensive experiments presented in Section 5.8.

Assumptions:

(i) for any hop h, the aggregate interference power obtained by the Algorithm 5.1 is an upper bound for the equivalent hop in the real system.

(ii) any vehicle in the real system drives in the middle of the lane in which it is situated.

(iii) if the distance between a hop h and the Tx in the real system is $\hat{d}_h$, its distance in the CA model is set to $d_h = \lceil \frac{\hat{d}_h}{\Delta} \rceil \Delta$.

Given the above assumptions, Lemma 5.6.1 states that the SINR obtained by the model for any given hop h is a lower bound to the real system with the condition that the hop h and the Tx are situated on the same lane. This case is referred to as *similar-lane* scenario.

Lemma 5.6.1. *Assume that a transmitter vehicle Tx and an intended recipient vehicle identified by hop number h are situated on a lane and the distance of h from the Tx in the real system is $\hat{d}_h$. The SINR obtained by the model for the hop h is, at most, as large as the SINR for the hop h in the real system.*

Proof. By assumption (i), the aggregate interference power at h obtained by the model is at least as large as in the real system. It remains to show that the received power in h from the Tx obtained by the model is, at most, as large as in the real system. Denote P_h^m the received power obtained by the model and P_h^s the power measured in the real system. Let d_h be the distance of hop h from the Tx calculated in the CA model. The assumption (iii) implies that $d_h \geq \hat{d}_h$. Assumption (ii) implies that in a similar-lane scenario any hop h beyond the first one is obstructed from the LOS of the Tx. By applying the assumption (iii) again, it follows that the likeliness of LOS obstruction between hop h and the Tx in the model is at least as high as in the real system. This result along with the previous one, i.e., $d_h \geq \hat{d}_h$, imply that $\mathrm{P}_h^m \leq \mathrm{P}_h^s$. □

The lower bound property of the model for reachable distance in a similar-lane scenario follows from Lemma 5.6.1.

If Tx and Rx are located on different lanes, the proof of lower bound property is not straightforward due to a complex obstruction behaviour. However, under certain conditions stated in Proposition 5.6.1 and Lemma 5.6.2, it can be proved that the reachable distance obtained by the model for a similar-lane scenario is a lower bound for the reachable distance obtained for a different-lane scenario. This implies that it is only necessary to find the reachable distance in a similar-lane scenario and consider it as a lower bound to the real system for both scenarios.

Proposition 5.6.1. *In a different-lane scenario, the likeliness of LOS obstruction between Tx and a hop h beyond the first hop is, at most, as high as in a similar-lane scenario.*

Proof. By assumption (ii), all hops but the first one are obstructed in a similar-lane scenario. In a different-lane scenario, on the other hand, the LOS obstruction occurs if at least one vehicle is present in the region between the hop h and Tx, and such vehicle obstructs the LOS of the hop h and the Tx. The chance that this occurs is less compared to the certain obstruction in a similar-lane scenario. Hence, for the same hop $h > 1$, the obstruction is less likely in a different-lane compared to a similar-lane scenario. □

Lemma 5.6.2. *Suppose Tx and its hop $h > 1$ (i.e., beyond the first hop) are situated on different lanes. Let δL be the absolute difference of the lane numbers of the Tx and its hop h. Also, let W_l, and HD be the lane width and headway distance, respectively. If $\delta L < \frac{\sqrt{3}HD}{2W_l}$, the SINR of the hop h in a similar-lane scenario is a lower bound on the SINR of the equivalent hop in a different-lane scenario.*

Proof. In a different-lane scenario, the average relative position of the hop h with respect to the Tx position is $\frac{h\,HD}{2}$. Thus, the average distance between the Tx and hop h is $d = \sqrt{\frac{(h\,HD)^2}{4} + (\delta L\,W_l)^2}$. Substituting $\delta L = \frac{\sqrt{3}HD}{2W_l}$ in the expression of d yields $d' = \frac{HD}{2}\sqrt{h^2+3}$. Using the fact that $\frac{\sqrt{h^2+3}}{2} \leq h \quad \forall h \geq 1$, it follows $d < d' \leq h\,HD$. The right side of the inequality is the distance between the Tx and the hop h in a similar-lane scenario. It follows that the distance of the Tx and the hop h in a different-lane scenario is on average less than the distance in a similar-lane scenario. Given the shorter distance and less severe LOS obstruction according to the Proposition 5.6.1, it follows that the received power in the hop $h > 1$ from the TX in a different-lane scenario is on average greater than in a similar-lane scenario.

It remains to show that the maximum interference power in hop h in a different-lane scenario is smaller compared to a similar-lane scenario. This can be inferred from the fact that on average, the distance between the hop h and interferers in the hidden terminal region is greater in a different-lane compared to the equivalent hop in a similar-lane scenario, because, as stated above, the hop is closer to the Tx in a different-lane compared to a similar-lane scenario. Also, with an increase in the distance of the hop from the hidden terminal region, the LOS obstruction between the hop and interferers increases, implying smaller interference power in the hop. It follows that in a different-lane scenario, on average, a hop h experiences less interference compared to a similar-lane scenario. The less severe LOS obstruction and the closer distance between the hop h and Tx in different-lane lead to greater SINR in h in a different-lane compared to a similar-lane scenario. □

5.7 Signalized Intersection Scenario

The hidden terminal effect is expected to demonstrate a highly complex behaviour in a traffic scenario with the presence of an intersection. An accurate study of such behaviour requires a traffic model to be in place for the characterization of the traffic behaviour at time instants during the red and green phases of a signalized intersection. Unfortunately, in spite of several decades having passed since the first studies were published on traffic behaviour at signalized intersections, to date there is no universal model capable of accurate describing the traffic parameters such as headway distance. Those models proposed so far mainly address the average delay and queue size during a red phase of the traffic light cycle [75]. The studies on the traffic behaviour in the green phase are confined to few parameters including saturation flow rate and the traffic indicators at the time of passing the stop line of an intersection [11]. In particular, there is no universal model capable of describing the headway distance parameter at any given time instant during a cycle of the traffic light. In the absence of appropriate models, the study of interference and the reachable distance of safety messages in spatial-temporal dimensions is extremely difficult. Consequently, our aim is to use an existing traffic model suitable for the investigation of interference in extreme case. Accordingly, we limit our study of hidden terminal interference to an upper bound interference for the system rather than for any given hop, as we addressed in the road stretch scenario.

The upper bound interference relates to the interference power experienced in some node assumed to be located on the boundary of the carrier sense distance of an anonymous target transmitter. Considering the highly dynamic traffic behaviour and the presence of heterogeneous traffic states in an intersection, the problem of finding upper bound interference involves the exploration of the interference power in potentially many nodes and in potentially many traffic conditions. We aim to reduce the extremely large size of the problem by identifying a scenario which exhibits the highest node concentration with respect to the intersection center. A probabilistic CA is proposed to model the identified traffic scenario and a simple procedure is proposed to find the upper bound interference power.

5.7.1 Assumptions

The intersection is assumed “drive through” without right and left turns. As shown in Figure 5.8, the intersection is comprised of a horizontal and a vertical bidirectional streets. The horizontal street, denoted by RW-RE, is comprised of two segments RW and RE situated to the right and left side of the intersection. Similarly, the vertical street, denoted by RN-RS, is comprised of two segments RN and RS above and below the intersection.

The intersection is assumed to be signalised with fixed timing of the traffic light. The total cycle is T_c and the green time for a given street is T_g. We assume the amber time is equally shared between the red and the green time. This implies that the red time of the given street is $T_{red} = T_c - T_g$. The intersection is assumed to be operating in perfect mode, i.e. the traffic queued up during a light cycle is discharged in the same cycle and over-saturation queue does not emerge.

The model is generally independent from the number of lanes in a road segment. The arguments hereafter are presented for a typical lane situated on a given road segment. The arguments can be easily extended to other lanes on the same road segment provided that the traffic direction and the timing of the traffic light are identical for those lanes.

5.7.2 Traffic Model

In Section 5.6, the CA model was deterministic in the sense that a cell was either occupied or empty. Such model is suitable for predictable traffic behaviour, where the traffic network is mainly dominated by a single traffic state. By contrast, in an intersection scenario multiple traffic states coexist with frequent transitions from one state to another [23]. Consequently, the application of a deterministic CA may not represent well the traffic behaviour in an intersection scenario. For this reason, we opt to model the traffic using a probabilistic CA, where the cell occupation is expressed probabilistically.

The base parameter used in the following arguments is headway distance. Two notions of headway distance are applied, each suitable for certain traffic states. Rear bumper to front bumper headway distance mainly suits jammed traffic states where the vehicle spacing is potentially smaller than the vehicle length. For other cases, rear bumper to rear bumper headway distance is applicable. In the following paragraphs, these two cases are addressed in the calculation of the probability of cell occupation.

Suppose the rear bumper to front bumper headway distance is $\mathrm{HD_{rf}}$ and measured in number of cells. Like the road stretch scenario, assume that three types of vehicles with different lengths exist in the network, even though it is possible to consider more types in the model. The notations related to size and population of vehicle classes are borrowed from Section 5.6. Denote the probability of cell occupation by $\mathrm{Pr_{oc}}$. To calculate $\mathrm{Pr_{oc}}$, we introduce the notion of basic blocks corresponding to different vehicle types. A basic block is a group of cells associated with a vehicle, and includes the cells accommodated in the headway distance and the cells occupied by the vehicle. Define b_s, b_m, and b_l as the block sizes corresponding to small, medium, and large vehicles respectively. It follows that

$$\begin{aligned} b_s &= L_s + HD_{rf} \\ b_m &= L_m + HD_{rf} \\ b_l &= L_l + HD_{rf} \end{aligned} \tag{5.32}$$

where L_s, L_m, and L_l are the the lengths of vehicles in number of cells.

The average size of a basic block, termed generic block size, is obtained as follows:

$$\bar{b} = p_s b_s + p_m b_m + p_l b_l \tag{5.33}$$

It follows that the probability of cell occupation is

$$Pr_{oc} = \frac{p_s L_s + p_m L_m + p_l L_l}{\bar{b}} \tag{5.34}$$

The probability that a cell contains the front part of a vehicle where the antenna is installed is obtained as:

$$Pr_{of} = Pr(OF|OC)Pr(OC) = \left(\frac{p_s}{L_s} + \frac{p_m}{L_m} + \frac{p_l}{L_l}\right) Pr_{oc} \tag{5.35}$$

where OF and OC are the events representing occupation by the front cell of a vehicle and the occupation by a vehicle, respectively.

If the rear bumper to rear bumper headway is given, we apply the following method. Let $\mathrm{HD_{rr}}$ be the headway distance measured in number of cells. In this case, only one basic block with size $\mathrm{HD_{rr}}$ is considered, since the vehicle length is included in $\mathrm{HD_{rr}}$. Thus, in Equation 5.34 the denominator $\bar{b}$ is replaced with $\mathrm{HD_{rr}}$. Accordingly, $\mathrm{Pr_{of}}$ is recalculated by Equation 5.35 and using the modified $\mathrm{Pr_{oc}}$.

The probability of cell occupation expressed by Equation 5.34 facilitates the calculation of LOS and OLOS probabilities for any pair of nodes. Suppose the cell indices h and i correspond to the cell locations of an intended recipient Rx and a potentially interfering node f. Denote by $\mathrm{LOS_{h,i}}$ and $\mathrm{OLOS_{h,i}}$, the LOS and OLOS events corresponding to these nodes. Initially, the set $\Omega_{\mathrm{h,i}}$ of cells obstructing the LOS between cell h and i are constructed using a similar approach to that described in Section 5.6. It should be noted that, in a probabilistic CA, obstruction by a single cell does not imply full obstruction, since cells are occupied probabilistically. Also, the obstructing cells may have different occupation probabilities due to the presence of different traffic states in the network. Therefore, in a second step, the obstructing cells are classified based on the similarity of occupation probability. Denote by $\mathbb{S}$ the union of the subsets of $\Omega_{\mathrm{h,i}}$ with distinct occupation probabilities. A member $s \in \mathbb{S}$ is the subset of cells with identical occupation probabilities. It follows that the probability of events $\mathrm{LOS_{h,i}}$

and $\mathrm{OLOS_{h,i}}$ can be obtained as follows:

$$\begin{aligned} Pr(LOS_{h,i}) &= \prod_{s\in\mathbb{S}} \left(1 - Pr_{(oc,s)}\right)^{\|s\|} \\ Pr(OLOS_{h,i}) &= 1 - Pr(LOS_{h,i}) \end{aligned} \tag{5.36}$$

where $\mathrm{Pr_{(oc\ ,\ s)}}$ and $\|s\|$ are the occupation probability and the number of cells in a given subset $s \in \mathbb{S}$, respectively.

5.7.2.1 Discretization Error and the Error Compensation Mechanism

Using cellular automata for the modelling of the traffic network introduces some error due to the discretization. In the proposed CA model, the discretization error is caused by two sources: transforming the actual headway distance, and the actual vehicle size, to discrete quantities measured in numbers of cells. Except for the small vehicles with the length equal to the base cell length (i.e., Δ), the discretization of the medium and large vehicles imposes some error with respect to the actual vehicle size. In the following, a simple error compensation mechanism is proposed, assuming that the discrete quantities are determined by upward rounding, i.e., $HD = \lceil \frac{\widehat{HD}}{\Delta} \rceil$, $L_m = \lceil \frac{\hat{L}_m}{\Delta} \rceil$, and $L_l = \lceil \frac{\hat{L}_l}{\Delta} \rceil$.

Denote by $\widehat{HD}$ the actual headway distance. Also denote by $\hat{L}_m$ and $\hat{L}_l$ the actual sizes of medium and large vehicles, respectively. A medium size vehicle contributes an error $e_m = L_m\Delta - \hat{L}_m$. Similarly, a large vehicle contributes $e_l = L_l\Delta - \hat{L}_l$. Given the populations of the medium and large vehicles denoted by p_m and p_l, the total error incurred due to vehicle size is as follows:

$$e_v = p_m e_m + p_l e_l \tag{5.37}$$

Transforming the headway distance into number of cells incurs an error of $e_{hd} = HD\ \Delta - \widehat{HD}$. It follows that the total error in a basic block described by Equation 5.33 is

$$e_b = e_v + e_{hd} \tag{5.38}$$

If two cells with indices i and j are situated on the same street, the distance between the cells, with the error taken into account, is obtained as follows:

$$\hat{d}_{ij} \quad = \quad \sqrt{\left(|j-i|\Delta - \tfrac{|j-i|}{b} e_b\right)^2 + (\delta L\, W_l)^2} \tag{5.39}$$

where δL is the lane difference of the cells, assuming the lanes are indexed by their ordering on the road segment (e.g., from top to bottom in horizontal street, and left to right in vertical street).

If the two cells are situated on different streets, the error compensation is performed with respect to the intersection center.

5.7.3 Traffic Discharge in a Green Phase of the Traffic Light

As highlighted previously, there is no model capable of describing the full course of traffic discharge in a green phase of the traffic light cycle. However, there are some well-established models proposed for describing the characteristics of discharging traffic at the stop line of a signalized intersection. One such model is proposed by Akcelik *et al.* [11]. Using extensive field experiments, they derived the following expressions for the queue discharge speed, flow rate, and headway as a function of the time since the start of green phase [11]:

$$\begin{aligned} v_s(t) &= V_n \left[1 - e^{-m_v(t-t_r)}\right] \\ q_s(t) &= Q_n \left[1 - e^{-m_q(t-t_r)}\right] \\ h_s(t) &= \tfrac{H_n}{\left[1-e^{-m_q(t-t_r)}\right]} \end{aligned} \tag{5.40}$$

The definitions of the above parameters are as follows [11]:
t: time elapsed in green phase (seconds),
t_r: average driver reaction time corresponding to the first vehicle in the queue (seconds),
$v_s(t)$: discharge speed of the queue at time instant t (km/h),
V_n: maximum discharge speed of the queue (km/h),
m_v: a model parameter,
$q_s(t)$: discharge flow rate of the queue at time instant t (veh/h/lane),

Q_n: maximum discharge flow rate of the queue (veh/h/lane),
m_q: a model parameter,
$h_s(t)$: discharge headway of the queue at time instant t and at the stop-line (seconds),
H_n: minimum discharge headway of the queue (seconds)
Akcelik *et al.* calibrated the parameters m_v, m_q, V_n, Q_n, and H_n by conducting measurements in various intersection sites including isolated, closely spaced, and right turn sites [11].

Figure 5.8: Signalized intersection scenario

5.7.4 An Extreme Node Concentration Scenario

We conjecture that the upper bound interference power in an intersection relates to an extreme node concentration from the perspective of a node Rx situated on the intersection. In this situation, the node density is high and the distance of the (interfering) nodes from the Rx is small. This suggests that, in general, the interference is the most severe when the traffic is jammed, because the node concentration in this state reaches its maximum. While this is true, the outcome interference power will not be a tight upper bound, especially when the normal traffic conditions are considered. In the following, we identify an extreme node concentration scenario which on one hand complies with the assumption of perfect operation and, on the other hand, it is expected to exhibit the maximum interference power in the intersection.

According to our results presented in Chapter 3, in a red phase, three traffic states can be identified on a road segment connected to the signalised intersection: a jammed traffic formed by queuing vehicles, transitional traffic joining the queue, and a free- or forced-flow traffic occupying the rest of the road segment. Our previous results also suggest that the maximum queue length on a road segment occurs sometime near $T_{red}+t_r$, where $\mathrm{T}_{\mathrm{red}}$ is the duration of a red phase and t_r is the reaction time of the first vehicle in the queue. At the time the queue reaches its maximum length on one road segment, the discharging vehicles on the other cross-road segments are still in the vicinity of the intersection. Depending on the traffic intensity on the different road segments, an extreme node concentration with respect to the intersection center corresponds to a situation where some road segments sharing the same phase of the traffic light reach their maximum queue length, while others have just discharged their queues. Therefore, to characterize the extreme node concentration, it is necessary to characterise the queue and the discharge traffic parameters.

The length of the queue relates to the input traffic flow of the road segment under investigation. To fulfil the perfect operation of the intersection, the input traffic flow should be determined based on a known saturation flow (Q_n) associated with the signalised intersection [11]. Given q_{in} for a lane on the road segment and the speed limit V_f of the road segment, the headway distance corresponding to the free- or forced-flow traffic state is obtained as follows:

$$\widehat{HD_f} = \frac{V_f}{q_{in}/3600} \tag{5.41}$$

$\widehat{HD_f}$ is then used to obtain the probability of cell occupation $\mathrm{Pr_{oc,f}}$ corresponding to the part of the road segment operating in the free- or forced-flow traffic state. The index of the starting cell with this traffic state is determined by the queue length N_{max} as we describe below. The last cell is located at the extreme end of the segment.

The probability of cell occupation $\mathrm{Pr_{oc,j}}$ corresponding to the cells within the queue region is determined by applying Equation 5.34 and using the jam space H_j as a rear bumper to front bumper headway distance. By ignoring the transitional traffic (for the sake of simplicity), the process of queue formation can be interpreted as the growth of cell occupation from $\mathrm{Pr_{oc,f}}$ to $\mathrm{Pr_{oc,j}}$ with rate q_{in}. This allows us to obtain the maximum number of cells on a lane occupied by a queue at time instant $T_{red} + t_r$ as follows:

$$N_{max} = \lceil \frac{\frac{q_{in}}{3600}(T_{red}+t_r)}{Pr_{oc,j}-Pr_{oc,f}} \rceil \tag{5.42}$$

N_{max} is identical for all lanes on the road segment with similar traffic direction.

In a green phase, we use the Akcelik model to find the discharge headway distance corresponding to the region of the road occupied by discharging traffic. It follows that at any time instant t after the start of the green phase, the discharge headway distance at the stop line is $HD_d(t) = \frac{v_s(t)h_s(t)}{3.6}$. Accordingly, occupation probability $\mathrm{Pr_{oc,d}}$ corresponding to the traffic discharged at time instant t is derived by applying $HD_d(t)$ to Equation 5.34. To find the number and the range of cells occupied by the discharged traffic up to a time instant, we need to know the evolution of the headway distance of the traffic after it discharges the queue. Such information can not be derived from the Akcelik model because it only describes the headway distance for the current time instant and only for the stop line. To obtain the headway distance of the previously discharged traffic, we enforce two assumptions in favour of an extreme node concentration. First, we assume that the discharging traffic travel in the form of a platoon with equal headway distance between consecutive vehicles in the platoon. Second, the headway distance of the previously discharged traffic is assumed to be equal to the current headway distance at the stop line. With these assumptions in effect, the number of cells corresponding to the maximum platoon size at the end of a green phase is obtained as follows:

$$N_d \quad = \quad \lceil \frac{N_{max} Pr_{oc,j}}{Pr_{oc,d}} \rceil \tag{5.43}$$

The initial position of the platoon discharged at the current green phase is a cell on the stop line and the end of the platoon on the lanes of the other road segment connected to the road segment under investigation is determined by $\mathrm{N_d}$. The starting location of a platoon discharged during the previous light cycle can be obtained as $\lfloor \frac{(T_c - t_r) v_s(T_g)/3.6}{\Delta} \rfloor$, where $\mathrm{T_c}$ is the cycle duration and $v_s(T_g)$ is the velocity of the platoon at the end of a green phase with duration $\mathrm{T_g}$, and determined by the the Akcelik model. This can be applied to as many previous cycles as appropriate with the condition that the length of the road segment where the platoon is situated is not exceeded.

5.7.5 Maximum Aggregate Interference Power

We obtain the maximum interference power in the intersection using a procedure comprised of three phases as follows:

Phase 1: Assignment of occupation probabilities

Initially, the road segments are categorized based on the traffic light phase they share. Assuming that the traffic light is scheduled in two phases, this, for the intersection depicted in Figure 5.8, leads to two categories with road segments RW and RE falling in one category, and RS and RN in the other. Denote the categories by $\mathrm{C_A}$ and $\mathrm{C_B}$, respectively. Arbitrarily, the red phase is assigned to $\mathrm{C_A}$. For each road segment in $\mathrm{C_A}$, the maximum queue length is obtained by Equation 5.42. The size(s) and the region(s) occupied by the previously discharged platoons up to a given number of cycles are obtained using Equation 5.43. The probabilities of cell occupation corresponding to each traffic state are obtained using Equation 5.34. In the meantime, the green phase is assigned to $\mathrm{C_B}$ and the traffic parameters and occupation probabilities corresponding to the current and previous discharged platoons are determined for each road segment in the category.

Phase 2: Calculation of aggregate interference power per lane

In the next phase, given a road segment and a lane on this road segment, a cell is selected on this lane as the initial location of the Rx. The initial cell location is chosen in such a way that its distance from the center of the intersection is at least NSD_H meters. By an iterative procedure, Rx is advanced towards the center of the intersection. In each iteration, the cells located in the region between Rx up to the boundary cells determined by NSD_H and NSD_V corresponding to the horizontal and vertical roads are considered as the locations of interferers. The NSD_H and NSD_V are obtained for all road segments using Equations 5.15 and 5.18. Next, the obstruction and distance maps are constructed using a similar approach to that described in Section 5.6. Using these information, the probability of LOS obstruction between the Rx and each interferer is calculated using Equation 5.36. At this point, the distance and the obstruction probabilities are known, and thus the aggregate interference power in Rx can be obtained.

Phase 3: Obtaining aggregate interference for the intersection
By iteration through the above procedure, for each lane, the maximum of the aggregate power values corresponding to all cell locations of Rx is recorded. For a given road segment, the aggregate interference power is the maximum of the values corresponding to all lanes on the segment. Accordingly, the maximum of the values corresponding to all segments will represent the interference power of the intersection under the current phase assignment. The above procedure is repeated for as many phase assignments. The upper bound interference power of the intersection is the largest outcome interference corresponding to the various phase assignments.

In a real traffic scenario with continuous vehicle position, it is possible that the instant position of a vehicle v driving on a road (e.g., RW-RE) coincides with a position in the range between two neighbouring lanes on the other road (e.g., RN-RS). If this occurs and if the width of vehicles are smaller than the lane width, vehicle v will have a full LOS with the vehicles on the two neighbouring lanes on the road RN-RS. Similarly, the instant position of v can fall between the intersection walls and a lane of the road RN-RS neighbouring the wall. If the distance to wall from the neighbouring lane on RN-RS is non-zero or vehicles' width are smaller than the lane width, vehicle v will have LOS with all vehicles situated on the lane of RN-RS neighbouring the wall. The two mentioned cases, if they occur, are predicted to exhibit a relatively large interference power in v. Therefore, these two cases are incorporated into the aforementioned procedure by enforcing a strategy that if the Rx cell is situated on the center area of the intersection, the Rx either has full LOS with the vehicle on the lane of cross-road neighbouring the wall or with any two neighbouring lanes on the cross-road, whichever yields the largest interference. The last assumption is that a discharging vehicle currently located on the intersection region will have LOS with the first vehicles queued on the cross-road. This assumption is applied in order to capture the fact that vehicles ahead of the queues are inclined to stop as close as possible to the stop line, thus having LOS with the crossing vehicles.

5.8 Experimental Results

Paramics [49] is used to construct the traffic networks corresponding to the urban road stretch and signalized intersection scenarios. We present the experimental results separately for the two scenarios. A set of parameters and the corresponding values used in both scenarios are shown in Table 5.4 with the exception that NLOS parameters are used only in the intersection scenario. The channel model parameters and the corresponding values are specified in [8] and are repeated in Table 5.4. Carrier sense power threshold (CSth), noise power $\mathrm{P_n}$, and SINR threshold (SINRth) are configured according to Torrent Moreno *et. al.* [163]. The value 16.535 dBm for transmission power (P) is chosen based on a desired transmission range of 300 m. With this power and in the absence of interference, an intended receiver located 300 m away from the transmitter can receive the signal with a power equal to a reception threshold (RCth) and with a sufficiently large Signal to Noise Ratio (SNR). The value of parameter RCth depends on the device sensitivity, modulation technique, FEC coding rate, and the data rate of the packet. A range of values from -85 to -94 dBm are used in the literature [76; 163]. We set the RCth to -89 dBm, representing an average sensitivity for data rate 3 Mbps and modulation BPSK. For robustness, the data rate R is set to 3 Mbps [163]. In both scenarios, without loss of generality, only periodic messages are considered and the case of event-driven messages is not

Table 5.4: Physical, DSRC, and traffic model parameters and configuration values

Group	Parameter	Value
Path Loss (global)	Implementation Loss (IL)	6.8 dBm
	Breakpoint Distance (d_b)	104 m
	Reference Distance (d_0)	10 m
Path Loss (LOS)	Free Space Path Loss (PL0)	56.5 dBm
	n_1	1.81
	n_2	2.85
Path Loss (OLOS)	Free Space Path Loss (PL0)	66.5 dBm
	n_1	1.93
	n_2	2.74
Path Loss (NLOS)	Constant Path Loss	3.75 dBm
	Wave Length (λ)	0.0508
	i_s	0
	n_{NLOS}	2.69
Other Physical	Frequency	5.9 GHz
	Carrier Sense Threshold (CSth)	-96 dBm
	Noise Power (P_n)	-99 dBm
	SINR Threshold (SINRth)	5 dB
	Transmission Power (P)	16.535 dBm
	Reception Threshold (RCth)	-89 dBm
	Data Rate (R)	3 Mbps
	Slot Time (σ)	16 μs
DSRC	Periodic Message Rate (λ_r)	10 Hz
	Periodic Message Length (M_b)	500 bytes
Traffic Model	Cell Length (Δ)	4 m
	Cell Width (Γ)	1.6 m
	Lane Width (W_l)	3.7 m
	Reaction Time (t_r)	1 s

covered. This conservative decision is justified by the fact that the generation rate of event-driven messages is not specified in the reference DSRC standard. Proprietary setting of the generation rate for the event-driven case is potentially misleading and affects the validity of conclusions. For periodic messages, on the other hand, the standard highlights 1–10 Hz as the recommended message generation rate. For the sake of high interference, as the main focus of the current work, the message generation rate is set to $\lambda_r = 10$ Hz, which is equivalent to a periodicity of 100 ms. Regarding the message length, a 200-byte message can accommodate the basic safety information. However, if the overhead imposed by security and privacy information is included, the resulting total message size amounts to values in the range 284 to 791 bytes [138]. We set the periodic message length $\mathrm{M_b} = 500$ bytes as the multiple of 100 bytes that is closest to the average value in the range $[284, 791]$. The slot duration σ is set to 16 μs. With these settings, the steady state probability of periodic message transmission in a time slot is obtained using the expression proposed in Chapter 4 for τ_b. The steady state τ_b is used for the experiments, both in the model and in the traces. Thus, the random MAC behaviour is not considered. Instead, the experiments are focused on the effects of the vehicular traffic.

While the investigation of the impacts of vehicle size on the interference behaviour merits its own dedicated experiment plan, without loss of the generality of the analytical models proposed in this chapter, we restrict the experiments to the case of a single type of vehicle. In that regard, passenger cars are used in our experiments. This choice is in agreement with the statistics on car populations in urban traffic systems [4], indicating the presence of a significantly large population of passenger vehicles ($> 80\%$) in Australia. We set $\hat{\mathrm{L}}_s = 4$ m and $\hat{\mathrm{W}}_s = 1.6$ m as the typical length and width of a passenger car. Also, the population of this car is set to $p_s = 1$. Accordingly, the length and width of a cell in the CA model are configured to $\Delta = \hat{\mathrm{L}}_s = 4$ m and $\Gamma = \hat{\mathrm{W}}_s = 1.6$ m respectively.

Regarding the mean driver reaction time (t_r), a relatively wide range of values have been addressed in the literature. In the literature of traffic science, the mean driver reaction time is assumed 1 second with values in range $[0.5, 2]$ seconds [9; 72; 168]. In Paramics, as our choice of traffic simulator, the recommended mean driver reaction time is also 1 second. We also use $t_r = 1$ second throughout the experiments. Finally, the lane width is set to $W_l = 3.7$ m, representing the width of a lane in an urban major road.

5.8.1 Road Stretch Scenario

In this experiment, the main objective is to cover the most prevalent urban traffic settings in terms of speed limits and the number of lanes accommodated by a road stretch. To this end, twelve bidirectional road stretches are implemented, each with an equal number of lanes in both directions. The scenarios include 4 velocities and 3 lane configurations per velocity setting. The selected velocities are 40, 50, 65, and 80 kph and the lane settings are 2, 4, and 6 lanes. The length of the road stretch in all scenarios is set to 8 km, with two traffic zones situated at the start and the end of the road stretch. The length of each zone is set to 500–800 m. To prevent the impact of traffic scarcity on the traffic dynamic and hence avoiding the potential biases in the measurements, traffic flows are set to a significantly large value of 3600 vehicles/hour/lane. With such traffic flow, the two zones are saturated in all scenarios. To force the simulator to reproduce – as much as possible – the capacity traffic state, a parameter in the simulator termed "target headway factor" is set to a value smaller than the reaction time. We set this parameter to 0.85 as the recommended minimum target headway factor for urban traffic. In each scenario characterized by a velocity and a lane configuration, the simulation time is set to one hour with the initial 20 minutes dedicated to warm-up period. In the remaining 40 minutes, 480 time instants are selected with a step of 5 seconds and the associated traces are extracted from the total recorded traces. At each time instant, the transmitter vehicles (i.e., Txs) are selected from different lanes. Given the lane, location, and identity of a Tx, the associated hops of the Tx are identified on various lanes. The hops information are then used for the measurement of the parameters of interest.

In the initial experiments, we address the similar-lane scenario, i.e., the Tx and its hops are situated on the same lane, followed by the different-lane scenario. Two scenarios corresponding to the minimum and maximum velocities (i.e., 40 kph and 80 kph) are selected to demonstrate a high level comparison between the model and the traffic traces. The SINR values, and the received and interference powers corresponding to the various lane configurations for the two velocities are shown in Figures 5.9 and 5.10, respectively.

A number of conclusions can be drawn from the results. First, the strong

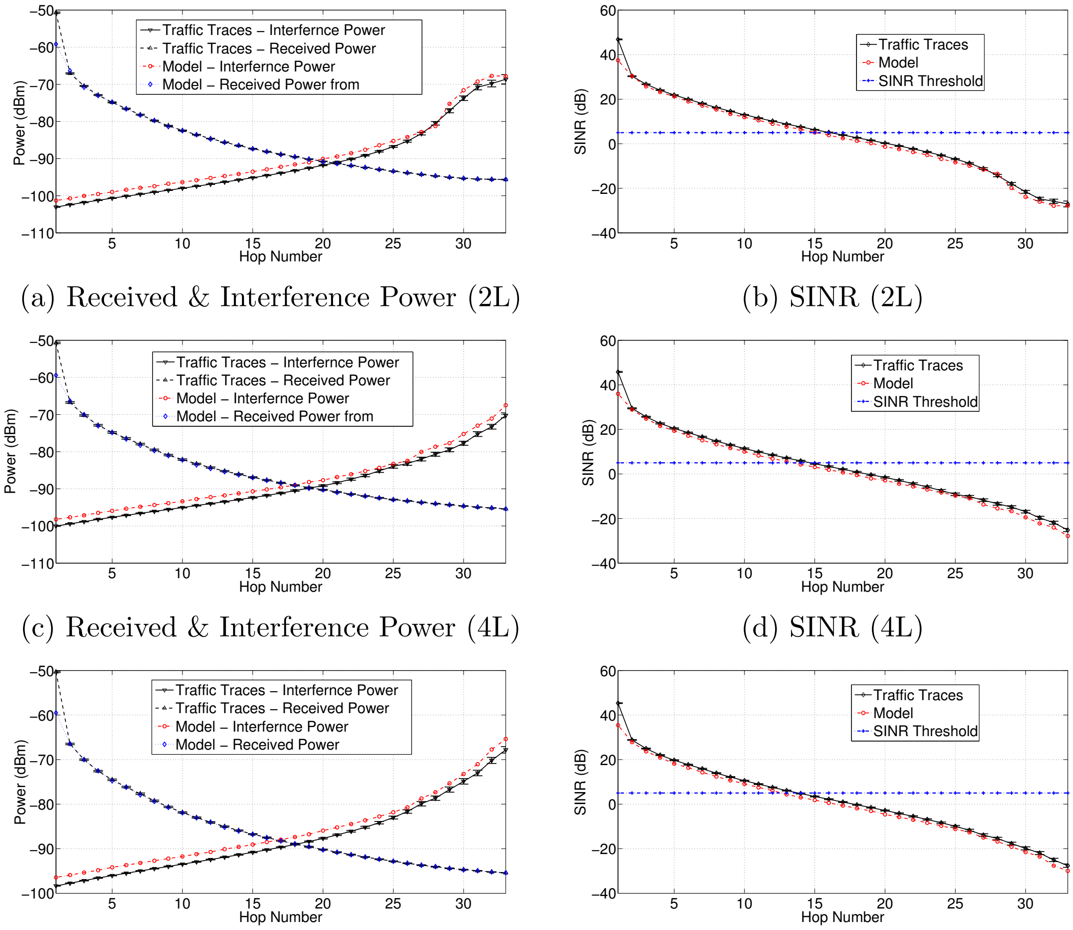

(a) Received & Interference Power (2L)

(b) SINR (2L)

(c) Received & Interference Power (4L)

(d) SINR (4L)

(e) Received & Interference Power (6L)

(f) SINR (6L)

Figure 5.9: 40 kph scenarios ("L" stands for lane)

similarity between the curves corresponding to the model and the traces indicates that the model has a high correlation with the traces. Second, the interference power increases with the increase in the number of lanes. Conversely, SINR decreases with the number of lanes increasing. In 2-lane scenarios, sharp increases (decreases) of interference power (SINR) can be observed for both velocities. At 40 kph, it starts from the 27^{th} hop (Figure 5.9a), whereas it starts from the 12^{th} hop in the 80 kph scenario (Figure 5.10a). A reasonable explanation for this phenomenon is the existence of LOS between the interferers and the hops close to the location of interferers. This, in turn, gives rise to the interference power experienced in those hops near the interferers. Observe that this phenomenon

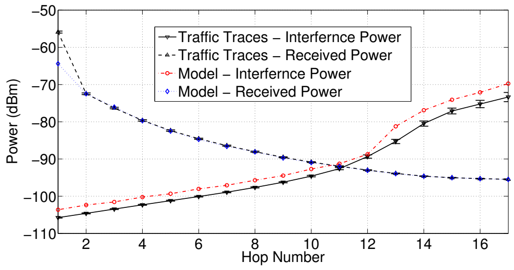

(a) Received & Interference Power (2L)

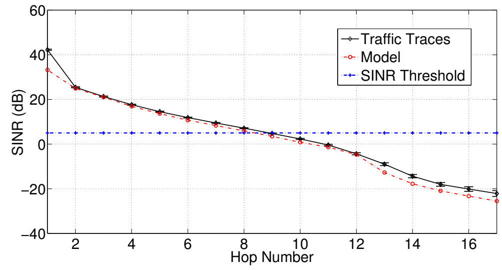

(b) SINR (2L)

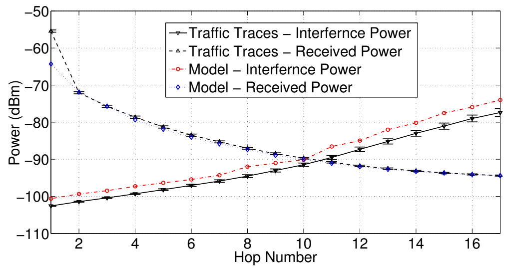

(c) Received & Interference Power (4L)

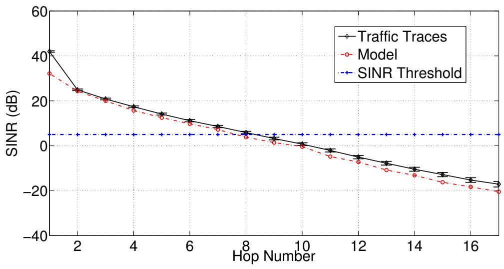

(d) SINR (4L)

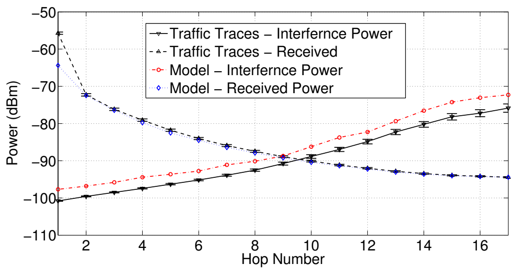

(e) Received & Interference Power (6L)

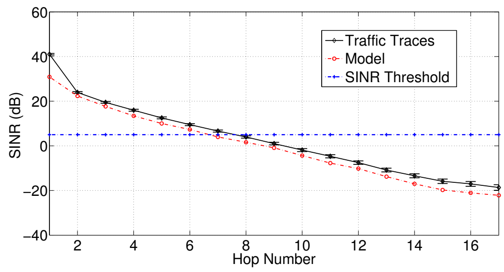

(f) SINR (6L)

Figure 5.10: 80 kph scenarios ("L" stands for lane)

rarely occurs in 4-lane and 6-lane scenarios, because with an increase in the number of lanes, the LOS obstruction increases irrespective of how close a hop is to the interferers. Comparing the 2-lane scenarios corresponding to 40 kph and 80 kph velocity scenarios (Figures 5.9a, 5.9b, 5.10a, and 5.10b) reveals that in the 80 kph scenario, the sharp increase in interference power (SINR decrease) starts when the receiver is at a shorter distance from the transmitter compared to the 40 kph scenario. A likely explanation is that the lower vehicle density in 80 kph scenario compared to 40 kph causes less LOS obstruction between a hop and the interferers, resulting in larger interference power. Another important conclusion is drawn from a global comparison of the interference power (and SINR) in 40 kph

Table 5.5: Actual and theoretical headway distances in capacity traffic state

Velocity (kph)	Traces (m)	Theoretic (m)	$\delta(\%)$
40	16.34	15.11	7.53
50	20.29	17.88	11.88
65	26.37	22.05	16.38
80	31.72	26.22	17.34

and 80 kph scenarios. We observe that, compared to 80 kph, in the 40 kph scenario the interference power and SINR curves corresponding to the model fit better to the curves pertaining to the traces. The reason is that at the 80 kph velocity (or generally at higher velocities), drivers tend to be more conservative and maintain excessively larger headway distances compared to the theoretical headway distance corresponding to the capacity traffic state. This phenomenon is explained in Table 5.5, which highlights the non-uniform difference between the theoretical and the actual headway distances corresponding to various velocities.

Column 4 (δ) in Table 5.5 shows the percentage difference between the actual and theoretical headway distances. According to the table, in all velocities, the mean headway distances measured from the traces are larger than the theoretical headway distances corresponding to the capacity state. This confirms that in real traffic situations, the capacity state is rarely reached, and thus it remains as a theoretical lower bound in terms of headway distance. Also, observe that the percentage difference between the actual and the theoretical headway distances increases from low to high velocities. This also verifies that the percentage difference is non-uniform in various velocities. For convenience, Figure 5.11 also presents a graphical demonstration of the actual and the theoretical headway distances.

Given the above observations and considering the fact that for all velocities, the headway distances calculated by the model are less than or equal to the theoretical headway distances corresponding to capacity traffic state, the model is expected to be an upper bound for the traces in terms of interference power and lower bound in terms of SINR (and reachable distance). These properties of the model are demonstrated in Table 5.6. The results in Table 5.6 are derived from

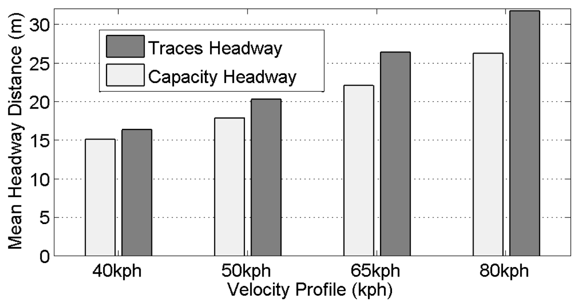

Figure 5.11: Actual and theoretical headway distances in capacity traffic state

the measured interference powers and the SINR data presented in Appendix C.

Table 5.6: Lower bound and upper bound properties of the model in terms of SINR and interference power

Velocity (kph)	Lanes	LB_SINR (%)	UB_INTF (%)
40	2	90.91	93.94
	4	91.43	91.43
	6	95.24	96.19
Scenario mean		92.52	93.85
50	2	92.59	100
	4	85	88.33
	6	96.67	97.78
Scenario mean		91.42	95.37
65	2	95	95
	4	95.83	97.92
	6	97.22	97.22
Scenario mean		96	96.71
80	2	94.12	100
	4	95	95
	6	100	100
Scenario mean		96.37	98.33
Mean (all scenarios)		94.08	96.07
Standard deviation		3.8	3.6

Column 3 (LB_SINR) and column 4 (UB_INTF) in Table 5.6 show the percentage of time that the SINR and interference power obtained from the model is below and above the 95% confidence interval of the SINR and interference powers measured from the traces, respectively. According to the results, on average, 96.07% of the time the interference powers obtained from the model are upper bounds to the traces. The upper bound becomes stronger as the velocity increases. This phenomenon is again explained by the observations shown in Figure 5.11. In case of SINR, on average, 94.08% of the time the SINRs obtained from the model are lower bounds to the traces. The lower bound property of the model in terms of reachable distance is similar to the case of SINR.

The tightness of the lower bound reachable distance is demonstrated in Table 5.7. RDT and RDM represent the average reachable distances measured from the traces and obtained from the model, respectively. δ is the difference between the reachable distances, i.e., $\delta = RDT - RDM$. α is the tightness of the lower bound defined as $\alpha = 100\frac{\delta}{RDT}$. According to the table, δ is 21.5 m on average, and does not exceed 29 m in any scenario. α is 8.11% on average, and does not exceed 11% in any scenario. A close observation of Table 5.7 reveals that in the traces, in 10 out of 12 ($\approx$ 83%) scenarios, the desired transmission range 300 m is not reached, whereas according to the model, in 100% of the time the reachable distances fall below 300 m. These results indicate a high potential of reliability degradation in some safety applications requiring medium to high coverage, e.g., Stop/Slow Vehicle Ahead (SVA) Advisor [17]. Applications with short coverage requirements ($\leq$ 150 m), such as Emergency Electronic Brake Light (EEBL) Advisor and Lane Change (& Blind Spot) Advisor (LCA), are less vulnerable to interference issues.

For the convenience of comparison, Figure 5.12 demonstrates the reachable distances described in Table 5.7. The outer and inner bars correspond to the traces and the model, respectively. According to the figure, in all scenarios the reachable distance obtained from the model is less than the average measured reachable distance. Also, observe that the reachable distance decreases from high to low velocities. Furthermore, in a given velocity, the reachable distance decreases with an increase in the number of lanes.

Table 5.8 demonstrates the decline of reachable distance as the result of hidden

Table 5.7: Tightness of lower bound reachable distance

Velocity (kph)	Lanes	RDT (m)	RDM (m)	δ (m)	α(%)
40	2	280.21	260	20.21	7.21
	4	248.54	228	20.54	8.26
	6	230.31	208	22.31	9.69
Scenario mean				21.02	8.39
50	2	291.43	276	15.43	5.29
	4	259.58	240	19.58	7.54
	6	241.31	220	21.31	8.83
Scenario mean				18.77	7.22
65	2	303.41	284	19.41	6.40
	4	269.71	252	17.71	6.57
	6	252.09	225	27.09	10.75
Scenario mean				21.40	7.90
80	2	312.84	292	20.84	6.66
	4	273.32	248	25.32	9.26
	6	260.26	232	28.26	10.86
Scenario mean				24.81	8.93
Mean (all scenarios)				21.5	8.11
Standard deviation				3.75	1.79

terminal interference. The values in the table are obtained by subtracting a reference reachable distance RD_{ref} from RDT and RDM entries in Table 5.7 respectively for the traces and the model. RD_{ref} is calculated in the absence of interference and with the same transmission power as in the Table 5.4 and with a SNR threshold of 5 dB. With these settings, the reference distance is obtained as $RD_{ref} = 456.67$ m. Also, recall that RDMs and RDTs in Table 5.4 were obtained using a SINR threshold of 5 dB. According to Table 5.8, the decline of the reachable distance increases with the number of lanes and decreases with velocity. In particular, the decline is most severe at velocity 40 kph. Also, the model shows more severe decline compared to the traces.

In this last experiment, we show that the SINRs in similar-lane scenarios are

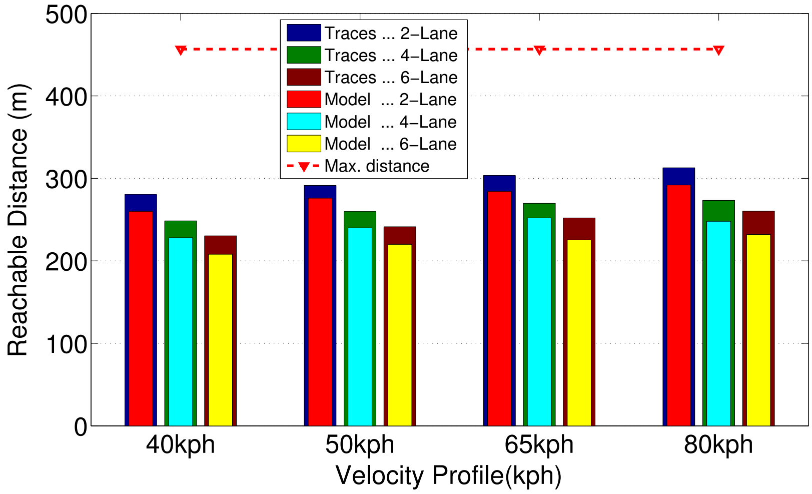

Figure 5.12: The impact of interference on reachable distance

Table 5.8: The decline of reachable distance due to hidden terminal interference. The reference reachable distance in the absence of interference is 456.67m.

		Lanes		
	Velocity (kph)	2L	4L	6L
Traces	40	176.46	208.13	226.36
	50	165.24	197.09	215.36
	65	153.26	186.96	204.58
	80	143.83	183.35	196.41
Model	40	196.67	228.67	248.67
	50	180.67	216.67	236.67
	65	172.67	204.67	231.67
	80	164.67	208.67	224.67

also lower bounds for different-lane scenarios. By applying the Lemma 5.6.2 in Section 5.6.4, we aim at extending the lower bound SINR results of the similar-lane scenarios to the different-lane conditions. According to the lemma, the σL (difference between lane numbers of the hop and Tx) must be less than $\frac{\sqrt{3}HD}{2W_l}$ in order to enforce such an extension. Given the lane width and also the theoretical headway distances pertaining to the different velocities, this leads to σL values 3, 4, 5, and 6 corresponding to 40, 50, 65, and 80 kph, respectively. The resultant lane differences are deemed to be sufficiently large to maintain the driver awareness required by the safety applications.

In Figure 5.13, a comparison between the per-hop SINRs in the different-lane and similar-lane situations is shown. The SINR values pertain to 6-lane scenarios with various velocities. According to the figure, from the second hop up to the fifth one, the SINR values in the similar-lane scenario fall far below those of the different lane scenario. The reason behind this is two-fold: first, as stated in the proof of Lemma 5.6.2, the average distance of a hop from the Tx in different-lane scenario is less than the distance of the equivalent hop in the similar-lane scenario. Second, in the different-lane scenario, the existence of LOS between a few hops beyond the first hop and the Tx is very likely, leading to a large received power in the hops from the Tx. In the similar-lane scenario, on the other hand, the LOS exists only for the first hop. This results in smaller received power in the hops beyond the first one. In the remaining hops, the SINR in the two scenarios are very close, although the similar-lane scenario still remains as a lower bound due to larger average distance from the Tx. In the 6-lane scenario with velocity 40 kph, 98.7% of the time, the SINR of the hops in the similar-lane scenario is smaller than the SINR of the equivalent hops in different-lane case. At other velocities (i.e., 50, 65, and 80 kph), on average 96.2%, 95.0%, and 94.4% of the time the lower bound occurs. In other lane scenarios, the percentages are slightly larger than for the 6-lane scenarios, implying a higher certainty of the lower bounds. In conclusion, we propose the SINR of a hop in the similar-lane scenario to be considered as a lower bound to SINR of the equivalent hop in the different-lane case.

5.8.2 Signalized Intersection Scenario

The intersection under investigation is as shown in Figure 5.8. The horizontal and vertical streets are identical in terms of the number of lanes, bidirectional traffic, and the number of lanes in each direction. Furthermore, they are symmetric in terms of traffic light timing. The experiment scenarios and parameters are shown in Table 5.9. Three different lane settings and three different configurations of the traffic light timing account for nine experiment scenarios. Jam spacing is

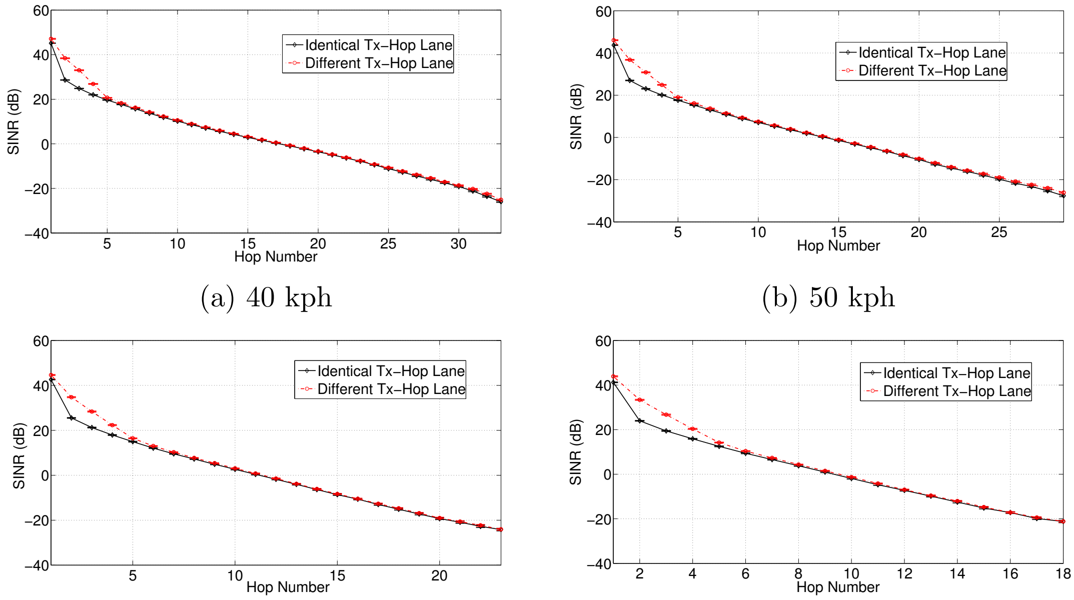

(a) 40 kph (b) 50 kph

(c) 65 kph (d) 80 kph

Figure 5.13: SINR comparison between similar-lane and different-lane scenarios

set to $H_j = 2$ m as the minimum recommended distance between vehicles in the queue, according to the Paramics simulator. The traffic parameters related to traffic discharge are configured similar to the isolated intersection scenario in the Akcelik model [11]. Given the saturation flow $Q_n = 2086$ vehicles/hour/lane and a reference speed limit $V_f = 69$ kph suggested in the Akcelik model, the input traffic flow is obtained as $q_{in} = 1043$ vehicles/hour/lane. Flows greater than this value result in frequent over-saturation of the intersection, a condition that violates the perfect operation of the intersection. Note that with speed limits other than 69 kph, the input flow and some other parameters in the discharge model must be re-calibrated. Covering all speed limits and parameter calibration is out of the scope of this work. The lane width and cell dimensions of the cellular automata is similar to the road segment scenario (i.e. $W_l = 3.7$ m, $\Delta = 4$ m and $\Gamma = 1.6$ m).

The warm-up and measurement durations are set to 20 and 40 minutes, respectively. After recording all traffic traces for a scenario, those traces belonging to the same light cycle are tagged. From the tagged traces corresponding to a cycle, the traces are extracted at each 0.5 second time step. In the resultant

Table 5.9: Intersection scenarios, parameters, and configuration values

Group	Parameter	Value
Scenarios	Lane (RW-RE Street)	2, 4, 6
	Lane (RN-RS Street)	2, 4, 6
	Traffic Light Timing	$T_c = 60$ s , $T_g = 30$ s $T_c = 100$ s , $T_g = 50$ s $T_c = 150$ s , $T_g = 75$ s
	Input Flow (q_{in})	1043 vehicles/hour/lane
	Speed Limit (V_f)	69 kph
	RN-RS Length	8 km
	RW-RE Length	8 km
	Junction Coordinates	(4000 m , 4000 m)
	Distance to Wall (x_t)	4 m
	Jam Spacing (H_j)	2 m
Traffic Discharge Model	Q_n	2086 vehicles/hour/lane
	V_n	45.1 kph
	H_n	1.725 s
	Other	$m_q = 0.369$, $m_v = 0.118$

traces, the interference power experienced by all vehicles within a circle of radius 1 km centred at the intersection are measured. The maximum interference power measured in all time steps during the cycle is recorded as the interference power corresponding to that cycle. Due to the symmetry of the intersection and the traffic light timing, the measurement is performed only for one road segment.

To verify that the interference power obtained by the model is an upper bound to the powers measured in the traces, a per-cycle comparison is performed for all individual light cycles and for all scenarios. Tables 5.10 and 5.11 show the maximum interference power measured from the traces for every individual cycle within the experiment duration. Table 5.12 shows the interference power obtained in a cycle by the model. The comparison of the results reveals that only in one cycle does the maximum interference power observed in the traces exceed the power obtained by the model (cycle 17 in Table 5.10). In this case, the surplus power is of the order of 10^{-9} mW, and thus negligible.

In Figure 5.14, the results obtained by the model are compared with the

Table 5.10: Per-cycle interference power (dBm) measured from traces. T_c is the duration of the traffic light cycle (seconds). "L" stands for lane.

	$T_c = 60s$			$T_c = 100s$			$T_c = 150s$		
cycle	2L	4L	6L	2L	4L	6L	2L	4L	6L
1	-57.39	-55.31	-54.15	-56.53	-54.59	-51.82	-55.83	-54.50	-51.84
2	-56.84	-54.87	-52.39	-55.88	-54.77	-53.35	-56.43	-55.03	-54.07
3	-56.97	-55.68	-54.07	-55.85	-54.05	-51.94	-56.36	-54.65	-54.08
4	-56.65	-55.06	-54.08	-56.49	-55.09	-53.85	-56.26	-54.03	-51.87
5	-57.37	-54.76	-54.57	-56.97	-54.81	-52.82	-56.38	-54.60	-53.73
6	-57.12	-55.33	-54.92	-56.61	-54.01	-53.24	-55.64	-54.61	-53.89
7	-56.98	-55.15	-54.07	-56.37	-54.94	-53.43	-56.88	-54.08	-53.44
8	-57.06	-55.27	-54.06	-56.48	-54.47	-53.86	-55.99	-54.54	-53.88
9	-57.25	-53.45	-53.25	-56.78	-53.97	-52.88	-56.23	-54.72	-52.75
10	-56.91	-55.11	-54.08	-56.54	-54.43	-53.82	-56.05	-54.44	-54.10
11	-55.75	-55.16	-54.67	-56.29	-53.20	-53.72	-56.34	-54.65	-53.69
12	-55.91	-54.50	-54.37	-55.74	-54.96	-53.96	-56.52	-54.19	-52.03
13	-56.83	-55.12	-53.94	-56.46	-55.33	-54.50	-56.65	-54.23	-54.19
14	-57.07	-55.31	-53.86	-56.92	-55.34	-54.15	-55.76	-54.47	-53.78
15	-57.12	-55.13	-54.33	-56.61	-54.41	-54.10	-56.27	-54.23	-53.74
16	-57.05	-54.90	-54.34	-56.36	-53.76	-53.69	-56.42	-54.98	-53.88
17	-57.23	-54.43	-54.49	-56.26	-52.73	-54.13	-	-	-
18	-57.22	-54.92	-54.41	-57.09	-54.97	-54.03	-	-	-
19	-56.87	-54.86	-54.07	-56.69	-54.86	-53.90	-	-	-
20	-56.07	-54.79	-53.49	-56.72	-53.95	-51.91	-	-	-

median of the interference power measured from the traces. A number of key conclusions can be derived by observing Figure 5.14. First, the interference power obtained by the model is an absolute upper bound to the median interference power in the traces. Second, the interference power significantly increases with the number of lanes. The power also increases with respect to the duration of the traffic light cycle, although the change is very small and in some cases negligible. Given the fact that the queue length increases with cycle duration, the negligible change of power with respect to the cycle length seems counter-intuitive. An explanation for this phenomenon is that although the queue length and node concentration around the intersection increase with the length of the light cycle, the distance between the intersection center and the new nodes joining the queue

Table 5.11: Per-cycle interference power (dBm) measured from traces. T_c is the duration of the traffic light cycle (seconds). "L" stands for lane. (continuing from Table 5.10).

	$T_c = 60s$			$T_c = 100s$			$T_c = 150s$		
cycle	2L	4L	6L	2L	4L	6L	2L	4L	6L
21	-56.81	-55.19	-54.88	-56.59	-54.54	-54.27	-	-	-
22	-56.38	-55.20	-55.00	-56.27	-54.76	-53.71	-	-	-
23	-56.49	-55.06	-53.86	-57.14	-53.56	-54.37	-	-	-
24	-57.23	-54.95	-54.46	-56.62	-54.33	-53.82	-	-	-
25	-57.06	-55.20	-54.21	-	-	-	-	-	-
26	-57.28	-55.76	-54.10	-	-	-	-	-	-
27	-56.39	-55.03	-53.78	-	-	-	-	-	-
28	-56.82	-55.17	-54.21	-	-	-	-	-	-
29	-56.71	-55.04	-54.57	-	-	-	-	-	-
30	-56.95	-55.27	-54.58	-	-	-	-	-	-
31	-57.09	-55.78	-54.03	-	-	-	-	-	-
32	-56.89	-55.14	-53.73	-	-	-	-	-	-
33	-56.74	-54.22	-51.94	-	-	-	-	-	-
34	-56.80	-54.80	-53.79	-	-	-	-	-	-
35	-56.93	-54.78	-54.90	-	-	-	-	-	-
36	-56.58	-53.96	-51.70	-	-	-	-	-	-
37	-56.44	-55.32	-54.29	-	-	-	-	-	-
38	-56.47	-54.09	-52.26	-	-	-	-	-	-
39	-56.98	-54.03	-54.06	-	-	-	-	-	-
40	-56.83	-55.00	-54.26	-	-	-	-	-	-

increases too. Also, with queue length growing, the LOS obstruction between the nodes at the tail of the queue and other nodes at or around the intersection increases. Consequently, the nodes at the tail of a long queue do not significantly impact the interference power experienced at the intersection. In fact, the most severe interference power is induced by the closest interferers to the intersection center, which in the meantime are not obstructed from the LOS of a receiver at the intersection.

The tightness analysis of the upper bound is performed using the results shown in Tables (5.13) and (5.14), corresponding to the tightness with respect to the median and mean interference powers measured from the traces, respectively. The

Table 5.12: Interference power (dBm) obtained by the model

	T_c = 60s	T_c = 100s	T_c = 150s
2L	-54.39	-54.32	-54.28
4L	-52.80	-52.75	-52.72
6L	-51.56	-51.52	-51.50

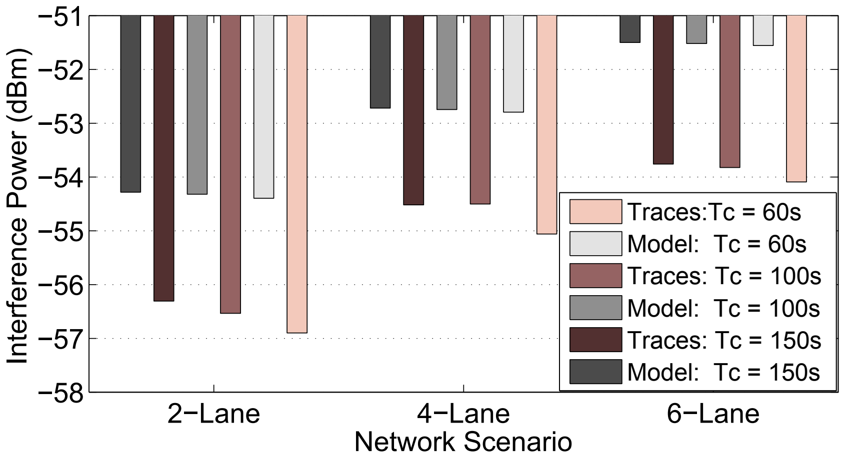

Figure 5.14: Comparison of interference power for all scenarios

left column in the tables corresponds to the three lane configurations. The second row shows the three traffic light settings. Columns α and β describe for each lane configuration the tightness of the upper bound interference power obtained by the model with respect to the median and mean powers measured in the traces, respectively. The tightness indicators α and β are defined as the percentage by which the power obtained by the model is above the median and mean of the traces.

According to the tables, in all lane configurations and traffic light timings, the interference power obtained by the model is above the median and mean interference power in the traces. Also, the tightness corresponding to the median and mean cases are on average 3.9% and 3.7%, respectively.

Another interesting finding is that the 14 largest interference powers measured in all cycles and in all scenarios occur on the intersection region. Also, in the model, the largest power is obtained in a cell located on the intersection region. In the traces, around 95% of the largest interference powers measured in all scenarios

Table 5.13: The tightness of the upper bound interference obtained by the model w.r.t median power in traces (powers are in dBm)

	Traces			Model			$\alpha(\%)$
	60s	100s	150s	60s	100s	150s	
2L	-56.9	-56.5	-56.3	-54.4	-54.3	-54.3	3.9
4L	-55.1	-54.5	-54.5	-52.8	-52.7	-52.7	3.5
6L	-54.1	-53.8	-53.7	-51.5	-51.5	-51.4	4.3
							$\bar{\alpha}$=3.9

Table 5.14: The tightness of the upper bound interference obtained by the model w.r.t the mean power in traces (powers are in dBm)

	Traces			Model			$\beta(\%)$
	60s	100s	150s	60s	100s	150s	
2L	-56.8	-56.5	-56.2	-54.4	-54.3	-54.3	3.9
4L	-54.9	-54.4	-54.5	-52.8	-52.7	-52.7	3.3
6L	-53.9	-53.5	-53.4	-51.5	-51.5	-51.4	3.8
							$\bar{\beta}$=3.7

are observed within 200 m of the intersection.

To gain more insight into the severity of interference in the intersection scenario, a comparison with the equivalent road stretch scenario operating in capacity state is performed and the results are shown in Figure 5.15. In the experiment, we selected the intersection scenario corresponding to T_c = 100 seconds and with three lane configurations. The speed limit parameter in the road stretch and the intersection scenarios is set to 69 kph. For comparability, in the road stretch scenario, we consider the interference power corresponding to the last hop (farthest from the Tx). Our experiment results show that in an intersection scenario the median interference power (in mW) can be as much as 56 times the median interference power in an equivalent road stretch scenario.

The above observations indicate the likeliness of the degradation in reliability of safety applications targeted to intersection scenarios. This include, but are not limited to, Cooperative Intersection Collision Avoidance System-Violation

(CICAS-V), Intersection Movement Assist (IMA), and Do Not Pass Warning (DNPW) [5].

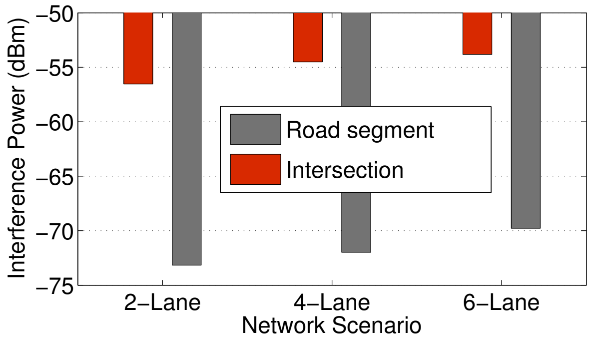

Figure 5.15: Comparison of interference powers measured in intersection and road segment scenarios (T_c = 100s, V_f = 69 kph)

5.9 Summary

In this chapter, a systematic approach was adopted to investigate the severity of hidden terminal interference as a primary cause of the degradation in reliability of broadcast communication in vehicular networks. With focus on the forced-flow traffic state dominating urban traffic systems, two major safety-critical traffic scenarios were identified and modelled using a well-established Cellular Automata (CA) traffic modelling paradigm. In an urban road stretch operating in capacity traffic state, a deterministic CA was designed to model the various traffic scenarios characterized by speed limit and lane configuration. Using a state-of-the-art radio propagation model targeted for vehicular environments, an analytical framework was designed to obtain the upper bound interference power and the lower bound reachable distance of broadcast safety messages. In a signalised intersection scenario, as the second safety-critical traffic scenario, a probabilistic CA was designed to model the traffic and the radio propagation model was employed to obtain an upper bound interference power for the entire intersection. Our extensive experiments with various velocities and lane configurations showed that in the road stretch scenario the interference power obtained by the model is an upper bound 96% of the time. The obtained reachable distance is a lower bound more than 94% of the time and exhibits a tightness of less than 9%. For the intersection scenario, the upper bound property of the model in terms of interference power was shown almost certain. Also, our experiments showed that the hidden terminal interference causes a significant decline in the reachable distance of broadcast messages, which in several cases drop to distances shorter than the minimum required coverage of medium range safety applications. In the intersection scenario, it was shown that the interference power of hidden nodes in the vicinity of the intersection region can be significantly large and may amount to values several times larger than the induced interference power in an equivalent road stretch scenario. The results demonstrate that the proposed analytical framework has the capability to be used as a benchmark for the assessment of the reliability risks of safety applications under safety-critical traffic scenarios.

Chapter 6

Information Dissemination: Background and Related Work

This chapter presents approaches and techniques of information dissemination in the general case of Delay Tolerant Networks (DTNs), and in Vehicular Ad hoc Networks (VANETs) as a particular example. The chapter begins with a definition of information dissemination and the classification of dissemination techniques (Section 6.1). The related work is presented in three sections: Section 6.2 surveys the related work in the context of VANETs; Section 6.3 addresses information dissemination in the context of general DTNs; and in Section 6.4, a new approach termed *popularity-based* content dissemination is introduced, which has received little attention in the contexts of VANETs and DTNs, but equally applicable to both. In Section 6.5, the related work is evaluated with a critical view. This section also builds the foundation of our contributions presented in Chapter 7. Finally, the chapter is summarised in Section 6.6.

6.1 Definition and Techniques

Information dissemination is the process of carrying information to a set of users potentially interested in the information. The set of target users can be limited to a single user, a certain number of users, or whoever interested in the information. As an extreme case, information flooding is a special type of information dissemination.

Dissemination of information is realized through a number of methods outlined as follows [65]:

- *Opportunistic:* a mobile node fetches information objects from other peer nodes or infrastructure once they are encountered [92].
- *Cooperative:* a node downloads a part(s) of a content and relies on other peer nodes to access the missing parts of the entire content [65]. This scheme is efficient when the size of the content is relatively large and the downloading time exceeds the contact duration of nodes.
- *Assisted by mobile nodes:* the information objects fetched by a mobile node during previous meetings are carried and delivered either to the fixed infrastructure units or to other nodes at the time of a meeting. The mobility pattern of nodes plays a key role in the performance outcome of this type of dissemination [65].

6.2 Information Dissemination in Vehicular Networks

6.2.1 Information Types

In the context of vehicular networks, the various types of information subject to dissemination are categorized as follows [65; 92]:

- *Safety and traffic information:* the objective of the dissemination of safety information is to promote the drivers' awareness of the hazardous events on a road. Traffic information, on the other hand, is used for traffic control and management purposes. It is also used to support the drivers to plan new routes in response to the traffic congestion in major urban roads.
- *Content:* the main difference between this type of information and the previous one is the relatively large size of a content object compared to other information types [65]. Therefore, the access to a content object is

generally longer compared to other information types. Due to the intrinsic differences, the techniques applicable to the dissemination of content objects differ from those applied to the dissemination of light-weight information. Chunk-based dissemination [50] is an example of an approach mainly used for content dissemination.

6.2.2 Literature Review

The dissemination process can be triggered by an information source/producer or a consumer. The former case is referred to as "push-based" dissemination, while the latter is termed "pull-based" content delivery [94].

6.2.2.1 Push-based information dissemination

Push-based dissemination allows applications to publish information to be served by multiple vehicles at the same time, e.g., information that concerns many vehicles such as traffic information, public service locations, city-wide events, etc. [94]. A well-known example in this class is AdTorrent [125] for the dissemination of commercial advertisements. Another example is a vehicle-assisted mechanism proposed in [187] for the extension of infrastructure coverage. In [132], an application framework was proposed for the distribution of videos with emergency nature. A content downloading framework relying on the cooperation of mobile nodes was proposed in [59]. [188] proposed an application framework with the objective of disseminating small-size information objects to vehicles situated in certain regions.

6.2.2.2 Pull-based information access

Lee *et al.* [87; 89] have identified a number of VANET services and applications relying on pull-based information retrieval. Examples of these applications are V3 [66], CarTorrent [86], MobEyes [90], and SPAWN [124].

6.3 Information Dissemination in DTNs

6.3.1 Literature Review

The main subject of dissemination proposals in the context of DTN is content. DTNs consist of mobile devices communicating in a "store-carry-forward" fashion, without any assumption on the presence of infrastructure [133]. Sporadic connectivity and the lack of permanent end-to-end paths in these kinds of networks hinder their applicability in delay sensitive applications; however, their potential utilization as a low cost network technology for delay tolerant content dissemination has attracted significant attention from the research community [35; 115; 129; 133; 181]. Content dissemination in DTNs is interpreted as a mechanism for carrying content to any node with interest in the content. Such a mechanism is typically realized in two different ways: routing and the subscribe/publish paradigm. In traditional routing, a consumer node demands a content object and the producer node(s) responds with the object carried through a pre-established route to the consumer. In the subscribe/publish paradigm [58], on the other hand, nodes advertise their interests or demands and a group of nodes acting as forwarding brokers are responsible for carrying the information of interest to the target consumer(s).

6.3.1.1 Routing

Routing as a message forwarding mechanism is addressed in [91; 99; 115; 158], to mention but a few studies. These works attempt to deliver content opportunistically, selecting next-hop nodes as carriers based mainly on their mobility and collocation information. In [99], a probabilistic routing algorithm is proposed, which relies on the period of collocation between nodes. [91] investigates methods to disseminate content to different target groups in an urban setting. [158] proposes a class of multi-copy protocols, termed *Spray* routing, to reach a trade-off between delay and the number of transmission attempts. In another study, Spyropoulos *et al.* [159] proposes a controlled replication scheme termed *Spray and Wait* to reduce the number of copies of a given message, and hence the number of transmissions per message, to L, with the flexibility to tune L in response to a delay requirement. Routing based on knowledge oracles is proposed in [71]. The authors considered various knowledge oracles to provide information about future contacts of nodes, available bandwidth, future traffic demand of the nodes, and the queue size at each node. Other routing schemes propose different forms of flooding control [186].

6.3.1.2 Publish/Subscribe scheme

The publish/subscribe paradigm was originally applied to Internet-based scenarios [58]. The authors in [51] introduced this paradigm to the context of mobile networks by establishing mobile publishers and subscribers and a set of backbone nodes responsible for content dissemination. In [134], a tree-based subscriber/publisher was proposed for relatively stable wireless environments. [181] proposed a broker-based content dissemination scheme targeted to dynamic wireless environments. Brokers are elected from mobile nodes based on an election mechanism which relies on knowledge of the community structure of the underlying network. The structure of the network in terms of the existing communities is identified and a broker(s) is selected from each community to disseminate content. The *Haggle* project released implementations of data and content-centric networks [129]. In Haggle, a node description represents a vector of interest attributes with weights assigned to the vector elements. The weights are then used for matching of the data attributes [31]. Content dissemination in Haggle is performed within two layers. The first layer involves ranked searches; that is, matching of nodes' individual interest vectors with the data in the cache. Ranked searches identify and prioritize data to be transmitted during a node contact. The second layer involves traditional forwarding among nodes to identify delegate forwarders, that is, nodes that are not interested in the data but are likely to deliver it. Bloom filters are used to avoid duplicate transmission of data that the other node already has; nodes exchange the Bloom filter instead of a long list with data in the caches. In [35], the authors suggest that each mobile node acts as a broker, arguing that building and maintaining the broker overlay is cost inefficient. In both [129] and [35], an autonomous community detection mechanism is used to identify communities and a weight is assigned to each cached object at the time of exchange to decide whether or not to fetch and forward that object, taking into account the current community of the node. In an attempt to minimise the computation and communication load imposed on intermediary nodes and in the meantime to achieve a high delivery ratio, Mashhadi *et al.* [115] proposed a mechanism termed *Habit* for content dissemination in Mobile Ad hoc Networks (MANETs).

6.4 Popularity-Based Information Dissemination

Popularity-based information dissemination aims at achieving network-wide performance of information delivery rather than individual node-based performance. The decision on which information to disseminate in a meeting incident is made based on the popularity of that information, which may or may not match perfectly with the individual interest of an encountered node. It departs from other dissemination approaches in several ways. First, the dissemination is not limited to a single recipient, i.e., the target of dissemination can be potentially many nodes with similar interests. Second, it relies only on one-hop forwarding as opposed to broadcast and multi-hop forwarding/routing where the information consumer is known in advance and the sender is able to route the content to its destination. Third, it is not necessarily bounded to a geographical area as in geocast-based services, although location-aware property can be presumed. Last, the dissemination trigger can be hybrid, that is, a combination of push and pull triggering mechanisms may be used. While content dissemination is the main task of a popularity-based system, it also can be employed as an information recommendation system that helps users discover new information. An example is a system that disseminates information about a special event (e.g., a concert) to users. The system decides to recommend the event to a user based on the popularity of the event and the user preferences.

While the idea of popularity-based dissemination appears highly promising in DTNs and particularly in VANETs, its potential merits and capabilities have not been explored well, except in few studies [94; 185]. CodeOn [94] is an information distribution framework designed for vehicular networks. CodeOn relies on proactive broadcast of contents from infrastructure units to vehicles in a region of interest. Also, it relies on dynamic selection of nodes to cooperatively relay the content. Roadcast [185] is a popularity-based content dissemination architecture proposed for vehicular networks. The motivation behind Roadcast is to avoid unnecessary delays of content access by disseminating popular contents first. This notion is in contrast with the conventional approaches of content dissemination in DTN, which emphasize on the delivery of the rare contents first. Zhang *et al.* [185] recommends the popularity-based content dissemination for vehicular applications, arguing that other approaches including the publish/subscribe paradigm may not suit the unique mobility and contact patterns of vehicles as they do for other DTNs.

6.5 Evaluation of Previous Studies

A major step towards fulfilling an efficient information-centric application is to fully understand the various tasks involved in the realization of the application. To achieve this aim, a reference framework describing the essential tasks and the involved inter-relations is highly demanded. The main criticism applied to the previous work in its entirety is the lack of such a framework. While the individual studies address some certain tasks, they stop short of addressing other possibly important ones and also the inter-play of the tasks. An example of missing functionalities in previous studies is an interaction model with the objective of describing the impacts of resource constraints and the state of the meeting nodes involved in information exchange.

Other criticisms are applied to the approaches employed in the implementation of functionalities. They are outlined as follows:

- In most previous work, content is seen as a black box without considering the content topic(s) or so-called content attribute(s). Furthermore, the approaches considering the content attributes rely only on atomic contents with a single attribute. Thus, these approaches are not applicable to compound contents with multiple attributes. This, in turn, overshadows the efficiency of the application due to the lack of discovery, matching and dissemination techniques appropriate for the case of compound contents.

- The above criticism is also applied to the way user interest(s) is modelled. In almost all existing approaches (except for Haggle), a user is assumed to have a single interest at a time. Furthermore, the user interest is expressed by the name of the information or content object. Thus, the notion of compound interests is missing in such approaches. This ultimately affects the user experience of the application due to the lack of appropriate discovery, matching and dissemination functionalities tailored to compound interests.

- Another criticism applied to the previous studies is the lack of adaptation to the shift in users' interests. Such a shortcoming is mainly seen in push-based approaches with inappropriate assumption of static interests. In these approaches, either the functionality of discovery is not implemented or they rely on predetermined user interests. With such assumption in effect, the users receive information objects matching with their past interests and not the ones related to their current interests.

- A criticism applied to the publish/subscribe scheme as the dominant approach in the context of DTNs relates to the reliance on a certain number of broker nodes taking the burden of content dissemination. This leads to several drawbacks. First, dependency on broker nodes turns into a system bottleneck because such nodes may leave the network or they are deactivated due to resource depletion (energy, buffer, etc). The selection of new brokers does not scale well, especially in highly dynamic environments such as vehicular networks. Second, it is not fair due to extreme resource usage of some nodes (i.e., brokers) while leaving the resources of others intact. A promising alternative scheme is to let each node participate in content distribution, but govern the degree of participation by the node's state and constraints. This approach avoids the drawbacks of publish/subscribe scheme; however, it requires a sophisticated interaction model accounting for various nodes' constraints and behaviours.

- While individual-oriented information dissemination strategies have been the mainstream focus of the previous studies, the capacity of social-oriented and also mixed dissemination strategies is not explored sufficiently. Central to the latter strategies is a popularity-based interest discovery and information dissemination mechanism. The promising efficiency of these strategies merits a focused study.

- The proposed solutions to content dissemination are restricted to a single technology and do not address the requirements for adaptation to various technologies under the broad class of DTNs. Ideally, an application framework targeted to various technologies contributes to significant saving of effort and cost, and in the meantime expands the information domain to a vast number of producers and consumers of information.

6.6 Summary

This chapter presented a survey of the solutions and approaches to information dissemination in the context of DTNs and VANETs. The drawbacks of existing approaches were identified and described, including the lack of a reference framework facilitating a full understanding of the various functionalities involved in the realization of information-centric applications.

Chapter 7

A Generic Application Framework for Information Dissemination in Delay Tolerant Networks

7.1 Introduction

As our main contribution in this chapter, we present a generic framework for describing the characteristics of content exchange among participating nodes in a Delay Tolerant Network (DTN). Among several components comprising the framework, we propose a distributed information popularity measurement and a pairwise node interaction formulated as a game theoretic problem. The framework is generally intended as a capstone for the investigation of information and content dissemination tasks, properties and various content exchange strategies in a DTN.

The main motivation of this study is to address the gaps and the drawbacks of the previous solutions to content dissemination, as we identified in Chapter 6. We aim to address those gaps by means of the following functionalities and properties incorporated in a generic framework:

(a) The proposed framework covers the missing functionalities in the previous solutions. As described in Chapter 6, one such functionality is the pairwise nodes' interaction on meeting incidents, which is deemed to influence the outcome of the content dissemination process in its entirety. The nodes' interaction is modelled as a game theoretic problem which takes into account the available network resource(s) and the current state of the meeting nodes to describe the pairwise content exchange process. The main objectives of the interaction model are the fair split of the network resource(s) and the maximization of nodes' utility.

(b) In contrast to the assumption of atomic content and the black-box content representation, we consider a content object as a compound object with multiple attributes (or topics). Accordingly, the associated functionalities including content popularity measurement and content ranking are adapted to the representation of compound contents.

(c) We propose a generic user model to represent users with compound interests, that is, multiple topics in the interest list of a user. The underlying functionalities are also adapted to this novel user representation model.

(d) Two realistic features of user interests are considered in the envisioned framework. First, user interests are not static. Second, the users' interests are not given *a priori*. To take these features into effect, the appropriate functionalities are incorporated in the framework to facilitate the learning of dynamic user interests.

(e) A popularity-based solution to information dissemination is developed which relies on the user interests learned in a distributed fashion.

(f) Instead of forcing a certain set of nodes, like brokers or central nodes as in the existing publish/subscribe proposals, to take the burden of content dissemination, we relax this limitation and let each node participate in content distribution; however, the degree of participation is governed by the current state and constraints of the node.

(g) Some essential guidelines are presented to facilitate the adaptation to various technologies under the broad class of DTNs.

The remainder of this chapter is organised as follows. In Section 7.2, the components and the associated tasks of the framework is briefly introduced. The user model component is presented in Section 7.3. In Section 7.4, we present the mechanisms designed in a mobile node for the measurement of information popularity from a network-wide standpoint. In Section 7.5, a game theoretic framework is proposed to model the interaction of nodes at the time of meeting and aiming at mutual content exchange. A similarity measurement mechanism is proposed in Section 7.6 which quantifies the degree of matching between the social view in a node with the cached contents in the node's buffer and also with the information interests of an encountered node. Section 7.7 presents the guidelines for the adaptation to various technologies. Section 7.8 presents the numerical study and finally, Section 7.9 summarises the chapter.

7.2 Model Component and Function Overview

The proposed framework consolidates all tasks required for the realization of information dissemination into a *node model* (Figure 7.1), which describes node behaviour in a DTN as it meets and exchanges information with peers. A *user model*, as a component of the node model, captures the information interests of individual nodes and assigns a weight to each information type the node is interested in. A second component termed *social popularity measurement model* collects peers' interest vectors on meeting incidents and constructs a pair of interest type and weight vectors representing the collective information interest of the network (i.e., social interests). We incorporate two fundamental features into the measurement mechanism: shift in information interests of nodes, and the formation of local communities. The former is a behavioural element while the latter is a structural element. We apply the measured information popularity to assign forwarding priorities to the content objects currently maintained in a node's cache. When it comes to the exchange of content objects, the measured information popularity is coupled with the *interaction model* of meeting nodes, taking into account the state and constraints of the nodes participating in an information exchange session. Figure 7.1 illustrates the essential components required to describe the behaviour of a node participating in information dissemination process. The internal functionalities associated with the components of the framework are described in the following sections.

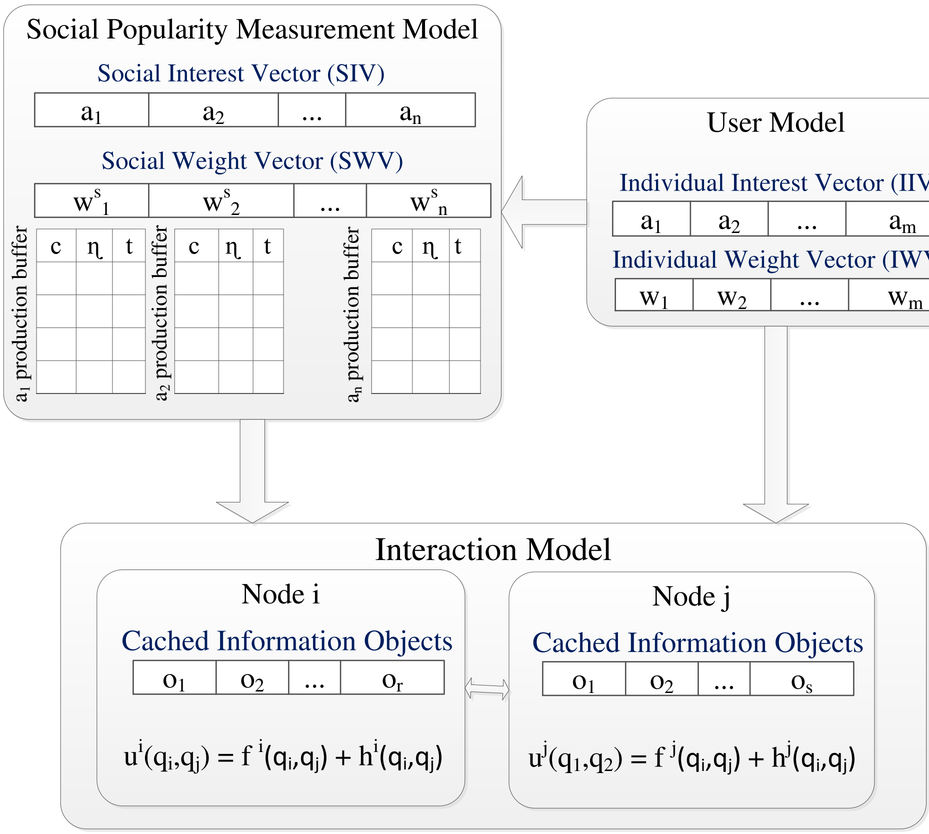

Figure 7.1: Model of a participant node in information dissemination process

7.3 User Model

We denote a consumer of information a “user”, regardless if the consumer is a person or a machine. The user model describes a node’s preferences or valuation of existing information attributes. It encompasses two major tasks: first, it uses a predefined internal process to identify the types of information the user is currently interested in. In practice, this can be implemented using direct feedback from a user or by implementing a background process which monitors the user’s activities and usage pattern of various information types. The second task is to represent the user interests and the associated valuation in order to enable other peers to collect the information interests of the user.

In this work, we assume a background user model is present and generates a ranked list of information attributes, sorted in descending order of attribute ranks. In Figure 7.1 this implies that attributes a_1 and a_m have the highest and lowest ranks, respectively. Such a ranked list determines the relative importance of information attributes rather than a quantified absolute significance of a given attribute in the list. To quantify the absolute significance, a weight is assigned to each attribute representing, e.g. the fraction of time a user spends on consuming information with the given attribute. The exact meaning of *attribute significance* can be defined for each type of information and also for various applications of the DTN.

We do not consider the implementation details of the actual user model. Thus, without loss of generality, we assign to each attribute a weight value generated by a distribution function. Among the candidate distribution functions, Zipf has proved to be a good representative model for many real life complex systems. The application of Zipf has also been introduced to the context of Internet and social networks [40]. We apply the Zipf distribution to obtain attribute weights according to the following expression:

$$f(k, \alpha, m) = \frac{\frac{1}{k^\alpha}}{\sum_{i=1}^{m}\left(\frac{1}{i^\alpha}\right)} \tag{7.1}$$

where m is the total number of attributes in the interest list of a node, k is the attribute rank, and α is an exponent.

To this end, the proposed user model is represented by a ranked attribute list termed *Individual Interest Vector* (IIV) and a weight vector termed *Individual Weight Vector* (IWV) (Figure 7.1). Given a list of ranked attributes in a node's IIV, the Zipf distribution determines the usage frequency for each attribute. Figure 7.2 demonstrates an example of Zipf's generated frequencies corresponding to attributes contained in IIVs with different sizes. The frequency values generated by Zipf distribution are then assigned to the elements of the node's IWV. Thus, a weight element in the IWV represents the valuation or significance of a corresponding attribute in the IIV.

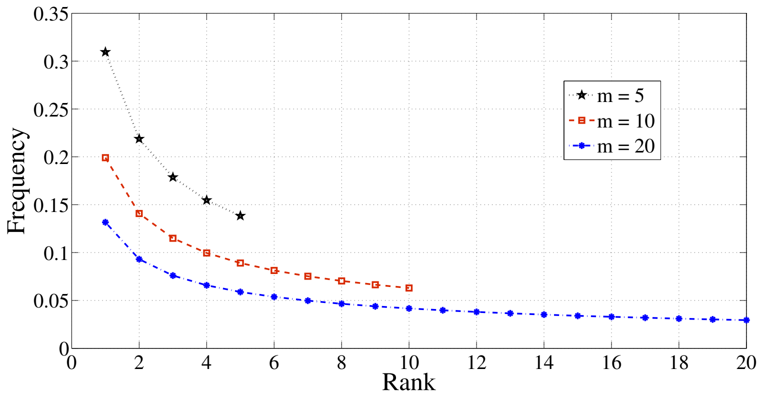

Figure 7.2: Zipf's probability mass function representing frequency distribution of ranked attributes contained in IIVs with different sizes. The exponent $\alpha = 0.5$ in all scenarios.

7.4 Measurement of Information Social Popularity

In the proposed node model, a vector termed *Social Interest Vector* (SIV) maintains in a node the information attributes advertised by other nodes as their information interests. A second vector termed *Social Weight Vector* (SWV) maintains for each attribute the social popularity (i.e., significance) of the attribute. Thus, an element in the SWV is a weight value representing the social significance of a corresponding attribute in the SIV. The SIV is a subset $\{a_i|a_i \in \Omega\}$ of information attributes, where Ω is the set of all possible information attributes in the system. The cardinality of Ω is assumed N. SIV is built and maintained continuously and incrementally by a node as it meets peers. More specifically, during a meeting incident, nodes exchange their individual interests and the valuation of those interests maintained in their IIVs and IWVs, respectively. In a node, the new attributes in the IIV of the peer node are added to the SIV and the attribute weights are adjusted accordingly and maintained in the SWV.

Our proposed model for information popularity measurement relies on two major social components: a behavioural component and a social structural component. The behavioural element reflects the transient nature of individual interests, that is, the shift in user's information interest over time. This implies that the model should not rely on one-time collected interest vectors corresponding to the peers encountered in the past. Instead, whenever a node is encountered, the SIV and SWV in a node are updated to reflect the possible changes of the information interests of the encountered node. This process guarantees that the model adapts to emerging events at all times during its life cycle. The social structural element involves the formation of *local communities*, among other structural entities representing the real world interactions of nodes. A local community from the standpoint of a given node is a set of nodes encountered frequently and recently compared to other peers in the network. It is not necessary for a node to have similar interests (i.e. IIV) to its local community. The notion of a local community implies that the social information popularity measured in a node will have a significant component induced by the local community compared to the component(s) induced by occasionally encountered peers. From a content exchange perspective, if the content in a node's cache is ordered with respect to the social interests measured in the node and represented by pair (SIV SWV), this leads to a state where a node with tight connection to its local community will prefer the dissemination of contents of interest to its own community to those interested by the rest of the network. This argument holds true if the information interests of the nodes comprising the local community of a node are not scattered. Therefore, we prefer to use the term *logical community* to be distinguished from physical community emerging based only on the contact patters of nodes. Moreover, nodes with balanced membership to several communities will act as *bridges*, muling content objects between those communities.

To this end, an adaptive information popularity measurement model is proposed, taking into account the properties described above. The popularity measurement process is described by Algorithm 7.1. In the following, we describe the process in more details.

When a node – termed *target node* for clarification – meets a peer node, it collects the peer's IIV and IWV. For each new attribute a detected in the peer's

Algorithm 7.1 Popularity Measurement of Information Attributes

Require: (SIV, SWV) , (IIV, IWV) , δ, T

$i \leftarrow 1$
while $i \leq size(IIV)$ **do**
  $j \leftarrow indexOf\,(SIV, IIV(i))$
  if $j \leq 0$ **then**
    $j \leftarrow createAttEntry(SIV)$
    $createWeightEntry(SWV)$
    $b_i^p \leftarrow assignBuffer(SWV(j))$
    $appendAtt(SIV(j), IIV(i))$
    $k \leftarrow appendWeight(b_i^p, IWV(i))$
  else
    $k \leftarrow findNearestNeighbour(b_i^p, IWV(i)$
    if $distance(b_i^p(k), IWV(i)) \leq \delta$ OR $isFull(b_i^p)$ **then**
      $b_i^p(k) \leftarrow aggregate(b_i^p(k), IWV(i))$
    else
      $k \leftarrow appendWeight(b_i^p, IWV(i))$
    end if
  end if
  $\eta_i(k) \leftarrow updateFrequncy(b_i^p(k), \eta_i(k), T)$
  $(b_i^p, \eta_i) \leftarrow aggregateClusters(b_i^p, \eta_i)$
  $SWV(j) \leftarrow updateSocialWeight(b_i^p, \eta_i)$
end while
$SWV \leftarrow normalize(SWV)$
$(SIV, SWV) \leftarrow sortDescend(SIV, SWV)$

IIV, an entry is created in the SIV of the target node. The weight value of attribute a, denoted by w_a, is fetched from the peer's IWV and is considered as the current social weight of a from the standpoint of the target node. Accordingly, a new entry in the target node's SWV is created which maintains the collected weight value. Obviously, the w_a reported by a peer node is not the only valuation of a in the network. Thus, it will not remain as the sole valuation of a contributing to the social weight of attribute a measured in the target node because, in future meetings, other nodes will report possibly different weight values for attribute a. This implies that a weight aggregation mechanism should be designed with the objective of producing a single value as the current designated social weight of the attribute. Such an aggregation mechanism requires that the reported weight values to be maintained in the target node, which in turn necessitates the allocation of a buffer space to the weight values of the attribute reported by various nodes in the previous meetings. However, if not handled properly, the size of the buffer will grow proportional to the number of encountered peers, which in turn raises scalability issues. To tackle this, a limited buffer space is assigned to the weight values of the attribute and a weight clustering scheme is designed for aggregation purpose. Denote by b_a^p a buffer with a fixed size P assigned to attribute a to maintain the weight clusters corresponding to this attribute. We denote this buffer *production buffer*. As shown in Figure 7.1, the following information entities are maintained in the b_a^p for each weight cluster: (i) c_i^a represents the weight value of the cluster i in b_a^p, (ii) t is the last time c_i^a was updated, and (iii) η_i^a represents the frequency at which the cluster i was selected as the nearest neighbour of the newly collected attribute weights. In other words, η_i^a is the update frequency of weight cluster c_i^a. We normalize η_i^a over a given time duration T in order to decay the old valuations of the attribute. To classify the newly collected attribute weight w_a, we determine the nearest neighbour based on $|w_a - c_i^a|$ and a parameter δ; if $|w_a - c_i^a| \leq \delta$ and $|w_a - c_i^a| = min(|w_a - c_j^a|) \quad \forall j \in [1, P] \wedge j \neq i$, w_a is classified to c_i^a and a new aggregated weight is obtained and assigned to c_i^a. If no cluster exists that satisfies $|w_a - c_i^a| \leq \delta$, but there exists an unused cluster entry among the P available clusters, w_a is assigned as the initial weight of a new cluster, otherwise a forced classification and aggregation is applied. Finally, η_i^a is incremented in order to account for this last update of the cluster weight c_i^a.

The aggregation procedure of a chosen weight cluster denoted by c_{old}^a[1] and a recently collected attribute weight w_a is defined as follows[2]:

$$c_{new}^a = (1 - \alpha(\Delta t))\, c_{old}^a + \alpha(\Delta t) w_a \tag{7.2}$$

where c_{new}^a is the weight cluster after aggregation. Δt indicates the time difference between the collection time of w_a and the last time the chosen weight cluster was updated. $\alpha(.) \in [0, 1]$ is a monotonically increasing function of time difference

[1] to highlight the fact that the weight of this cluster is old and subject to change
[2] for simplicity, the index i is eliminated from the cluster name

Δt. We apply $\alpha(.)$ in order to grant a larger contribution to the new attribute weight (i.e., w_a) compared to the old weight cluster. This ensures that a recently collected attribute weight will have a larger contribution in the new weight cluster and thus decays the stale attribute weights.

In the aftermath of an aggregation event, the new weight cluster may become the neighbour of an existing cluster. Thus, in step (19) of the algorithm, the entire production buffer is evaluated to find and apply potential aggregations. The aggregation of two weight clusters is slightly different from the aggregation of a weight cluster and a single attribute weight as described by Equation 7.2. In the former case the update frequencies of the two weight clusters should also be aggregated to obtain a single frequency. Denote by η_1 and η_2 the update frequencies of weight clusters c_1 and c_2. We define the aggregate update frequency η_{12} of the two weight clusters as $\eta_{12} = \min(\eta_1+\eta_2, 1)$. This implies that the update frequency of the resultant weight cluster is the accumulated update frequencies of the two neighbour weight clusters. The aggregation of the two weight clusters is expressed as follows:

$$c_g^a = \begin{cases} (1-\alpha(\Delta t))c_1^a + \alpha(\Delta t)c_2^a & s.t. \quad t_2 \geq t_1 \\ (1-\alpha(\Delta t))c_2^a + \alpha(\Delta t)c_1^a & \text{otherwise} \end{cases} \tag{7.3}$$

where c_g^a is the aggregate weight corresponding to attribute a. Also, $\Delta t = |t_2 - t_1|$ where t_1 and t_2 are the last update (or aggregation) times of c_1^a and c_2^a, respectively.

The aggregation mechanism described by Equation 7.3 ensures that a weight cluster with more recent update will have a larger contribution in the ultimate social weight of the attribute.

Two complementary tasks are performed in a node before exchanging content objects with a peer: first, using the various weight clusters corresponding to an attribute, the aggregate weight value is obtained for that attribute. Second, the social weight vector is normalized to obtain the relative popularity of different attributes currently maintained in the SWV. These tasks are implemented to facilitate the ranking of the various content objects maintained in the node's cache. Also, they facilitate the measurement of similarity between a node's view of information social popularity and the individual interest of an encountered peer (Section 7.5). The first task is indicated in line (20) of the Algorithm 7.1. The aggregate weight of attribute a is calculated as the normalized weighted sum of the cluster weights associated with that attribute, that is,

$$\bar{w}_a = \frac{\sum_{j=1}^{|c^a|} c_j^a \eta_j^a}{\sum_{j=1}^{|c^a|} \eta_j^a} \tag{7.4}$$

where $|c^a| \leq P$ is the effective (i.e., used) number of cluster weights corresponding to the attribute a. The second task is indicated in step (22). In this case, the aggregate weights of all attributes calculated by the first task are normalized with respect to the attribute with the highest update frequency. A ranked list of attributes is then created in step (23). The resultant weight of each attribute is considered as the social weight of that attribute (w^s in Figure 7.1). Note that the social weights are temporary and are subject to change in the next meeting(s).

The information popularity measured in a node and represented by the pair (SIV, SWV) is used to evaluate the relevance of content objects cached in a node with respect to the aggregate information interests of all peers in the network encountered so far. The evaluation process involves two steps: (i) weights are assigned to the attributes contained in a content object. We assume weights are generated using Zipf distribution in similar way to user representation described in Section 7.3, (ii) a disjoint vector comparison (as described in Section 7.6) is applied to evaluate the similarity between the attributes of a content object and the social attributes maintained in vector SIV.

On a meeting incident with a limited contact time, the evaluated relevance of content objects, in addition to other factors, is used to choose a subset of available content objects in a node to exchange with a peer. The object exchange decision is also influenced by the interaction features of the meeting nodes, which we detail next.

7.5 Interaction Model of Meeting Nodes

When two nodes carrying a number of content objects meet, each node tends to pursue a content exchange strategy which produces the highest possible payoff, where payoff is the difference between the profit and the cost involved in the enforcement of a strategy. Considering the content exchange as the main subject of interaction, each node, as its strategy, aim at establishing a balance between amounts of content it receives and transmits from/to the encountered party so that the content exchange will maximize the node's payoff. In a more general form, given a limited contact duration d during which nodes are able to exchange content objects, nodes seek a balance between the fractions of time d consumed for reception and transmission. The time fractions identified by a node as its strategy of choice can be different from those identified by the other party and, in some cases, the mutual strategies may conflict due to the selfish behaviour of nodes. In this sense, the behaviour of the meeting nodes can be captured using a two-player *bargaining problem*. The main step towards characterizing the bargain problem is to design the utility function describing the node's payoff. To this end, a generic utility function of a node i can be expressed as:

$$u^i(q_i, q_j, S_i) = f^i(q_j, S_i) + h^i(q_i, S_i) \quad s.t. \quad q_i + q_j \leq d \tag{7.5}$$

q_i and q_j are the individual strategies chosen by nodes i and j, respectively. More specifically, q_i is the fraction of the total transmission opportunity d which node i desires to acquire for the transmission of its cached contents. Similarly, q_j is the desired transmission opportunity of node j. S_i represents the current state of node i. f^i is the payoff accrued by node i if node j plays strategy q_j. h^i is the payoff accrued by player i if it chooses strategy q_i. h^i can have a negative value corresponding to the net cost involved in data transmission, e.g., due to fast depletion of energy resource. Conversely, a buffer discharge in a node with limited buffer space is a representative example where h^i admits a positive value. The constraint in Equation 7.5 ensures that the total transmission opportunities of the two meeting nodes do not exceed the contact duration d. We assume the meeting nodes have an identical estimate of the contact duration. The utility function of node j denoted by u^j is symmetric to u^i.

To characterize the generic utility function expressed by Equation 7.5, the utility parameters associated with nodes' interaction must be identified. The utility parameters impact the strategy played by a node, and are classified in two categories. The first category includes parameters describing the state of the node at the time of a meeting. In order to keep the model parsimonious, we restrict these parameters to a minimal set including the fraction of buffer space occupied in the node (denoted by b), the fraction of total energy consumed in the node (denoted by ξ), and the current satisfaction level of the node (denoted by ν). The satisfaction parameter $\nu \in [0, 1]$ is determined by the meeting history of the node and increases accumulatively as the node receives content objects matching its interest list. The model can be easily extended to incorporate additional parameters corresponding to more specific cases. The second parameter category is not directly related to a node's state; these parameters rather provide complementary information about the encountered party, hence impact the strategy selected by the node. The parameter r defined as the similarity between the social interest vector (i.e. SIV) maintained in a node and the individual interest vector (i.e. IIV) of an encountered node is an example of parameters belonging to this category. In our bargaining problem formulation, we apply parameters r and ν to describe the willingness of a node to receive content objects from the other party. The aforementioned interaction parameters corresponding to a pair of meeting nodes i and j are shown in Figure 7.3. To demonstrate the effect of the above mentioned parameters on the players' strategies, without loss of generality, we instantiate the generic utility function described by Equation 7.5 with a more practical and concrete function defined as follows:

$$\begin{aligned} u^i(q_i, q_j, S_i) &= r_{ji}(1-\nu_i)q_j + b_i(q_i - q_j) - \xi_i q_i \\ & s.t. \quad q_i + q_j \leq d \end{aligned} \tag{7.6}$$

Rearranging the Equation 7.6 with respect to the transmission opportunities q_i and q_j leads to a more straightforward expression as follows:

$$\begin{aligned} u^i(q_i, q_j, S_i) &= (r_{ji}(1-\nu_i) - b_i)\, q_j + (b_i - \xi_i)\, q_i \\ & s.t. \quad q_i + q_j \leq d \end{aligned} \tag{7.7}$$

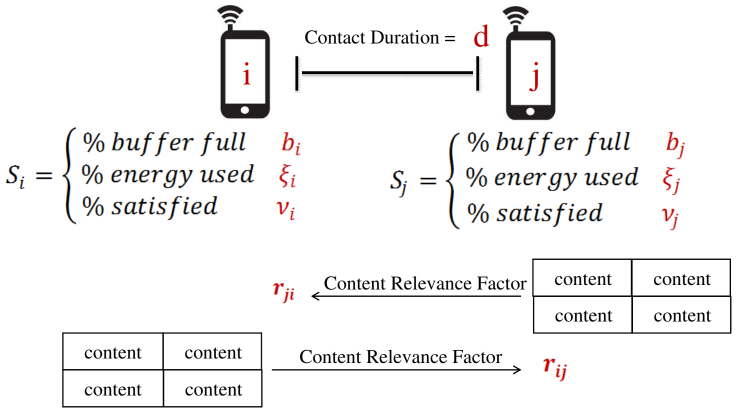

Figure 7.3: Interaction parameters of two meeting nodes

By analogy between Equations 7.5 and 7.7, $f^i = (r_{ji}(1 - \nu_i) - b_i)\, q_j$ and $h^i = (b_i - \xi_i)\, q_i$.

The definitions of f^i and h^i in Equation 7.7 are intuitive; a node i tends to choose a large fraction of time for transmission (i.e. q_i) if a significant fraction of its buffer space is occupied (represented by b_i) and/or the fraction of its energy consumed is low enough to permit the node to transmit more content objects. On the other hand, node i is willing to accept content objects from node j if: (i) node i has enough buffer space, (ii) node i realizes that the other party has interesting content objects, and/or (iii) node i is currently starving, e.g. due to not being satisfied during the previous interactions with other nodes. It is emphasized that the utility function described by Equation 7.7 is a representative example of potentially many alternatives. Therefore, it can be redefined with respect to the characteristics of the application under investigation.

A further step towards full characterization of the proposed game theoretic framework described by Equation 7.7 is to address scenarios emerging with respect to selfish and cooperative behaviours of meeting nodes.

7.5.1 Non-Cooperative Game Scenario

To identify the Nash equilibria of the game described by Equation 7.7, we obtain the mutual best response strategies of the nodes. Fixing the strategy of node j at any q_j, the best response strategy q_i of node i is only dependent on h^i. Thus, the best response strategy can be found by maximizing h^i while taking into account the constraint $q_i + q_j \leq d$. This leads to the following setting for q_i:

$$q_i = \begin{cases} 0 & \beta_i < \alpha_i \\ d' \leq d & o.w \end{cases} \tag{7.8}$$

where $\alpha_i = r_{ji}(1 - \nu_i) - b_i$ and $\beta_i = b_i - \xi_i$. Applying the same argument to node j, the best response q_j is obtained as follows:

$$q_j = \begin{cases} 0 & \beta_j < \alpha_j \\ d'' \leq d & o.w \end{cases} \tag{7.9}$$

where $\alpha_j = r_{ij}(1 - \nu_j) - b_j$ and $\beta_j = b_j - \xi_j$. Combining Equations 7.8 and 7.9, the set of equilibria existing in the game are obtained as $(\mathbf{q_i^*}, \mathbf{q_j^*}) = \{(0, 0),$ $(d', 0)$, $(0, d'')$, $(d', d'')\}$. If $d' + d'' > d$, the last equilibrium (i.e., (d', d'')) is not feasible since it violates the game constraint on the total transmission opportunity d. In fact, this equilibrium is the only case when an actual contention between nodes takes place. However, due to the infeasibility of the equilibrium, none of nodes benefits from the competition. We tackle this situation in the context of a cooperative bargaining problem as detailed in the next section.

7.5.2 Cooperative Bargaining Scenario

In cooperative games, players (in this case, meeting nodes) aim to reach an agreement on the splitting of a resource that yields mutual advantage. In this case, the resource is the amount of time available for transmission, that is, the contact duration d. A player i has its own utility function $u^i(q_i, q_j, S_i)$ which is determined by the allocated resource and its current state. Player i also has a minimum desired utility ($u_0^i(q_i, q_j, S_i)$) termed *disagreement point* which corresponds to the minimum utility that the player expects to accrue by participating in a game without cooperation. In a cooperative bargaining, it is guaranteed that each player at least gains the minimum desired utility. Let $U = \{(u^i, u^j)\} \subset R^2$ be the feasible utility set assumed to be convex, non-empty, closed, and bounded.

Also, let $U_0 = \left\{ \left(u_0^i, u_0^j \right) \right\} \subset R^2$ be the disagreement points of the meeting nodes. The pair (U, U_0) together describes the bargaining problem. The solution of the bargaining problem is reduced to finding a Pareto optimal point in the set U. A Pareto optimal point is a point such that it is impossible to discover other points resulting in strictly larger advantage for the two players, simultaneously.

Definition 1. *Pareto Optimality: in a two-player game with players i and j and a utility pair $(u^i, u^j) \subset R^2$ corresponding to a resource allocation pair (q_i, q_j), if for each $(\bar{u}^i, \bar{u}^j) \in U$, $(\bar{u}^i, \bar{u}^j) \geq (u^i, u^j)$ implies $(\bar{u}^i, \bar{u}^j) = (u^i, u^j)$.*

Definition 1 implies that there may exist an infinite number of Pareto optimal points in the game. Hence, selection criteria are needed for the bargaining solution in order to identify a Pareto optimal point which is in the best interest of both players. Different bargaining solutions provides different criteria in terms of optimality and fairness for different bargaining problems. Nash Bargaining Solution (NBS) [126] and Kalai-Smorodinsky Bargaining Solution (KSBS) [74] are the most popular approaches used in the literature for different application domains. KSBS differs from NBS in that it replaces the axiom of irrelevant alternatives with the axiom of individual monotonicity [131]. The KSBS does not impose strict requirements on the convexity of feasible utility set, while the convexity is a strict condition in Nash bargaining solution. Moreover, various types of fairness can be realized by KSBS as opposed to the Nash bargaining solution [131]. As we avoid to be bounded to a specific utility function and utility set and also due to the potential fairness requirements, we opt for KSBS as our choice of bargaining solution in this work.

To find the Pareto optimal point of the bargaining problem, we determine the bargaining set B consisting of the Pareto frontier points. In the game problem described by Equation 7.7 for node i (and a symmetric equation for the other node j), a Pareto frontier point is the pair (u^i, u^j) of utilities corresponding to a feasible resource allocation (q_i, q_j) such that $q_i + q_j = d$. We solve Equation 7.7 for q_i and q_j as functions of u^i and u^j and obtain the bargaining set B as follows:

$$B \;=\; \left\{ (u^i, u^j) \,|q_i\,(u^i, u^j) + q_j\,(u^i, u^j) = d \quad s.t \quad u^i \quad and \quad u^j > 0 \right\} \qquad (7.10)$$

Assuming that each node is aware of its desired utility, the KSB solution must satisfy the following equation [139]:

$$\mathbf{u}^* = \mathbf{u_0} + k^* \left(\mathbf{u_{max}} - \mathbf{u_0} \right) \tag{7.11}$$

where $\mathbf{u}^* = ((u^i)^*, (u^j)^*)$ is the KSB solution, k^* is the maximum value of k such that $\mathbf{u}^* \in U$, and $\mathbf{u_{max}} = (u^i_{max}, u^j_{max}) \geq \mathbf{u_0}$ specifies the best alternative (or the desired utility pairs) in U for each player. From Equation 7.11 and recalling that $\mathbf{u_0} = (0, 0)$, it can easily be verified that $\frac{u_i}{u^i_{max}} = \frac{u_j}{u^j_{max}}$. The KSBS is the intersection of bargaining set B described by Equation 7.10 and the line S defined as follows:

$$S = \left\{ \left(u^i, u^j \right) \middle| \ \frac{u_i}{u^i_{max}} = \frac{u_j}{u^j_{max}} \quad s.t \quad u^i \quad and \quad u^j > 0 \right\} \tag{7.12}$$

Setting $u^i = k u^i_{max}$, $u^j = k u^j_{max}$, and substituting in Equation 7.10 determines k, and hence $\mathbf{u}^* = ((u^i)^*, (u^j)^*)$. Correspondingly, q_i and q_j are obtained by applying $(u^i)^*$ and $(u^j)^*$ to Equation 7.7. Figure 7.4 shows a graphical illustration of the bargaining solution determined by the KSBS approach described above.

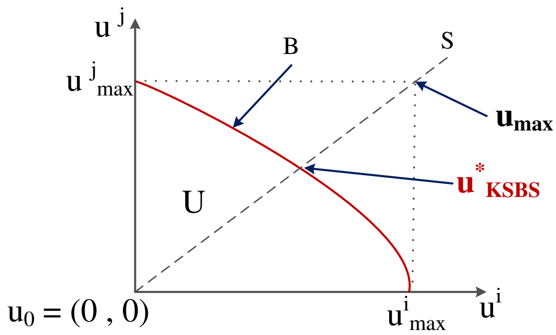

Figure 7.4: An illustration of KSBS with two players

It is worth mentioning that KSBS determines the share of transmission opportunities in such a way that the fairness in terms of utilities accrued by the meeting nodes is guaranteed. The fairness criterion for the meeting nodes should also be fulfilled during the exchange of each content object. Considering the stochastic nature of the communication channel which may cause some disruptions during the content exchange, a scheduling mechanism similar to Weighted Fair Queuing

(WFQ) must be employed to maintain fairness at all time during the content exchange.

7.6 Similarity of Individual and Social Information Interests

Parameter r_{ij} (and similarly r_{ji}) in Equation 7.7 plays an important role in the proposed game theoretic model of node interaction, since it determines the degree of a node's willingness for cooperation. Recall that we defined r_{ji} (r_{ij}) as the amount of similarity between node j's (i's) SIV and node i's (j's) IIV. Also recall that content objects in a node are weighted and ranked for forwarding according to SIV and the corresponding weight vector SWV measured by the node. It follows that a large r_{ji} can be interpreted as a high probability that node j is carrying a number of objects in top positions of its buffer that are likely to be of interest to node i, thus giving node i enough motivation to receive those objects.

To calculate r_{ji}, we assume that node i shares its pair (IIV , IWV) with node j during the meeting incident before the game starts. Then node j measures the similarity between node i's IIV ranked with respect to IWV and its own SIV ranked using SWV. Thus, the entire process can be reduced to the similarity measure of two ranked vectors. As per similarity measurement techniques [39; 175], the vectors subject to comparison here are generally disjoint and of different sizes. Furthermore, the top rank positions of the two vectors are expected to exhibit larger contributions to the overall similarity of vectors. Such unique measurement requirements prevent direct application of the existing similarity measure techniques. Most relevant to our case is [175], where an indicator termed Ranked-Biased Overlapping (RBO) is calculated as the similarity measure of two infinite size vectors. RBO of two vectors S and T is defined as [175]:

$$RBO(S,T,p) = (1-p)\sum_{d=1}^{\infty} p^{d-1} A_d \tag{7.13}$$

where A_d is the degree of overlapping at depth d of the vectors and $0 < p < 1$ is a constant devised to assign an overlapping contribution proportional to the position in the vectors where overlapping occurs. In this sense, RBO is classified as a top-weighted technique. On the other hand, RBO is classified as an equal-size similarity measure, since the sizes of both vectors are assumed to be infinite. The latter characteristic of RBO hinders its direct applicability to our case. The main reason is that the overlap weights in Equation 7.13 (i.e. $(1-p)p^{d-1}$) form a geometric series with their sum converging to 1 as the depth d approaches ∞. However, in our case, we deal with finite size vectors, thus the weighting scheme in Equation 7.13 cannot be applied. Furthermore, in our case the vector sizes are not equal, which necessitates the design of a proprietary similarity measure. In the following, we propose a new similarity measure which copes with the drawbacks of RBO while preserving its top-weighted feature.

Assume that the lengths of node j's SIV (and SWV) and node i's IIV (and IWV) are denoted by m and n, respectively. It follows that $m \geq n$. This is supported by the fact that the nodes exchange their IIVs on a meeting incident and update their previous SIVs with respect to the received IIV from the other party. Thus, the size of the updated SIV in a node is at least as large as the other party's IIV. We are also aware of the facts that IWV in a node i determines the relative importance of attributes contained in the node's IIV and that the sum of weight elements in IWV is 1 (due to normalization). Likewise, the relative importance of attributes in SIV is determined by weight elements in SWV and the sum of weight elements of SWV is 1. These features imply that the attribute weight elements maintained in node i's IWV and node j's SWV are good candidates for position-based weighting in the envisioned similarity measure. In other words, using the weight elements in IWV and SWV enables the similarity measure with top-weightedness property. Taking all these into consideration, we propose the following expression to calculate r_{ji}:

$$
\begin{aligned}
r_{ji} = \quad & \operatorname{argmax}_k \left(p^k \sum_{d=1}^{n} \left(\frac{IWV_d + SWV_{k+d}}{2} \right) A\left(IIV_{1:d}, SIV_{k:k+d}\right) \right) \\
& s.t.\ 0 \leq k \leq m-n
\end{aligned}
\tag{7.14}
$$

where k is the number of positional shifts applied to the smaller vector, IWV_d and SWV_{k+d} are the weight elements of IIV and SWV at positions d and $k+d$, respectively. $IIV_{1:d}$ and $SIV_{k:k+d}$ are the subset of attributes located at positions 1 to d of IIV, and k to $k+d$ of SIV, respectively. We apply the arithmetic average of IWV and SWV as the overlapping weight. It is straightforward to show that $0 \leq \sum_{d=1}^{n}\left(\frac{IWV_d+SWV_{k+d}}{2}\right) \leq 1$, thus the similarity measure is normalized. Generally, any normalized combination of IWV and SWV provided that it preserves the top-weighted property can be used in Equation 7.14. Figure 7.5 demonstrates a physical interpretation of the proposed similarity measure with $p = 0.7$. In the example depicted in the figure, the maximum similarity is obtained after one shift and the relevance factor is obtained as $r_{ji} = 0.1715$. In Figure 7.6, we illustrate how the similarity measure preserves the top-weighted property. Two vectors IIV_1 and IIV_2 only differ with respect to the ranks of attributes a and b. The vector with higher overlapping in the top positions (i.e. IIV_1) exhibits a larger similarity to the SIV. In both figures, the weight values of attributes are generated using Zipf distribution.

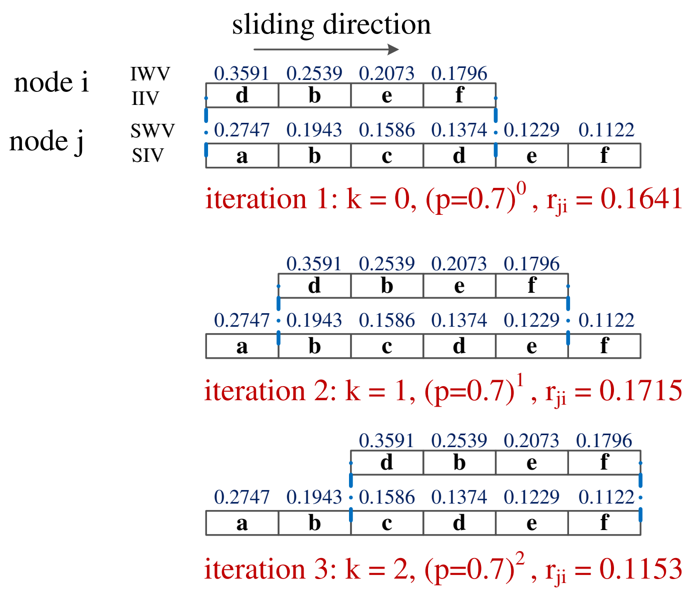

Figure 7.5: Similarity measure of individual and social interests. With $p = 0.7$, the maximum relevance $r_{ji} = 0.1715$ is obtained after a single shift (i.e., $k = 1$).

The similarity measurement described by Equation 7.14 is also employed as a generic similarity measure of disjoint vectors to calculate the matching between the topics of the content objects in a node's cache and the social information view of the node maintained in vectors (SIV SWV). The measured similarity is

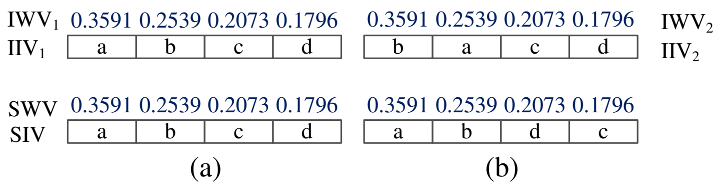

Figure 7.6: Top-weighted property of the proposed similarity measure. (a) $A = [1, 1, 1, 1]$, $r = 1$, and (b) $A = [0, 1, 1, 1]$, $r = 0.6408$

then used for the purpose of ranking and sorting of the cached contents in the node with respect to the social interests of the network. This further enables the prioritized forwarding of contents based on their relative social significance.

7.7 Adaptation to Different Technologies

The generic game theoretic framework described above can be further customized based on the target technology in use and also the user preferences. In a 3G/4G network with memory rich user devices, buffer space is presumably large and thus the energy parameter will act as the major driving factor influencing the strategy of a node. On the other hand, with technologies lacking the energy constraint, e.g., VANETs, the available energy reserve is large most of the time and a node's transmission is restricted mainly by the amount of content objects available in its cache and the contact duration d. To enable the model with this flexibility, we define threshold parameters b_{th} and ξ_{th} and redefine b and ξ as follows:

$$\hat{b} = \begin{cases} \frac{b}{b_{th}} & b < b_{th} \\ 1 & o.w \end{cases} \tag{7.15}$$

$$\hat{\xi_i} = \begin{cases} \frac{\xi}{\xi_{th}} & \xi < \xi_{th} \\ 1 & o.w \end{cases} \tag{7.16}$$

In devices with strict buffer or energy constraints, b_{th} and ξ_{th} admit small values. These settings will also enable nodes to become generous or conservative in content dissemination process depending on their current state and the values of the threshold parameters.

Another parameter influencing the outcome information dissemination is the contact duration d. The contact duration depends on the type of the communication platform. While in 3G/4G networks the contact duration is in the order of several minutes, in highly dynamic networks such as VANETs, it is in the order of few seconds. Furthermore, in 3G/4G networks, users are free to remain in contact until the contents of interest are exchanged completely, whereas in VANETs such freedom does not exist due to the external restrictions and the transportation specific regulations. The awareness about contact duration, as it is assumed in our proposed framework, can be viewed as a strong advantage compared to the counterpart approaches. In particular, the proposed interaction model has the capability to adapt to the available contact duration in order to enforce optimal exchange of cached contents in the meeting nodes.

7.8 Experimental Results

Numerical studies are carried out to validate that the model behaves correctly according to basic elements of a content dissemination network. We focus on structural and behavioural elements to validate the proposed model. To validate the structural element, the impacts of the size of node communities with similar interests and the meeting pattern of nodes on the outcome content dissemination behaviour are addressed. To perform validation with respect to the behavioural element, we address the impacts of strategies chosen by nodes as well as the shift in nodes' interests on the dissemination process. Performance aspects are left for the evaluation of such specific extensions in content dissemination strategies. For this reason, our studies are independent of performance considerations such as mobility rates and patterns, probabilities of successful transmissions etc.

We implemented a discrete event simulator in MATLAB to simulate meetings. Nodes are divided into separate groups, where nodes in a group are assigned a subset of similar content attributes at the top of their interest vectors and the rest of the nodes' content attributes are chosen randomly and assigned to random positions in the interest vector. Different groups have different sets of attributes at the top of their nodes' interest vectors. The grouping scheme further allows us to achieve high level of flexibility in representing various network conditions

Table 7.1: Configuration of global simulation parameters

Ω	$d(sconds)$	p	$T(hours)$	δ	b_{th}	ξ_{th}
6	1.2	0.8	5	10^{-2}	0.7	0.2

by defining custom meeting patterns inside and between nodes' groups. Similar to the node grouping, we also group the content objects with respect to the contained topics (i.e. attributes). The objects' attributes are assigned in a similar way to nodes' attributes. Each object group is targeted to a node group. Depending on the objectives of a simulation scenario, different numbers of groups are used. Throughout the simulations we assume the total number of unique content attributes (Ω) in the network is 6 attributes indexed by a_1, $a_2, \cdots, a_6$. Using larger number of attributes only complicates our discussions hereafter, and does not affect the validity of the model in general. The object buffer in each node is set to a size of 1000 objects, and the attribute weight clusters used for popularity measurement in a node has a size of 4. Packet time and energy usage per packet are fixed to 0.3 second and 10^{-3} unit of energy, respectively. The satisfaction parameter ν is set to 0, meaning that nodes are always willing to receive contents as long as other constraints allow to do so. However, in field experiments with real users, the satisfaction parameter should be adapted with respect to the implicit or explicit user feedback after each meeting incident. Table 7.1 shows the configuration of the remaining simulation parameters.

Figures 7.7 and 7.8 demonstrate the behaviour of the model in response to difference in the size of node groups involving in object forwarding. The meeting rates of all nodes are identical. Practically, this setting results in different distributions of object popularity among node groups. The x-axis represents the number of iterations and can be interpreted as the number of hours, days, or other meaningful units. The y-axis represents the penetration rate of objects of different types targeted to different node groups. Figure 7.7 addresses a scenario where a weak majority exists in the network. Two groups of nodes are defined with sizes of 51 and 49 nodes. The nodes in the former group are mainly interested in attributes a_1 and a_2 while the nodes in the latter group are mostly interested in attributes a_3 and a_4. Two groups of content objects of equal size 100 are shared among two source nodes, each chosen from a group of nodes. Each

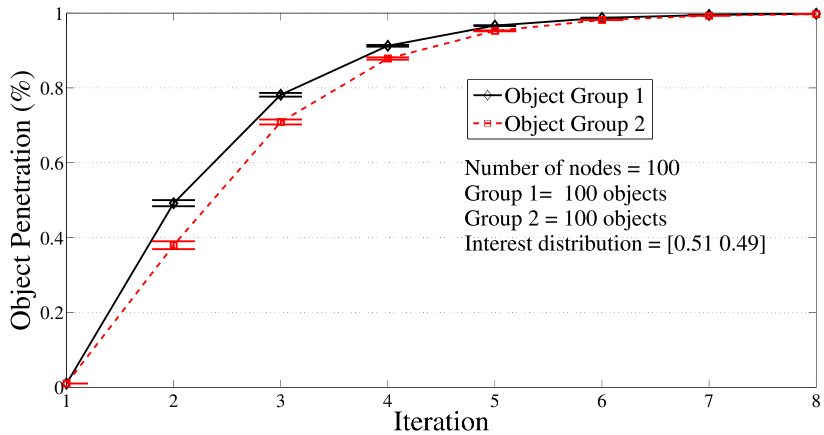

Figure 7.7: Weak majority: group 2 objects are slightly less popular than group 1 objects (0.49 vs. 0.51)

group of objects are of interest to a group of nodes; i.e. at the top of the nodes' attribute vectors, group 1 have attributes a_1 and a_2 and group 2 have attributes a_3 and a_4.

As shown in Figure 7.7, the content of interest to the majority group (with size 51) is disseminated faster than the content targeted to the minority (with size 49). This scenario verifies that the popularity measurement and object forwarding model is capable of majority oriented dissemination even in the presence of a weak majority. Figure 7.8a demonstrates a strong majority scenario. Three groups of nodes with sizes of 30, 10, and 10 are defined and the interest vectors of the nodes in these three groups consist of attribute pairs (a_1 , a_2), (a_3 , a_4), and (a_5 , a_6), respectively. 540 objects from three different types are initially shared by three sources selected from these groups. As expected, the group with a larger population dominates the community and receives its objects of interest faster. As the remaining two minority groups have identical sizes, they receive their objects of interest at identical rate as expected. In Figure 7.8b, the three groups have equal sizes. Since the meeting rates of the three groups are also identical, no single group has an advantage and thus the content dissemination is performed uniformly. Figure 7.8c is an extension of the scenario demonstrated by 7.8a. In this scenario, the group sizes are set to 30, 20, and 10 nodes. The result of this scenario leads us to conclude that in case of identical meeting rates, the

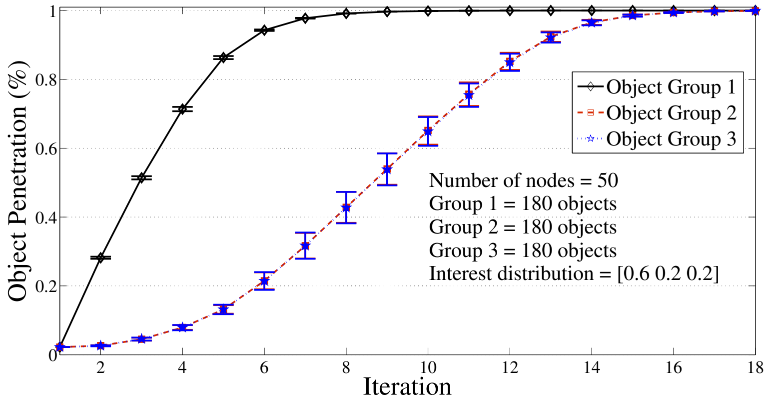

(a) Group 1: high, Group 2 & 3: medium popularity

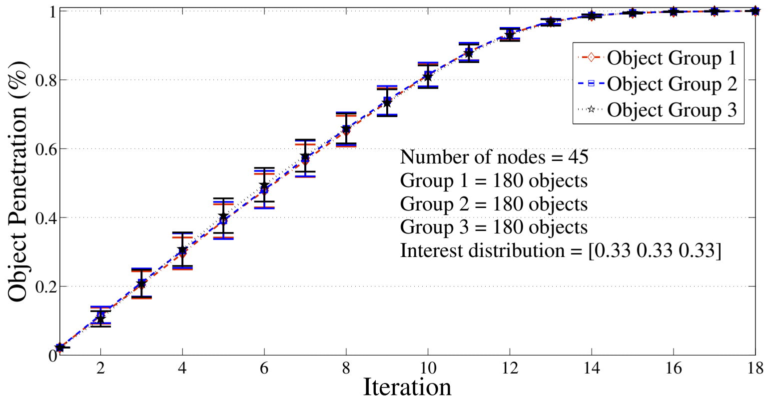

(b) Three object groups with similar popularity

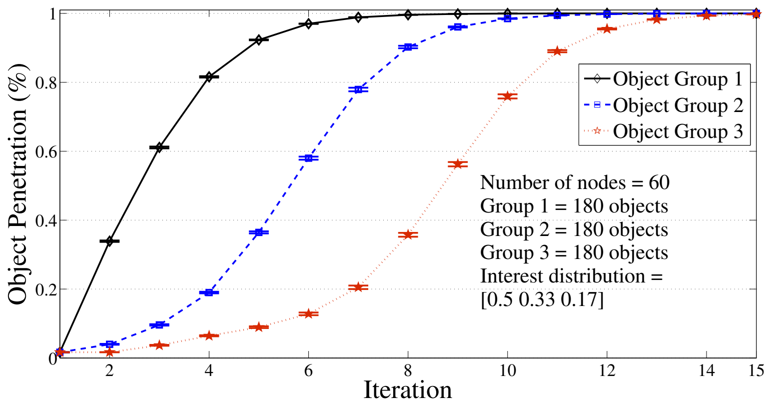

(c) Group 1: high, Group 2: medium, Group 3: low popularity

Figure 7.8: Impact of content popularity distribution on the outcome dissemination behaviour

dissemination priority of contents targeted to different node groups is identified based on the size of groups with similar interests. It is worth mentioning that the interpretation of the network structure with respect to its physical and logical elements yields different number of communities in the above scenarios. The similar contact patterns of nodes implies for the presence of only a single community in all scenarios, whereas the content popularity distribution in the network implies for 2, 3, and 3 communities in scenarios (a), (b), and (c), respectively. The conclusion to be drawn here is that given a uniform physical network structure (i.e, uniform contact rates), the dissemination behaviour is driven by the logical structure formed based on content popularity distribution. Accordingly, the network tends to serve majority communities with high priority.

Following this, we study scenarios where the contact patterns of nodes play a key role in the outcome behaviour of content dissemination. Two scenarios of this kind are selected as demonstrated in Figure 7.9. In these scenarios the node groups are of identical sizes. We assign a larger intra-group meeting rate to nodes in one of the groups, whereas the meeting rates for the remaining groups and the inter-group meetings are kept smaller but identical. This setting only holds for a warm-up period where nodes build their view of information social popularity. In the content dissemination phase, we assign identical contact rates to all groups. This approach enables us to evaluate the function of the social popularity measurement component of the model. It is observed in Figure 7.9a that the content dissemination behaviour in this scenario is comparable to the scenario depicted in 7.8a. This leads us to conclude that contact patterns also contribute to the formation of a majority, thus forcing others to dedicate more resources to disseminate the content of interest to the majority. In the second scenario in this experiment, we introduced a degree of isolation in one of the two groups; i.e. a subset of nodes in a group never visits the others in the same group. As in the previous scenario, we defined this setting only for a warm-up period. As shown in Figure 7.9b, the content of interest to the isolated group (group B) is disseminated at a lower rate compared to the tighter group A. The intuition behind this phenomenon is that the nodes in an isolated community will have a weaker belief in their social interests compared to the communities with strong internal bonds. This motivates the isolated nodes to join the non-isolated ones, forming a local community and contributing to the dissemination of the content they favour.

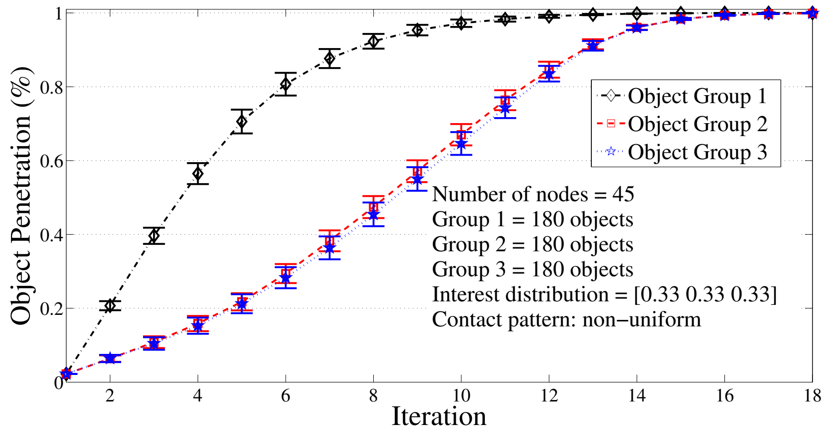

(a) Group 1 and group 2 objects are interested by groups of nodes with high and low contact rates, respectively.

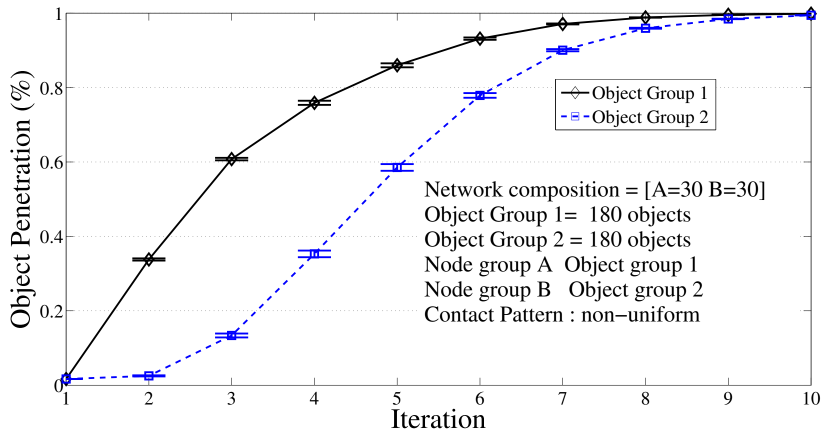

(b) Group 1 and group 2 objects are interested by tight and scattered communities, respectively.

Figure 7.9: Impact of non-uniform contact patterns on the content dissemination behaviour

We investigate the impacts of social and individual-oriented dissemination strategies on the outcome content dissemination behaviour in Figure 7.10. The solid curves show the penetration of object groups when the ordering of information objects are determined based on the individual interests of the encountered party and the dotted curves demonstrate the social-oriented object dissemination. As in the scenario in Figure 7.8c, three groups of nodes of sizes 30, 20, and 10 with identical meeting rates are configured. According to Figure 7.10, an individual-oriented strategy causes the dominance of majorities on the content ordering to be reduced in favour of minorities, and to be only proportional to the size of node groups. This leads to less inclination of nodes towards the dissemination of network-wide popular contents.

Finally, we address the impact of nodes' shifting interests on the content dissemination behaviour. Two groups of nodes with sizes 12 and 10 and identical contact rates are established. The nodes in each group have identical interests with nodes in the same group. A number of 2000 content objects are initially shared by two sources selected from the two groups. After 10 iterations, 2 nodes from the larger group change their interests and become members of the smaller group. According to Figure 7.11, in the first 10 iterations, the first group becomes dominant and their targeted contents gain higher penetration. After the shift in interest, the second group becomes dominant and the dissemination priority changes as a result. The relatively higher fluctuations of the curves in 7.11 (compared to previous scenarios) are attributed to the elimination of the warm-up period, which in turn introduce some degree of randomness in the popularity measurement model. However, this result confirms that the integration of warm-up and dissemination phases is possible in the proposed model.

As a general observation of all simulation scenarios, the pace of content dissemination decreases when the content density in the network increases. Such a finding is in agreement with other similar findings in the context of DTN.

7.9 Summary

We proposed a generic framework intended as a capstone architecture incorporating various content dissemination functionalities and properties. This framework, while being independent from the underlying network architecture and the mobility and meeting patterns among nodes, enables a typical node to dynamically build its view of the information interests of other participating nodes. Such capability coupled with the interaction model of meeting nodes facilitate the realization of various content dissemination strategies while fulfilling the individual nodes' constraints in terms of buffer space, energy, etc. We numerically validated

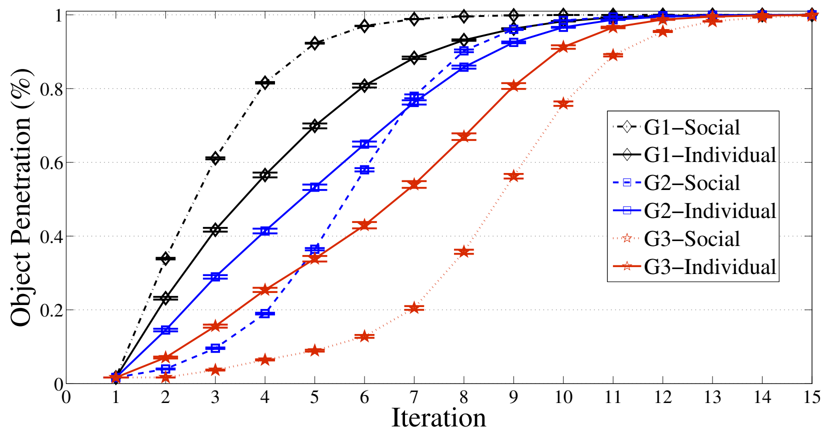

Figure 7.10: Comparison of social and individual-oriented content dissemination strategies

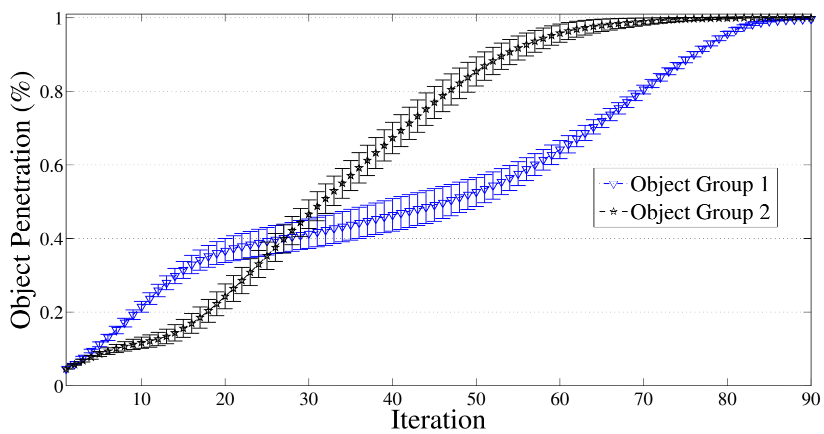

Figure 7.11: The impact of shift in nodes' interests

the model with respect to structural and behavioural elements of content dissemination network, where we showed that the model well captures the essential network properties such as dynamic composition of nodes' communities, and in the meantime reacts quickly to the shift in information interests of nodes. We further showed that, opposed to the widely accepted assumption that the physical structure of the network is the main factor driving the outcome behaviour of the dissemination task, the logical structure formed by the contact and interest patterns of the participant nodes is the key influential factor.

Chapter 8

Conclusions and Future Directions

Through a number of contributions, this thesis has advanced the state of the art in safety applications of vehicular communication networks in terms of reliability issues. Also, the generic information dissemination framework proposed for the case of non-safety applications provides a reference architecture for accurate characterization of diverse tasks and factors affecting the efficiency of applications.

The main contributions of this thesis were presented in four chapters. In this chapter, we summarise the conclusions and directions for future work on a chapter by chapter basis.

8.1 Traffic Density Model (Chapter 3)

8.1.1 Conclusions

In Chapter 3, we proposed a traffic density model for urban traffic systems with heterogeneous traffic phases. It was shown that the model captures well the traffic dynamics of road segments connected to signalised intersections. Using the traffic density model, we showed that the overlapping radios behave in a highly dynamic manner, which cannot be adequately captured by the widely used uniform density models with steady-state traffic assumption. Based on the proposed density model, we also investigated the radio overlap and channel load of safety beacon messages. We showed that, in an intersection scenario with 3-lane road segments and applying the nominal settings of DSRC parameters (500 byte messages, 10 Hz beaconing, and 1000 m transmission range), the channel load can be as high as 18 Mbps, indicating that the use of data rates in the lower part of the DSRC's range is highly questionable, especially in congested traffic scenarios.

8.1.2 Future Directions

Extension of the radio overlapping model

While our emphasis in Chapter 3 was to capture the realism in one component of the host system, this is the vehicular traffic model, for tractability of the analytical model we relaxed the evaluation of the radio overlap by adopting a unit disk model to represent the other component, i.e., radio propagation. This is a conservative approach, and using a more realistic propagation model with channel errors would indeed further increase the channel occupancy due to excessive uncoordinated transmissions.

Extension to bidirectional traffic

The traffic density model was developed with the assumption of one-way traffic, and the evaluation of radio overlap and channel load were also performed based on one-way traffic. Although it is expected that the radio overlap intensifies and channel load increases in two-way traffic scenarios, accurate understanding of such factors calls for extension of the model to a two-way traffic scenario in road segments connected to signalised intersections. Unfortunately, traffic models for two-way scenarios in signalised road segments do not exist in the literature. Therefore, a dedicated research is demanded for the development of new traffic models.

Our proposed traffic density model was based on a bivariate logistic function, that is, time and position variables. The extension of this model to a bidirectional road segment involves the convolution of two bivariate functions or designing an integrated multivariate logistic function. The development of the theoretical framework for such a problem is an interesting research direction.

Extension to cascaded intersections

The proposed traffic model was developed based on the assumption that a road segment is only connected to one intersection, or that the impact of other intersections on the traffic flow in the road segment under investigation is negligible. Incorporating more intersections into the model is extremely challenging due to the filtering and platooning effects of a downstream intersection, which in turn influence the outgoing traffic into the connected road segments. Full-feature models for cascaded intersections have not been developed by the research body in the field of traffic science, which leaves the extension of our single intersection model to multi-intersection scenarios an open problem. Similarly, the extension of our model to non-signalised intersections (e.g., give way intersections) opens a new direction for future research.

Our proposed density model has the capacity for such extensions. For extension to the cascaded case, instead of assuming a continuous traffic arrival described by a mean traffic flow, one can employ *on-off* processes to model the filtering and platooning effects of the upstream intersection(s). Accordingly, the duration and the amount of traffic released during the *on* stage is determined by the traffic light timing and the traffic intensity in the upstream intersection(s). For extension to the second case, the assumption of fixed timing of the traffic light must be replaced with adaptive timing. Correspondingly, the expected duration of the red and green phases as perceived by a typical vehicle can be modelled by a stochastic process.

Load balancing based on local traffic estimation

The scarcity of the radio resource underscores the need for careful design of applications and protocols in urban VANETs in order to mitigate channel load in dense traffic regions, based on vehicles' estimations of their local traffic density or traffic information provided by roadside infrastructure. To this aim, as the first step, the development of a robust mechanism for estimation of local traffic is highly important. Second, the design of an adaptive and robust mechanism to adjust transmission power and assign proper data rates based on the perceived radio overlap opens a new direction for research.

8.2 Reliability of Safety Message Broadcast in VANETs (Chapter 4)

8.2.1 Conclusions

In Chapter 4, it was stressed that previous studies on the reliability issues of safety applications were focused on investigating the reliability of communication networks in free-flow scenarios, where vehicles are uniformly distributed or traffic is in steady state. We argued that this does not hold true in urban settings, where traffic is regulated by signalized intersections and influenced by peculiar driving behaviour. In Chapter 4, we addressed the urban case by studying the performance of safety messages using a realistic vehicular mobility model which captures the heterogeneous node densities at and around signalized intersections. In line with previous work, we constructed Markov models for capturing the delivery probability for event-driven warning messages and the packet inter-reception time for periodic beacons. By combining the Markov models with the urban vehicular density model, for the first time we are able to accurately capture the resulting performance characteristics in a non-uniform density setting. Through a numerical evaluation, we demonstrated that the major impact of the hidden node problem on the reliability performance of safety messages extends to the urban case as well. Importantly, we found that the impact is most significant in sections where the vehicle velocities are highest. Bearing in mind the relationship between traffic safety and vehicle's velocity, one can draw the conclusion that the hidden terminal problem potentially overshadows the degree of improvement in traffic safety expected to be achieved by means of safety applications.

8.2.2 Future Directions

Extension of the reliability model

The reliability model should be revisited based on the extensions of the traffic density and radio overlap model as mentioned in Section 8.1.

Reliability of applications targeted to intersection scenarios

Intersections have proven to be accident-prone regions [80]. This motivated the standard bodies including VSC [5] to design safety applications specifically targeted for intersection scenarios, including intersection collision warning, left or right turn assistance and traffic light violation warning. An interesting direction for future research is to investigate the reliability of such applications. This, firstly, demands accurate characterization of the traffic behaviour at intersections. In the next phase, a risk model should be designed which maps the traffic parameters to the safety level of vehicles. Finally, the capacity of the safety application in enhancing the safety level of drivers at the intersections should be explored. The first case was addressed in this thesis (Chapter 3). However, the latter cases call for future research.

Kinematic-aware countermeasures and control mechanisms

Our findings on reliability issues generally call for further work on mechanisms to mitigate the effect of hidden nodes in order to ensure the viability of DSRC/WAVE-based safety applications. Transmission power control and suppression of message transmission rates are examples of countermeasures which will potentially lead to mitigation of the hidden terminal problem. The idea of power or transmission rate control is not new in itself; however, most of the the existing proposals rely on channel sensing or some form of traffic density estimation. In the context of vehicular networks, the traffic safety also should be taken into account, a factor missing in the current approaches and proposals. In more concrete terms, the control mechanisms should estimate the potential hazards incurred by vehicles and apply the hazard information to the power or rate adaptation decisions. An example of a decision of this type would be the suppression of the beaconing rate in less hazardous vehicles stopping in a queue, while increasing the power level or transmission rate for vehicles joining the queue with potentially high velocity and small headway distances. Enforcement of these types of control mechanisms in a vehicle demands the monitoring of the kinematic status of the vehicle itself and the kinematic information of other surrounding vehicles.

8.3 Severity of Hidden Terminal Interference in VANETs (Chapter 5)

8.3.1 Conclusions

The degree of realism incorporated into the host system representation culminated in the work presented in Chapter 5. First of all, we represented urban traffic scenarios characterised by a forced-flow traffic regime using a well-established Cellular Automata (CA)-base traffic modelling paradigm, which has proven to be highly efficient in describing various traffic scenarios [30; 123; 161]. Second, a special-purpose shadow-fading radio propagation model [8] targeted for VANETs was used to represent the radio propagation environment. Finally, two major safety-critical traffic scenarios were identified with theoretical and empirical support from traffic science and evidence from car crash statistics. With realism captured in these three dimensions, we addressed hidden terminal interference as a primary cause of reliability degradation in broadcast communications. To this aim, analytical models and geometric algorithms were developed to quantify the severity of hidden terminal interference under safety-critical scenarios. For a road stretch operating in a capacity traffic state and with various speed limits, the upper bound interference power and the lower bound reachable distance of safety messages were obtained. Our extensive experiments with various velocities and lane configurations showed that, in a stretch of road, the interference power obtained by the model is an upper bound 96% of the time. It was also shown that the obtained reachable distance is a lower bound more than 94% of the time and exhibits a tightness of less than 9%. For the intersection scenario, the upper bound property of the model in terms of interference power was shown to be almost certain. Also, our experiments showed that the hidden terminal interference causes a significant decline in the reachable distance of broadcast messages, which in several cases drop to distances shorter than the minimum required coverage of medium range safety applications. In the intersection scenario, it was shown that the aggregate interference power of hidden nodes in the vicinity of the intersection region can be significantly large and may amount to values several times larger than the induced interference power in an equivalent road stretch scenario. The results demonstrate that the proposed analytical framework has the capability to be used as a benchmark for the assessment of the reliability risks of safety applications under safety-critical traffic scenarios.

8.3.2 Future Directions

Extension to radio propagation with path loss variation

In the analytical framework developed in Chapter 5, the path loss variation was discarded for the sake of model tractability. Hence, our analysis in that chapter was restricted to average path loss. Consequently, the upper bound interference and lower bound reachable distance were obtained on an average basis. Further extension with the aim of absolute worst case analysis requires the path loss variation to be taken into account. In a second dimension, investigating the impacts of device sensitivity on the successful decoding of a signal in the presence of interference is an interesting research direction.

Reachable distance in intersection scenarios

In the intersection scenario, we used a measurement-based traffic discharge model [11] capable of describing the traffic properties at the stop line of the intersection. With the limitations of this model (and other similar models), it was only possible to obtain the upper bound interference for the *entire* intersection. Such discharge models are not adequate for obtaining the upper bound interference corresponding to any position of a road segment connected to the intersection. An accurate spatial-temporal analysis of upper bound interference, and hence worst case reliability, calls for the development of comprehensive traffic discharge models for intersection scenarios. The traffic density model proposed in Chapter 3 is a good starting point to serve this purpose; however, extra development is needed to map from traffic density to the spatial distribution of vehicles.

Characterization of other safety-critical traffic scenarios

Identification of various safety-critical scenarios other than the two cases addressed in this thesis, and investigation of the reliability issues in such scenarios is an interesting direction for future research. Particularly, more research is needed to characterise traffic safety and to develop a traffic risk model. Incorporating such a risk model in a framework intended for reliability analysis will facilitate a better understanding of the bottlenecks of the DSRC/WAVE technology, especially in scenarios where safety is most needed.

Investigation of other reliability metrics

The reliability metric addressed in the proposed framework was reachable distance. Investigation of other reliability metrics, including network level metrics such as packet delivery ratio, and application level metrics like message inter-reception time and effective range, opens a new direction for future research.

Investigation of other factors affecting reliability

The analysis of reliability can be extended to account for other factors besides hidden terminal interference, which was our main focus in Chapter 5. The internal interference caused by concurrent transmissions, the controlled factors including transmission power and data rate, and MAC layer parameters are candidate factors for investigation within a realistic host system.

Development of a rich geometric calculus for vehicular traffic scenarios

Simple geometric algorithms were proposed to obtain the upper bound interference and lower bound reachable distance for two safety-critical scenarios. Given that there are many other traffic scenarios that are highly significant from the perspective of communication reliability, a rich geometric computation framework customized for vehicular traffic scenarios is demanded to describe such diverse scenarios. The envisioned framework would facilitate the capture of the core properties of complicated traffic scenarios and transform them to parsimonious and analytically tractable procedures and algorithms. This, in turn, advocates advanced studies of reliability and other performance aspects of vehicular networks.

8.4 Generic Framework for Information Dissemination (Chapter 7)

8.4.1 Conclusions

We proposed a generic framework intended as a capstone architecture incorporating various content dissemination functionalities and properties. This framework, while being independent from the underlying network architecture and the mobility and meeting patterns among nodes, enables a typical node to dynamically build its view of the information interests of other participating nodes. Such capability, coupled with the interaction model of meeting nodes, facilitate the realization of various content dissemination strategies while fulfilling the individual nodes' constraints in terms of buffer space, energy, etc. We numerically validated the model with respect to structural and behavioural elements of the content dissemination network, where we showed that the model captures well the essential network properties, such as dynamic composition of nodes' communities, and in the meantime reacts to the shift in information interests of nodes.

8.4.2 Future Directions

Verification by field experiments and subjective tests

The efficiency of information-centric applications is substantially determined by the user experience of the dissemination outcome. Knowing that users may have diverse opinions on the quality of information they receive, the validation and verification of the information dissemination framework should be performed using a diverse sets of users on a subjective basis. Furthermore, since the generic framework is intended for users of various technologies, the verification mechanisms should account for heterogeneous user constraints imposed by the target technologies.

Extension to information recommendation system

The autonomous and distributed information popularity measurement designed as part of the proposed framework is a generic functionality which can serve several purposes with minimal changes. In Chapter 7, we highlighted its application in social-oriented content exchange. Similarly, the information popularity adaptively learned by mobile nodes or infrastructure units can be used in recommendation systems with the objective of enhancing automated information discovery. In this use-case, a mobile node or infrastructure unit informs the passing-by nodes about some popular information they are not aware of.

Extension to multi-player interaction model

Our proposed interaction model as a component of the generic framework currently describes the pairwise node interaction. Accordingly, the game theoretic problem defined for the interaction model was a two-player game problem. However, in real situations it is likely that multiple nodes simultaneously come into contact and desire to participate in content exchange. Therefore, a general interaction model is needed to account for multiple nodes with potentially diverse constraints and contact times.

Mechanism design for the game theoretic interaction model

In the proposed interaction model, we assumed that the meeting nodes are cooperative. In a real system, incentive mechanisms are needed to enforce cooperative behaviour. In view of that, some cooperation enforcement mechanisms including incentive and reputation-based mechanisms are deemed to be highly advantageous compared to other alternatives [128]. The design of such mechanisms to facilitate cooperative content exchange by nodes with unique constraints and states opens a new direction for future research.

Appendices

Appendix A

Vehicular Communication Networks: Standards, Protocols and Applications

This appendix presents an overview of DSRC/WAVE technology in Section A.1, followed by a description of the applications envisioned for future deployment in vehicular networks in Section A.2. In Section A.3, a number of existing added-value applications and frameworks are introduced, emphasising the strong motivation of the research body in developing information and content-centric applications for vehicular communication networks. In Section A.4, we present the current trend of vehicular network applications with some examples.

A.1 DSRC/WAVE

The DSRC/WAVE initiative [2; 121] addresses the communication services and protocols required for the realization of vehicle to vehicle and infrastructure communications. The initiative targets a broad range of services spanning from traffic safety, management and control to location and facility discovery, content delivery, and many more [3; 5]. Provision of short and medium range data communications with high data rate and low delay is the primary objective of the initiative [96]. Data communications take place either directly between On-Board Units (OBUs) installed in vehicles or between OBUs and infrastructure equipment such as Road-Side Units (RSUs) [96; 153]. As part of the deployment plan in the US, a spectrum with 75 MHz bandwidth in the 5.9 GHz band is dedicated to vehicular communications [76]. The spectrum is divided into 7 channels. A control channel is dedicated to life-related safety services and also for the exchanging of physical and link layer control information. The convenience and commercial services must rely on the remaining six channels [76]. The physical layer parameters such as transmission power, data rate, and modulation scheme are regulated with respect to the type of application and the on-board unit installed in a vehicle [76; 96].

A.1.1 Standards and Protocols

DSRC/WAVE architecture is comprised of the IEEE802.11p protocol [7], the IEEE 1609.x series of standards and protocols [5; 76], and the information models specified by the Society of Automotive Engineers (SAE) J2735 [5; 6] (Figure A.1). For further information about the WAVE physical (WAVE PHY) and WAVE medium access control (WAVE MAC), the interested reader is referred to [7; 76; 96].

A.2 Overview of Applications and Services

A large number of services and applications with various objectives have been proposed by the Vehicle Safety Communication Project [3; 5] for future deployment in vehicular networks. Yet, more applications are predicted to be proposed by research body in the near future. The benefit to the user from the various applications and services are not the same; hence, a number of applications have a high priority for deployment. Of the high priority applications, 16 applications have been identified in [15] with safety services as the primary focus.

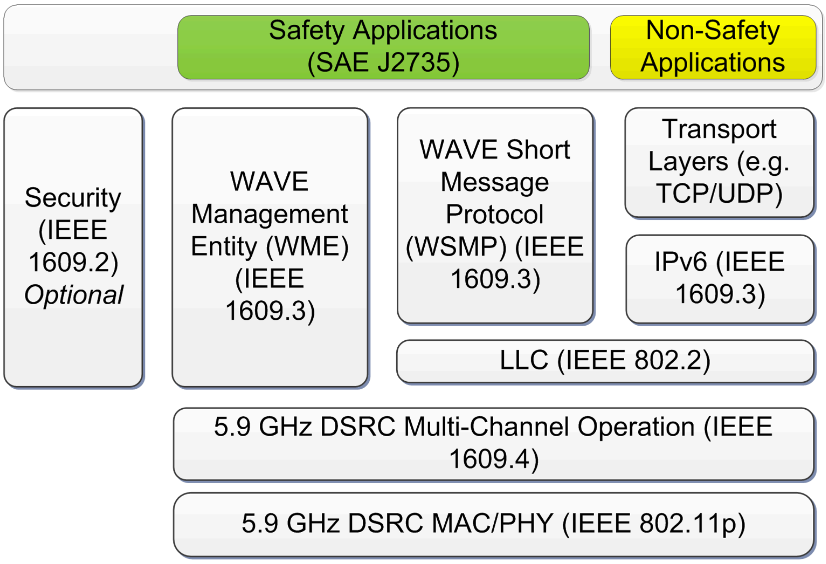

Figure A.1: DSRC/WAVE protocol stack [5]

A.2.1 Application Types

VANET applications are classified into three main classes: safety, convenience, and commercial applications [3; 15].

- *Safety applications* monitor actively the surrounding environment to keep track of the kinematic state of the neighbouring vehicles and the road conditions by means of inter-vehicle message communication. The information received from the nearby environment enables the drivers to react to potentially hazardous incidents. Two classes of safety applications are envisioned for future deployment [15]. In the first class, the applications are aimed to facilitate automatic actions such as automatic braking or slowing down to prevent potential accidents. In the second class, the applications assist drivers only if they activate the applications and grant them a permission for assistance [15]. Examples of safety applications are Emergency Electronic Brake Light (EEBL), and Lane Change Warning (LCW) [5].

- *Convenience applications* share traffic information, road conditions, and various types of information associated with urban sensing among vehicles, infrastructure entities, and centralized traffic monitoring and control systems [15; 16]. These applications aim to enhance traffic flow, travel time, pollution measurement and control, etc. Yet, another goal of these applications is to provide a convenience to drivers. Congested Road Notification (CRN), and toll services (TOLL) [15] are examples of this type.

- *Commercial applications* facilitate access to a wide variety of content and information services. Internet access and audio and video communications are considered as two generic types of commercial services. Applications with more specific objectives include, but are not limited to, Real-Time Video Relay (RTVR) and Service Announcement (SA) [15].

A.2.2 Application Attributes and Scopes

Applications are further characterized by application and network specific attributes [15; 147]. The application attributes describe the inherent properties of the application, while network attributes mainly describe the communication aspects of the application.

- **Application Attributes:** describe the internal properties of the application. These attributes include, but are not limited to, region of interest, trigger conditions, lifetime of events, and the entities enabling the application [15].

- **Network Attributes:** specifies the communication features of an application. These attributes include, but are not limited to, routing mechanism, channel attributes, and the dependency on infrastructure equipment [15; 147].

A complete list of attributes have been identified for 16 high priority applications, which can be found in [15]. According to [15], the applications relying on periodic exchange of safety messages also rely mainly on single hop communication, while for others who exploit event-based messaging, multi hop communication is an alternative choice. Also, the periodic-based applications rely mainly on broadcast mode, whereas the event-based applications can use geocast dissemination.

In convenience and commercial applications, on the other hand, the dominant communication mode is unicast.

In a more recent study, Bai *et al.* [16] classified the VANET applications into six categories. In this classification, one can find new application types such as wide-area alert services, file sharing services, and interactive applications [16]. Using this classification, Bai *et al.* identified three key characteristics indicating the scope over which the information subject to communication is relevant. These scopes are temporal, spatial, and interest groups [16].

A study with a greater focus on broadcast safety applications can be found in [43]. In this study, Chen *et al.* specified the latency and the desired communication range for a number of safety applications including intersection collision avoidance, public safety, and traffic sign extension. According to Chen *et al.*, most applications require a latency of $\leq$ 100 milliseconds and transmission range of $\leq$ 300 meters. An example of a very strict application is Pre-Crash Sensing (PCS) [43], which needs a latency of $\leq$ 20 milliseconds. Approaching Emergency Vehicle Warning (AEVW) [43] is also considered a strict application, which requires a transmission range up to 1000 meters. Bai *et al.* [17] investigated the required transmission (or application) range and a factor termed tolerance time window for a set of four popular safety applications. Tolerance time window is a time duration within which the reception of at least one message is necessary for a receiver vehicle to be able to predict and update the status of a neighbour vehicle accurately [17]. The communication patterns of VANET applications are studied in [147], which highlights that most safety applications must rely on one-hop broadcast of safety messages. In cooperative forward collision avoidance, for instance, vehicles are required to broadcast regularly the current kinematic information to other neighbouring vehicles [3; 147]. In vehicle to infrastructure applications such as curve speed warning, the RSU(s) must broadcast regularly the information about road surface type, weather conditions and more to the approaching vehicles [147].

A.3 Added Value Applications and Service Frameworks

Safety applications have been the primary focus of car to car communications. However, viewing the information in an abstract form and considering the variety of roles a vehicle can play in an information-centric framework, a vast number of services with unique features can be envisioned. The roles of a vehicle can be summarized into four categories including information consumer, information producer, information consumer and producer, and intermediary [87]. With such roles in mind and considering the fact that a vehicle can play the intermediary role in almost all cases, the services can be classified into three broad classes as we survey in the following sections.

A.3.1 Information Consumer Services

The information or content is produced by external infrastructure units. Vehicles access the information from the external units using either a pull- or push-based method. Opportunistic dissemination is then used to exchange the information among vehicles beyond the coverage of the infrastructure units. Location- aware advertisements and content dissemination account for two broad categories of information consumer services [87]. AdTorrent [125] was designed to facilitate the delivery of advertisements relevant to drivers' interests. Mershad *et al.* [118] proposed a data routing mechanism termed CAN DELIVER. This mechanism relies on the cooperation of vehicles and road side units to route information to vehicles far from the coverage of road side units. In [124], an application framework was proposed to facilitate the dissemination of content.

A.3.2 Information Producer Services

Easy and low-cost equipment of vehicles with special purpose sensors and location services empowered by navigation systems enables a series of added value urban sensing services [87]. In [68], an application framework was proposed to facilitate the processing and resolution of queries of various topics. [57] addressed an application which provides the drivers with information about road conditions, and [90] proposed an enabling framework for a broad range of services targeted to urban sensing.

A.3.3 Information Consumer and Producer Services

In this type of services, a vehicle can be viewed as a consumer and a source of information, simultaneously. Example services are proactive reporting of traffic conditions and incidents, voice and video over vehicular communications, and peer to peer services [87]. In [88], the authors addressed a trading service over vehicular communication platform. [66] proposed a framework to facilitate the communication of live videos about incidents in a vehicular traffic system. [154] proposed an application framework targeted to virtual mobile communities such as chat groups. A proposal for traffic information system based on vehicle to vehicle and infrastructure communications can be found in [144].

A.4 Trends of VANET Applications

The idea of using vehicular networks as a communication infrastructure to realize sophisticated applications dates back to 2003 when Goel *et al.* proposed "sensor-on-wheels" architecture [63] for the realization of traffic information systems. At the time this novel architecture was proposed, standards and protocols dedicated for vehicular communications did not exist. This led the authors to base their proposal on a generic IEEE 802.11-based short range communication interface or wide-area communication links (cellular network or two-way paging network) [63]. Since then, as highlighted in the previous sections, the research has been focused on exploring new applications and versatile frameworks to facilitate the implementation and deployment of such applications. In particular, the idea of Content Centric Networking (CCN) [69] in VANET has recently gained significant momentum. The CCN framework was originally proposed for the future Internet [130]; however, this framework has the capacity of being employed independent from the underlying communication technology. In CCN, a content is referred to by a unique name instead of the address of the host device where the content is stored [13]. The functionality of content distribution in CCN is controlled by the information consumer(s). A consumer issues a content request by advertising their *interest* through existing channels, that is, communication interfaces. In the basic form, a single interest results in the retrieval of a single content object [69]; however, the extension to the retrieval of multiple content objects demands further modification of the basic architecture. A transparent implementation of CCN requires that the underlying communication architecture supports name-based content retrieval instead of traditional host-based routing.

IC NOW [16] and CRoWN [13] frameworks represent two major attempts for realizing versatile application frameworks. The aim of IC NOW is to provide a holistic and versatile framework for the development of information-centric applications targeted to vehicular networks. The founders of IC NOW seek consistent and flexible mechanisms enabling the development of various applications with different natures (i.e., safety, convenience, etc.) and with different scopes (i.e., spatial, temporal, and user interests) [16]. In the CRoWN framework, two objectives are pursued: (i) conformance to 802.11p/WAVE standards, and (ii) provision of content-centric vehicular communications relying on vehicles and infrastructure as content providers. Both IC NOW and CRoWN frameworks conform to the CCN architecture. Compared to IC NOW, CRoWN is more compatible with the DSRC/WAVE architecture for VANETs and also does not need an overlay network as is required in IC NOW.

A.5 Summary

DSRC/WAVE initiative covers a wide variety of a services ranging from safety to convenience, and commercial services. While safety services are the primary focus of standard bodies, the research campaign continues to explore other added value services and application frameworks. Such a campaign is motivated by the easy and low-cost equipment of vehicles with various facilities ranging from special purpose sensors to high power processors, and location services.

Appendix B

Vehicular Traffic Models

In this appendix, we present an overview of traffic concepts and the traffic modelling paradigms addressed frequently in the context of vehicular traffic networks.

B.1 What is a Traffic Model?

A traffic model is characterised by a network topology and vehicular mobility. The network topology is described by a graph, where the graph vertices represent the intersections and the edges are the road segments connected to those intersections. The topology is further described by the dimension of the road segments in terms of segment length, curvature, the number of lanes, and the lane width. Traffic mobility is described by constraints and regulations governing the motion of individual vehicles [67]. A wide variety of constraints can be found in the constraint set, including those related to driving habits, velocity regulations, vehicle kinematics, road topology, *etc.*

B.2 Factors Affecting the Vehicular Mobility

Mahajan [110] identified a number of key factors affecting the mobility behaviour. These factors include:

B.2.1 Streets Layout

The motion of vehicles is restricted by the predefined paths formed by streets and roads. Streets are comprised of single or multiple lanes. Furthermore, they are characterized by unidirectional or bidirectional traffic flow.

B.2.2 Size of Block

A block corresponds to an urban region surrounded by a number of streets connected by intersections. The size of a block in urban centre is generally smaller than in a suburb. The size of a block affects the motion of vehicles by affecting the frequency of stopping. Traffic density is also influenced by the size of block [110].

B.2.3 Traffic Control Mechanisms

Stop signs along the streets and traffic lights at intersections account for the major mechanisms deployed for the goal of traffic control or enforcement of traffic regulations [110]. These control mechanisms significantly affect the motion pattern of vehicles due to queuing and frequent accelerations and decelerations.

B.2.4 Mutual Dependency of Vehicular Mobility

Traffic safety implies maintaining safe distance between vehicles. To this aim, the interaction between a vehicle and its neighbouring vehicles is inevitable for preserving a safe distance.

B.2.5 Average Velocity

The frequency at which a vehicle changes its position is determined by its velocity. The average velocity is influenced by the vehicles' acceleration and deceleration and also the topological aspects of the traffic network. In particular, the density of intersections highly affects the average velocity of vehicles in a region of interest [110].

B.3 Granularity of Traffic Mobility Model

Mobility models are generally categorized by the degree of details they describe vehicular motion. In view of that, the granularity of a mobility model falls within one of three categories as follows [62]:

B.3.1 Microscopic

Microscopic models aim to describe the motion details of individual vehicles accurately. Hence, all features related to the dynamic interaction of a vehicle with their surrounding vehicles, the transportation regulations, etc, are taken into consideration in these models.

B.3.2 Macroscopic

These models describe the traffic behaviour by means of high level traffic parameters including density, flow, or average velocity. They do not emphasize on the detailed motion of vehicles individually, but rather on traffic features corresponding to a segment of a road or street.

B.3.3 Mesoscopic

The features of microscopic and macroscopic models are integrated into a mesoscopic model. In this model, macroscopic parameters such as density, flow, or average velocity are used to describe the individual motion behaviour of vehicles.

B.4 Theoretic Motion Models

Given the granularity of the mobility model as described above, the vehicular mobility is realized, that is, motions are generated using one of the following mathematical models.

B.4.1 Stochastic Models

Stochastic models determine the movement of nodes within the network graph using a random process. Motion elements include, but are not limited to, node destination, pause time at destination, motion direction, and speed. All or a subset of motion elements are determined randomly. Random Waypoint (RWP) [73] is a well-known stochastic mobility model widely used in the simulation of ad hoc networks. According to this model, a node stays in a location and waits for a duration termed *pause time*. When this time ends, the waiting node selects randomly a new location within a production area. Afterwards, it moves to the new destination with a velocity chosen randomly from a predefined velocity range. Random Walk [145] and Random Direction [143] mobility models also fall within the class of stochastic models [38]; however, their applications in the context of ad hoc networks is rare. RWP as an abstract model has been used mainly in the context of Mobile Ad hoc NETworks (MANETs). Recently, some mobility models derived from RWP have been applied to vehicular networks. City Section (CS) mobility model [52] and Constant Speed Motion (CSM) [52] are typical examples of such models. Freeway [18] and Manhattan [155] models are also considered as stochastic models applied to vehicular networks in few studies.

B.4.2 Traffic Stream Models

In these models, the motion of a vehicle is modelled as a hydrodynamic phenomenon characterized by some equations derived from the broad concept of fluid dynamic [26]. Fluid Traffic Model (FTM) [152] is an example of traffic stream models. According to this model, the velocity of a vehicle decreases proportional to traffic density. When the traffic density reaches a threshold termed *critical density*, the vehicles decelerate in order to preserve a minimum velocity known as lower bound velocity [26]. The FTM is generally characterized by a velocity update mechanism as follows [61]:

$$v_n\left(t+\Delta t\right) = \max\left(v_{min}, v_{max}\left(1-\tfrac{m/r}{d_{jam}}\right)\right)$$

m is the number of vehicles situated on the road where a vehicle n under investigation is situated, t is the current time instant, Δt is a predefined time step used for velocity update, r is the length of the road under investigation, and d_{jam} is the vehicular density corresponding to jammed traffic state. The ratio m/r indicates the instant traffic density. With m/r growing to jammed traffic density, vehicles decelerates in order to preserve a predetermined minimum velocity. In non-congested or less congested situations, vehicles increase their velocities to a predetermined maximum velocity [61].

B.4.3 Car Following Models

Car Following [142] models are the basis for many synthetic traffic simulation frameworks. Based on this traffic modelling scheme, the motion dynamic of a given vehicle is determined with respect to the kinematic information of the neighbouring vehicles. The kinematic information includes vehicle position, velocity, acceleration rate, and driving direction [62]. An example of numerous models derived from car following is Intelligent Driver Model (IDM) [62; 167]. In this model, the motion dynamic of a given vehicle is determined by its kinematic status and the kinematic information of a leading vehicle. Let n, x_n, and v_n be the index, the position, and the velocity of a vehicle of interest at time t. Also, let l_n be the effective length of the vehicle n. The spacing of vehicle n with a leading vehicle $n-1$ is expressed as $s_n := x_{n-1} - x_n - l_{n-1}$ and the relative velocity of the two vehicles is defined as $\Delta v_n := v_n - v_{n-1}$. With these settings, the motion dynamic of vehicle n is defined by a number of differential equations as follows [62]:

$$
\begin{aligned}
\dot{x}_n &= \frac{\mathrm{d}x_n}{\mathrm{d}t} = v_n \\
\dot{v}_n &= \frac{\mathrm{d}v_n}{\mathrm{d}t} = a\left(1 - \left(\frac{v_n}{v_0}\right)^{\delta} - \left(\frac{s^*(v_n, \Delta v_n)}{s_n}\right)^2\right) \\
s^*(v_n, \Delta v_n) &= s_0 + v_n T + \frac{v_n \Delta v_n}{2\sqrt{a\,b}}
\end{aligned}
$$

v_0 is the desired velocity, s_0 is the minimum spacing, T is the desired headway time, a is the acceleration rate, b is the comfortable deceleration rate, and σ is an exponent usually set to 4 [62].

IDM model was further extended to support motion dynamics at intersections and also to lane changing maneuvers [62]. MOBIL [166] is another motion model for lane changing. In this model, a lane change maneuver is considered as a game theoretic problem characterized by appropriate utility functions.

B.4.4 Traffic Cellular Automaton Models

Traffic Cellular Automaton (TCA) [123] describes traffic motion using discrete variables (i.e., integer or binary variables). In these models, a given road segment is viewed as pieces of equal length Δx termed *cells* and the time is fragmented to slots of equal duration Δt. In a deterministic TCA, the CA states including velocity, position, or cell occupation are chosen from a predetermined set. In stochastic CA models, on the other hand, the state variables (or a subset of them) are determined probabilistically. In TCA, the dynamics of vehicular motion are generally described by the following expressions for position and velocity update:

$$\begin{aligned} v_n(t+1) &= f\left(s_n(t), v_n(t), v_{n-1}(t), \ldots\right) \\ x_n(t+1) &= g\left(x_n(t), v_n(t+1)\right) \end{aligned}$$

where f is a function which implements the velocity update by means of a set of rules governing the TCA model and a set of parameters. The key parameters determining the node n's velocity at time $t+1$ are the current spacing of vehicle n ($s_n(t)$), current velocity of vehicle n ($v_n(t)$), and the current velocity of the front vehicle ($v_{n-1}(t)$). Function g determines the next position of vehicle n using the information of the current position and the next velocity of n represented by $x_n(t)$ and $v_n(t+1)$, respectively. In some CA models [161], g is simply the summation of $x_n(t)$ and $v_n(t+1)$, that is, $g\left(x_n(t), v_n(t+1)\right) = x_n(t) + v_n(t+1)$.

Examples of deterministic TCA models are Wolframs rule 184 (CA-184) [82] and Biham-Middleton-Levine traffic model [30]. The former is a generic model used for the description of many forms of particle systems, with the traffic system as an example. Biham-Middleton-Levine model is a two-dimensional version of Wolframs rule 184. A well-known example of stochastic TCA (STCA) is Nagel-

Schreckenberg model (NaSch) [123]. This model is able to reproduce several characteristics of real-life traffic features such as the spontaneous emergence of jammed traffic. It explicitly includes a stochastic noise term in at least one of its rules. The computational model in the NaSch is defined on a one dimensional array of a number of known sites. Each site is either occupied or empty. Each vehicle has an integer velocity with values in range $[0, v_{max}]$. With an arbitrary configuration, the system update is realized by the following four steps performed in parallel for all vehicles [123]:

1. Acceleration:

$$v_n(t) < v_{max} \wedge s_n(t) > v_n(t) + 1 \quad \Rightarrow \quad v_n(t+1) \leftarrow v_n(t) + 1$$

2. Braking:

$$s_n(t) < v_n(t+1) \wedge s_n(t) > v_n(t) + 1 \quad \Rightarrow \quad v_n(t+1) \leftarrow s_n(t) - 1$$

3. Randomization:

$$\xi(t+1) < p \quad \Rightarrow \quad v_n(t+1) \leftarrow max\,(0, v_n(t+1) - 1)$$

   where $\xi(t+1)$ is a random number generated for the next update, p is stochastic noise parameter or slow-down probability.

4. Movement:

$$x_n(t+1) \quad \leftarrow \quad x_n(t) + v_n(t+1)$$

Extensions of NaSch for two dimensional streets can be found in [48] and [161]. Both models support traffic mobility at intersections with the difference that the latter assigns different priorities to the turning and drive- through traffic at an intersection.

As a final remark, it is worth mentioning that due to quantization in the time or space domain, CA models are generally less accurate compared to car following models. However, these models are more efficient in terms of scalability with network size and computation complexity [161].

Appendix C

Interference Power and SINR Results for Road Stretch Scenario

C.1 Description

The interference power and SINR results corresponding to the road stretch scenario (Chapter 5) are presented in the following tables. Due to the lack of space, the hop numbers are not shown in the tables, however, they can be implicitly realized from the row number of the tables. In the tables corresponding to the interference power, the row numbers are equivalent to the hop numbers. Thus, for example, the first row belongs to the first hop and the last row represents the last hop in the carrier sense range of the transmitter. Similarly, in SINR tables, the row numbers represent the hop numbers. The interference powers and SINRs are measured in dBm and dB respectively. Some abbreviations used in the tables are described as follows:

- **"L"**: stands for lane, e.g., 2L is equivalent to 2 lanes.

- **"T_mean"**: represents the mean value of a quantity (either interference power or SINR) measured from the traces.
- **"T_CI"**: represents the 95% confidence interval of a quantity (either interference power or SINR) measured from the traces.
- **"M"**: stands for a quantity (either interference power or SINR) obtained by the model.

C.2 Interference Power and SINR Tables

Table C.1: Interference power (velocity = 40kph)

2L			4L			6L		
T_mean	T_CI	M	T_mean	T_CI	M	T_mean	T_CI	M
-103.05	0.06	-101.28	-100.06	0.06	-98.22	-98.31	0.05	-96.45
-102.40	0.06	-100.72	-99.42	0.07	-97.69	-97.68	0.06	-95.93
-101.80	0.06	-100.05	-98.84	0.07	-97.04	-97.07	0.07	-95.25
-101.23	0.06	-99.54	-98.25	0.09	-96.49	-96.49	0.07	-94.76
-100.66	0.06	-98.98	-97.71	0.09	-95.94	-95.93	0.08	-94.14
-100.12	0.06	-98.37	-97.18	0.09	-95.41	-95.38	0.09	-93.61
-99.58	0.06	-97.87	-96.64	0.10	-94.88	-94.84	0.09	-93.07
-99.04	0.06	-97.43	-96.12	0.10	-94.42	-94.31	0.10	-92.59
-98.51	0.06	-96.77	-95.60	0.11	-93.87	-93.78	0.10	-92.01
-97.97	0.06	-96.34	-95.08	0.11	-93.36	-93.25	0.10	-91.54
-97.43	0.06	-95.82	-94.56	0.12	-92.83	-92.71	0.11	-90.99
-96.89	0.07	-95.23	-94.02	0.13	-92.32	-92.14	0.12	-90.44
-96.31	0.07	-94.65	-93.48	0.13	-91.82	-91.58	0.13	-89.89
-95.74	0.07	-94.14	-92.94	0.14	-91.23	-91.00	0.14	-89.28
-95.15	0.07	-93.53	-92.36	0.15	-90.69	-90.42	0.15	-88.74
-94.53	0.08	-92.91	-91.78	0.16	-90.17	-89.79	0.16	-88.13
-93.91	0.08	-92.22	-91.15	0.18	-89.59	-89.15	0.18	-87.50
-93.24	0.09	-91.58	-90.45	0.21	-88.92	-88.45	0.20	-86.89
-92.55	0.10	-91.01	-89.76	0.23	-88.20	-87.71	0.23	-86.20
-91.79	0.11	-90.05	-89.02	0.25	-87.62	-86.97	0.25	-85.52
-90.98	0.12	-89.41	-88.22	0.27	-86.85	-86.14	0.28	-84.77
-90.13	0.13	-88.53	-87.24	0.33	-85.96	-85.22	0.32	-83.93
-89.15	0.15	-87.63	-86.16	0.39	-85.13	-84.23	0.36	-83.13
-88.06	0.19	-86.41	-84.86	0.49	-84.22	-83.14	0.41	-82.19
-86.78	0.22	-85.26	-83.86	0.52	-83.33	-81.94	0.47	-81.25
-85.31	0.27	-84.15	-82.89	0.55	-82.44	-80.75	0.51	-80.31
-83.28	0.36	-82.74	-82.02	0.55	-80.83	-79.39	0.58	-77.52
-80.49	0.48	-81.24	-80.99	0.52	-78.85	-78.30	0.60	-76.62
-77.10	0.55	-75.21	-79.48	0.55	-77.94	-77.05	0.63	-75.44
-73.74	0.62	-71.51	-77.84	0.57	-76.34	-75.59	0.66	-73.67
-70.76	0.71	-69.51	-75.53	0.65	-73.96	-73.84	0.68	-71.55
-69.78	0.90	-67.77	-73.33	0.65	-71.16	-71.67	0.71	-68.78
-68.63	1.26	-67.82	-69.96	0.68	-67.56	-69.47	0.67	-66.67

Table C.2: SINR (velocity = 40kph)

2L			4L			6L		
T_mean	T_CI	M	T_mean	T_CI	M	T_mean	T_CI	M
46.85	0.19	37.46	45.86	0.22	36.12	45.17	0.21	35.24
30.32	0.17	30.39	29.40	0.25	28.92	28.58	0.24	27.86
26.70	0.15	25.75	25.66	0.24	24.44	24.68	0.25	23.18
24.06	0.14	23.24	22.80	0.26	21.54	21.74	0.25	20.55
21.88	0.14	21.23	20.60	0.25	19.40	19.40	0.26	18.00
19.96	0.15	19.01	18.68	0.26	17.42	17.35	0.27	16.03
18.08	0.15	17.11	16.79	0.27	15.32	15.44	0.28	13.80
16.24	0.14	15.39	14.88	0.27	13.55	13.45	0.27	11.96
14.57	0.14	13.36	13.13	0.27	11.62	11.64	0.27	9.97
13.00	0.13	11.95	11.53	0.26	10.06	9.97	0.27	8.42
11.56	0.13	10.54	10.02	0.27	8.44	8.38	0.27	6.80
10.19	0.13	8.96	8.55	0.27	7.06	6.84	0.27	5.27
8.83	0.13	7.63	7.19	0.27	5.75	5.40	0.28	3.84
7.55	0.13	6.48	5.90	0.27	4.31	4.01	0.28	2.33
6.31	0.13	5.07	4.59	0.28	3.09	2.70	0.29	1.08
5.09	0.13	3.86	3.35	0.29	1.89	1.37	0.30	-0.24
3.91	0.14	2.48	2.09	0.30	0.70	0.09	0.31	-1.55
2.71	0.14	1.34	0.78	0.33	-0.64	-1.24	0.33	-2.75
1.53	0.15	0.25	-0.48	0.35	-1.99	-2.57	0.35	-4.05
0.27	0.16	-1.32	-1.75	0.36	-3.03	-3.85	0.37	-5.28
-0.99	0.17	-2.41	-3.06	0.38	-4.38	-5.20	0.39	-6.54
-2.28	0.18	-3.73	-4.55	0.43	-5.81	-6.61	0.43	-7.92
-3.69	0.20	-5.03	-6.10	0.50	-7.11	-8.06	0.47	-9.15
-5.20	0.23	-6.78	-7.83	0.59	-8.47	-9.59	0.51	-10.54
-6.88	0.26	-8.31	-9.19	0.62	-9.73	-11.18	0.56	-11.89
-8.72	0.31	-9.83	-10.51	0.63	-10.95	-12.74	0.61	-13.17
-11.13	0.40	-11.62	-11.69	0.62	-12.91	-14.44	0.67	-16.29
-14.27	0.52	-13.47	-13.03	0.58	-15.12	-15.81	0.67	-17.47
-17.97	0.58	-19.84	-14.85	0.62	-16.38	-17.34	0.70	-18.96
-21.58	0.65	-23.82	-16.78	0.63	-18.28	-19.06	0.72	-20.99
-24.75	0.75	-25.98	-19.37	0.71	-20.94	-21.07	0.74	-23.36
-25.80	0.95	-27.82	-21.80	0.70	-23.93	-23.47	0.76	-26.36
-27.01	1.32	-27.77	-25.42	0.72	-27.80	-25.86	0.71	-28.64

Table C.3: Interference power (velocity = 50kph)

2L			4L			6L		
T_mean	T_CI	M	T_mean	T_CI	M	T_mean	T_CI	M
-103.97	0.09	-102.44	-100.92	0.07	-99.34	-99.14	0.06	-97.56
-103.20	0.09	-101.67	-100.15	0.08	-98.51	-98.37	0.08	-96.71
-102.44	0.09	-100.91	-99.42	0.09	-97.85	-97.64	0.09	-96.07
-101.74	0.09	-100.31	-98.72	0.11	-97.22	-96.95	0.10	-95.36
-101.04	0.09	-99.44	-98.05	0.11	-96.47	-96.27	0.11	-94.71
-100.37	0.09	-98.90	-97.38	0.12	-95.84	-95.60	0.12	-94.02
-99.72	0.09	-98.33	-96.71	0.13	-95.24	-94.92	0.13	-93.38
-99.04	0.09	-97.48	-96.01	0.14	-94.50	-94.25	0.13	-92.71
-98.35	0.09	-96.94	-95.32	0.15	-93.84	-93.55	0.15	-92.04
-97.68	0.09	-96.19	-94.61	0.17	-93.17	-92.84	0.16	-91.35
-97.01	0.09	-95.47	-93.85	0.19	-92.44	-92.12	0.17	-90.69
-96.28	0.10	-94.87	-93.05	0.21	-91.71	-91.35	0.19	-89.93
-95.55	0.10	-94.24	-92.22	0.24	-91.02	-90.52	0.23	-89.25
-94.74	0.10	-93.21	-91.35	0.27	-90.23	-89.70	0.25	-88.45
-93.83	0.11	-92.42	-90.36	0.32	-89.40	-88.78	0.28	-87.62
-92.89	0.12	-91.48	-89.32	0.36	-88.59	-87.81	0.31	-86.77
-91.88	0.14	-90.36	-88.05	0.43	-87.61	-86.67	0.36	-85.90
-90.74	0.16	-89.42	-86.59	0.51	-86.59	-85.33	0.42	-84.47
-89.46	0.20	-88.19	-85.25	0.57	-85.59	-83.91	0.49	-83.34
-87.83	0.26	-86.49	-83.80	0.63	-82.61	-82.56	0.52	-81.03
-85.52	0.36	-85.07	-82.46	0.70	-81.77	-80.78	0.60	-78.98
-82.20	0.49	-81.38	-81.83	0.70	-80.29	-79.13	0.67	-77.35
-78.41	0.59	-74.75	-81.05	0.68	-79.06	-78.20	0.69	-76.34
-74.92	0.67	-72.49	-79.62	0.73	-77.68	-76.75	0.74	-74.26
-72.44	0.81	-70.39	-77.79	0.78	-75.73	-75.38	0.75	-72.62
-71.39	1.04	-69.63	-76.22	0.81	-72.84	-73.54	0.80	-70.64
-70.27	1.43	-68.19	-74.22	0.86	-70.95	-72.03	0.83	-68.59

Table C.4: SINR (velocity = 50kph)

2L			4L			6L		
T_mean	T_CI	M	T_mean	T_CI	M	T_mean	T_CI	M
45.39	0.21	36.47	44.68	0.27	35.45	43.84	0.28	34.55
28.88	0.18	29.16	27.99	0.28	27.34	27.16	0.30	26.06
25.06	0.17	24.37	24.08	0.28	22.98	23.12	0.31	21.87
22.34	0.16	21.83	21.16	0.31	20.28	20.17	0.31	18.92
19.93	0.18	19.12	18.77	0.32	17.75	17.65	0.32	16.60
17.68	0.18	16.89	16.52	0.33	15.08	15.33	0.33	13.68
15.58	0.17	14.88	14.27	0.33	12.97	13.00	0.33	11.47
13.64	0.16	12.63	12.16	0.34	10.78	10.88	0.33	9.36
11.82	0.16	11.04	10.25	0.34	8.86	8.90	0.33	7.35
10.22	0.15	9.18	8.43	0.35	7.07	7.04	0.34	5.53
8.71	0.15	7.63	6.68	0.36	5.33	5.30	0.35	3.90
7.20	0.15	6.24	4.96	0.38	3.66	3.60	0.36	2.15
5.77	0.15	4.90	3.33	0.40	2.21	1.91	0.38	0.67
4.30	0.16	3.12	1.73	0.43	0.67	0.34	0.40	-0.94
2.74	0.16	1.58	0.05	0.47	-0.89	-1.32	0.42	-2.52
1.21	0.17	0.07	-1.64	0.50	-2.34	-2.96	0.44	-4.04
-0.34	0.19	-1.70	-3.52	0.57	-3.94	-4.73	0.49	-5.50
-2.00	0.21	-3.16	-5.55	0.64	-5.53	-6.66	0.54	-7.56
-3.76	0.25	-4.86	-7.36	0.70	-7.03	-8.61	0.61	-9.22
-5.87	0.30	-7.15	-9.25	0.74	-10.44	-10.42	0.63	-11.92
-8.65	0.40	-9.04	-10.94	0.81	-11.61	-12.66	0.70	-14.49
-12.41	0.53	-13.15	-11.83	0.80	-13.32	-14.69	0.78	-16.46
-16.56	0.63	-20.20	-12.87	0.77	-14.80	-15.86	0.78	-17.72
-20.33	0.71	-22.74	-14.60	0.81	-16.55	-17.60	0.83	-20.10
-23.01	0.85	-25.03	-16.73	0.86	-18.78	-19.21	0.83	-21.97
-24.15	1.09	-25.86	-18.55	0.89	-21.92	-21.31	0.88	-24.17
-25.35	1.49	-27.40	-20.77	0.93	-24.04	-23.01	0.90	-26.45

Table C.5: Interference power (velocity = 65kph)

2L			4L			6L		
T_mean	T_CI	M	T_mean	T_CI	M	T_mean	T_CI	M
-104.96	0.11	-103.07	-101.90	0.10	-99.92	-100.09	0.09	-98.12
-103.97	0.11	-102.14	-100.93	0.11	-99.04	-99.12	0.11	-97.29
-103.02	0.11	-101.18	-99.98	0.13	-98.11	-98.18	0.13	-96.27
-102.13	0.10	-100.42	-99.08	0.15	-97.28	-97.32	0.15	-95.52
-101.26	0.10	-99.41	-98.17	0.17	-96.36	-96.43	0.16	-94.38
-100.37	0.10	-98.63	-97.28	0.19	-95.57	-95.54	0.19	-93.62
-99.44	0.10	-97.77	-96.34	0.22	-94.65	-94.58	0.23	-92.78
-98.53	0.11	-96.83	-95.35	0.26	-93.74	-93.63	0.25	-91.37
-97.58	0.12	-96.03	-94.34	0.28	-92.92	-92.55	0.30	-90.56
-96.57	0.12	-94.87	-93.30	0.31	-92.00	-91.44	0.34	-89.77
-95.49	0.14	-93.86	-92.01	0.38	-90.26	-90.12	0.39	-87.88
-94.27	0.16	-92.49	-90.74	0.42	-89.38	-88.59	0.46	-87.03
-92.88	0.19	-91.34	-89.25	0.49	-88.41	-87.10	0.53	-85.92
-91.33	0.24	-89.71	-87.72	0.55	-86.21	-85.72	0.58	-83.67
-89.01	0.35	-87.92	-85.82	0.64	-84.35	-84.14	0.63	-81.87
-85.76	0.47	-86.01	-84.23	0.68	-82.35	-82.40	0.68	-80.01
-81.61	0.59	-78.14	-82.30	0.77	-80.63	-80.21	0.77	-77.53
-77.39	0.68	-74.25	-80.94	0.83	-79.08	-78.65	0.82	-75.97
-74.60	0.80	-71.74	-79.95	0.87	-77.65	-77.30	0.88	-74.02
-73.16	1.22	-70.82	-78.48	0.91	-75.24	-75.35	0.99	-72.15

Table C.6: SINR (velocity = 65kph)

2L			4L			6L		
T_mean	T_CI	M	T_mean	T_CI	M	T_mean	T_CI	M
43.59	0.26	33.88	43.13	0.33	32.89	42.43	0.35	32.12
26.82	0.23	26.40	26.28	0.35	25.13	25.47	0.37	24.43
22.96	0.21	22.29	22.10	0.37	20.89	21.20	0.39	19.64
19.88	0.21	19.23	18.94	0.39	17.63	18.04	0.41	16.79
17.12	0.20	16.09	16.09	0.42	14.38	15.14	0.42	13.11
14.51	0.19	13.54	13.37	0.42	11.84	12.33	0.43	10.46
12.16	0.18	11.29	10.85	0.43	9.22	9.71	0.45	7.96
10.11	0.17	9.14	8.51	0.45	6.98	7.33	0.46	5.19
8.16	0.18	7.25	6.31	0.47	5.05	4.97	0.50	3.01
6.28	0.18	5.21	4.29	0.48	3.13	2.76	0.52	1.19
4.42	0.19	3.16	2.05	0.54	0.47	0.43	0.56	-1.73
2.48	0.21	1.07	0.02	0.57	-1.28	-2.01	0.63	-3.56
0.44	0.24	-0.84	-2.20	0.64	-2.99	-4.25	0.69	-5.44
-1.73	0.29	-3.15	-4.36	0.69	-5.77	-6.27	0.73	-8.29
-4.62	0.40	-5.59	-6.85	0.77	-8.22	-8.43	0.77	-10.65
-8.43	0.52	-8.14	-8.90	0.81	-10.69	-10.70	0.82	-13.07
-13.08	0.63	-16.43	-11.27	0.89	-12.83	-13.39	0.90	-16.07
-17.69	0.72	-20.79	-12.94	0.95	-14.74	-15.29	0.95	-17.99
-20.75	0.84	-23.58	-14.19	0.97	-16.41	-16.93	1.00	-20.20
-22.32	1.28	-24.60	-15.92	1.01	-19.12	-19.20	1.11	-22.37

Table C.7: Interference power (velocity = 80kph)

2L			4L			6L		
T_mean	T_CI	M	T_mean	T_CI	M	T_mean	T_CI	M
-105.75	0.13	-103.61	-102.57	0.12	-100.43	-100.77	0.09	-98.34
-104.61	0.13	-102.38	-101.37	0.17	-99.29	-99.54	0.12	-97.25
-103.46	0.13	-101.53	-100.30	0.18	-98.36	-98.45	0.14	-96.22
-102.31	0.12	-100.23	-99.15	0.22	-97.19	-97.36	0.16	-94.94
-101.20	0.12	-99.34	-98.01	0.25	-96.18	-96.24	0.19	-93.86
-100.09	0.12	-98.02	-96.82	0.32	-95.20	-95.04	0.23	-92.93
-98.93	0.13	-97.07	-95.61	0.36	-94.14	-93.73	0.28	-91.06
-97.64	0.15	-95.70	-94.19	0.43	-92.44	-92.33	0.34	-90.14
-96.25	0.16	-94.48	-92.72	0.49	-91.51	-90.50	0.44	-88.83
-94.60	0.20	-92.70	-91.21	0.54	-90.48	-88.61	0.52	-85.92
-92.60	0.28	-91.30	-89.68	0.59	-87.16	-86.67	0.58	-84.02
-89.35	0.44	-88.74	-87.67	0.66	-85.65	-84.70	0.65	-82.06
-85.29	0.56	-81.28	-85.66	0.73	-83.03	-82.57	0.70	-79.81
-80.48	0.69	-76.91	-83.85	0.77	-81.59	-80.52	0.75	-77.38
-77.11	0.78	-74.10	-81.75	0.85	-79.34	-78.05	0.83	-74.43
-75.23	0.99	-72.02	-79.83	0.92	-76.54	-76.12	0.91	-72.24
-73.36	1.24	-69.97	-77.83	1.07	-74.16	-74.63	1.08	-71.15

Table C.8: SINR (velocity = 80kph)

2L			4L			6L		
T_mean	T_CI	M	T_mean	T_CI	M	T_mean	T_CI	M
42.23	0.28	33.23	41.88	0.37	31.48	41.10	0.36	30.70
25.43	0.24	24.91	24.77	0.42	23.70	23.86	0.39	22.39
21.31	0.23	21.01	20.56	0.43	19.56	19.38	0.41	17.87
17.66	0.23	16.89	16.97	0.47	15.28	15.85	0.43	13.78
14.53	0.22	13.66	13.74	0.50	11.97	12.46	0.44	10.17
11.88	0.20	10.71	10.79	0.55	9.28	9.33	0.46	7.38
9.46	0.20	8.30	8.15	0.57	6.78	6.44	0.50	3.90
7.13	0.22	5.93	5.43	0.62	3.92	3.72	0.53	1.63
4.76	0.22	3.47	2.91	0.67	1.88	0.70	0.62	-0.91
2.30	0.25	0.81	0.47	0.71	-0.08	-2.20	0.70	-4.81
-0.41	0.33	-1.37	-1.81	0.74	-4.09	-4.98	0.74	-7.52
-4.33	0.48	-4.71	-4.54	0.80	-6.35	-7.68	0.80	-10.28
-8.99	0.61	-12.71	-7.16	0.87	-9.62	-10.43	0.84	-13.15
-14.36	0.73	-17.77	-9.45	0.90	-11.54	-13.01	0.88	-16.11
-18.04	0.82	-20.95	-12.01	0.97	-14.27	-15.98	0.95	-19.58
-20.13	1.04	-23.30	-14.29	1.04	-17.47	-18.26	1.04	-22.15
-22.12	1.31	-25.52	-16.59	1.20	-20.20	-20.00	1.21	-23.44

References

[1] Quadstone Paramics: Microscopic Traffic Simulation. http://www.paramics-online.com/. (Cited on page 41.)

[2] *Standard Specification for Telecommunications and Information Exchange Between roadside and Vehicle Systems - 5 GHz Band Dedicated Short Range Communications (DSRC) Medium Access Control (MAC) and Physical Layer (PHY) Specifications ASTM E2213-03*. September 2003. (Cited on pages 1, 60, 79, and 195.)

[3] *Vehicle Safety Communications Project: Task 3 Final Report: Identify Intelligent Vehicle Safety Applications Enabled by DSRC*. National Highway Traffic Safety Administration, Office of Research and Development, Washington, D.C., 2004. (Cited on pages 1, 196, 197, and 199.)

[4] Motor Vehicle Census. *Australian Bureau of Statistic*, 2005. (Cited on page 127.)

[5] Vehicle Safety Communications–Applications VSC-A, First Annual Report. 2009. (Cited on pages xvi, 1, 2, 143, 187, 196, and 197.)

[6] DSRC Implementation Guide – A guide to users of SAE J2735 message sets over DSRC. SAE International. 2010. (Cited on page 196.)

[7] IEEE Standard for Information technology– Local and metropolitan area networks– Specific requirements– Part 11: Wireless LAN Medium Access Control (MAC) and Physical Layer (PHY) Specifications Amendment 6:

Wireless Access in Vehicular Environments. *IEEE Std 802.11p-2010*, pages 1–51, 2010. (Cited on page 196.)

[8] T. Abbas, F. Tufvesson, and J. Karedal. Measurement based Shadow Fading Model for Vehicle-to-Vehicle Network Simulations. *ArXiv e-prints*, March 2012. (Cited on pages 36, 37, 82, 86, 91, 125, and 188.)

[9] Kazi Iftekhar Ahmed. *Modeling drivers' acceleration and lane changing behavior*. PhD thesis, Massachusetts Institute of Technology, 1999. (Cited on page 127.)

[10] Rahmi Akcelik. Speed-flow models for uninterrupted traffic facilities. *Akcelik and Associates, Technical Report*, 2003. (Cited on page 91.)

[11] Rahmi Akçelik and Mark Besley. Queue discharge flow and speed models for signalised intersections. In *Transportation and Traffic Theory in the 21st Century, Proceedings of the 15th International Symposium on Transportation and Traffic Theory*, pages 99–118, 2002. (Cited on pages 114, 119, 120, 121, 137, and 189.)

[12] Rahmi Akçelik and Nagui M Rouphail. Overflow queues and delays with random and platooned arrivals at signalized intersections. *Journal of Advanced Transportation*, **28**[3]:227–251, 1994. (Cited on page 40.)

[13] Marica Amadeo, Claudia Campolo, and Antonella Molinaro. CRoWN: Content-Centric Networking in Vehicular Ad Hoc Networks. 2012. (Cited on page 202.)

[14] Maen M Artimy, William Robertson, and William J Phillips. Assignment of dynamic transmission range based on estimation of vehicle density. In *Proceedings of the 2nd ACM international workshop on Vehicular ad hoc networks*, pages 40–48. ACM, 2005. (Cited on page 40.)

[15] Fan Bai, Tamer Elbatt, Gavin Hollan, Hariharan Krishnan, and Varsha Sadekar. Towards characterizing and classifying communication-based automotive applications from a wireless networking perspective. In *Proceedings of IEEE Workshop on Automotive Networking*

and Applications (AutoNet), pages 1–25, 2006. (Cited on pages 196, 197, and 198.)

[16] Fan Bai and Bhaskar Krishnamachari. Exploiting the wisdom of the crowd: localized, distributed information-centric VANETs [Topics in Automotive Networking]. *IEEE Communications Magazine*, **48**[5]:138–146, 2010. (Cited on pages 198, 199, and 202.)

[17] Fan Bai and H. Krishnan. Reliability Analysis of DSRC Wireless Communication for Vehicle Safety Applications. In *IEEE Intelligent Transportation Systems Conference (ITSC '06)*, pages 355–362, 2006. (Cited on pages 22, 55, 90, 133, and 199.)

[18] Fan Bai, Narayanan Sadagopan, and Ahmed Helmy. The IMPORTANT framework for analyzing the Impact of Mobility on Performance Of RouTing protocols for Ad hoc NeTworks. *Ad Hoc Networks*, **1**[4]:383–403, 2003. (Cited on pages 33 and 206.)

[19] Fan Bai, Narayanan Sadagopan, Bhaskar Krishnamachari, and Ahmed Helmy. Modeling path duration distributions in MANETs and their impact on reactive routing protocols. *IEEE Journal on Selected Areas in Communications*, **22**[7]:1357–1373, 2004. (Cited on page 33.)

[20] Fan Bai, Daniel D Stancil, and Hariharan Krishnan. Toward understanding characteristics of dedicated short range communications (DSRC) from a perspective of vehicular network engineers. In *Proceedings of the sixteenth annual international conference on Mobile computing and networking*, pages 329–340. ACM, 2010. (Cited on page 21.)

[21] Fan Bai, DD Stancil, and Hariharan Krishnan. Toward understanding characteristics of Dedicated Short Range Communications (DSRC) from a perspective of vehicular network engineers. In *Proceedings of the sixteenth annual international conference on Mobile computing and networking*, MobiCom '10, pages 329–340. ACM, 2010. (Cited on pages 18 and 35.)

[22] Nathan Balon and Jinhua Guo. Increasing broadcast reliability in vehicular ad hoc networks. In *Proceedings of the 3rd international workshop on Vehicular ad hoc networks (VANET '06)*, pages 104–105, New York, NY, USA, 2006. (Cited on pages 25 and 79.)

[23] S. Bastani, B. Landfeldt, and L. Libman. A traffic density model for radio overlapping in urban vehicular ad hoc networks. In *IEEE 36th conference on Local Computer Networks (LCN)*, pages 85–92, 2011. (Cited on pages vii, 10, and 116.)

[24] Saeed Bastani, Bjorn Landfeldt, and Lavy Libman. On the reliability of safety message broadcast in urban vehicular ad hoc networks. In *Proceedings of the 14th ACM international conference on Modeling, Analysis and Simulation of Wireless and Mobile Systems*, MSWiM '11, pages 307–316, New York, NY, USA, 2011. ACM. (Cited on pages vii and 11.)

[25] Saeed Bastani, Bjorn Landfeldt, Christian Rohner, and Per Gunningberg. A social node model for realising information dissemination strategies in delay tolerant networks. In *Proceedings of the 15th ACM international conference on Modeling, Analysis and Simulation of Wireless and Mobile Systems*, MSWiM '12, pages 79–88, New York, NY, USA, 2012. ACM. (Cited on pages vii and 15.)

[26] Nicola Bellomo, M Delitala, and V Coscia. On the mathematical theory of vehicular traffic flow I: Fluid dynamic and kinetic modelling. *Mathematical Models and Methods in Applied Sciences*, **12**[12]:1801–1843, 2002. (Cited on page 206.)

[27] Laura Bernadó, Anna Roma, Alexander Paier, Thomas Zemen, Nicolai Czink, Johan Karedal, Andreas Thiel, Fredrik Tufvesson, Andreas F Molisch, and CF Mecklenbrauker. In-tunnel vehicular radio channel characterization. In *Vehicular Technology Conference (VTC Spring), 2011 IEEE 73rd*, pages 1–5. IEEE, 2011. (Cited on page 35.)

[28] Giuseppe Bianchi. Performance analysis of the IEEE 802.11 distributed coordination function. *IEEE Journal on Selected Areas in Communications*, **18**[3]:535–547, 2000. (Cited on page 31.)

[29] Scott Biddlestone, Student Member, Keith Redmill, and Senior Member. An Integrated 802 . 11p WAVE DSRC and Vehicle Urban (LOS and NLOS) Propagation Models. *IEEE Transactions on Intelligent Transportation Systems*, **13**[4]:1792–1802, 2012. (Cited on page 35.)

[30] Ofer Biham, A Alan Middleton, and Dov Levine. Self-organization and a dynamical transition in traffic-flow models. *Physical Review A*, **46**[10]:R6124–R6127, 1992. (Cited on pages 188 and 208.)

[31] F. Bjurefors, P. Gunningberg, E. Nordström, and C. Rohner. Interest dissemination in a searchable data-centric opportunistic network. In *Proc. of European Wireless Conference (EW)*, pages 889 –895, 2010. (Cited on page 149.)

[32] Jeremy J Blum, Azim Eskandarian, and Lance J Hoffman. Challenges of intervehicle ad hoc networks. *IEEE Transactions on Intelligent Transportation Systems*, **5**[4]:347–351, 2004. (Cited on pages 20 and 21.)

[33] Mate Boban, Tiago TV Vinhoza, Michel Ferreira, Joao Barros, and Ozan K Tonguz. Impact of vehicles as obstacles in vehicular ad hoc networks. *Selected Areas in Communications, IEEE Journal on*, **29**[1]:15–28, 2011. (Cited on page 35.)

[34] H. Boeglen, B. Hilt, P. Lorenz, J. Ledy, A.-M. Poussard, and R. Vauzelle. A survey of V2V channel modeling for VANET simulations. In *Wireless On-Demand Network Systems and Services (WONS), 2011 Eighth International Conference on*, pages 117–123, 2011. (Cited on page 36.)

[35] Chiara Boldrini, Marco Conti, and Andrea Passarella. ContentPlace: social-aware data dissemination in opportunistic networks. In *Proc. of ACM MSWiM*, pages 203–210, USA, 2008. (Cited on pages 148 and 149.)

[36] Martin Burkhart, Pascal von Rickenbach, Rogert Wattenhofer, and Aaron Zollinger. Does topology control reduce interference? In *Proceedings of the 5th ACM international symposium on Mobile ad hoc networking and computing*, pages 9–19. ACM, 2004. (Cited on page 19.)

[37] Federico Cali, Marco Conti, and Enrico Gregori. IEEE 802.11 wireless LAN: capacity analysis and protocol enhancement. In *Seventeenth Annual Joint Conference of the IEEE Computer and Communications Societies*, **1**, pages 142–149. IEEE, 1998. (Cited on page 31.)

[38] Tracy Camp, Jeff Boleng, and Vanessa Davies. A survey of mobility models for ad hoc network research. *Wireless communications and mobile computing*, **2**[5]:483–502, 2002. (Cited on page 206.)

[39] Ben Carterette. On rank correlation and the distance between rankings. In *Proceedings of ACM SIGIR*, pages 436–443, USA, 2009. (Cited on page 171.)

[40] C. Cattuto, V. Loreto, and L. Pietronero. Semiotic dynamics in online social communities. **46**[2]:33–37, 2006. (Cited on page 158.)

[41] Kun chan Lan and Chien-Ming Chou. Realistic mobility models for Vehicular Ad hoc Network (VANET) simulations. In *8th International Conference on ITS Telecommunications*, pages 362–366, 2008. (Cited on page 33.)

[42] Periklis Chatzimisios, Vasileios Vitsas, and Anthony C Boucouvalas. Throughput and delay analysis of IEEE 802.11 protocol. In *IEEE 5th International Workshop on Networked Appliances, 2002. Liverpool. Proceedings*, pages 168–174. IEEE, 2002. (Cited on page 31.)

[43] Rex Chen, Wen-Long Jin, and Amelia Regan. Broadcasting safety information in vehicular networks: issues and approaches. *IEEE Network*, **24**[1]:20–25, 2010. (Cited on pages 55, 90, and 199.)

[44] Xianbo Chen, Hazem H Refai, and Xiaomin Ma. A quantitative approach to evaluate DSRC highway inter-vehicle safety communication.

In . *IEEE Global Telecommunications Conference (GLOBECOM'07)*, pages 151–155. IEEE, 2007. (Cited on page 27.)

[45] David R. Choffnes and Fabián E. Bustamante. An integrated mobility and traffic model for vehicular wireless networks. In *Proceedings of the 2nd ACM international workshop on Vehicular ad hoc networks*, VANET '05, pages 69–78, New York, NY, USA, 2005. ACM. (Cited on page 33.)

[46] Jong-Mu Choi, Jungmin So, and Young-Bae Ko. Numerical analysis of IEEE 802.11 broadcast scheme in multihop wireless ad hoc networks. In *Information Networking. Convergence in Broadband and Mobile Networking*, pages 1–10. Springer, 2005. (Cited on page 25.)

[47] B. Chopard and M. Droz. *Cellular Automata Modeling of Physical Systems*. Cambridge University Press, 2005. (Cited on pages 11 and 96.)

[48] Bastien Chopard, PO Luthi, and Pierre-Antoine Queloz. Cellular automata model of car traffic in a two-dimensional street network. *Journal of Physics A: Mathematical and General*, **29**[10]:2325, 1996. (Cited on pages 96 and 209.)

[49] Lianyu Chu, Henry Liu, Michael McNally, and Will Recker. Development of the capability-enhanced Paramics simulation environment. 2005. (Cited on pages 93 and 125.)

[50] Byung-Gon Chun, Peter Wu, Hakim Weatherspoon, and John Kubiatowicz. ChunkCast: An Anycast Service for Large Content Distribution. In *IPTPS*. Citeseer, 2006. (Cited on page 147.)

[51] G. Cugola, E. Di Nitto, and A. Fuggetta. The JEDI event-based infrastructure and its application to the development of the OPSS WFMS. *IEEE Transactions on Software Engineering*, **27**[9]:827 –850, September 2001. (Cited on pages 14 and 149.)

[52] Vanessa Ann Davies et al. *Evaluating mobility models within an ad hoc network*. Master's thesis, Department of Mathematical and Computer Sciences. Colorado School of Mines, 2000. (Cited on page 206.)

[53] L. Du and Rensselaer Polytechnic Institute. *Fundamental Problems in Vehicular Ad Hoc Networks: Connectivity, Reachability, Interference, Broadcast Capacity, and Online Routing Algorithms*. Rensselaer Polytechnic Institute, 2008. (Cited on page 20.)

[54] S. Eichler, C. Schroth, T. Kosch, and M. Strassberger. Strategies for Context-Adaptive Message Dissemination in Vehicular Ad Hoc Networks. In *Third Annual International Conference on Mobile and Ubiquitous Systems - Workshops*, pages 1–9, 2006. (Cited on page 29.)

[55] Tamer ElBatt, Siddhartha K. Goel, Gavin Holland, Hariharan Krishnan, and Jayendra Parikh. Cooperative collision warning using dedicated short range wireless communications. *Proceedings of the 3rd international workshop on Vehicular ad hoc networks (VANET'06)*, pages 1–9, 2006. (Cited on pages xiv, 23, 29, 30, 58, 60, 70, 71, 73, and 77.)

[56] Paal E Engelstad and ON Osterbo. The Delay Distribution of IEEE 802.11 e EDCA and 802.11 DCF. In *International Performance, Computing, and Communications Conference (IPCCC 2006)*, pages 10–pp. IEEE, 2006. (Cited on pages 31, 63, and 67.)

[57] Jakob Eriksson, Lewis Girod, Bret Hull, Ryan Newton, Samuel Madden, and Hari Balakrishnan. The Pothole Patrol: using a mobile sensor network for road surface monitoring. In *ACM MobiSys*, 2008. (Cited on page 201.)

[58] Patrick Th. Eugster, Pascal A. Felber, Rachid Guerraoui, and Anne-Marie Kermarrec. The many faces of publish/subscribe. *ACM Computing Surveys*, **35**[2]:114–131, June 2003. (Cited on pages 148 and 149.)

[59] Marco Fiore and Jose Maria Barcelo-Ordinas. Cooperative download in urban vehicular networks. In *Proceedings of the 6th International Conference on Mobile Adhoc and Sensor Systems (MASS'09)*, pages 20–29. IEEE, 2009. (Cited on page 147.)

[60] MARCO FIORE AND JÉRÔME HÄRRI. The networking shape of vehicular mobility. In *Proceedings of the 9th ACM international symposium on Mobile ad hoc networking and computing*, pages 261–272. ACM, 2008. (Cited on pages 33 and 59.)

[61] MARCO FIORE, JEROME HARRI, FETHI FILALI, AND CHRISTIAN BONNET. Understanding vehicular mobility in network simulation. In *IEEE Internatonal Conference on Mobile Adhoc and Sensor Systems (MASS 2007)*, pages 1–6. IEEE, 2007. (Cited on pages 59, 206, and 207.)

[62] MARCO FIORE, JEROME HARRI, FETHI FILALI, AND CHRISTIAN BONNET. Vehicular mobility simulation for VANETs. In *40th Annual Simulation Symposium*, pages 301–309. IEEE, 2007. (Cited on pages 205, 207, and 208.)

[63] SAMIR GOEL, TOMASZ IMIELINSKI, KAAN OZBAY, AND BADRI NATH. Sensors on Wheels–towards a zero-infrastructure solution for intelligent transportation systems. In *Proceedings of the 1st international conference on Embedded networked sensor systems*, pages 338–339. ACM, 2003. (Cited on page 201.)

[64] JAVIER GOZALVEZ, MIGUEL SEPULCRE, AND RAMON BAUZA. Impact of the radio channel modelling on the performance of VANET communication protocols. *Telecommunication Systems*, **50**[3]:149–167, December 2010. (Cited on page 34.)

[65] GIANLUCA GRILLI. *Data dissemination in vehicular networks*. PhD thesis, PhD dissertation in Computer Science and Automation Engineering, 2010. (Cited on page 146.)

[66] MENG GUO, MOSTAFA H AMMAR, AND ELLEN W ZEGURA. V3: A vehicle-to-vehicle live video streaming architecture. *Pervasive and Mobile Computing*, **1**[4]:404–424, 2005. (Cited on pages 147 and 201.)

[67] JEROME HARRI, FETHI FILALI, AND CHRISTIAN BONNET. Mobility models for vehicular ad hoc networks: a survey and taxonomy. *IEEE Commu-*

nications Surveys and Tutorials, **11**[4]:19–41, 2009. (Cited on pages 59 and 203.)

[68] Bret Hull, Vladimir Bychkovsky, Yang Zhang, Kevin Chen, Michel Goraczko, Allen Miu, Eugene Shih, Hari Balakrishnan, and Samuel Madden. CarTel: a distributed mobile sensor computing system. In *Proceedings of the 4th international conference on Embedded networked sensor systems*, pages 125–138. ACM, 2006. (Cited on page 200.)

[69] Van Jacobson, Diana K Smetters, James D Thornton, Michael F Plass, Nicholas H Briggs, and Rebecca L Braynard. Networking named content. In *Proceedings of the 5th international conference on Emerging networking experiments and technologies*, pages 1–12. ACM, 2009. (Cited on pages 201 and 202.)

[70] Kamal Jain, Jitendra Padhye, Venkata N Padmanabhan, and Lili Qiu. Impact of interference on multi-hop wireless network performance. In *Proceedings of the 9th annual international conference on Mobile computing and networking*, pages 66–80. ACM, 2003. (Cited on pages 19 and 20.)

[71] Sushant Jain, Kevin Fall, and Rabin Patra. Routing in a Delay Tolerant Network. *SIGCOMM Computer Communications Review*, **34**[4]:145–158, 2004. (Cited on page 149.)

[72] Gunnar Johansson and Kåre Rumar. Drivers' brake reaction times. *Human Factors: The Journal of the Human Factors and Ergonomics Society*, **13**[1]:23–27, 1971. (Cited on page 127.)

[73] David B Johnson and David A Maltz. Dynamic source routing in ad hoc wireless networks. *Kluwer International Series in Engineering and Computer Science*, pages 153–179, 1996. (Cited on page 206.)

[74] Ehud Kalai and Meir Smorodinsky. Other Solutions to Nash's Bargaining Problem. *Econometrica*, **43**[3]:513–18, May 1975. (Cited on page 169.)

[75] Youn-Soo Kang. *Delay, stop and queue estimation for uniform and random traffic arrivals at fixed-time signalized intersections*. PhD thesis, Virginia Polytechnic Institute and State University, 2000. (Cited on page 114.)

[76] John B Kenney. Dedicated Short-Range Communications (DSRC) Standards in the United States. *Proceedings of the IEEE*, **99**[7]:1162–1182, 2011. (Cited on pages 125 and 196.)

[77] M. Khabazian, S. Aissa, and M. Mehmet-Ali. Performance Modeling of Safety Messages Broadcast in Vehicular Ad Hoc Networks. *Intelligent Transportation Systems, IEEE Transactions on*, **14**[1]:380–387, 2013. (Cited on pages 23 and 26.)

[78] Mehdi Khabazian, Sonia Aïssa, and Mustafa Mehmet-Ali. Performance modeling of message dissemination in vehicular ad hoc networks. In *5th IEEE International Symposium on Wireless Pervasive Computing (ISWPC)*, pages 174–179. IEEE, 2010. (Cited on pages 5, 18, 26, and 79.)

[79] S.E. Kingsland. *Modeling Nature: Episodes in the History of Population Ecology*. Science and Its Conceptual Foundations. University of Chicago Press, 1985. (Cited on page 41.)

[80] Keith K Knapp and John Campell. *Intersection crash summary statistics for Wisconsin*. University of Wisconsin-Madison, Traffic Operations and Safety Laboratory, 2005. (Cited on pages 96 and 187.)

[81] Jochen Koberstein, Sören Witt, and Norbert Luttenberger. Model complexity vs. better parameter value estimation: comparing four topography-independent radio models. In *Proceedings of the 2nd International Conference on Simulation Tools and Techniques*, page 92. ICST (Institute for Computer Sciences, Social-Informatics and Telecommunications Engineering), 2009. (Cited on pages 32 and 34.)

[82] Joachim Krug and Herbert Spohn. Universality classes for deterministic surface growth. *Physical Review A*, **38**[8]:4271, 1988. (Cited on page 208.)

[83] Anis Laouiti, Paul Muhlethaler, and Yasser Toor. Reliable opportunistic broadcast in VANETs. In *IEEE 9th International Conference on Intelligent Transport Systems Telecommunications,(ITST)*, pages 382–387. IEEE, 2009. (Cited on page 26.)

[84] Jonathan Ledy, Hervé Boeglen, Anne-Marie Poussard, Benoît Hilt, and Rodolphe Vauzelle. A semi-deterministic channel model for VANETs simulations. *International Journal of Vehicular Technology*, **2012**, 2011. (Cited on page 36.)

[85] John Lee and Wai Chen. Reliably suppressed broadcasting for Vehicle-to-Vehicle communications. In *Vehicular Technology Conference (VTC 2010-Spring), 2010 IEEE 71st*, pages 1–7. IEEE, 2010. (Cited on page 25.)

[86] Kevin C Lee, Seung-Hoon Lee, Ryan Cheung, Uichin Lee, and Mario Gerla. First experience with CarTorrent in a real vehicular ad hoc network testbed. In *Mobile Networking for Vehicular Environments*, pages 109–114. IEEE, 2007. (Cited on page 147.)

[87] Uichin Lee, Ryan Cheung, and Mario Gerla. Emerging vehicular applications. *Vehicular Networks: From Theory to Practice. Chapman and Hall/CRC*, 2009. (Cited on pages 1, 147, 200, and 201.)

[88] Uichin Lee, Jiyeon Lee, Joon-Sang Park, and Mario Gerla. FleaNet: A virtual market place on vehicular networks. *IEEE Transactions on Vehicular Technology*, **59**[1]:344–355, 2010. (Cited on page 201.)

[89] Uichin Lee, Joon-Sang Park, Joseph Yeh, Giovanni Pau, and Mario Gerla. Code torrent: content distribution using network coding in VANET. In *Proceedings of the 1st international workshop on Decentralized resource sharing in mobile computing and networking*, pages 1–5. ACM, 2006. (Cited on page 147.)

[90] Uichin Lee, Biao Zhou, Mario Gerla, Eugenio Magistretti, Paolo Bellavista, and Antonio Corradi. MobEyes: smart mobs for urban monitoring with a vehicular sensor network. *IEEE Wireless Communications*, **13**[5]:52–57, 2006. (Cited on pages 147 and 201.)

[91] Jérémie Leguay, Anders Lindgren, James Scott, Timur Friedman, and Jon Crowcroft. Opportunistic content distribution in an urban setting. In *Proceedings of ACM CHANTS*, pages 205–212, USA, 2006. (Cited on page 148.)

[92] Ilias Leontiadis. *A content dissemination framework for vehicular networking*. PhD thesis, UCL (University College London), 2010. (Cited on page 146.)

[93] Ming Li and Wenjing Lou. Opportunistic Broadcast of Emergency Messages in Vehicular Ad Hoc Networks with Unreliable Links. In *Proceedings of the 5th International ICST Conference on Heterogeneous Networking for Quality, Reliability, Security and Robustness*, QShine '08, pages 47:1–47:7. ICST (Institute for Computer Sciences, Social-Informatics and Telecommunications Engineering), 2008. (Cited on page 29.)

[94] Ming Li, Zhenyu Yang, and Wenjing Lou. Codeon: Cooperative popular content distribution for vehicular networks using symbol level network coding. *IEEE Journal on Selected Areas in Communications*, **29**[1]:223–235, 2011. (Cited on pages 147 and 150.)

[95] Xiaoyan Li, Thu D Nguyen, and Richard P Martin. An analytic model predicting the optimal range for maximizing 1-hop broadcast coverage in dense wireless networks. In *Ad-Hoc, Mobile, and Wireless Networks*, pages 172–182. Springer, 2004. (Cited on page 25.)

[96] Yunxin Jeff Li. An overview of the DSRC/WAVE technology. In *Quality, Reliability, Security and Robustness in Heterogeneous Networks*, pages 544–558. Springer, 2012. (Cited on page 196.)

[97] K. Lidstrom and T. Larsson. Cooperative Communication Disturbance Detection in Vehicle Safety Systems. In *Intelligent Transportation Systems Conference, 2007. ITSC 2007. IEEE*, pages 522–527, 2007. (Cited on page 28.)

[98] K. Lidstrom and T. Larsson. Model-based Estimation of Driver Intentions Using Particle Filtering. In *Intelligent Transportation Systems,*

2008. ITSC 2008. 11th International IEEE Conference on, pages 1177–1182, 2008. (Cited on page 28.)

[99] Anders Lindgren, Avri Doria, and Olov Schelén. Probabilistic routing in intermittently connected networks. *ACM SIGMOBILE Mobile Computing and Communications Review*, **7**[3]:19–20, 2003. (Cited on page 148.)

[100] AI Lyakhov, VM Vishnevsky, and P Poupyrev. Analytical study of broadcasting in 802.11 ad hoc networks. In *2nd International Conference on e-Business and Telecommunication Networks (ICETE)*, 2005. (Cited on page 31.)

[101] Xiaomin Ma and Xianbo Chen. Delay and broadcast reception rates of highway safety applications in vehicular ad hoc networks. In *IEEE INFOCOM2007 workshop on Mobile Networking for Vehicular Environments*, pages 85–90. IEEE, 2007. (Cited on pages 22, 23, 27, and 62.)

[102] Xiaomin Ma and Xianbo Chen. Saturation performance of IEEE 802.11 broadcast networks. *Communications Letters, IEEE*, **11**[8]:686–688, 2007. (Cited on pages 22 and 27.)

[103] Xiaomin Ma and Xianbo Chen. Performance analysis of IEEE 802.11 broadcast scheme in ad hoc wireless LANs. *IEEE Transactions on Vehicular Technology*, **57**[6]:3757–3768, 2008. (Cited on pages 27 and 31.)

[104] Xiaomin Ma, Xianbo Chen, and Hazem H Refai. Unsaturated performance of IEEE 802.11 broadcast service in vehicle-to-vehicle networks. In *IEEE 66th Vehicular Technology Conference (VTC-2007 Fall)*, pages 1957–1961. IEEE, 2007. (Cited on page 27.)

[105] Xiaomin Ma, Xianbo Chen, and Hazem H Refai. On the broadcast packet reception rates in one-dimensional MANETs. In *IEEE Global Telecommunications Conference (GLOBECOM 2008)*, pages 1–5. IEEE, 2008. (Cited on pages 27 and 79.)

[106] Xiaomin Ma, Xianbo Chen, and Hazem H. Refai. Performance and reliability of DSRC vehicular safety communication: A formal analysis. *EURASIP Journal on Wireless Communications and Networking*, **2009**:3:1–3:13, January 2009. (Cited on pages 5, 18, 20, 23, 27, 31, and 79.)

[107] Xiaomin Ma and Hazem H Refai. Analytical model for broadcast packet reception rates in two-dimensional MANETs. In *IEEE International Conference on Communications (ICC 2011)*, pages 1–5. IEEE, 2011. (Cited on page 27.)

[108] Xiaomin Ma, Jinsong Zhang, and Tong Wu. Reliability analysis of one-hop safety-critical broadcast services in VANETs. *IEEE Transactions on Vehicular Technology*, **60**[8]:3933–3946, 2011. (Cited on pages 5, 17, 18, 20, 21, 22, 23, 24, and 27.)

[109] Xiaomin Ma, Jinsong Zhang, Xiaoyan Yin, and Kishor S Trivedi. Design and analysis of a robust broadcast scheme for VANET safety-related services. *IEEE Transactions on Vehicular Technology*, **61**[1]:46–61, 2012. (Cited on pages 20 and 27.)

[110] Atulya Mahajan, Niranjan Potnis, Kartik Gopalan, and Andy Wang. Urban mobility models for VANETs. In *2nd IEEE International Workshop on Next Generation Wireless Networks*, 2006. (Cited on pages 33, 203, and 204.)

[111] Thomas Mangel, Oliver Klemp, and Hannes Hartenstein. 5.9 GHz inter-vehicle communication at intersections: a validated non-line-of-sight path-loss and fading model. *EURASIP Journal on Wireless Communications and Networking*, **2011**[1]:1–11, 2011. (Cited on page 35.)

[112] Thomas Mangel, Friedrich Schweizer, Timo Kosch, and Hannes Hartenstein. Vehicular safety communication at intersections: Buildings, Non-Line-Of-Sight and representative scenarios. In *International Conference on Wireless On-Demand Network Systems and Services (WONS)*, pages 35–41. IEEE, 2011. (Cited on page 35.)

[113] Francisco J Martinez, Chai-Keong Toh, J-C Cano, Carlos T Calafate, and Pietro Manzoni. Realistic radio propagation models (RPMs) for VANET simulations. In *Wireless Communications and Networking Conference, WCNC 2009*, pages 1–6. IEEE, 2009. (Cited on page 34.)

[114] Francisco J. Martinez, ChaiKeong Toh, Juan-Carlos Cano, CarlosT. Calafate, and Pietro Manzoni. Determining the Representative Factors Affecting Warning Message Dissemination in VANETs. *Wireless Personal Communications*, **67**[2]:295–314, 2012. (Cited on page 30.)

[115] A.J. Mashhadi, S. Ben Mokhtar, and L. Capra. Habit: leveraging human mobility and social network for efficient content dissemination in Delay Tolerant Networks. In *Proceedings of International Symposium on a World of Wireless, Mobile and Multimedia Networks (WoWMoM)*, pages 1–6, 2009. (Cited on pages 148 and 150.)

[116] David W Matolak. V2V Communication Channels: State of Knowledge, New Results, and Whats Next. In *Communication Technologies for Vehicles*, pages 1–21. Springer, 2013. (Cited on pages 32 and 34.)

[117] Rui Meireles, Mate Boban, Peter Steenkiste, Ozan Tonguz, and Joao Barros. Experimental study on the impact of vehicular obstructions in VANETs. *IEEE Vehicular Networking Conference*, pages 338–345, 2010. (Cited on page 35.)

[118] Khaleel Mershad, Hassan Artail, and Mario Gerla. We can deliver messages to far vehicles. *IEEE Transactions on Intelligent Transportation Systems*, **13**[3]:1099–1115, 2012. (Cited on page 200.)

[119] Friedhelm Meyer auf de Heide, Christian Schindelhauer, Klaus Volbert, and Matthias Grünewald. Energy, congestion and dilation in radio networks. In *Proceedings of the fourteenth annual ACM symposium on Parallel algorithms and architectures*, pages 230–237. ACM, 2002. (Cited on page 19.)

[120] A Molisch, Fredrik Tufvesson, Johan Karedal, and C Mecklenbrauker. A survey on vehicle-to-vehicle propagation channels. , *IEEE Wireless Communications*, **16**[6]:12–22, 2009. (Cited on pages 4, 32, and 34.)

[121] Yasser L Morgan. Notes on DSRC & WAVE standards suite: Its architecture, design, and characteristics. *IEEE Communications Surveys and Tutorials*, **12**[4]:504–518, 2010. (Cited on pages 1, 79, and 195.)

[122] Thomas Moscibroda and Roger Wattenhofer. Minimizing interference in ad hoc and sensor networks. In *Proceedings of the 2005 joint workshop on Foundations of mobile computing*, pages 24–33. ACM, 2005. (Cited on page 19.)

[123] Kai Nagel and Michael Schreckenberg. A cellular automaton model for freeway traffic. *Journal de Physique I*, **2**[12]:2221–2229, 1992. (Cited on pages 188, 208, and 209.)

[124] Alok Nandan, Shirshanka Das, Giovanni Pau, Mario Gerla, and MY Sanadidi. Co-operative downloading in vehicular ad-hoc wireless networks. In *Second Annual Conference on Wireless On-demand Network Systems and Services (WONS 2005)*, pages 32–41. IEEE, 2005. (Cited on pages 147 and 200.)

[125] Alok Nandan, Saurabh Tewari, Shirshanka Das, Mario Gerla, Leonard Kleinrock, et al. Adtorrent: Delivering location cognizant advertisements to car networks. In *Third Annual Conference on Wireless On-demand Network Systems and Services (WONS 2006)*, pages 203–212, 2006. (Cited on pages 147 and 200.)

[126] John Nash. The Bargaining Problem. *Econometrica*, **18**[2]:155–162, April 1950. (Cited on page 169.)

[127] Qiang Ni, Tianji Li, Thierry Turletti, and Yang Xiao. Saturation throughput analysis of error-prone 802.11 wireless networks. *Wireless Communications and Mobile Computing*, **5**[8]:945–956, 2005. (Cited on page 31.)

[128] Noam Nisan. *Algorithmic game theory*. Cambridge University Press, 2007. (Cited on page 193.)

[129] Erik Nordström, Per Gunningberg, and Christian Rohner. Haggle: a data-centric network architecture for mobile devices. In *Proc. of ACM MobiHoc S3 Workshop*, pages 37–40, 2009. (Cited on pages 148 and 149.)

[130] Jianli Pan, Subharthi Paul, and Raj Jain. A survey of the research on future internet architectures. *IEEE Communications Magazine*, **49**[7]:26–36, 2011. (Cited on page 201.)

[131] Hyunggon Park and Mihaela van der Schaar. Bargaining strategies for networked multimedia resource management. *Signal Processing, IEEE Transactions on*, **55**[7]:3496–3511, 2007. (Cited on page 169.)

[132] Joon-Sang Park, Uichin Lee, Soon Y Oh, Mario Gerla, and Desmond S Lun. Emergency related video streaming in VANET using network coding. In *Proceedings of the 3rd international workshop on Vehicular ad hoc networks*, pages 102–103. ACM, 2006. (Cited on page 147.)

[133] L. Pelusi, A. Passarella, and M. Conti. Opportunistic networking: data forwarding in disconnected mobile ad hoc networks. *IEEE Communications Magazine*, **44**[11]:134 –141, 2006. (Cited on page 148.)

[134] Gian Pietro Picco, Gianpaolo Cugola, and Amy L. Murphy. Efficient Content-Based Event Dispatching in the Presence of Topological Reconfiguration. In *Proc. of IEEE ICDCS*, USA, 2003. (Cited on page 149.)

[135] Louis A Pipes. An operational analysis of traffic dynamics. *Journal of applied physics*, **24**[3]:274–281, 1953. (Cited on page 40.)

[136] Rajmohan Rajaraman. Topology control and routing in ad hoc networks: a survey. *ACM SIGACT News*, **33**[2]:60–73, 2002. (Cited on page 59.)

[137] Theodore S Rappaport. *Wireless Communications: Principles and Practice*. Prentice Hall communications engineering and emerging technologies series. Dorling Kindersley, 2009. (Cited on page 32.)

[138] Maxim Raya and Jean-Pierre Hubaux. The security of vehicular ad hoc networks. In *Proceedings of the 3rd ACM workshop on Security of ad hoc and sensor networks*, pages 11–21. ACM, 2005. (Cited on page 127.)

[139] Guillaume Rocheteau and Christopher Waller. Bargaining and the value of money. Working Paper 0501, Federal Reserve Bank of Cleveland, 2005. (Cited on page 170.)

[140] Roger P. Roess, Elena S. Prassas, and William R. McShane. *Traffic Engineering, 4/E*. Pearson Prentice Hall, 2010. (Cited on pages xiv, 6, and 7.)

[141] David A Rosenblueth and Carlos Gershenson. A model of city traffic based on elementary cellular automata. *Complex Systems*, **19**[4]:305, 2011. (Cited on page 96.)

[142] Richard W Rothery. Car following models. *Traffic Flow Theory*, 1992. (Cited on pages 6, 37, 41, 42, 96, 97, and 207.)

[143] Elizabeth M Royer, P Michael Melliar-Smith, and Louise E Moser. An analysis of the optimum node density for ad hoc mobile networks. In *IEEE International Conference on Communications*, **3**, pages 857–861. IEEE, 2001. (Cited on page 206.)

[144] Jedrzej Rybicki, Björn Scheuermann, Wolfgang Kiess, Christian Lochert, Pezhman Fallahi, and Martin Mauve. Challenge: peers on wheels-a road to new traffic information systems. In *Proceedings of the 13th annual ACM international conference on Mobile computing and networking*, pages 215–221. ACM, 2007. (Cited on page 201.)

[145] Miguel Sánchez and Pietro Manzoni. ANEJOS: a java based simulator for ad hoc networks. *Future generation computer systems*, **17**[5]:573–583, 2001. (Cited on page 206.)

[146] T.K. Sarkar, Zhong Ji, Kyungjung Kim, A. Medouri, and M. Salazar-Palma. A survey of various propagation models for mobile

communication. *IEEE Antennas and Propagation Magazine*, **45**[3]:51–82, 2003. (Cited on page 80.)

[147] Elmar Schoch, Frank Kargl, Michael Weber, and Tim Leinmuller. Communication patterns in VANETs. *IEEE Communications Magazine*, **46**[11]:119–125, 2008. (Cited on pages 198 and 199.)

[148] H. Schumacher, H. Tchouankem, J. Nuckelt, T. Kurner, T. Zinchenko, A. Leschke, and L. Wolf. Vehicle-to-Vehicle IEEE 802.11p performance measurements at urban intersections. In *Communications (ICC), 2012 IEEE International Conference on*, pages 7131–7135, 2012. (Cited on page 35.)

[149] M. Sepulcre and J. Gozalvez. On the importance of application requirements in cooperative vehicular communications. In *Eighth International Conference on Wireless On-Demand Network Systems and Services (WONS2011)*, pages 124–131, 2011. (Cited on page 28.)

[150] Miguel Sepulcre and Javier Gozalvez. On the importance of radio channel modeling for the dimensioning of wireless vehicular communication systems. In *Telecommunications, 2007. ITST'07. 7th International Conference on ITS*, pages 1–5. IEEE, 2007. (Cited on page 35.)

[151] Miguel Sepulcre and Javier Gozalvez. Experimental evaluation of cooperative active safety applications based on V2V communications. In *Proceedings of the ninth ACM international workshop on Vehicular internetworking, systems, and applications*, pages 13–20. ACM, 2012. (Cited on page 24.)

[152] Ivan Seskar, Svetislav V Maric, Jack Holtzman, and Jack Wasserman. Rate of location area updates in cellular systems. In *IEEE 42nd Vehicular Technology Conference*, pages 694–697. IEEE, 1992. (Cited on page 206.)

[153] Steven E Shladover and Swe-Kuang Tan. Analysis of vehicle positioning accuracy requirements for communication-based cooperative colli-

sion warning. *Journal of Intelligent Transportation Systems*, **10**[3]:131–140, 2006. (Cited on page 196.)

[154] STEPHEN SMALDONE, LU HAN, PRAVIN SHANKAR, AND LIVIU IFTODE. RoadSpeak: enabling voice chat on roadways using vehicular social networks. In *Proceedings of the 1st Workshop on Social Network Systems*, pages 43–48. ACM, 2008. (Cited on page 201.)

[155] ETSI SMG. Universal Mobile Telecommunications System (UMTS); Selection procedures for the choice of radio transmission technologies of the UMTS. *ETSI Document TR*, **101**:112, 1997. (Cited on page 206.)

[156] C. SOMMER, D. ECKHOFF, R. GERMAN, AND F. DRESSLER. A computationally inexpensive empirical model of IEEE 802.11p radio shadowing in urban environments. In *Wireless On-Demand Network Systems and Services (WONS), 2011 Eighth International Conference on*, pages 84–90, 2011. (Cited on page 36.)

[157] PHILIPP SOMMER. *Design and analysis of realistic mobility models for wireless mesh networks*. Master's thesis, ETH Zurich, 2007. (Cited on page 33.)

[158] T. SPYROPOULOS, K. PSOUNIS, AND C.S. RAGHAVENDRA. Efficient Routing in Intermittently Connected Mobile Networks: The Multiple-Copy Case. *IEEE/ACM Transactions on Networking*, **16**[1]:77 –90, 2008. (Cited on page 148.)

[159] THRASYVOULOS SPYROPOULOS, KONSTANTINOS PSOUNIS, AND CAULIGI S RAGHAVENDRA. Spray and Wait: an efficient routing scheme for intermittently connected mobile networks. In *Proceedings of the 2005 ACM SIGCOMM workshop on Delay-tolerant networking*, pages 252–259. ACM, 2005. (Cited on page 148.)

[160] GREGORY STEPHANOPOULOS, PANOS G MICHALOPOULOS, AND GEORGE STEPHANOPOULOS. Modelling and analysis of traffic queue dynamics at signalized intersections. *Transportation Research Part A: General*, **13**[5]:295–307, 1979. (Cited on page 40.)

[161] Ozan K Tonguz, Wantanee Viriyasitavat, and Fan Bai. Modeling Urban Traffic: A Cellular Automata Approach. *IEEE Communications Magazine*, **47**[5]:142–150, 2009. (Cited on pages 11, 37, 96, 188, 208, 209, and 210.)

[162] M. Torrent-Moreno. Inter-vehicle communications: assessing information dissemination under safety constraints. In *Fourth Annual Conference on Wireless on Demand Network Systems and Services (WONS 2007)*, pages 59–64, 2007. (Cited on page 28.)

[163] M. Torrent-Moreno, J. Mittag, P. Santi, and H. Hartenstein. Vehicle-to-Vehicle Communication: Fair Transmit Power Control for Safety-Critical Information. *IEEE Transactions on Vehicular Technology*, **58**[7]:3684–3703, 2009. (Cited on pages 30, 97, and 125.)

[164] Marc Torrent-Moreno, Steven Corroy, Felix Schmidt-Eisenlohr, and Hannes Hartenstein. IEEE 802.11-based one-hop broadcast communications: understanding transmission success and failure under different radio propagation environments. In *Proceedings of the 9th ACM international symposium on Modeling, Analysis and Simulation of Wireless and Mobile Systems (MSWiM '06)*, pages 68–77, New York, NY, USA, 2006. (Cited on pages 5, 9, 19, 20, 21, 30, 79, 80, and 97.)

[165] Marc Torrent-Moreno, Daniel Jiang, and Hannes Hartenstein. Broadcast reception rates and effects of priority access in 802.11-based vehicular ad-hoc networks. In *Proceedings of the 1st ACM international workshop on Vehicular ad hoc networks (VANET '04)*, pages 10–18, New York, NY, USA, 2004. (Cited on pages 5, 19, 20, 21, 22, 30, 79, and 80.)

[166] Martin Treiber and Dirk Helbing. Realistische Mikrosimulation von Strassenverkehr mit einem einfachen Modell. In *16th Symposium Simulationstechnik ASIM*, **2002**, page 80, 2002. (Cited on page 208.)

[167] Martin Treiber, Ansgar Hennecke, and Dirk Helbing. Congested

traffic states in empirical observations and microscopic simulations. *Physical Review E*, **62**[2]:1805, 2000. (Cited on page 207.)

[168] Thomas J Triggs and Walter G Harris. Reaction time of drivers to road stimuli. 1982. (Cited on page 127.)

[169] Alexey Vinel, Yevgeni Koucheryavy, Sergey Andreev, and Dirk Staehle. Estimation of a successful beacon reception probability in vehicular ad-hoc networks. In *Proceedings of the 2009 International Conference on Wireless Communications and Mobile Computing: Connecting the World Wirelessly*, pages 416–420. ACM, 2009. (Cited on page 27.)

[170] Alexey Vinel, Dirk Staehle, and Andrey Turlikov. Study of beaconing for car-to-car communication in vehicular ad-hoc networks. In *IEEE International Conference on Communications Workshops (ICC Workshops*, pages 1–5. IEEE, 2009. (Cited on page 27.)

[171] Alexey Vinel, Vladimir Vishnevsky, and Yevgeni Koucheryavy. A simple analytical model for the periodic broadcasting in vehicular ad-hoc networks. In *IEEE GLOBECOM Workshops*, pages 1–5. IEEE, 2008. (Cited on page 27.)

[172] VM Vishnevsky and AI Lyakhov. IEEE 802.11 wireless LAN: Saturation throughput analysis with seizing effect consideration. *Cluster Computing*, **5**[2]:133–144, 2002. (Cited on page 31.)

[173] Francesco Viti and Henk J van Zuylen. Modeling queues at signalized intersections. *Transportation Research Record: Journal of the Transportation Research Board*, **1883**[1]:68–77, 2004. (Cited on page 40.)

[174] Pascal Von Rickenbach, Stefan Schmid, Roger Wattenhofer, and Aaron Zollinger. A robust interference model for wireless ad-hoc networks. In *Proceedings of 19th IEEE International Parallel and Distributed Processing Symposium*, pages 8–pp. IEEE, 2005. (Cited on page 19.)

[175] William Webber, Alistair Moffat, and Justin Zobel. A similarity measure for indefinite rankings. *ACM Trans. on Inf. Syst.*, **28**[4]:20:1–20:38, 2010. (Cited on page 171.)

[176] Graeme West. Better approximations to cumulative normal functions. *Wilmott Magazine*, **9**:70–76, 2005. (Cited on page 87.)

[177] Ravi M Yadumurthy, Mohan Sadashivaiah, Ranga Makanaboyina, et al. Reliable MAC broadcast protocol in directional and omni-directional transmissions for vehicular ad hoc networks. In *Proceedings of the 2nd ACM international workshop on Vehicular ad hoc networks*, pages 10–19. ACM, 2005. (Cited on pages 22, 23, and 25.)

[178] Lin Yang, Jinhua Guo, and Ying Wu. Channel Adaptive One Hop Broadcasting for VANETs. In *11th International IEEE Conference on Intelligent Transportation Systems (ITSC 2008)*, pages 369–374, 2008. (Cited on page 79.)

[179] Fei Ye, Raymond Yim, Sumit Roy, and Jinyun Zhang. Efficiency and reliability of one-hop broadcasting in vehicular ad hoc networks. *IEEE Journal on Selected Areas in Communications,*, **29**[1]:151–160, 2011. (Cited on pages 22 and 26.)

[180] Xiaoyan Yin, Xiaomin Ma, and Kishor Trivedi. Performance Evaluation for DSRC Vehicular Safety Communication: A Semi-Markov Process Approach. In *The Fourth International Conference on Communication Theory, Reliability, and Quality of Service (CTRQ 2011)*, pages 9–14, 2011. (Cited on page 27.)

[181] Eiko Yoneki, Pan Hui, ShuYan Chan, and Jon Crowcroft. A socio-aware overlay for publish/subscribe communication in delay tolerant networks. In *Proc. of ACM MSWiM*, pages 225–234, USA, 2007. ACM. (Cited on pages 148 and 149.)

[182] S. Yousefi, M. Fathy, and S. Bastani. *Mobile Ad Hoc Networks: Current Status and Future Trends*, chapter Vehicular Ad Hoc Networks:

Current Issues and Future Challenges, pages 329–377. CRC Press, Boca Raton, 2012. (Cited on page 6.)

[183] Saleh Yousefi, Saeed Bastani, and Mahmood Fathy. On the performance of safety message discrimination in vehicular ad hoc networks. In *Proceedings of the 4th European Conference on Universal Multiservice Networks*, ECUMN '07, pages 377–390, Washington, DC, USA, 2007. IEEE Computer Society. (Cited on pages 18, 23, 29, 60, and 77.)

[184] Saleh Yousefi and Mahmood Fathy. Metrics for performance evaluation of safety applications in vehicular ad hoc networks. *Transport*, **23**[4]:291–298, 2008. (Cited on pages 24 and 30.)

[185] Yang Zhang, Jing Zhao, and Guohong Cao. Roadcast: a popularity aware content sharing scheme in VANETs. *ACM SIGMOBILE Mobile Computing and Communications Review*, **13**[4]:1–14, 2010. (Cited on pages 150 and 151.)

[186] Zhensheng Zhang. Routing in intermittently connected mobile ad hoc networks and delay tolerant networks: overview and challenges. *IEEE Communications Surveys Tutorials*, **8**[1]:24 –37, quarter 2006. (Cited on page 149.)

[187] Jing Zhao, Todd Arnold, Yang Zhang, and Guohong Cao. Extending drive-thru data access by vehicle-to-vehicle relay. In *Proceedings of the fifth ACM international workshop on VehiculAr Inter-NETworking (VANET'08)*, pages 66–75. ACM, 2008. (Cited on page 147.)

[188] Jing Zhao, Yang Zhang, and Guohong Cao. Data Pouring and Buffering on the Road: A New Data Dissemination Paradigm for Vehicular Ad Hoc Networks. *IEEE Transactions on Vehicular Technology*, **56**[6]:3266–3277, 2007. (Cited on page 147.)

[189] Wei Zhou and Sheng-rui Zhang. Analysis of distance headways. *Eastern Asia Society for Transportation Studies*, **4**:556–561, 2003. (Cited on page 97.)